Reynir Fjalar Reynisson

Deep structure and sub-basalt exploration of the mid-Norwegian margin with emphasis on the Møre margin

Thesis for the degree of Philosophiae Doctor

Trondheim, October 2010

Norwegian University of Science and Technology
Faculty of Engineering Science and Technology
Department of Petroleum Engineering and Applied Geophysics

NTNU – Trondheim
Norwegian University of
Science and Technology

NTNU
Norwegian University of Science and Technology

Thesis for the degree of Philosophiae Doctor

Faculty of Engineering Science and Technology
Department of Petroleum Engineering and Applied Geophysics

ISBN 978-82-471-2277-8 (printed ver.)
ISBN 978-82-471-2278-5 (electronic ver.)
ISSN 1503-8181

Doctoral theses at NTNU, 2010:154

Printed by NTNU-trykk

Acknowledgements

This thesis is the result of a project initiated by Jan Reidar Skilbrei in September 2005. Jan Reidar was initially the main supervisor of the project but was early replaced by Jörg Ebbing. I am grateful for their guidance and help during the past years. I also wish to thank Per Terje Osmundsen for his ideas and input during the project.

The project was funded by a project scholarship from Shell. Initially, Olav Norvik was my contact at Shell. He was later replaced by Jan Strømmen. In addition to financial support Shell provided access to data and interpretations that were of great value to the project. I wish to thank Olav, Jan and Shell's exploration team in Stavanger for their assistance and support.

The Continental Shelf Geophysics Team at the Geological Survey of Norway provided working facilities for the majority of the work period. I wish to express my gratitude to Odleiv Olesen and Jörg Ebbing for giving me the opportunity to be a member of their team. The interaction with team has been enormously beneficial for the project and my education. I wish to acknowledge my appreciation for the help and advice from the team members: Albert Eyike, Aziz Nasuti, Christophe Pascal, John Olav Mogaard, Jomar Gellein, Laura Marello, Laurent Gernigon, Marco Brönner, Ola Kihle, Stephanie Werner, Susann Wienecke, and Torleif Lauritsen. Special thanks go to my roommate Cécile Barrére who expanded my french vocabulary to three words in as many years.

I want to thank my colleagues Christine Fichler, Erik Lundin and Susann Wienecke for the support and motivation to finish the thesis. I also wish to thank Jón Steinar Guðmundsson for good advice since I contacted him in relation to applying to this project.

This work would not have been possible without the support of my wife and daughter.

Dedicated to Dagný and Ása Dröfn

Contents

1. Introduction **1**
1.1 Thesis objectives 1
1.2 Contribution of thesis 2
1.3 Thesis layout 3

2. Introduction to the gravity and magnetic methods **5**
2.1 Implementation of gravity and magnetic data on the Norwegian argin 5
2.1.1 Norwegian margin 6
2.1.2 Perspectives 7
2.2 Elementary potential field theory 8
2.2.1 Gravity fields 9
2.2.2 Magnetic fields 11

3. Sub-basalt imaging: an overview **15**
3.1 Seismic methods 16
3.2 Potential field methods 19
3.3 EM methods 21

4. The nature and evolution of the mid-Norwegian margin with emphasis on the Møre margin: a review **23**
4.1 Stratigraphic settings 23
4.2 Tectonic setting 25
4.2.1 Møre Basin 25
4.2.2 Møre Marginal High 27
4.2.3 Transfer systems 31
4.3 Magmatic setting 33
4.3.1 Extrusive volcanics 33
4.3.2 Intrusives 35
4.3.3 Magmatic underplate 36
4.4 Rifting and margin formation 37
4.4.1 Caledonian orogenic climax and extensional collapse 37
4.4.2 Permo-Triassic extension 38
4.4.3 Jurassic extensional events 38
4.4.4 Cretaceous extensional events 39
4.4.5 From rift to drift 40
4.4.6 Paleogene evolution 40
4.4.7 Neogene uplift and erosion 41

5. The use of potential field data in revealing the basement structure in sub-basaltic settings: an example from the Møre margin 43
5.1 Tectonic settings ... 46
5.2 Methodology ... 47
5.2.1 Gravity gradients ... 47
5.2.2 Euler depth estimation ... 48
5.2.3 Forward modelling ... 49
5.3 Synthetic model ... 50
5.3.1 Magnetic and gravity signals from the model ... 52
5.3.2 Euler Deconvolution ... 52
5.3.3 Sensitivity of Forward Modelling ... 54
5.4 Application to the Møre margin ... 59
5.5 Discussion ... 61
5.6 Conclusions ... 64

6. A regional 3D model of the Møre margin 65
6.1 Data Sources ... 66
6.1.1 Potential Field Data ... 66
6.1.2 Seismic Data ... 68
6.1.3 Well Data ... 69
6.2 Seismic Interpretation ... 69
6.3 3D Potential Field Model ... 71
6.3.1 Model Geometry ... 73
6.3.2 Layer Properties ... 74
6.3.3 Modelling Procedure ... 76
6.4 Modelling Results ... 77
6.5 Discussion ... 82
6.5 Conclusions ... 85

7. Origin of lower crustal bodies on the Møre margin from isostatic considerations 87
7.1 Deep structure of the Møre margin from a 3D model ... 88
7.2 Isostatic Flexural Moho ... 89
7.3 Isostatic effect of the LCB ... 91
7.4 Flexural effect of the LCB ... 92
7.5 Implications for evolution of the margin ... 96
7.6 Conclusions ... 102

8. Properties and distribution of lower crustal bodies on the mid-Norwegian margin 103
8.1 Compilation of 3D models ... 104
8.2 Isostatic considerations ... 106
8.3 Process oriented approach ... 112
8.4 Regional considerations ... 113
8.5 Discussion and conclusion ... 115

9. Concluding remarks **119**

Bibliography **121**

Appendix **139**

Chapter 1
Introduction

1.1 Thesis objectives

The mid-Norwegian passive margin offers a unique opportunity to study a variety of tectonic processes and perhaps holds the answers to some key questions regarding the evolution of continental passive margins. Previous studies on the margin have contributed significantly in the general understanding of passive margins worldwide. The nature and evolution of the margin has been studied extensively and to date reasonable knowledge exists on the margin's stratigraphic, tectonic, and magmatic evolution. However, questions remain regarding the role of inherited structural grain in margin formation, the properties of the so-called lower crustal bodies (LCB), the development of a marginal high, the evolution from rift to drift, the cause of large-scale volcanism, and the petroleum prospectivity on volcanic margins in general.

Large areas of volcanic passive margins are covered by basalt that may conceal large reserves of hydrocarbons. For example, the outer parts of the northeast Atlantic margin is relatively unexplored and holds the promise of very large hydrocarbon accumulations. However, in most of this area, the Mesozoic and Palaeozoic sediments that are of interest for hydrocarbon exploration are covered by Cenozoic flood basalts. The Norwegian margin has been strongly affected by the volcanism, in particular in the outer part of the commercially exploitable Møre and Vøring Basins, where extrusive and intrusive rocks form an important part of the basin fill (Planke *et al.* 1999a).

Standard seismic acquisition and processing fail to deliver interpretable images of the sub-basalt sequences. One of the keys to unlocking the huge potential of the margin is to characterize the basalt and find better methods to image beneath it (Ziolkowski *et al.* 2003). A useful technique in the presence of seismically problematical lithologies is modelling of potential field data (Smallwood *et al.* 2001). Gravity modelling can significantly improve the seismic interpretation and may especially help with understanding the structural interpretation under areas obscured by volcanics (Ashcroft *et al.* 1999). Gravity modelling has for example improved the geological interpretation of the sedimentary fill and the depth to basement of the Faroe-Shetland Basin (Ashcroft *et al.* 1999, England *et al.* 2005, White *et al.* 2005). The combined use of both gravity and magnetic potential fields add a further constrain to the interpretations (e.g. Smallwood *et al.* 2001).

Imaging problems caused by the large volumes of magmatic material and substantial sedimentary thickness on the mid-Norwegian margin hamper our interpretation of deep structures and basin on the outer margin. To address this problem an integrated approach

of various geophysical methods and geological reasoning needs to be undertaken. Potential field studies (gravity and magnetics) integrated with seismic- and electromagnetic data hold the promise to bring us still one step closer to understanding of the margin. The following chapters are an attempt towards this goal.

The main aim of this study was to utilize potential fields data to construct an improved regional geological model of the Møre margin and the Møre Marginal High. Interpretation and modelling (both forward and inverse) of the potential fields data were required. Interpretation of available seismic data within the study area were important to establish necessary constraints on the potential field data. Additional constraints were gained by incorporating interpretations of all available geophysical data. Processing of other geophysical data than potential fields data were outside the scope of the study as well as interpretation of geophysical data other than potential fields and seismic.

The main objectives of this thesis were to construct synthetic models of sub-basalt structures and examine the sensitivity of potential fields in sub-basalt imaging. Observations and learnings from the synthetic models were used to aid the construction of a regional geological model of the Møre margin area. The conclusions from the sub-basalt synthetic models on the Møre Margin area were used to estimate the thickness of volcanic layers and pre-Tertiary sediments. Investigation of the isostatic balance of the lithosphere were undertaken to limit the ambiguity of the deeper part of the model. It was necessary to delineate extrusives and intrusives within the study area from seismic to test if and possibly how the potential fields are sensitive to the basalt in the study area. The results of the Møre margin allowed estimation of thickness of the crust and estimate of the total stretching factor (beta). Segmentation of the study area were extracted from the modelling results. Distribution of the LCB acquired by the model and comparison to other geological feature provided means to address its character and origin.

1.2 Contribution of thesis

This thesis addresses the utilization of gravity and magnetic data in volcanic settings with special focus on the Møre margin. Synthetic models and forward models of the Møre margin were constructed to test the sensitivity of the various potential field methods. The results were then applied to a 3D gravity and magnetic model of the Møre margin.

The synthetic models demonstrated that deep sills, as observed in the Møre Basin, cannot be identified from the gravity and magnetic data alone. The lava flows have a clear effect on the gravity and magnetic signature if thicker than ~1 km. Experiments with Euler Deconvolution demonstrated the limitations of the method in sub-basaltic settings both as a tool for basement depth estimation and edge detection. Forward modelling of the gravity and magnetic data were shown by the synthetic models to be a valuable tool in basement recognition in sub-basaltic settings. The use of gravity gradients was shown to limit the modelling ambiguity and improve the basement mapping in sub-basaltic settings.

A 3D regional gravity and magnetic model of the Møre margin integrated with seismic and well data was constructed. The model extends from the Norwegian coast line to the oceanic crust. The model gives a view on the architecture of the continental crust, the distribution of high density lower crust, and the Moho topography. It provides means to estimate for example sub-basalt sedimentary thickness, crustal thickness and total thinning

of the margin. The distribution of lava flows and sills was mapped on extensive industry seismic data set.

The effect of water and sediment loading on the continental crust was estimated and compared to the results of the 3D model. The isostatic response of the loading reflected by the Moho was used to gain insight in the origin of the high density lower crust on the Møre margin. Isostatic backstripping was also used to explain the results of the 3D model. By combining the isostatic concept with the results of the 3D model an improved regional understanding of the margin is acquired.

The results of the model of the Møre margin was merged with a 3D model of the Vøring and Lofoten margins to construct a model for the whole mid-Norwegian margin. The water and sediment loading on the crust was estimated by applying the same methods as on the Møre margin. An enhanced understanding on the character of the high density lower crust was obtained and hence a better regional picture for the whole mid-Norwegian margin achieved.

1.3 Thesis layout

An introduction to the fundamentals of the gravity and magnetic methods used in this study is given in Chapter 2. The first section provides an overview of the implementation of gravity and magnetic data on the Norwegian margin and gives a brief description on the potential of gravity and magnetic data in sub-basaltic settings. A brief summary of the potential theory is given in the second section. Description on what is measured by gravi- and magnetometers is provided and the units of the measurements used in this thesis.

Chapter 3 is an overview of the challenges in sub-basalt imaging and their proposed solutions. The contributions of all the main geophysical methods used by the petroleum industry are discussed.

The object of Chapter 4 is to outline the main structural features and the tectonic evolution of the mid-Norwegian margin. The focus is mainly on the Møre margin and its immediate neighbours. A description of the stratigraphic, tectonic, and magmatic settings is provided, followed by a summary of the rifting and margin formation.

The study presented in Chapter 5 is from an article published in Geophysical Prospecting (Reynisson *et al.* 2009). The article is based on my own work with support from Jörg Ebbing and Jan Reidar Skilbrei. The study systematically investigates the utility of potential field data (gravity and magnetics) for basement mapping in sub-basaltic settings. The applied methods are Euler deconvolution on magnetic data, gravity gradients, and integrated 3D gravity and magnetic forward modelling. The different methods are tested on a synthetic model that has the same dimensions, ambient magnetic field, and similar tectonic settings as the Møre margin. The results from the different methods are finally compared to a seismic line that extends from the Norwegian mainland to the oceanic domain west of the Møre Marginal High.

The data, 3D modelling method, and modelling results of the Møre margin are presented in Chapter 6. This chapter is a publication in preparation and is based on my work with support from Jörg Ebbing. The data sources and limitations are discussed. The implementation of the constraining data and modelling methodology is described. The results of the modelling study and seismic interpretations are presented.

Chapter 7 focuses on the LCB on the Møre margin. The study is a publication in preparation and is based on my own contribution with support from Jörg Ebbing and Per Terje Osmundsen. Results from the 3D model of the Møre margin (Chapter 6) are employed in isostatic investigation of the margin. Comparison between the model results and the isostatic concept provide new insights into the characteristics and possible origin of the LCB.

Chapter 8 addresses the origin of the LCB on the whole mid-Norwegian continental margin. The chapter is from an article that has been accepted for publication in Proceedings of the 7th Petroleum Geology Conference (Reynisson *et al.* in press). My own work is the major contribution of the study supported by Jörg Ebbing, Erik Lundin and Per Terje Osmundsen. For this work Jörg Ebbing provided a basement map of the whole of the mid-Norwegian margin, whereas Erik Lundin wrote the section on the regional considerations. Per Terje Osmundsen is the author of the underlying idea of early magma poor evolution of the mid-Norwegian margin. The results of the 3D model of the Møre margin (Chapter 6) were merged with models of the Vøring and Lofoten margins. The combined model of the whole mid-Norwegian margin provided means to address the properties of the LCB by incorporating flexural isostasy considerations.

A summary of the thesis with its main conclusions and recommendations for further studies are provided in Chapter 9.

Chapter 2

Introduction to the gravity and magnetic methods

2.1 Implementation of gravity and magnetic data on the Norwegian margin

This section is largely based on a publication by Ebbing *et al.* (2008) that describes how magnetic and gravity data have been used on the Norwegian margin to understand its geological evolution. The measurement and interpretation of gravity data is called 'gravimetry', which means gravity measurement. Magnetometry is the geophysical discipline where magnetic data is measured and interpreted. Data on the Earth's gravity and magnetic fields is often collectively referred to as 'potential field data', which involves the measurement of a field strength that is composed of fields from a number of different sources. Every rock exerts an influence on the Earth's gravity and magnetic fields through its density and magnetic properties respectively. Geophysical anomaly fields, which are used to interpret the structure of the upper crust, are corrected for the normal geofield. The anomaly field therefore describes the deviation from the normal field caused by varying densities and structures in the crust, i.e. the uppermost layer of the Earth.

An anomaly map shows deviations from the normal field such that only the part that is unknown, i.e. the anomaly, is interpreted. By looking at a gravity map or a magnetic map, anomalies can be related to properties in the crust. On a gravity anomaly map, low gravity values mean that the material in the underground must have a lower density than the surroundings, while high gravity means a material with a higher density. However, it is not always easy to determine the depth or size of the body causing the anomaly. Figure 2.1 shows that different sources at different depths can give the same anomaly on the surface. Geological knowledge or other information is needed to interpret an anomaly map, so that the bedrock can be followed at depth, and the size of the various structures can be determined. Interpreting magnetic fields is more complicated, but the principle is the same.

Geophysicists use different techniques such as filtering, or correction for known structures, in order to interpret anomaly maps. If we look at the Norwegian shelf, we often interpret isostatic gravity anomalies and total magnetic anomalies (Figure 2.2). Isostatic gravity anomalies are anomalies after the gravitational field has been corrected for the effects of known structures such as the Earth's shape, topography and variation in crust thickness. Total magnetic anomalies are anomalies after correction for the Earth's magnetic field as defined in global reference models, one is then left with a field which originates from

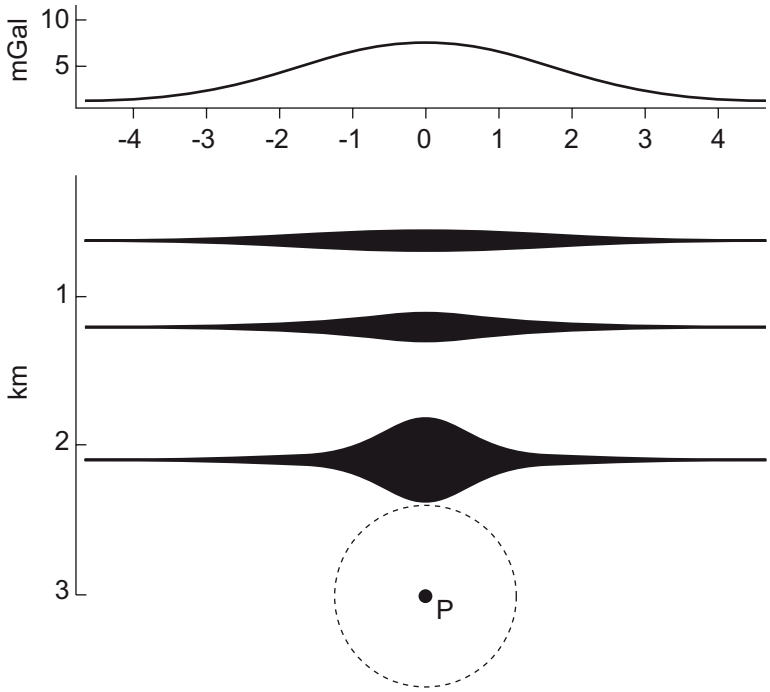

Figure 2.1. Ambiguity in potential field data. Different underground structures can all produce the same gravitational field. A good geological understanding is therefore necessary in order to interpret such geophysical anomalies. The gravitational field is often measured in milligals. The gal is named after Galileo Galilei (1564-1642), who tried to determine the Earth's gravitational field using experiments from the Leaning Tower of Pisa.

structures in the Earth's crust. Both the anomaly fields are therefore corrected in such a way as to give a special insight into the upper crust, i.e. the thickness of sediment basins and the transition from sediments to the underlying gneiss (basement).

2.1.1 Norwegian margin

Anomaly maps clearly show the transition from Norwegian shelf to the deep sea. The crust under the sea was formed at mid-oceanic ridges and is youngest at the spreading ridges and oldest furthest away from these ridges. In the early 1950s Jan Hospers, by his work on Icelandic basalts, convinced many in the geoscience community that most rocks with reversed magnetism were not self reversed but were relics of epochs when the Earth had reversed magnetic polarity (Hospers 1951). New crust is being formed today along the mid-oceanic ridges, as on Iceland and Jan Mayen Island, where molten magma is flowing up from the deep and solidifying to form volcanic rocks. The magnetic pattern shows a series of stripes which is virtually parallel to the mid-oceanic ridges. This striped pattern finishes at the boundary between the Norwegian shelf and the deep-sea (the continent-ocean boundary), because the rocks on the shelf have a different geological history in terms of their formation, and therefore different magnetic properties.

On the basis of new data sets from 2003 and 2005, an alternative geodynamic model for the historical development of the Norwegian Sea was developed (Olesen *et al.* 2002).

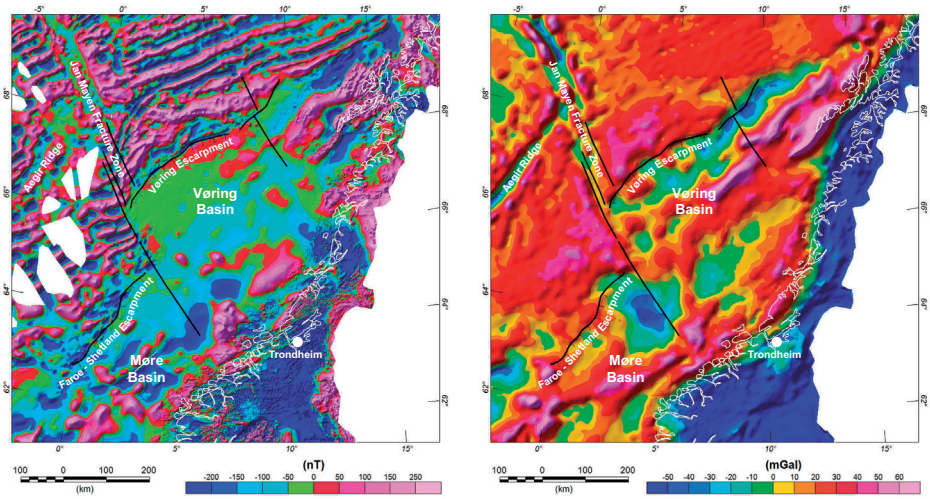

Figure 2.2. Magnetic (left) and isostatic (right) anomalies in Central Norway and the Norwegian Sea.

Previous interpretations indicated a large number of fracture zones in the deep sea, which it was assumed controlled the opening of the North Atlantic. New aeromagnetic data has shown that these fracture zones do not actually exist, but were the result of incomplete coverage and inaccurate positioning of the aircraft during the taking of measurements.

The anomaly map also shows that the outer part of the central Norwegian shelf (the Vøring Basin) contains fewer and smaller magnetic anomalies than the inner part (the Trøndelag Platform). The difference between these two areas is also clear on isostatic anomaly maps. The reason for this is that sediment basins on the outer shelf have depths of up to 14 km, while the basins on the Trøndelag Platform are only 5–8 km deep. Sedimentary rocks have a low density and therefore show negative gravity anomalies. These rock types are also virtually non-magnetic and therefore give very small magnetic anomalies. On the Trøndelag Platform, the distances from the surface to the gneiss basement are not as great, and the Upper Precambrian and Caledonian rocks (marked "Bedrock") show up clearly on the magnetic anomaly map (Figure 2.3).

2.1.2 Perspectives

Gravimetry and magnetometry are the oldest geophysical methods, yet they are still being developed and given new life. In recent years, two new developments have led to renewed interest in the methods: the Earth's gravity and magnetic fields are being measured with great precision from new satellites, giving new information on relatively inaccessible areas such as the Antarctic. However, of greater importance to the Norwegian shelf is the development of gradiometer measurements, which enables better information to be obtained concerning the underground in areas that are difficult to interpret from seismics. On the outer part of the Norwegian shelf, in many places there are volcanic rocks in the form of sheets (sills or lavas) in sedimentary rocks. Using seismic methods, it is difficult to map structures beneath volcanic rock types, but by combining seismics with the interpretation of gravimetry and magnetometry, a picture of the large-scale geological structures in these problem areas can be obtained (Ashcroft *et al.* 1999, Smallwood *et al.* 2001, Reynisson

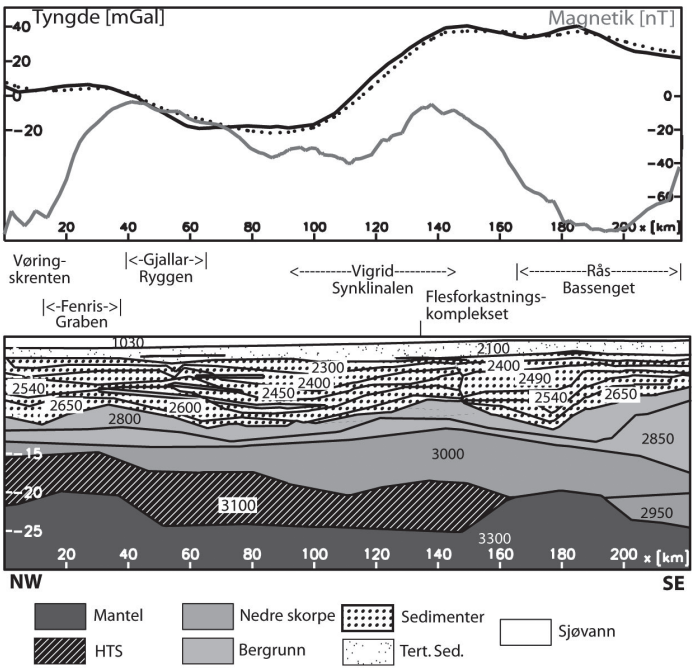

Figure 2.3. Interpreted profile through the outer part of the Norwegian Shelf. The figures show densities of geological structures in kg/m^3. HDC=High Density Crust.

et al. 2007). In addition, electromagnetic methods can provide new information on the outer shelf and the opportunities for new oil and gas discoveries. The combination and co-interpretation of seismic and gravimetric data will also become even more important in the future. The relatively simple relationship between seismic wave velocity and density is used for automatic interpretation (inversion) in unknown areas and can give information which is more accurate than that which can be obtained from the individual methods in isolation.

Gradiometers, which measure a particular component of the gravitational field, can also help to measure changes in the underground. With repeated measurements, changes can be observed both in oil reservoirs and along fault zones. This provides scientists with new opportunities for studying dynamic processes. Gravimetry and magnetometry are still important geophysical methods and will remain so in the years to come. One of the last big gaps in our knowledge of the formation of the Norwegian Sea is currently in the process of being filled through aeromagnetic measurements in the Norwegian Basin off the continental slope of Central Norway.

2.2 Elementary potential field theory

Gravitational and magnetic fields are both potential fields. In general the potential at any point is defined as the work necessary to move a unit mass or pole from an infinite distance to that point through the ambient field. Potential fields obey Laplace's equation which states that the sum of the rates of change of the field gradient in three orthogonal directions

is zero. In a normal Cartesian coordinate system with horizontal axes *x*, *y* and a vertical axis *z*, Laplace's equation is stated:

$$\frac{\delta^2 A}{\delta x^2}+\frac{\delta^2 A}{\delta y^2}+\frac{\delta^2 A}{\delta z^2}=0 \qquad (2.1)$$

where *A* refers to a gravitational or magnetic field and is a function of (x, y, z).

2.2.1 Gravity fields

The gravitational field is defined in terms of the gravitational potential *U*:

$$U=\frac{GM}{r} \qquad (2.2)$$

Where *G* is the Gravitational Constant, *M* is the mass of the Earth, and *r* is the distance from the centre of the Earth.

The gravitational acceleration *g* is a vector quantity that has both magnitude and direction but the gravitational potential *U* is a scalar, which has magnitude only. The first derivative of *U* in any direction gives the component of gravity in that direction.

The gradient of *U* (*grad U*) is equal to the gravity *g*:

$$g=\nabla U \qquad (2.3)$$

where $grad=\nabla=\frac{\partial}{\partial x}i+\frac{\partial}{\partial y}j+\frac{\partial}{\partial z}k$

So the gravity field *g* is:

$$g=\frac{\partial U}{\partial x}i+\frac{\partial U}{\partial y}j+\frac{\partial U}{\partial z}k \qquad (2.4)$$

Where *i*, *j*, *k* represents unit vectors in the direction of the positive *x*, *y*, *z* axes respectively.

The gradient of the gravity field *g* with g_x, g_y, g_z as its components along the *x*, *y*, *z* axes respectively is:

$$g=\nabla U$$

$$\nabla g=\nabla^2 U$$

$$\frac{\partial g_x}{\partial x}+\frac{\partial g_y}{\partial y}+\frac{\partial g_z}{\partial z}=\frac{\partial^2 U}{\partial x^2}+\frac{\partial^2 U}{\partial y^2}+\frac{\partial^2 U}{\partial z^2} \qquad (2.5)$$

In non mass-free space:

$$\nabla g=\nabla^2 U=-4\pi G\rho \qquad (2.6)$$

where *G* is the Gravitational Constant and ρ is the density of mass distribution at the point considered. Equation 2.6 is Poisson's equation and describes the potential at all points, even inside the mass distribution. Laplace's equation (2.1) is simply a special case of Poisson's equation valid for mass-free regions of space (Blakely 1996).

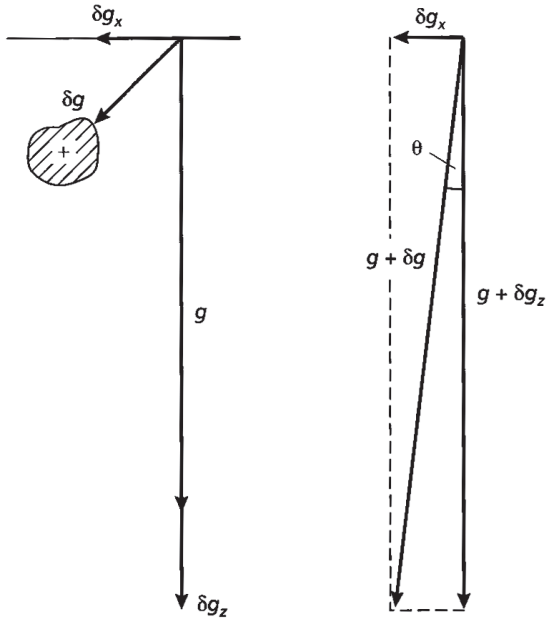

Figure 2.4. Relationship between the gravitational field and the components of the gravity anomaly of a small mass (from Kearey *et al.* (2002)).

The gravity field *g*, which is measured by gravimeters varies with height, hence there is a vertical gradient of the gravity field *g*, given by:

$$g' = \frac{\partial g}{\partial z}$$

Over a non-uniform earth in which density varies laterally, the vertical gradient changes. The rate of change of the vertical gradient is thus the second vertical derivative of the gravity field *g*.

$$\frac{\partial g'}{\partial z} = \frac{\partial}{\partial z}(g') = \frac{\partial}{\partial z}\left(\frac{\partial g}{\partial z}\right) = \frac{\partial^2 g}{\partial z^2}$$

This quantity is very sensitive to the effects of shallow features and to the effect of noise and topography.

Gravimeters effectively respond only to the vertical component of the gravitational attraction of an anomalous mass. Consider the gravitational effect of an anomalous mass δg, with horizontal and vertical components δg_x and δg_z, respectively, on the local gravity field *g* and its representation on a vector diagram (Figure 2.4). Solving the rectangle of forces gives:

$$g + \delta g = \sqrt{(g + \delta g_z)^2 + \delta g_x{}^2}$$

$$g + \delta g = \sqrt{(g^2 + 2g\delta g_z + \delta g_z{}^2 + \delta g_x{}^2)}$$

Term in δ^2 are insignificantly small and can thus be ignored. Binomial expansion of the equation then gives:

$$g + \delta g \approx g + \delta g_z$$

so that

$$\delta g \approx \delta g_z$$

Consequently, measured perturbations in gravity effectively correspond to the vertical component of the attraction of the causative body. Very large mass anomalies such as mountain ranges can, however, produce noticeable local vertical deflections (Kearey *et al.* 2002).

Before the results of a gravity survey can be interpreted it is necessary to correct for all variation in the Earth's gravitational field which do not result from the differences of density in the underlying rocks. This process is referred to as gravity reduction (LaFehr 1991). The main corrections are instrumental drift correction, latitude correction, elevation correction, tidal correction (at fixed location), and Eötvös correction (on moving platforms). The free-air anomaly includes all these corrections and represents the contribution of mass in the Earth to the gravity field at the measuring point. The free-air correction ignores mass that exist between the measuring point and sea level. The Bouguer correction accounts for this additional mass (Blakely 1996).

The mean value of gravity at the Earth's surface is about 9.8 ms^{-2}. Variations in gravity caused by density variation in the subsurface are of the order of 100 μms^{-2}. In honour of Galileo, the cgs unit of acceleration due to gravity (1 cms^{-2}) is the Gal. The sensitivity of gravimeters is about ten parts per million. Such small numbers have resulted in sub-units being used such as the milliGal (1 mGal=10^{-3} Gals) (Reynolds 1997). The measurement of gravity gradients is often given in the Eötvös unit which equals 10^{-4} mGal/m or 0.1 mGal/km. In the following chapters the milliGal (mGal) and mGal/km are employed.

2.2.2 Magnetic fields

Magnetic fields can be defined in term of magnetic potentials in a similar manner to gravitational fields. For a single dipole of strength m the magnetic potential V at a distance r from the pole is given by:

$$V = \frac{\mu_0 m}{4\pi\mu_R r} \qquad (2.7)$$

where μ_0 and μ_R are constants corresponding to the magnetic permeability of vacuum and the relative magnetic permeability of the medium separating the poles. The magnetic field component in any direction is then given by the partial derivative of the potential in that direction.

The closeness of the flux lines shown in Figure 2.5b is the flux density B which is a vector quantity. The magnetic field can also be defined in terms of a force field which is produced by electric currents. This magnetising field strength H is defined as being the field strength at the centre of a loop of wire of radius r through which a current I is flowing such that $H=I/2r$. The ration of the flux density B to the magnetising field strength H is a constant called the absolute magnetic permeability μ. The relationship between B and H can be expressed in terms of a geologically diagnostic parameter, the magnetic susceptibility k. Susceptibility is

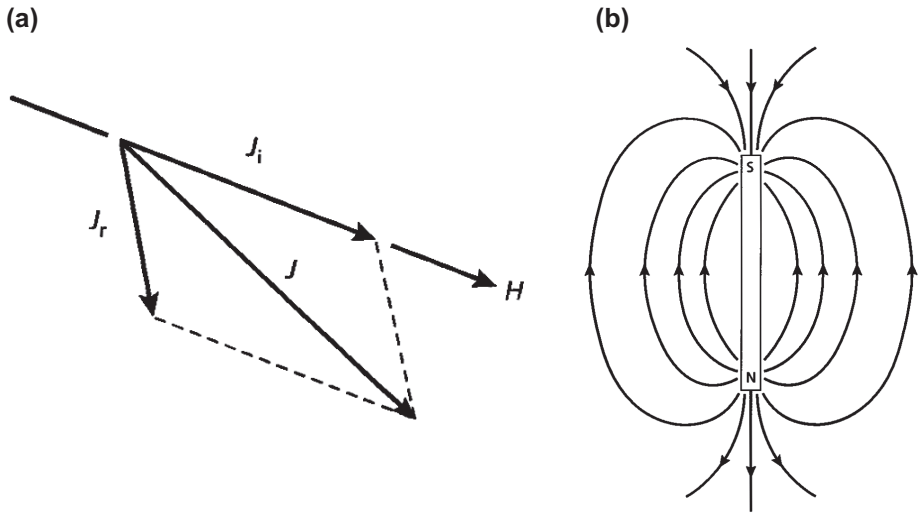

Figure 2.5. (**a**) Vector diagram illustrating the relationship between induced J_i, remanent J_r and total J magnetization components. (**b**) The magnetic flux surrounding a bar magnet (from Kearey *et al.* (2002)).

in essence a measure of how susceptible a material is to becoming magnetised (Reynolds 1997).

When a material is place in a magnetic field it may acquire a magnetization in the direction of the field which is lost when the material is removed from the field. This phenomenon is referred to as induced magnetization. The induced intensity of magnetization J_i is proportional to the strength of the magnetizing force H of the inducing field:

$$J_i = kH \tag{2.8}$$

Any rock containing magnetic minerals may possess both induced and remanent magnetizations J_i and J_r. The relative intensities of induced and remanent magnetizations are commonly expressed in terms of the Königsberger ratio Q:

$$Q = \frac{J_r}{J_i} \tag{2.9}$$

These may be oriented in different direction and may differ significantly in magnitude. The magnetic effects of a rock arise from the resultant J of the two magnetization vectors (Figure 2.5a). The magnitude of J controls the amplitude of the magnetic anomaly and the orientation of J influences its shape (Kearey *et al.* 2002).

Magnetic anomalies caused by rocks are localized effects superimposed on the normal magnetic field of the Earth. Consequently, knowledge of the behaviour of the magnetic field is necessary both in the reduction of magnetic data to a suitable datum and in the interpretation of the resulting anomalies. The magnetic field is geometrically more complex than the gravity field of the Earth and exhibits irregular variation in both orientation and magnitude with latitude, longitude and time (Kearey *et al.* 2002).

The ambient geomagnetic field is described in terms of the declination *D*, inclination *I* and the total field vector *B*. The horizontal angle between geographic and magnetic north is the declination and the dip of *B* is the inclination. The strength of *B* varies from about 25000 nT in equatorial regions to about 70000 nT at the poles (Kearey *et al.* 2002, Reynolds 1997).

The SI unit of magnetic field strength is the tesla (T). The tesla is too large a unit in which to express the small magnetic anomalies caused by rocks and therefore a subunit, the nanotesla (nT), is commonly used ($1\ nT=10^{-9}T$).

Chapter 3
Sub-basalt imaging: an overview

The problem of imaging through basalt is particularly acute in areas where potential hydrocarbon bearing structures are overlain by basalt flows up to several kilometres thick (e.g., the North Atlantic, west African and Brazilian margins) (Martini *et al.* 2005). Other terrains with severe imaging problems, such as those associated with salt deposits, have received extensive attention within the seismic processing industry. It is important to note that fundamentally different petrophysical properties of volcanic and salt deposits suggest that new solutions should be considered to improve the sub-basalt and intrabasalt images (Planke *et al.* 1999a).

Intra-lava flow velocity variation, caused by compositional and structural variability within the individual flows (low velocity at the top and base versus high velocity in the massive core), combined with inter-layering between lava flows, sediments, tuff, sills, and hyaloclastites, contribute to the heterogeneous internal structure of the volcanic succession. This complex 3D structure attenuates scatters and multiply reflects the energy that gets transmitted into the basalt layers through the high impedance contrast at the top of the flows. Also, top and base basalt are not flat regular surfaces, but often have a complex topography, which compounds the disruptive effect on wave propagation. All these factors combine to reduce the quality of sub-basalt seismic imaging substantially (Martini *et al.* 2005).

The internal characteristics of basalt flows can seriously degrade the seismic image quality below them. Flood basalts are often extruded as a sequence of laminar flows alternating with sediments and volcanoclastics (Planke 1994, Smallwood *et al.* 1998, Fliedner & White 2001). This leads to high impedance contrasts internal to the flow itself, generating internal reverberation and mode conversion. The P-wave velocity range of igneous rocks produced by the same melt can be as large as 1.5–7.5 km/s. Typically, poorly consolidated tuff are in the lower velocity range, intrusives at depth are in the higher range, and basalt flows are in the intermediate range. Velocities can also change drastically in a basalt flow. The P-wave velocity in subaerial flow shows cyclical asymmetric variations related to emplacements and alteration processes and interbedding of flows and sediments. Planke (1994) developed a characteristic velocity and density basalt flow distribution (CFD) based on log responses in Ocean Drilling Program (ODP) hole 642E. In single flows the velocity increases gradually (velocity gradient of ~400–600 s^{-1}) from ~3 km/s at the top to 5.3 km/s, corresponding to a decreasing number of voids and cracks in the flow. The velocity in the massive central flow is 5.0–6.0 km/s, decreasing very rapidly near the base (velocity gradient of 1000–2000 s^{-1}). The S-wave velocity follows the same trend, with a V_p/V_s ratio of 1.7 to 2.0. The density logs often show a similar pattern, ranging from 2300 to 2800 kg/m^3 (Planke 1994, Planke

& Eldholm 1994). This density and velocity distribution reflects changes in porosity, pore aspect ratio distribution, and alteration. The proportional thickness of the massive interior increases with flow thickness. Consequently, the average velocity and density increases with the thickness. Differences in lava thickness have been observed systematically in many flood basalt sequences (Planke & Eldholm 1994). These observations point to the highly heterogeneous nature of basalts. This heterogeneity leads to strong seismic wave scattering which results in image contamination (Martini & Bean 2002).

3.1 Seismic methods

Much emphasis has been put on solving the imaging problem during the past years by enhancing of seismic methods. The modelling and inversion of long offset and low frequency data have proved particularly promising, as have various processing-based approaches, but the fix-all solution has yet not been found.

One aid in imaging through basalts is to record seismic arrivals at longer offsets than what is normal in seismic reflection profiling. Most of the multiples produced between the sea-surface, the sea-bed and top of the basalt layer that contaminate the near-offset wavefield are not present in the wide-angle data because their low apparent move-out velocities mean that they arrive considerably later. Another advantage of using seismic data from large offsets is that, for most reflectors, the amplitude of the reflection increases as the angle of incidence increases towards the critical angle. Finally, there is a greater possibility of recording converted shear waves at wide angles, and these may be useful for both imaging and for constraining the rock types and properties (Fliedner & White 2003, White *et al.* 2003).

Long-offset data have two major disadvantages. One is that the long travelpaths mean that the higher-frequency components of the waveform tend to be absorbed with reduction in finer details. Another factor is that the further the distance over which the energy travels, the larger will be the errors introduced by incorrect velocity models used in migrating the arrivals back to normal incidence (White *et al.* 2003).

There are three main ways of recording data to large offsets. One is to use fixed receivers on the sea-bed, so called ocean-bottom seismograph (OBS), in which case it is feasible to use three-component seismometers in addition to hydrophones (Wang & Singh 2003). This carries the additional advantages of the possibility of removing the water multiple by separating the upgoing and downgoing waves, and that converted shear waves can be detected directly. The second way is to use longer hydrophone streamers, up to 12 000 m. The third way of acquiring large-offset data, which is unconstrained by the streamer length available, is to use a second seismic acquisition ship steaming at a fixed distance behind a lead seismic acquisition vessel to synthesize a super-long streamer (White *et al.* 2003).

Wide-angle seismic imaging may be considered complementary to exploration seismic surveying in that it focuses on the information content of the post-critical seismic wavefield which usually lies beyond the mute in conventional, sub-critical processing. Whereas short-offset seismic data contain information on impedance contrasts, wide-angle data mainly contain information on the velocity structure. Long-offset wavefields have the merit that diving waves are often first arrivals with good signal-to-noise ratios and can be identified unambiguously as primary events. Although a velocity reversal does not give rise to a diving wave, high velocity (e.g. basalt) layer thickness can often be inferred from the offset

termination of the diving wave and the resulting 'step-back' to the underlying basement reflector (White *et al.* 2003). Wide-angle reflections and diving waves may be tracked back in offset to identify sub-critical events. Their arrival times may also be picked and modelled with ray-tracing (e.g. Zelt 1999) to develop a velocity model in support of that derived from sub-critical velocity analysis. Although wide-angle events are typically low frequency and lack the resolution of conventional seismic data, when correctly imaged, they may be used to distinguish deep primaries from multiples on migrated sub-critical seismic sections (Christie & Robein 2005).

Wide-angle reflections and refractions from the basalt and underlying strata allow building a velocity model down to the crystalline basement. The velocity models give a first-order picture of the geology, including the presence of low-velocity sediments beneath the basalt flows. They also provide velocity control for pre-stack depth migration of the entire seismic dataset, thus allowing us to produce good depth images of the structure (Fruehn *et al.* 2001).

Usually, the data are processed using a pre-stack depth migration process which requires a velocity-depth model on input. Applying data migration and velocity model updating processes iteratively significantly improves results from seismic imaging. This is because subsequent updates in the velocity model improve focusing of seismic energy at deeper targets (Smit *et al.* 2005).

The solution to the sub-basalt problem is clearly to build a velocity model that is sufficiently accurate to allow proper pre-stack depth migration of the disrupted wavefield. The length-scale of structures at top basalt, and within the basalts, can be small, and both the velocity model and the migration algorithm must properly deal with this. Almost certainly, Kirchhof type migrations are inadequate, and full wave-equation methods will be required, possibly even methods that use the two-way rather than approximate one-way wave-equation. The key to applying such methods is to be able to determine a sufficiently accurate and well resolved velocity model (Warner *et al.* 2002).

Estimating a velocity model is a crucial aspect of seismic data analysis, as it is required to map seismic information into spatial coordinates. One of the problems facing the 'conventional' processor attempting to obtain a sub-basalt image is the determination and validation of a velocity model. Several authors suggest that acquiring long-offset data can help with this. Two recent examples are given below.

White *et al.* (2003) built crustal velocity models by inverting the traveltimes of the recorded reflections and diving waves using ray-tracing methods. Finer details of the velocity structure were then refined by analysis of the amplitudes and waveforms of the arrivals. Then prestack depth migration of selected wide-angle arrivals of known origin, such as the base-basalt reflection, using the crustal velocity model, allowed building a composite image of the structure down to the pre-rift basement.

Barton and Barker (2003) proposed an automatic method for generating a velocity field from traveltimes picked on refracted arrivals. The picks were effectively transformed into the tau-p (intercept-slope) domain from both source and receiver gathers, and the apparent velocities were mapped into depth under some simplifying assumptions about the nature of the (2D) field on the scale length of the cable.

Much activity has focused on the generation and recording of low frequency seismic energy (e.g. Mjelde *et al.* 1998, Ziolkowski *et al.* 2003) which are less affected by scattering from basalt heterogeneities (Christie & Robein 2005). Ziolkowski *et al.* (2003) argue

that the acquisition system for sub-basalt targets should be modified to emphasize the low frequencies. Scattering theory predicts that the lower the frequency, the lower the proportion of energy scattered. Therefore the use of low-frequency seismic waves may avoid the scattering problem of thin layering and lateral heterogeneity. To obtain this the source and receiver must be towed deep and much larger airguns than normal must be used. A comparison of data obtained with larger airguns towed at 15 m and with the streamer at the same depth show improved deep reflection below the top of the basalt.

Martini and Bean (Martini & Bean 2002) compared body and interface scattering through acoustic finite-difference modelling and showed that interface scattering seems to have the most detrimental effect on imaging at depth. A wave equation prestack datuming procedure was applied to synthetic acoustic data to remove the effects of rough interfaces. This computational process transforms seismic data to a new datum plane in the subsurface, eliminating propagation effects between the surface and the new datum plane. The technique led to a much improved image below the basalt. The technique has the same objective as prestack migration but with the great advantage that an accurate representation of only the overburden and the interface (which can be digitized from the data) are required, as opposed to the entire velocity-depth model.

Roberts *et al.* (2005) report the acquisition of low-frequency OBS data together with low-frequency, long-offset, towed-streamer data, to image sub-basalt structure, including lower crustal reflectivity and the Moho. The integration of OBS and towed seismic data may also allow correlation of mixed-mode events from the OBS data with double-mode conversions on the towed streamer data, thereby establishing greater confidence in the method of mode-converted shear wave imaging proposed by Fruehn *et al.* (1999).

Conventional streamer surveys are narrow azimuth (NAZ) but deploying sources on multiple vessels to widen the effective receiver array are wide azimuth (WAZ). WAZ data has shown proven benefits in many areas around the world, and is becoming more common. WAZ surveying is appropriate for any area of complex structural geology, or where velocity contrasts are significant. For example, in basins where deep sedimentary geology is overlain by basalts, which are notoriously difficult to penetrate by conventional seismic methods (Firth & Taylor 2009).

Seafloor compliance is a geophysical prospecting technique that uses the seafloor deformation under ocean waves to determine the subsurface shear modulus. Seafloor compliance is the transfer function between the seafloor pressure and displacement fields as a function of frequency. It is measured by deploying a broad-band seismometer and differential pressure gauge to the seafloor for two or more days. Multiple seafloor compliance measurements can be used to create 2D or 3D subsurface shear modulus models. Seafloor compliance measurements are most sensitive to low shear modulus regions and are insensitive to impedance contrasts such as reflectors in the basalt layer. Compliance data can be inverted to determine the shear velocity/modulus structure of the subsurface, which is very sensitive to the existence and distribution of fluids. The measurements are even more useful when combined with compressional velocity constraints from seismic data (Crawford 2002, 2004).

The sensitivity of seafloor compliance to sub-basalt sediments depends mostly on the water depth and the sub-basalt sediment layer depth, thickness and shear modulus. If the water depth is 1 km or more, seafloor compliance measurements will detect a sub-basalt sediment layer 0.6 km or more thick and will constrain the depth to the top and bottom

of a 2 km thick sub-basalt sediment layer to within 0.2 km. If the water depth is 0.25 km, the thinnest detectable layer will be 1.2 km and the depth uncertainty for a 2 km thick sub-basalt sediment layer will be 0.5–0.8 km. Neither interlayered sediments within the basalt nor sediments above the basalt layer have a strong effect on the measurement sensitivity (Crawford 2004).

3.2 Potential field methods

Subsurface de-risking is presently almost exclusively done by methods using seismic data. Indeed, all other data collected at the surface is referred to as 'non-seismic'. However, there are emerging gravity and electromagnetic measurement technologies that could fundamentally change subsurface risk management by involving 'non-seismic' methods more prominently (Smit *et al.* 2005).

Non-seismic methods have been successful in improving understanding of overall geometry for sub-basalt targets, e.g., electric and electromagmatic methods, gravity, compliance methods. Integration of seismic and non-seismic data has been tested for some of the methods and has yielded promising results. However, these methods cannot produce the clarity of image required for conventional risk assessment for hydrocarbon exploration (Martini *et al.* 2005).

A useful technique in the presence of seismically problematical lithologies is modelling of potential field data (Smallwood *et al.* 2001). Gravity modelling can significantly improve the seismic interpretation and may especially help with understanding the structural interpretation under areas obscured by volcanics (Ashcroft *et al.* 1999). Gravity modelling has for example improved the geological interpretation of the sedimentary fill and the depth to basement of the Faroe-Shetland Basin (Ashcroft *et al.* 1999, England *et al.* 2005, White *et al.* 2005). The combined use of both gravity and magnetic potential fields adds a further constrain to the interpretations (e.g. Smallwood *et al.* 2001).

Extensive 3D modelling was conducted on Abrolhos Bank, offshore Brazil, using seismic, gravity and magnetics data. Integrated geophysical analysis of these complimentary datasets greatly improved the understanding of the extent of the flood basalts, as well as the thickness of the sub-volcanic sediments and the basement structure. No single one of these geophysical methods would have given all the information in isolation. The seismic data together with magnetic depth estimation techniques was used to constrain the depth to the basement. Inversions of the gravity data in 3D were used to produce an isopach of the basalt, which was in turn constrained with the seismic and magnetic data interpretation (Parsons *et al.* 2001).

In some cases, results from gravity modelling have provided valuable insights into the geology below a salt body, enabling the seismic processors to refine their migration velocity model, and as a result refine the seismic image through re-migration of the data using the new velocity model. From data, acquired from off-shore Brazil, an enhancement process was used to generate a velocity model constrained by the combination of seismic and potential field data in a single integrated earth model. The resulting potential-fields-enhanced velocity model was used to generate a prestack depth migration (PSDM) image that showed significant improvement over the PSDM images derived solely from seismic data (Weber *et al.* 2000).

Modern instruments based on the old concept of measuring directly the gradients of the gravity field can record minute changes in the Earth's gravity field and may hold the potential to resolve subsurface structures that seismic methods have difficulty to image (Smit *et al.* 2005). Full Tensor Gradiometry (FTG), or high precision, high-resolution marine gravity gradiometry, is a multiple accelerometer system that records all 9 components or tensors of the gravity field. The result is an increased signal bandwidth that contains the full spectrum and allows identification and mapping of subtle density contrasts that arise from complex geological features (Murphy *et al.* 2002).

Conventional gravimeters usually determine only the vertical component U_z of the three-component gravity acceleration vector at each measurement point. Gradiometers, in contrast, measure first-order changes in the gravity field, for example by measuring the difference field between two accelerometers placed closely together. These first-order changes form a nine-component tensor, U_{ij}. Newton's theory of gravity implies, however, that only five of the nine components are independent and four are redundant. U_{xx} represents the gradient in the x direction of the x component of the gravity (U_x). U_{yy} represents the gradient in the y direction of the y component of the gravity (U_y). U_{yz} represents the gradient in the y direction of the vertical component of the gravity (U_z). U_{zz} represents the vertical gradient of the vertical component of the gravity (U_z), and so forth. The measured gravity gradients thus provide a more detailed picture of the subsurface by reflecting the edges, shape, and approximate depth of dominant mass anomalies (Huston *et al.* 1999, Smit *et al.* 2005).

Although fundamentally gravity gradient data contain no more information than conventional gravity data, both being governed by a single scalar potential satisfying Poisson's equation, they are of great interest from a practical point of view. Firstly, the horizontal resolution is about an order of magnitude better because of the absence of linear acceleration noise (the so-called common mode) inherent to gravity measurements. This has a further practical consequence in that acquisition may be done at a coarser grid and under rougher condition leading to reduced acquisition time. Secondly, gradients provide additional information in practice. Although the gradient field falls off with distance as r^{-3} as opposed to r^{-2} for gravity and hence is more sensitive to structures (anomalies) at shallow depth, this is actually less of a problem than is seems. The better signal to noise ratio at shorter wavelengths has shown to provide tighter constraints on overburden structure. This is often critical to achieve better subsurface definition at deeper targets. Furthermore, the sensitivity of gradients to the geometrical structure of the anomaly is theoretically about 30% better than that of gravity vectors (Smit *et al.* 2005).

Gravity gradiometer data have been fully integrated in the cycle of iterative PSDM model, updating to arrive at a high-fidelity subsurface model in complex geological settings where seismic data is of poor quality. Upon integrating FTG data it has been shown that significantly improved seismic imaging can be achieved near salt overhangs (sub-salt) as well as below hard layers (Smit *et al.* 2005).

FTG data were acquired in the Faroe-Shetland Basin in 1999 for the purpose of resolving basalt complexity/characterisation and imaging sub-basalt geology. The results demonstrated FTG's ability to image basalt and the underlying geology. FTG's identification of density contrasts on both the regional and localised scale make it a useful independent constraint for other geophysical methods deployed in the Faroe-Shetland area, i.e. seismic (long offset, PSDM exercises), magnetic, MT data etc. (Murphy *et al.* 2002).

3.3 EM methods

One consideration that makes electromagnetic techniques attractive as a prospecting tool is that sequences of basalt flows, salt or carbonate layers, which are commonly distressingly opaque to seismic waves, have high electrical resistivities typically in the range 100–1000 Ωm. This is in marked contrast to the resistivities of the surrounding sedimentary sequences, which are typically less than 10 Ωm. These high-resistivity layers can act as electromagnetically transparent window to the underlying sedimentary structure in electromagnetic surveys (MacGregor & Sinha 2000). Electromagnetic soundings are therefore a valuable compliment to seismic surveys in such areas, providing information which may be interpreted independently or which may be used to constrain parameters in the interpretation of seismic data (Jegen *et al.* 2002).

The controlled source electromagnetic (CSEM) method can be used to provide valuable information on the structure and properties of the subsurface in technically demanding environments (Chave *et al.* 1991, Eidesmo *et al.* 2002). The CSEM method uses a horizontal electric dipole source with a dipole moment of about 104 Am, to transmit a discrete frequency electromagnetic signal to an array of sea-bottom receivers which record two orthogonal components of the horizontal electric field at the seafloor. During a typical survey, the source is towed at a height of about 50 m from the sea bottom, within an array of receiving instruments. By studying the variation in the separation and geometry, and the frequency of the signal, the resistivity structure of the underlying crust can be determined. Frequencies in the range of 0.25–40 Hz are transmitted in a typical survey. Depths of investigation up to 30 km have been achieved in the past, although the technique is most effective for probing rather shallower (0–5 km depth) structure (MacGregor & Sinha 2000).

Model studies suggest that CSEM data which are well within the limits of current technology can be used to detect sediments beneath 2–3 km of basalt, and provide useful constraints on their geometry and properties. The base-basalt boundary can be located to within about 10% of its depth, and the base-basalt/sediment boundary topography resolved (MacGregor & Sinha 2000).

The CSEM technique is particularly powerful if combined with the results of other geophysical surveys. For example inclusion of the upper-basalt boundary determined from seismic studies, can improve resolution of deeper structure observed in the CSEM data. Resistivity values from well-logs can also be used to constrain the CSEM interpretation and hence improve the resolution achieved (MacGregor & Sinha 2002).

The use of a marine CSEM method is technologically challenging, and the method favours the more resistive hard-rock sea floor of the deep ocean over the conductive sediments of petroleum targets on the continental shelf. Modelling a 3D source field also presents a greater difficulty than modelling the magnetotelluric plane-wave source (Constable *et al.* 1998).

The magnetotelluric (MT) method has been used to map sedimentary structure as an aid to petroleum exploration for several decades. The method uses natural magnetic field variations as the energy source. These naturally occurring waves induce electric currents in the subsurface, the strength of which is proportional to the electrical conductivity. The essence of the method is the computation of electromagnetic earth impedance from measurements of orthogonal horizontal magnetic and electric fields at the surface.

Estimates of impedance magnitude (transformed to an apparent resistivity) and phase at various frequencies allow investigation of electrical conductivity as a function of depth. Impedance measured at several locations allows investigation of conductivity as a function of horizontal position (Constable *et al.* 1998, Jegen *et al.* 2002).

In practice, the applicability of MT spans the range from stand-alone techniques for resolving gross structures to sophisticated joint applications where structure derived from seismic is essential for fixing some the parameters in the electrical model of the subsurface. The effective resolution of MT depends entirely on the constraints that can be imposed on the interpretation by other data (Hoversten *et al.* 1998).

Chapter 4

The nature and evolution of the mid-Norwegian margin with emphasis on the Møre margin: a review

The mid-Norwegian margin is part of the NE Atlantic margin (Figure 4.1) and the North Atlantic Igneous Province (NAIP), one of the bigger Large Igneous Provinces (LIPs) in the world (White & McKenzie 1989, Eldholm & Grue 1994, Saunders *et al.* 1997, Eldholm & Coffin 2000, Holbrook *et al.* 2001). The NAIP was formed by transient, voluminous igneous activity during continental break-up between Greenland and Eurasia (Eldholm *et al.* 1989). Norway's Atlantic margin is a classic example of a passive margin that finally went from rifting to drifting in the early Tertiary (Mosar 2003).

The mid-Norwegian margin is divided into two rift segments the Vøring margin in the north and the Møre margin in the south, offset by a transform margin. The two segments have some similar structural characteristics, such as a marginal high, an escarpment, and wide and thick Cretaceous basins. The main differences between the two margins are the presence of the ~150 km wide Trøndelag Platform SE of the Vøring Basin, the normal fault system affecting the NW Vøring Basin, and the Tertiary domes and arches in the Vøring Basin. Both margins contain severly thinned continental crust, anomalously thick oceanic crust, and voluminous lower crustal bodies (LCB) (Mutter *et al.* 1982, Fernàndez *et al.* 2005, Breivik *et al.* 2006).

4.1 Stratigraphic settings

From wells and seismic surveys, a total of nine regional unconformities have been identified in the stratigraphy of the Møre and Vøring margins (Brekke 2000). The three oldest unconformities may be identified only in the platform areas: these are of late Early Permian, Mid-Triassic and late Mid-Jurassic age. Dating of these unconformities is based on exploration well data and analogies with East Greenland (Surlyk *et al.* 1984). The six younger regional unconformities in the stratigraphy are identified in both the basin and platform-terrace areas: these are of base Cretaceous, top Cenomanian, base Tertiary, Upper Eocene–Lower Oligocene, Middle Miocene and intra Upper Pliocene positions in the sequence (Brekke 2000).

The base of the Cretaceous sequence in the central Vøring and Møre basins lies at depths between 9000 and 13 000 m (Brekke 2000). However, there is yet no consensus

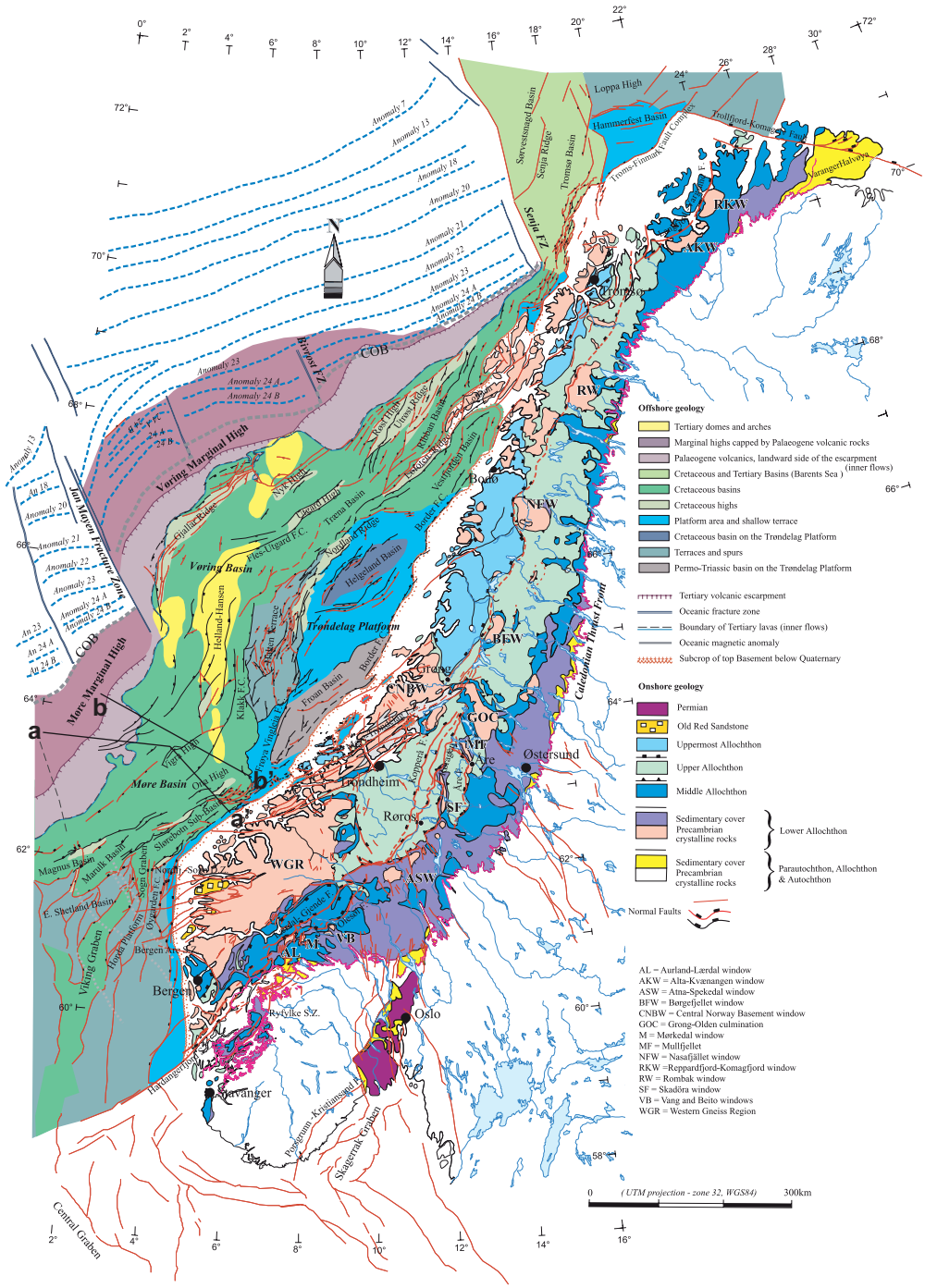

Figure 4.1. Tectonostratigraphic map of the Atlantic Scandinavian passi margin and nomenclature of the mid-Norwegian margin (modified from Mosar *et al.* 2002). Profiles a-a' and b-b' are shown in figures 4.2 and 4.3, respectively.

about the base Cretaceous level in the central and western Møre and Vøring basins (cf. Ren *et al.* 1998). In fact, Vøring Basin models vary by several kilometres in depth. Thus, large uncertainties may exist in pre-Cretaceous sediment thickness estimates and in the depth to crystalline basement, which is often inferred from the seismic velocity-depth distribution (Eldholm & Mutter 1986, Ólafsson *et al.* 1992, Mjelde *et al.* 1998, Eldholm *et al.* 2002), or magnetic depth estimates (Åm 1970, Skilbrei *et al.* 2002, Skilbrei & Olesen 2005).

4.2 Tectonic setting

The overall tectonic framework of the mid-Norwegian margin (Figure 4.1) consists of a central area of NE-SW trending deep Cretaceous basins, the Vøring and Møre Basins, flanked by palaeo-highs and -platforms and the elevated mainland. The eastern flank of the Vøring margin is dominated by the Trøndelag Platform which in turn, is flanked to the east by the eroded mainland. The Møre margin is on the other hand immediately flanked by the mainland to the east. The platforms to the west are the Møre and Vøring Marginal Highs and are characterized by thick, Early Eocene basalt flows overlying an unknown substrate. The boundary between the marginal highs and the basin area is formed by the Faroe-Shetland Escarpment to the south and the Vøring Escarpment to the north (Blystad *et al.* 1995, Brekke 2000).

To the north, the main basin area is bounded by the NW-SE trending Bivrost Lineament, which separates the wide and deep Vøring Basin from the narrow and tectonically uplifted continental margin around the Lofoten Ridge. To the south, the southeastern boundary of the Møre Basin is located where the NE-SW trending Møre-Trøndelag Fault Complex truncates the N-S and NNE-SSW trends of the northern North Sea. To the southwest, the Møre Basin borders upon the Faroe-Shetland Basin along the NW-SE trending Erlend Platform. Apart from the main NE-SW structural grain, the continental margin is subdivided by a NW-SE trending lineament, the Jan Mayen Lineament that continues into the oceanic crust as the Jan Mayen Fracture Zone (Brekke 2000).

Commonly the onshore-offshore transition has been considered the transition from a domain of mountain building processes to one of rift-related process. Mosar (2003) demonstrated that a large part of the onshore mountain belt is part of the extended continental crust that forms the passive margin of the North Atlantic. The position of the rift flank is then given by the locus of its associated innermost boundary fault system (IBF).

4.2.1 Møre Basin

The Møre Basin is defined at the base of the Cretaceous and by a greatly expanded Cretaceous sequence (Blystad *et al.* 1995). In map view, the Cretaceous Møre Basin (Rønnevik *et al.* 1975, Gabrielsen *et al.* 1984, Hamar & Hjelle 1984, Blystad *et al.* 1995) is an elongated, wedge-shaped feature, the axis of which strikes NE-SW (Figure 4.1). In its axial parts Cretaceous and younger strata exceed 5000 m in thickness (Grunnaleite & Gabrielsen 1995).

To the southeast and east of the Møre Basin are the Møre-Trøndelag and Klakk Fault Complexes (Blystad *et al.* 1995). The northern border to the basin is diffuse, but it is separated from the Vøring Basin at the Jan Mayen Lineament, which lies in the projection of the Jan Mayen Fracture Zone. To the west the Møre Basin terminates against the Møre

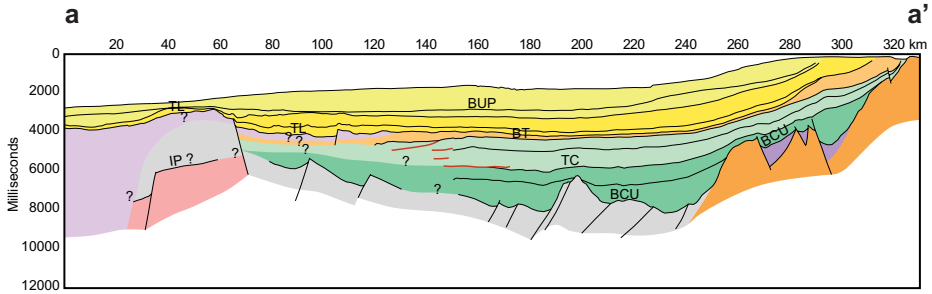

Figure 4.2. Geoseismic section from Blystad *et al.* (1995). See Figure 4.1 for location of profile (a-a'). BUP=Base Upper Pliocene, BT=Base Tertiary, TC=Top Cenomanian, BCU=Base Cretaceous Unconformity, IP=Intra Permian, TL=Top lava.

Marginal High, the oceanward margin of which corresponds to the Faroe-Shetland Escarpment. To the south the Jurassic-Cretaceous basins, including the Sogn Graben and the northernmost Viking Graben, limit the Møre Basin. This border is diffuse and Hamar & Hjelle (1984) included the Sogn Graben within the Møre Basin domain. In the formal definitions the Marulk and Magnus Basins border the southern margin of the Møre Basin and the northern termination of the Tampen Spur defines the southern limit of the basin (Blystad *et al.* 1995). The most prominent internal features of the Møre Basin is the Vigra High (Hamar & Hjelle 1984).

Blystad *et al.* (1995) and Brekke (2000) describe the basin with an overall NE-SW trend which reflects the structure of the unconformity at the base of the Cretaceous. According to these authors, the Cretaceous sediments onlap this unconformity along the western and eastern basin margins, indicating that the Møre Basin was a symmetrical feature mainly formed by downwarping of its flanks on which the early faults show polarity away from the basin centre (Figure 4.2). Conversely, Osmundsen *et al.* (2002) followed by Osmundsen & Ebbing (2008) interpret the deep basin structure as dominated by arrays of rotated fault blocks separated by NW-dipping faults (Figure 4.3).

The depth of the deepest sedimentary basins on the mid-Norwegian margin is largely unknown due to poor seismic imaging below the base of the Cretaceous. Potential field data (gravity and magnetics) have been used to estimate depth to top crystalline basement in the Møre Basin. The basement depths in the basin are reported to exceed 14 km based on magnetic inversions (Skilbrei *et al.* 1995, Skilbrei *et al.* 2002, Skilbrei & Olesen 2005). From density forward modelling studies the basin depth is estimated 12–15 km (Skilbrei *et al.* 1995, Ebbing *et al.* 2006, Osmundsen & Ebbing 2008, Ebbing *et al.* 2009).

Several authors have suggested that the Møre Basin started to open as an ocean in the Cretaceous (Bott 1975, Roberts *et al.* 1981). This interpretation was not supported by

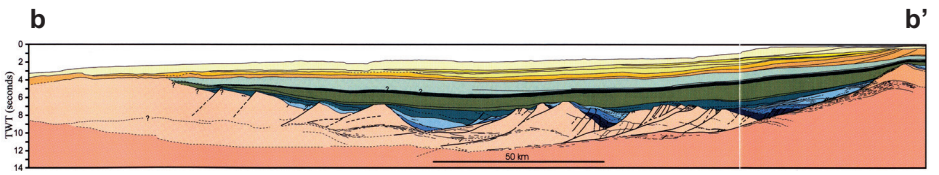

Figure 4.3. Geoseismic section from Osmundsen *et al.* (2002). See Figure 4.1 for location of profile (b-b').

Eldholm *et al.* (1984). However, Lundin & Rundhovde (1993) later proposed that nearly successful rift took place in the basin.

A NW-oriented refraction profile across the Møre margin indicates that only a few km of crust remains in the central part of the basin (Ólafsson *et al.* 1992). The profile crosses series of NE-trending positive magnetic anomalies (trough to peak anomalies of approx. 450 nT) in the central Møre Basin, the pronounced crustal thinning coincides with the magnetic anomalies. These anomalies have been interpreted as seamounts (Lundin & Rundhovde 1993), by analogy with characteristics of such features in the northern Red Sea (Cochran & Martinez 1988). If so, their presence implies a nearly successful rift event (Lundin & Doré 1997).

The structural expression of the anomalies cannot be imaged well in the Møre Basin, but the anomalies continue northwards into the southern Vøring Basin, where a large upstanding feature is observed. The feature is onlapped by ~4–5 km of Lower Cretaceous strata and is peneplaned and transgressed near the Cenomanian level. Gravity and magnetic modelling indicates a mafic or ultramafic composition. If this feature is related to the magnetic anomalies in the Møre Basin, it may be a seamount. Alternative interpretations are that the magnetic anomalies are highly magnetic basement blocks or major mafic intrusions of latest Cretaceous to Early Tertiary age. However, the bed geometry around the described feature suggests an onlap relationship and rules out the latter possibility with reasonable confidence. The NE axial trend of the anomalies, at the age of onlapping strata where observed and a Neocomian age was suggested for their formation. Evidence of Early Cretaceous magmatic activity in the region includes report of pyroclastic rocks in the North Sea (Crittenden *et al.* 1991), off mid-Norway (Dalland 1980), and on East Greenland (Lundin & Doré 1997, Doré *et al.* 1999).

Skilbrei *et al.* (2002) claim that the absence of a coinciding belt of pronounced gravity anomalies along the axis of the basin makes it unlikely that Cretaceous seamounts exist at the centre of the Møre Basin. They suggested an alternative interpretation that is a combination of high-grade basement highs, possibly with increased magnetization due to intrusions that form a 'Christmas tree' of dykes and sills.

4.2.2 Møre Marginal High

The Møre Marginal High is situated to the west of the Faroe-Shetland Escarpment and bounded to the north by the Jan Mayen Fracture Zone. To the south, the Møre Marginal High merges with the Faroe Plateau, which includes the Faroe Islands. The high comprises Tertiary sediments on top of thick early Eocene flood basalts, and, like the Vøring Marginal High, probably contains continental crust that westwards becomes increasingly more intruded, faulted, thinned and stretched (Brekke 2000).

The marginal high is widest in the south where it maps as a continuous volcanic sheet, including the Faroe Islands. The southeastern termination at the escarpment only appears to be a volcanic flow limit and build-up (Smythe *et al.* 1983). Gibb & Kanaris-Sotiriou (1988) correlated this with the Faroe Middle Series Lavas.

The substrate to the flood lavas in the continental part of the marginal high is unknown. Regional information shows that the area is likely underlain by pre-Cretaceous sedimentary rocks varying in thickness between 3 and 10 km, which infill an older, uneven basement relief (Bøen *et al.* 1984, Eldholm & Mutter 1986, Skogseid & Eldholm 1989, Planke *et al.* 1991).

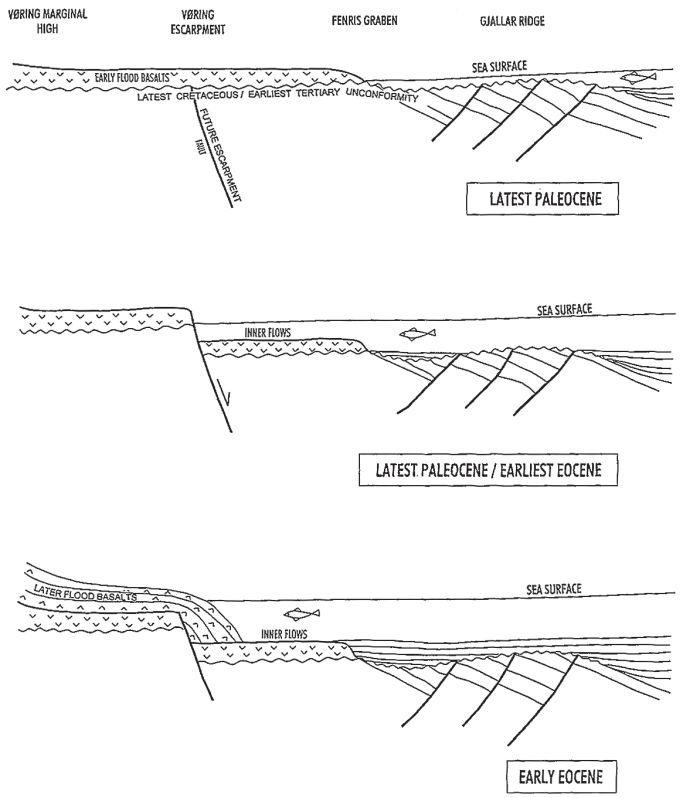

Figure 4.4. Model for the development of the Vøring Escarpment and the formation of the 'inner flows'. The same model is inferred for the Faero-Shetland Escarpment (Brekke 2000).

Hinz *et al.* (1982) demonstrated the occurrence of a high-amplitude, low-frequency reflector (the 'K reflector') at the assumed base of the volcanics, and Smythe *et al.* (1983) traced this reflector continuously beneath the marginal high to correlate it with volcanic rocks landwards of the Faroe-Shetland Escarpment. Gibb & Kanaris-Sotiriou (1988) correlated these volcanics with the Faroe Lower Series Lavas.

Planke *et al.* (1999a) identified two seaward dipping reflectors (SDR) units on a transect across the Møre margin, where the seaward one is overlaid by an internally stratified Outer High. Based on the drilling results elsewhere in the northeast Atlantic, the SDRs are interpreted as dominantly subaerially emplaced and erupted basalts, while the stratified Outer High is interpreted as consisting of shallow-marine volcaniclastics. The deeper landward-dipping reflectors are not drilled anywhere but are interpreted as feeder dikes that likely followed weakness zones such as fault planes. The dikes may originally have been emplaced as near vertical feeders but have acquired their landward dip by synconstructional margin flexuring and subsidence (Planke & Alvestad 1999).

According to Brekke (2000) the westward thinning and onlap of the Cretaceous units of the Møre Basin indicate that the Cretaceous sequence is very thin or missing beneath the lavas on the high. The Paleocene sequence in the Møre Basin seems to thicken westwards towards the Faroe-Shetland Escarpment, suggesting early fault activity along the escarpment and differential uplift and erosion of the marginal high at that time. The

fact that the early lavas flowed far eastward of the present escarpment indicates that the area was above sea level in Late Paleocene-Early Eocene time. Subsequent faulting along the escarpment probably submerged and separated the 'inner flows' from the marginal high (Figure 4.4). The present morphology of the Faroe-Shetland Escarpment seems to be mainly the result of the build-up of a volcanic front along that fault-related shoreline (cf. Smythe *et al.* 1983). However, in the northern segments it is enhanced by minor faulting in Late Eocene time (Brekke 2000).

Brekke (2000) also claims that it is possible to identify a deep-seated, faulted angular unconformity within the marginal high because of a relatively thin cover of lava in some places. As it is juxtaposed by the Cretaceous sequence of the Møre Basin in the hanging wall, it must be older than the Cretaceous sequence. In Figure 4.2 it is suggested that it may be correlated with the Upper Permian unconformity identified in the Trøndelag Platform.

Osmundsen *et al.* (2002) found no indication of a SE-throwing normal fault adjacent to the Møre escarpment and claim this may be due to the juxtaposition of the marginal high with high-seated basement rocks in the hanging wall, or, alternatively, that no such fault exists in the area. Major escarpments in the late-stage lava flows observed on seismic data represent the transition from subaerial to submarine lavas according to some authors (e.g. Andersen 1988, Naylor *et al.* 1999).

The change from the top of oceanic to continental crystalline basement is the continent-ocean boundary (COB). The continent-ocean transition (COT) is a distinct zone of steeply dipping Moho between oceanic and continental levels (Eldholm *et al.* 2002). The COB is frequently associated with, but also masked by, magmatic extrusives along the North Atlantic volcanic margin. It is located in the transition zone between the oldest magnetic anomaly and the continental crust. According to Mosar (2003), offshore Norway, this correlates to anomaly 24 and the main break-off fault which is located to the W-NW of the Møre and Vøring marginal highs (Figure 4.1). The precise position of the COB in the Vøring and Møre marginal highs remains a matter of debate and is difficult to resolve given the problems with the resolution and penetration of the seismic surveys (Mosar 2003).

Various models have been proposed for the origin of the volcanic marginal highs. One proposes rifting at the escarpment, initiating mantle convection and significant volcanic activity leading to the formation of an abnormally thick ocean layer 3 (Hinz 1987, Mutter *et al.* 1988). Other models explain the marginal high adjacent to the escarpment as representing a transitional intruded crust, with the continent-ocean boundary located just west of the termination of reflector K (Smythe *et al.* 1983, Skogseid & Eldholm 1989), while the local thickening of the crust is explained by magmatic underplating (White *et al.* 1987, Pedersen & Skogseid 1989). In addition it is not known whether Late Jurassic rifting spanned the entire region from East Greenland to mid-Norway or if two or more rift arms existed. A mid-Jurassic land bridge or central high has been postulated between East Greenland and northern Norway based on sediment provenance studies (e.g. Doré 1991).

The different models can be divided into two main categories-those that relate the construction of the volcanic complex to infilling and capping of a rifted terrain (e.g. Hinz 1981, Eldholm *et al.* 1989, Planke & Eldholm 1994) and those that are focused on the volcanics being formed during a phase of subaerial seafloor spreading (e.g. Mutter *et al.* 1982, Larsen & Saunders 1998). Drill hole data have not been able to distinguish between these end-member models, and both processes may actually form constructions imaged as SDR (Planke & Alvestad 1999). ODP sites 642 and 917 provide direct evidence that the

Landward Flows are underlain by extended continental crust (Eldholm *et al.* 1989, Larsen & Saunders 1998). The seaward continuation of the deep reflector patterns below the SDR suggest that at least the inner parts of the SDR are underlain by continental material. However, the results from Site 918 suggest that the entire crust below the Inner SDR on the Southeast Greenland margin is of igneous nature (Larsen & Saunders 1998).

ODP Site 642 on the Vøring Marginal High, which terminated almost 1 km below the top of the acoustic basement, provides key information of the composition and vertical motion history of a marginal high. The basement rocks consist of two different lava series and interbedded volcanoclastic sediments. The lower series is andesitic to dacitic in composition, emplaced by infrequent eruptions of crustal melts during the late rift stage, and interbedded sediments indicate fluvial or shallow-water deposition. The upper series has been dated radiometrically to 55 Ma, whereas the lower series is not more than one million years older (Sinton *et al.* 1998). The ~800 m thick upper lavas consist of transitional, mid-oceanic tholeiitic basalts and altered, interbedded, basaltic vitric tuffs. Subaerial and neritic environments are inferred during and after break-up, when the lavas erupted during an intense phase of explosive, subaerial basaltic volcanism (Eldholm *et al.* 2002).

After break-up, the oldest 'Icelandic'-type oceanic crust accreted above or near sea level. The intense volcanism abated in 2–3 million years, and the injection centre submerged to mid-oceanic ridge levels. The change in production volume and emplacement mode left the marginal highs trailing behind new crust accreted at the mid-oceanic ridge (Figure 4.5). As the ocean basin widened and deepened, the highs subsided at rates similar to oceanic crust, maintaining the basement relief (Eldholm *et al.* 1989). Thus, across-margin circulation barriers, induced by regional uplift along the initial plate boundary and the subsequent formation of marginal highs, were maintained also after breakup.

The elevated plate boundary region, which probably had an accentuated along plate boundary relief, was rapidly denuded. Thus, a major early Palaeogene sedimentary source region existed first in the central epicontinental sea between Greenland and Eurasia and

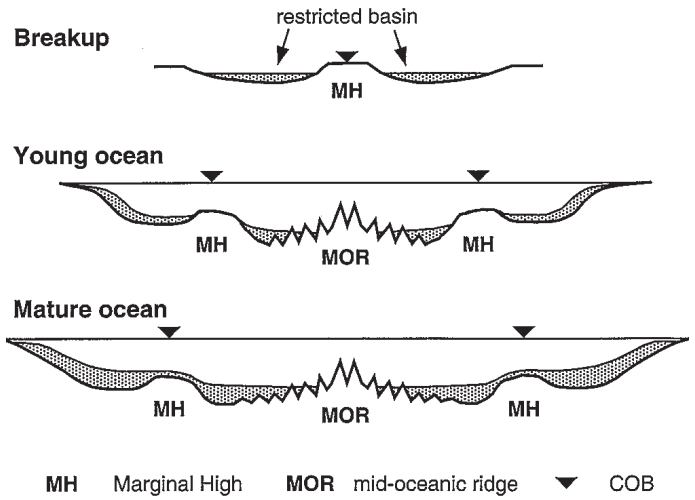

Figure 4.5. Schematic illustration of volcanic margin basin segmentation creating across-margin barriers for water mass circulation caused by late rift uplift and construction of extrusive edifices along the COB (Eldholm *et al.* 2002).

later on the young margins, dominating the sediment supply and deposition in the Møre and Vøring basins. Sediments from the east reached the marginal high in middle Eocene. Later, the relief of the outer margin was gradually smoothed and the high became sediment-covered during the middle Oligocene to early Miocene. This model is consistent with recovered basal sediments on the high derived from continental soils formed under a hot, seasonably humid, climate followed by an initially restricted marine depositional regime (Thiede *et al.* 1989).

4.2.3 Transfer systems

The transfer zones within extended continental crust are commonly spatially connected to early opening, small-offset fracture zones. Following Tsikalas *et al.* (2001) the term transfer system is used here to include both the transfer zone (lineament) and the fracture zone. The fracture zone trend may represent a different stress regime, thus it may differ from that of the transfer zone while the initial fracture zone location is governed by the older zone of weakness (Eldholm *et al.* 2002).

The Jan Mayen Fracture Zone (JMFZ) is a major offset in the Mid-Atlantic Ridge and has been active since early Tertiary continental breakup (Skogseid & Eldholm 1987). Talwani and Eldholm (1977) divide it into two segments, which are associated with strong free-air gravity anomalies. The southeastern segment has been further divided into two individual fracture zones – the East Jan Mayen Fracture Zone and the Central Jan Mayen Fracture Zone – with approximately 50 km separation (Skogseid & Eldholm 1987).

To the southeast the JMFZ terminates in a 200 km long transform margin (Berndt *et al.* 2001a). Transform margins are continent-ocean boundaries that develop due to offsets in the rift axis (Le Pichon & Hayes 1971, Scrutton 1979). They are characterized by a steep, fault-controlled continental slope commonly bordering a marginal plateau on the upper continental slope or a wide continental shelf. Frequently, transform margins are associated with a transform margin high (Reid 1989, Basile *et al.* 1993, Faleide *et al.* 1993).

Through the whole of Late Cretaceous and Tertiary time the Jan Mayen Lineament was a tectonic barrier between the tectonically very active Vøring Basin and the quiet and non-active Møre Basin, confirming the significance of this lineament (Brekke 2000).

The Vøring and Lofoten-Vesterålen margins are separated by the Bivrost transfer system. Structurally, the fracture zone marks the northern termination of the Vøring Plateau and the Vøring Marginal High, and thus also the Vøring Escarpment. The Bivrost Lineament represents a dextral shift in main structural elements which may have been rejuvenated during several tectonic episodes (Blystad *et al.* 1995).

The landward prolongation of the Gleipne Fracture Zone is described as a diffuse Late Cretaceous-Paleocene structural lineament, whereas the coeval Surt Lineament farther north marks a change in fault polarities between the Gjallar Ridge and the Hel Graben, offsetting the Gjallar Ridge and Nyk High fault complexes (Eldholm *et al.* 2002). The Surt Lineament coincides with a change in magnetic signature (Doré *et al.* 1997b) and it may be a basement-controlled feature (Brekke *et al.* 1999). Ebbing *et al.* (2006) showed that not all of the proposed crustal lineaments appear to be major tectonic boundaries in the mid-Norwegian margin. The Bivrost Lineament, which separates the Lofoten and the Vøring margins, is clearly related to changes in the crustal petrophysical parameters. The Gleipne and Surt Lineaments do not seem to be major tectonic features, because neither the interpreted profiles nor the calculations of basement thickness reveal the presence of

these lineaments (Ebbing *et al.* 2006). Furthermore, Olesen *et al.* (2007) proposed that all the small fracture zones previously proposed to exist along the Norwegian margin north of the East Jan Mayen Fractue Zone are artefacts.

Basement grain is believed to have played an important role in structural development, in that NE Atlantic rifting and opening partially exploited the Caledonian orogen. The formation of extensional zones and new ocean along the line of old orogens, is common in the geological record and is a basic constituent of the 'Wilson Cycle' (Doré *et al.* 1999). Its causes are still poorly understood, although it has been suggested by Ryan & Dewey (1997) that eclogite-facies roots of collapsed orogens, weaker than adjacent lithosphere, provide preferred sites for rifting and hence ocean formation.

While transfer zones may be formed during rifting as a means of accommodating displacement between adjacent rift segments (Morley *et al.* 1990), work on extensional terrains has shown that the position of such zones may be determined by pre-existing cross-cutting lineaments or tectonic grain (Cartwright 1992). Doré *et al.* (1997a) believe that this was the case with elements of the NW-SE transfer trend of the NE Atlantic margin. Other, lesser NW-SE transfers are more difficult to assign to a basement origin. It is, however, established that NW-SE fracture systems are prominent in the Precambrian basement on both sides of the Caledonian orogen.

Doré *et al.* (1997b) argue that many of the key lineaments observable in the extensional basins along the NE Atlantic margin can be ascribed a Caledonian or older origin. More importantly, however, they argue that the current dominance and visibility of the lineament sets is because these, out of a wide variety of basement fracture trends, were conveniently orientated to accommodate the extensional forces leading to NE Atlantic break-up. Most prominent are NE-SW shears such as the Møre-Trøndelag Fault Zone, which trend parallel to the present-day continental margin and almost precisely normal to the Cretaceous-Cenozoic extension direction.

The evidence is reasonably good that Precambrian and Caledonian lineaments striking at a low angle to the extension direction were predisposed to form major NW-SE transfer zones (Doré *et al.* 1997b). A basement origin for the N-S trends is less clear, but is suggested by some North Sea studies (e.g. Færseth *et al.* 1995). An inception of these fractures in post-Caledonian strike-slip duplexes is possible and is consistent with the field evidence along the Møre-Trøndelag Fault Zone (Doré *et al.* 1997b).

Osmundsen *et al.* (2002) interpreted long-offset seismic data on the mid-Norwegian margin. They showed that Palaeozoic phases of extension left a structural imprint that was exploited by Mesozoic rift phases. Doré *et al.* (1999) also claim that most of the offshore lineaments on the mid-Norwegian margin can probably be explained in terms of Permian or later extension.

The Jan Mayen Lineament and the Bivrost Lineament probably reflect an old structural grain in the crystalline basement according to Brekke (2000). This is substantiated by the NW-SE strike of the fjords and major fractures where the lineaments meet the mainland.

Complete continental separation along the Jan Mayen Fracture Zone (Skogseid & Eldholm 1987) was achieved in the early middle Eocene, ~48 Ma. Its landward prolongation, the Jan Mayen Lineament (Blystad *et al.* 1995), offsets large, positive gravity and magnetic anomaly belts more than 200 km in a left-lateral sense probably reflecting Palaeozoic or older crustal lineaments (Talwani & Eldholm 1972). Similarly, the Mesozoic basin axes are shifted westward and Torske & Prestvik (1991) suggested that the lineament represents a

transfer zone separating opposing, pre-opening, simple-shear detachment systems in the Møre and Vøring basins.

4.3 Magmatic setting

Passive, rifted margins are commonly classified as volcanic margins if there is evidence of excessive, transient magmatic activity during final continental breakup and initial sea floor spreading (Eldholm *et al.* 2002). The main evidence are (1) prominent wedges of SDR, near the continent-ocean transition and (2) high P wave velocity bodies, V_p>7 km/s, in the lower crust (Eldholm *et al.* 1995, Planke *et al.* 2000).

Breakup volcanism is common, although its intensity and character may vary significantly along a margin and between margins. Typical volcanic and nonvolcanic rifted margins, such as the northeast Atlantic and Iberia margins, respectively, appear to be end-member cases (Eldholm *et al.* 1995). On transition-type volcanic margins, such as the Western Australia margin, the characteristic SDR are regionally absent or poorly developed (Symonds *et al.* 1998).

Onshore and offshore studies combined with scientific drilling show that the rifted volcanic margins offshore Norway belong to the North Atlantic Large Igneous Province (cf. Eldholm *et al.* 1989, White & McKenzie 1989). The magmatism was initiated at about 62–60 Ma by sporadic, and small volume melting of variable composition (Saunders *et al.* 1997), followed by an intense, break-up phase producing voluminous mafic melts lasting 1–1.5 million years, gradually changing into waning, small-volume melting of variable compositions. About three million years after break-up the system returned to relatively normal mid-oceanic ridge production rates and the injection centre had subsided to the NE Atlantic mid-oceanic ridge depth (Eldholm *et al.* 2002).

Igneous rocks emplaced during the breakup event comprise three main units: (1) voluminous extrusive complexes, including the SDRs, (2) intrusives, and (3) thick initial oceanic/transitional crust, often with a high-velocity lower crustal body (LCB). Between individual margin segments, there is variability in the extent and volume of these magmatic features (Meyer *et al.* 2007).

4.3.1 Extrusive volcanics

Planke *et al.* (1999a) observed several distinct volcanic seismic facies units on volcanic margins (Figure 4.6). The Inner SDR unit is perhaps the most spectacular feature in the seismic profiles, and its presence is commonly used to classify margins as volcanic. The Outer High unit appears near the seaward termination of the Inner SDR. Farther seaward, weak or no intrabasement reflectivity is observed. The landward flow unit pinches out toward the continent but merges with the lava delta and inner flows unit on the European north-eastern Atlantic margin.

The nature of the intra-basement reflectivity on volcanic rifted margins is largely unconstrained (Planke & Eldholm 1994, Barton & White 1997, Smallwood *et al.* 1998). Currently, only the landward flows unit has been sampled by several deep drill holes. Only a few, very shallow holes have been drilled into the SDR, and only one hole has recovered material from the Outer High. None of the other seismic facies units have been sampled. Moreover, none of the northeast Atlantic drill holes have penetrated any well-defined

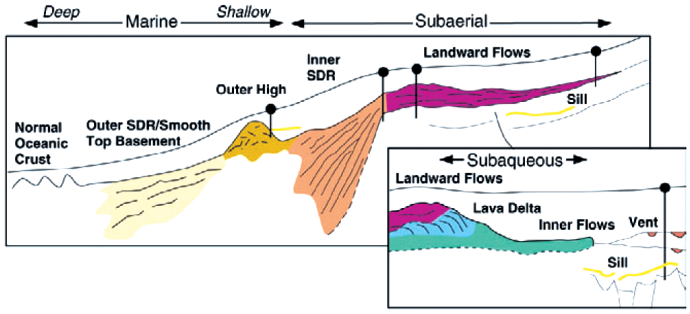

Figure 4.6. Schematic volcanic margin transect illustrating seismic facies units associated with extrusive volcanic deposits (Planke *et al.* 1999a). Additional units commonly observed on the European Northeast Atlantic margins shown by inset. Proposed emplacement environment (arrows) and wells (ball-and-line) schematically located.

intrabasalt reflectors, with the exception of reflector K, representing the lower boundary of the SDR on the Vøring margin (Planke & Alvestad 1999).

In spite of lack of direct observations the seismic facies units have been interpreted in terms of volcanic eruption, emplacement, and sedimentation history (Alvestad 1997, Planke & Alvestad 1999, Planke *et al.* 1999a). Landward Flows are penetrated at the Ocean drilling program (ODP) sites 917 and 642, where they represent subaerially erupted and emplaced volcanics. The lava delta unit has not been penetrated by any drill holes but is interpreted to represent a volcaniclastic lava delta formed as subaerially erupted lavas reached a paleo-shoreline (Planke & Alvestad 1999). This interpretation is compatible with the hypothesis that the Faroe-Shetland Escarpment is a coastal feature (Smythe *et al.* 1983). Hydroclastite lava delta constructions are found exposed, for example, on Nuussuaq Island off western Greenland (Pedersen *et al.* 1996), and are well developed along the coastline of Hawaii (Moore *et al.* 1973). The inner flows are interpreted as dominantly hydroclastite deposits consisting of a mixture of massive and fragmented basalts. Together, the three facies units form a coarse-grained Gilbert-type clastic delta, where the Landward Flows, Lava Delta, and Inner Flows represent the top- and bottom-set facies of the delta (Planke & Alvestad 1999).

Local, restricted rift basins are formed as the extension accelerates toward breakup, and probably also by synconstructional faulting just after breakup. The Inner SDR are constructed by the in-filling of such basins, and accommodation space is provided by a combination of tectonic forces and loading by the thick basalt pile (Pálmason 1980). Initial flood basalt volcanism commonly forms shallow intrusions, peperites, or hydrovolcanic deposits generated by the interaction of magma and wet sediment. Continued flood basalt volcanism leads to effusive, subaerial volcanism where lavas in-fill and pond in topographic lows and basins. If lava reaches the shoreline, it will fragment in contact with water, constructing a fore-set bedded lava delta consisting of hydroclastites and locally massive flows. The eruption character changes dramatically when the volcanic fissures submerge to shallow marine conditions. In this case, extensive fragmentation and formation of pyroclasitics occurs (Surtseyan eruptions). The lavas build upward, occasionally to above the sea level, forming the Outer High units. Additonally, tuffs will spread over large areas. Examples are the primary and resedimented smectite-rich clay deposits recognized in

the North Sea (e.g., Balder Formation) and elsewhere in northwest Europe. Subsequent subsidence of the injection center to water depths >100–200 m leads to decreased magma fragmentation, and the lavas are emplaced as deep marine flood or pillow basalts (Planke & Alvestad 1999, Planke *et al.* 1999a).

4.3.2 Intrusives

Based on the work of Mudge (1968), Lister & Kerr (1991), and Walker (1993), sills are defined as tabular intrusive bodies of magmatic origin, that are predominantly layer parallel, and thin compared to their lateral extent. The Vøring and Møre basins are classical examples of intruded volcanic basins located on a rifted volcanic margin (e.g. Skogseid *et al.* 1992a, Skogly 1998, Berndt *et al.* 2000, Brekke 2000, Gernigon *et al.* 2003, Planke *et al.* 2005). The volcanic activity in these basins was associated with Late Paleocene rifting and continental breakup in the NE Atlantic. Similar intrusive basin provinces are located along the entire European NE Atlantic margin (e.g. Gibb & Kanaris-Sotiriou 1988, Bell & Butcher 2002, Smallwood & Maresh 2002) and onshore in central-east Greenland (e.g. Larsen & Marcussen 1992, Price *et al.* 1997).

Skogseid *et al.* (1992a) noted a first-order spatial correspondence of Late Cretaceous–Paleocene rifting and magmatic intrusions in the Vøring and Møre basins. In the Vøring Basin most sills appear to be intruded in Cretaceous sediments (Berndt *et al.* 2000). Igneous sills of Palaeocene–earliest Eocene age are found within the Cretaceous and lowermost Palaeocene basin-fill of the Møre Basin (Roberts *et al.* 1999, Brekke 2000).

Planke *et al.* (2005) mapped an extensive Palaeogene sill complex with an extent of at least 80 000 km^2 in the Vøring and Møre basins. The sheet intrusions are saucer-shaped in undeformed basin segments and the size of the saucers becomes larger with increasing emplacement depth. More varied intrusion geometries are found in structured basin segments, where the melt was emplaced along weakness zones such as fault planes and along stratigraphic layers.

Physical properties and compositional data on the intrusives in the Vøring Basin have only been sampled in NPD well 6607/5-2 on the Utgard High. The well penetrated a 2 m thick microgabbroic sill within late Campanian claystones at a depth of 3419 m below seafloor. Another 91 m thick unit, intruded into altered claystones of the Campanian Shetland Group, was reached at 3792 m below seafloor. The well terminated 50 m into a third sill below Turonian sandstones. Cuttings of the two lower units show microgabbroic mafic rocks with only little secondary alteration, millimeter grain sizes, and a tholeiitic composition (Berndt *et al.* 2000). The thick, second sill apears as a distinct anomaly in the downhole sonic and density logs. The mean sill velocity is 7.0 km/s. On either side of the sill is an approximately 80 m thick transition zone where the velocity increases gently form 3 to 4 km/s toward the sill. This velocity increase is probably caused by contact metamorphism as described by Fowler & Nisbet (1982). Similarly, there is a density contrast of 500 kg/m^3 between the sediments and the 2750 kg/m^3 mean sill density, but no transition zone is recorded by the density log. The sonic velocities at well 6607/5-2 are similar to OBS measurements (Berndt *et al.* 2000).

Based on both field analogue and seismic data Svensen *et al.* (2004) suggest that the major part of the sill complexes were formed in a short time span. The seismic interpretation reveals that the intrusive volcanism mainly occurred before the main extrusive events that initiated in Early Eocene. Individual sills may be up to hundreds of kilometres long and

must have formed very rapidly (tens of years) to avoid solidification. Seismic observations indicate that a small number of large-volume intrusive episodes have formed the entire intrusive complex of the Vøring and Møre basins.

4.3.3 Magmatic underplate

The igneous activity associated with Early Tertiary break-up is generally believed to result from migration of plume-generated mantle melts into the thinned axis of incipient opening (e.g. Eldholm *et al.* 1989, Skogseid *et al.* 1992a). Eldholm *et al.* (2002) describe the influence of a plume as subsidence and sediment deposition within the growing rift that continued into Paleocene time when the Iceland Plume approached the base of the lithosphere (Skogseid *et al.* 1992a, Saunders *et al.* 1997) inducing dynamic and thermal uplift of the rift basins. When the plume head material preferentially migrated into the pre-existing region of thinned lithosphere, decompressional partial melting accelerated, and culminated with massive subaerial volcanism during breakup and early sea floor spreading. The change in thermal regime in the continental lithosphere caused by the approaching and impinging plume may have affected the rheology of the continental crust (Buck *et al.* 1988, Pedersen & Skogseid 1989), thus contributing to a change from brittle to more ductile extensional deformation from Campanian to Paleocene times.

A lower crustal body (LCB) characterized by high seismic velocity, 7.1–7.7 km/s (Eldholm & Grue 1994, Mjelde *et al.* 1997, Mjelde *et al.* 1998) is characteristic for the outer parts of volcanic margins (Eldholm *et al.* 1989, White & McKenzie 1989, Eldholm *et al.* 2002).

A widely accepted interpretation is that the LCB represents magmatic underplating, formed by ponded magmatic material trapped beneath the Moho, or magmatic sills injected into the lower crust (Furlong & Fountain 1986, White & McKenzie 1989). Paleocene uplift of provenance areas adjacent to the Atlantic margin has been attributed to magmatic underplating associated with the Iceland Plume (White 1988, White & McKenzie 1989, Milton *et al.* 1990).Suspicion regarding the magmatic nature of the LCB has been emerging however (Ebbing *et al.* 2006, Gernigon *et al.* 2006). Gernigon *et al.* (2006) propose that the LCB-characteristics may partly be explained by the presence of pre-existing high-velocity rocks, such as eclogites or migmatites. Ebbing *et al.* (2006) proposed that the LCB could be remnants of the Caledonian root. A non-magmatic interpretation of the LCB will lower the estimated NAIP melt volumes (Eldholm & Grue 1994) significantly. This, in turn, would affect most conventional models for NAIP formation that generally link melt volumes to potential mantle temperature (White & McKenzie 1989).

According to Doré *et al.* (1999) a key question is why underplating should have caused uplift of the cratonic areas (e.g. the Scottish Highlands) while the Faroe-Shetland Basin, positioned between Scotland and the impacting plumehead, underwent anomalously rapid subsidence (Hall & White 1994). The simplest explanation involves extension-related subsidence in the Faroe-Shetland Basin which has been documented by Dean *et al.* (1999). An explanation is still required, however, as to how buoyant plume material could bypass this area of crustal thinning to cause significant magmatic underplating of the adjacent craton (Doré *et al.* 1999).

Only high-velocity lower crustal bodies beneath thinned continental crust satisfy the criteria of Herzberg *et al.* (1983) and Furlong & Fountain (1986) in which underplated bodies are ponded mafic melts trapped by the density filter at the base of the crust.

Alternatively, this body has been considered as pervasively intruded lower crust similar to the Ivrea-Verbano zone in northern Italy, where field observations show a complex system of mafic intrusions within the lower crustal metasediments (Rutter *et al.* 1993, Handy & Streit 1999). Berndt *et al.* (2000) investigated the Hel Graben sill complex that has seimic velocities similar to those which characterize the lower crust on volcanic margins and concluded that seismic refraction arrivals do not allow to distinguish whether the 7+ km/s velocity of the LCB represents relatively homogeneous, ponded, and underplated mafic crust or pervasively intruded crust. White *et al.* (2008) found that near the Faroe Islands the lower crust is intruded by sills rather than underplated by 100 per cent melt. The lower crustal intrusions are focused mainly into a narrow zone of ~50 km wide on the continent–ocean transition.

The LCB is well developed on the Møre and Vøring segments where it forms the lower part of the thickened crust beneath the marginal highs, continuing east below the crust that was extended and thinned prior to break-up (Mutter *et al.* 1988, Planke *et al.* 1991, Ólafsson *et al.* 1992, Skogseid *et al.* 1992b, Mjelde *et al.* 1997, Mjelde *et al.* 1998, Eldholm *et al.* 2002). According to Fernàndez *et al.* (2004, 2005) the maximum thickness of LCB beneath the Møre Marginal High is about 7–8 km, whereas in the Vøring Marginal High it reaches values of up to 15–16 km. Mjelde *et al.* (2009a, 2009b) suggest a maximum thickness of ~9 km for the Vøring and ~5 for the Møre margin.

The apparently good fit between the interpreted lower crustal high velocity bodies, the gravity anomalies, and the magnetic anomalies suggest that these bodies are real, and not artefacts resulting from different data quality, data collection methods or poor interpretation (Planke *et al.* 1991).

4.4 Rifting and margin formation

Since the collapse of the Caledonian orogen (~400 Ma) to early Eocene break-up (~53 Ma) several rifting episodes have been documented on the mid-Norwegian margin. Regional rift episodes off Norway have been interpreted as being of Late Carboniferous to Permian times, and of Triassic to Jurassic age (Bukovics *et al.* 1984, Blystad *et al.* 1995). Moreover, the definition and the timing of the late Middle Jurassic to Early Cretaceous tectonism are under discussion. Late Middle Jurassic to earliest Cretaceous rifting is recognized by most authors (Blystad *et al.* 1995, Brekke *et al.* 1999, Brekke 2000), but there is less consensus on how far into Early Cretaceous time the extension continued. For example, Lundin & Doré (1997) and Doré *et al.* (1999) divide this episode into separate Late Jurassic and Early Cretaceous tectonic phases, suggesting that the Vøring Basin was mainly formed by subsidence following the latter phase. In the following sections we follow Doré *et al.* (1999) who argue that episodes of Permo-Triassic, Late Jurassic, Early Cretaceous, 'middle' Cretaceous and latest Cretaceous–Early Eocene age can be distinguished from one another in space and time.

4.4.1 Caledonian orogenic climax and extensional collapse

In Late Silurian times Baltica collided with Laurentia and caused the Scandian phase of the Caledonian Orogeny. Wholescale westward subduction of Baltic continental crust beneath Laurentia gave rise to crustal thickening in the Caledonian Belt, examplified by the

preserved high-pressure eclogite-bearing terranes in western Norway (Torsvik *et al.* 2002). The collisional climax was followed by a generalized collapse of the orogen (e.g. Andersen & Jamtveit 1990, Osmundsen & Andersen 1994). The development of intramontane detrital Devonian basins followed the orogenic climax and is linked to the collapse of the mountain belt that occurred in the Devonian to Early Carboniferous. The rifting occurred from then on in a succession of phases (Mosar 2003).

Extensional movements began in immediate post-Caledonian (Devonian) times with post orogenic collapse, back-sliding of the nappe pile, and the development of molasse basins in Norway (Séranne & Séguret 1987). Intra-mountain basins formed as Scandian compression gave way to collapse and extension and initiated the formation of a series of extensional supra-detachment basins which were filled with thick successions of continental deposits (Ziegler 1988, Coward 1993, Hartz & Andersen 1995). Rift structures between Greenland and Norway followed the Caledonian and possibly, pre-Caledonian structural grain, northward to the SW Barents Shelf and connected to the Arctic rift system (Skogseid *et al.* 2000, Torsvik *et al.* 2002). However, sediment packages associated with these movements are poorly resolved seismically, mainly because of the overprint by younger events (Doré *et al.* 1999).

4.4.2 Permo-Triassic extension

Permo-Triassic extension is generally poorly dated, but is best constrained onshore in East Greenland where a major phase of normal faulting culminated in the Middle Permian and further block faulting took place in the Early Triassic (Surlyk 1990). Early Permian magmatism associated with the rifting has been described from East Greenland (Surlyk 1990) and from the West Shetland Basins–southwestern Møre margin area (Hitchen *et al.* 1995).

The Permian and Triassic periods saw a grouping together of most of the world's continents as the supercontinent Pangea was formed. The supercontinent appears to have been inherently unstable, with the result that assembly and the beginnings of continental rfiting were simultaneous. In the region of the future Atlantic margin, Permo-Triassic basins followed the Caledonian fold belt. Usually, Permo-Triassic extension is characterized by half-grabens, commonly containing significant thicknesses of continental sediments. Large portions of the northwest European Atlantic margin are flanked by such basins, generally with a Caledonide trend and lying inboard of the younger depocenters. The sedimentary successions in the basins are up to 8 km thick (e.g. Evans 1997).

Offshore mid-Norway the Froan Basin is one of several NE-trending half-grabens arranged in a left-stepping, en echelon pattern. The significant thicknesses of the Permo-Triassic on the Nordland Ridge and Halten Terrace, and evidence of Permo-Triassic faulting in this area, suggests that fragments of Permo-Triassic basins are likely to be present beneath the Cretaceous-Cenozoic basins to the west (Doré *et al.* 1999). Marine influences periodically penetrated the basin network from the northern (Boreal) and southeastern (Tethyan) oceans bordering Pangea, but never succeeded in breaching the supercontinent (Doré 1992).

4.4.3 Jurassic extensional events

The Triassic-Jurassic transition in the North Atlantic region saw a change to rift tectonics associated with incipient ocean floor spreading in the Tethys to the southeast and in the proto-Central Atlantic to the southwest. Marine flooding of the old Permo-Triasssic rift

basins took place as rifting breached Pangea (Doré 1992). Some extensional fault activity of this age is documented offshore mid-Norway (Blystad *et al.* 1995). In comparison to later Jurassic extension, however, this activity was limited (Doré *et al.* 1999).

The most intense phase of rifting occurred in latest Middle to Late Jurassic times. An approximately E-W least principal stress direction was regionally prevalent, as exemplified by the consistent close-to-northerly trend of Jurassic rift basins in North Atlantic region. The regional picture of Jurassic basin geometry is of a series of parallel or en echelon rifts, strongly overstepped by later (Cretaceous-Cenozoic) depocenters. A N-S dogleg in the south-western Vøring Basin may reflect Jurassic basin geometry underlying the thick Cretaceous-Tertiary section (Doré *et al.* 1999).

The Late Jurassic extension was characterized by a regional E-W least principal stress direction, as reflected in the N-S strike of those basins that can unequivocally be described as Jurassic rifts bordering the NE Atlantic margin (Doré *et al.* 1997b). This stress direction may have been inherited from an earlier (Permo-Triassic) extensional episode (Færseth *et al.* 1995).

Doré *et al.* (1999) noted that the fabric and stress patterns of the Late Jurassic differed strongly from those of the subsequent extension leading to north Atlantic separation. They claim this observation is a critical element of their model of migrating, rather than repeating, rifts. They also suggest that the Late Jurassic rifting in northwest Europe was less influenced by central Atlantic spreading than by the imposition throughout northwest Europe of a stress regime associated with seafloor spreading in Tethys. Thus on the Atlantic margin, the existence of which is largely the result of later tectonics, evidence of Late Jurassic activity is very variable along present strike.

4.4.4 Cretaceous extensional events

In Early Cretaceous times Tethyan seafloor spreading had ceased and was replaced by subduction on the northern margin of the ocean (Ziegler 1988). Tectonics on the future Atlantic margin switched from a system dominated by N-S Tethyan rift propagation to one dominated by NE-SW trending rifts, an extension vector that was maintained intermittently through to break-up. A series of coeval NE-SW faults bounding the Magnus and Manet highs and Margareta Spur postdate the Viking Graben faults of Late Jurassic age and effectively delineate the southeastern margin of the Møre Basin (Doré *et al.* 1999).

Early Cretaceous faulting has not been reported in the Møre and Vøring Basins, probably because of poor seismic imaging due to the unusually thick Cretaceous basin fill (up to ~10 km). The rift flanks provide the least ambiguous clues to timing of rifting. Near the Norne Field on the Nordland Ridge, seismic mapping reveals Early Cretaceous NE-trending normal faults offsetting N-trending Late Jurassic normal faults. Also, the major Klakk Fault Complex bounding the east side of the Rås Basin (SE Vøring Basin) is interpreted to have been active in Early Cretaceous (Blystad *et al.* 1995).

In particular, considerable quantities of sands were deposited on the basin flanks and around structural highs, particularly after a hiatus emanating from a mid-Cenomanian tectonic pulse. However, the regional character and the inter-relationships of the tectonism need further studies (Eldholm *et al.* 2002).

A number of tectonic and stratigraphic observations in the Vøring Basin reported by Lundin & Doré (1997) point to an extensional tetonic event of mid-Cretaceous age. Biostratigraphic data from the Vøring margin also reveal a change from neritic to bathyal

conditions and increase in sediment accommodation space change in the Aptian-Albian, attributed to eustatic sea-level rise and regional tectonism (Gradstein *et al.* 1999). In places this tectonic event is narrowly time-constrained approximately to the Cenomanian, while elsewhere there appears to have been some continuity through the late Cretaceous with the break-up rifting of approximately Paleocene age. The mid-Cretaceous event is seen on seismic data as a gentle to angular unconformity in the outer Vøring Basin (Gjallar Ridge and Nyk High), Træna Basin and Ribban Basin. Expansions of the early Late Cretaceous section immediately east of the Utgard High and Fles Fault Zone also indicate significant extension (Doré *et al.* 1999).

4.4.5 From rift to drift

At the onset of the Late Cretaceous-Paleocene rifting, the area between Norway and Greenland was an epicontinental sea covering a region in which the crust had been attenuated by the multiple post-Caledonian rift events (Doré 1991). There is little direct tectono-stratigraphic evidence to precisely date the onset of the rift episode leading to complete lithospheric breakup (Eldholm *et al.* 2002). The most abundant ash layers occur in the lower Balder Formation where a regional seismic marker has been attributed to the intensive breakup volcanism (e.g. Eldholm *et al.* 1989, Skogseid & Eldholm 1989). According to Lundin & Doré (1997) latest Cretaceous-Early Tertiary rifting appears to have started in late Maastrichtian (~65 Ma) (based on Norwegian Petroleum Directorate (NPD) wells 6607/5-1, and 2 on the Utgard High), while break-up occurred in the Early Eocene. However, in the northern Vøring Basin Ren *et al.* (1998) and Skogseid *et al.* (2000) inferred that rifting occurred for a ~20 Ma period prior to breakup at ~55 Ma (Campian).

The rifting resulted in low-angle detachment structures that updome thick Cretaceous sequences and sole out at medium to deep intra-crustal levels on the Vøring margin (Eldholm *et al.* 2002). Faulting is well expressed in the Vøring Basin, where two regions were affected (Skogseid *et al.* 1992a). In the east, the mildly reactivated Utgard High and its southward continuation, the Fles Fault Complex. In the west, the more intensely faulted Gjallar Ridge highs and the Hel Graben/Nyk High. Between the two regions lie the unfaulted Vigrid and Någrind Synclines. The Møre Basin margin also broke up in Early Tertiary time, but there are few signs of preceding brittle faulting of the margin. Only in the outermost part of the basin can some Tertiary faulting be documented. Isopach maps show that the Palaeocene section thickens westward until masked by Early Tertiary lava, suggesting an increase in lithospheric thinning toward the basin margin (Lundin & Doré 1997).

4.4.6 Paleogene evolution

During plate separation in the early Eocene (chron 24b), a reversal of the horizontal stress patterns took place whereby NW-SE extension gave way to SE-directed compression, attributable to ridge push forces from the adjacent ocean. The new compressive regime gave rise to widely-distributed inversion structures along the Atlantic margin (Doré *et al.* 1999). According to Eldholm *et al.* (2002) the Eocene and Oligocene epochs reflect the early margin history, governed by differential subsidence caused by thermal cooling and contraction of the lithosphere and by sediment lading and compaction. In addition, Stuevold *et al.* (1992) and Hjelstuen *et al.* (1997) point out that differential sediment loading has also to be considered when evaluating dome geometry and location, and doming mechanisms.

The most commonly observed inversion features are elongate domes which, although only gently deformed, are aerially and vertically extensive. For example, the Helland Hansen Arch in the Norwegian Sea has a long axis of about 200 km, is 50 km wide and has a structural relief in the order of 1 km. Reverse faulting is observed in the Norwegian Sea, where the Fles Fault Zone reversely reactivates a Cretaceous normal fault (Doré & Lundin 1996). A more general bulge of some of the Cretaceous depocentre axes is probably also attributable to Cenozoic compression (see for example the Någrind Syncline axis) (Doré *et al.* 1999).

Many features show a multiphase inversion, in some cases reactivating older rift structures, and there are indications that the timing becomes younger to the north. The main inversion of the domes is dated as late Eocene-early Oligocene on the Ormen Lange Dome, late Eocene-early Miocene on the Helland-Hansen Arch, and early-middle Miocene on the Naglfar Dome by Doré *et al.* (1999), whereas Hjelstuen *et al.* (1997) suggest a late Oligocene-Miocene age for both Vema and Naglfar domes. Eldhom *et al.* (2002) note that a detailed study of the Ormen Lange Dome reveals only moderate, <2–3%, contraction and that it has been growing continuously from Eocene to Present.

Plate reorganization of Oligocene-Miocene age gave rise to local renewed extension of the north Atlantic margin. Doré *et al.* (1999) suggest that rifting propagated from south to north between the Jan Mayen Block and SE Greenland, counterbalancing the fan-shaped spreading (widening northwards) along the Aegir Ridge. The extension culminated in the separation of the Jan Mayen microcontinent along the Kolbeinsey spreading ridge, and extinction of the Aegir Ridge, at chron 7 time (25 Ma, Oligocene-Miocene boundary).

Extension on the Norwegian margin may represent a failed attempt at splitting off a microcontinent similar to Jan Mayen (Doré *et al.* 1999). The relationship between the Cenozoic extension and inversion is not yet clear. As suggested by (Doré & Lundin 1996), it is possible that these tectonic effects occurred simultaneously as transtensional and transpressional elements of a strike-slip regime. Doré *et al.* (1999) propose, however, that the extension was a discrete event and interrupted a general background of mild compression deriving from ridge-push, as also suggested for East Greenland (Price *et al.* 1997).

4.4.7 Neogene uplift and erosion

The last major tectonic phase on the Atlantic margin was regional uplift of Neogene age. Cretaceous and Cenozoic sedimentary units rise and are truncated close to the emergent basement of the Norwegian coast. A major sedimentary wedge of Pliocene age progrades away from the mainland, and is itself truncated by the unconformity at the base of the Quaternary. This pattern is consistent around most of the Norwegian mainland, which is ringed by concentric subcrops indicating domal uplift and late emergence (Doré *et al.* 1999).

There is now a reasonable consensus among Norwegian workers that initial uplift was tectonic in nature and occurred in several phases during the Cenozoic, but that the most severe uplift and erosion was in the Plio-Pleistocene and was closely associated with glaciations taking place in the last 2.5 Ma (Solheim *et al.* 1996).

The domes and arches controlled the sedimentation on the Vøring margin in post-middle Miocene times when Late Miocene muds and oozes filled in and buried the existing relief (Brekke *et al.* 1999). Sedimentation continued into the Pliocene interspersed with ice-rafted debris signifying regional cooling and formation of mountain glaciers (Thiede *et al.* 1989, Stuevold & Eldholm 1996).

In terms of total post-opening sediment volume the glacial component constitutes as much as about 50% on the margins of Norway (Eldholm *et al.* 2002). The high-density glacial load on sediments of lower density and higher water content may, in part, explain recent margin deformation such as large-scale sliding (Bugge *et al.* 1987), mud volcanoes and extensive provinces of mud diapirism (Hjelstuen *et al.* 1997, Vogt *et al.* 1997, Hjelstuen *et al.* 1999), and possibly rejuvenation of older faults triggering earthquakes (Byrkjeland *et al.* 2000).

The morphology of Fennoscandia and the almost complete absence of onshore Mesozoic and Cenozoic sediments have for more than a century been interpreted in terms of epeirogenic uplift (Eldholm *et al.* 2002). In particular, a lower to middle Miocene hiatus on the Norwegian shelf (Gradstein & Backstrøm 1996, Brekke 2000) may be related to renewed tectonic uplift of the eroded landmass in late Oligocene or early Miocene time, later amplified by the isostatic response to the numerous glacials and interglacials since the late Pliocene. This induced large-scale glacial erosion of the shelf and mainland sourcing the voluminous wedges of glacial sediments centred near the present shelf edge (Faleide *et al.* 1996, Stuevold & Eldholm 1996).

Chapter 5

The use of potential field data in revealing the basement structure in sub-basaltic settings: an example from the Møre margin

Reynisson, R. F., Ebbing, J. & Skilbrei, J. R. 2009. The use of potential field data in revealing the basement structure in sub-basaltic settings: an example from the Møre margin, offshore Norway. *Geophysical Prospecting* **57**(4), 753-771.

This study investigates the usability of potential fields (gravity and magnetics) in volcanic settings as observed on volcanic continental margins. The Møre margin (Figure 5.1) is a typical example of a continental passive margin that has been heavily affected by Early Tertiary volcanism. The volcanism has left sills intruded in the Møre Basin and basalt flows on the Møre Marginal High that extend into the basin. The volcanic emplacement is the main reason for the geophysical imaging problems encountered on the margin. A simple synthetic model is used to test the effect of volcanics on the gravity and magnetic fields and to study the feasibility of potential field interpretation in sub-basalt imaging. The same tests are made on the Møre margin and compared to the synthetic model.

Our study focuses on using the potential fields to map basement structure. The knowledge of crystalline (i.e. metamorphic/igneous) basement is of crucial interest as the basement is representative of the tectonic situation and geological history of a specific area. In petroleum exploration, the basement depth (or equivalently sedimentary thickness) is a primary exploration risk parameter. Estimates of basement depth are directly applicable to basin modelling (e.g. source rock volume estimation) and thermal maturity applications (e.g. source rock burial depth).

Basement structure is most commonly imaged on seismic data but lithologies like salt and basalt can severely perturb the imaging of the underlying basement. The problem of seismic imaging through basalt is particularly acute where potential hydrocarbon bearing structures are overlain by basaltic sequences of stacked flows up to several kilometres thick (e.g., the North Atlantic, west African and Brazilian margins; Martini *et al.* 2005). Other areas with severe imaging problems, such as those associated with salt deposits, have received extensive attention within the seismic processing industry but fundamentally different petrophysical properties of volcanic and salt deposits suggest

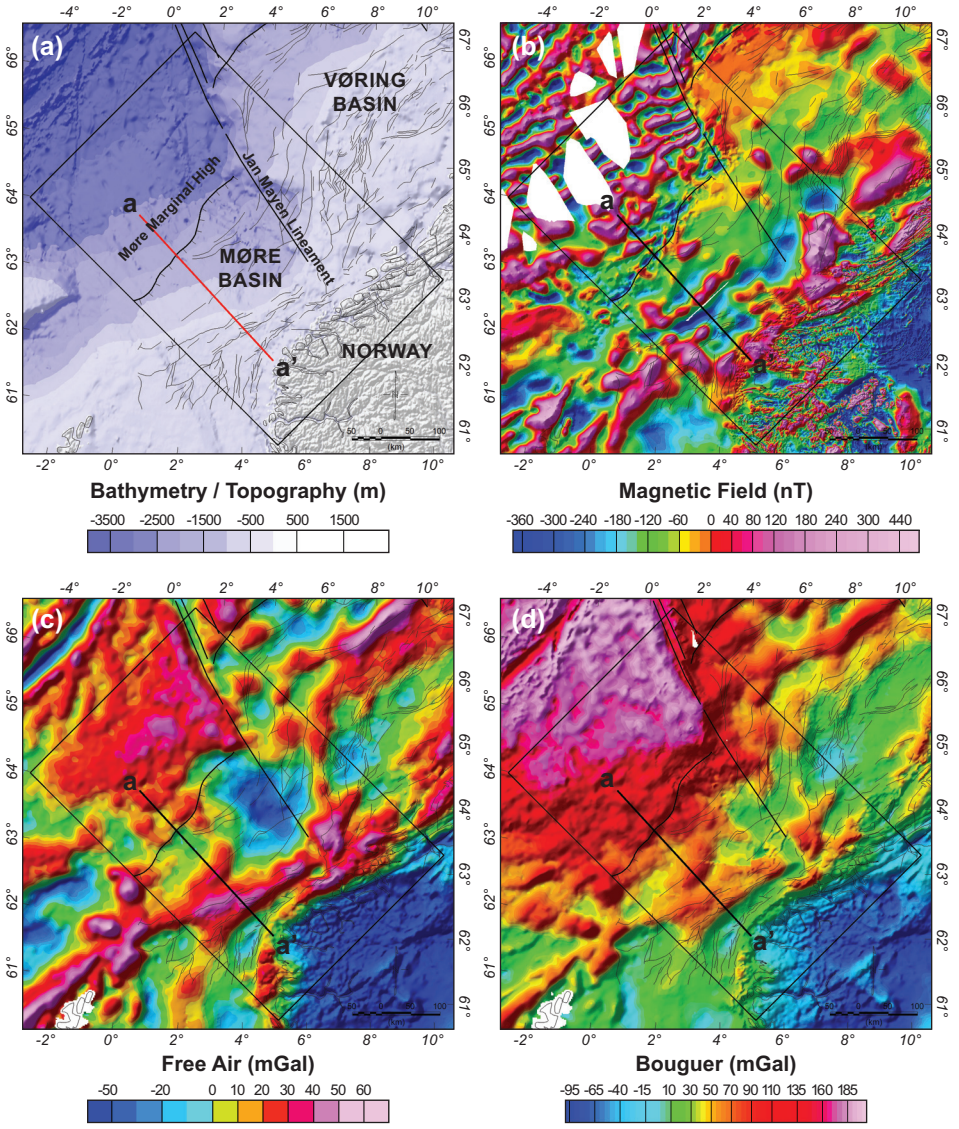

Figure 5.1. Outline of study area. (**a**) Bathymetry and tectonic setting of the Møre margin. Fault boundaries are marked by thin black lines and major tectonic features with thick black lines (after Blystad *et al.* 1995). The box outlines the study area and the red line marks the profile a-b (GMNR94-102) presented in Figure 5.12. (**b**) total magnetic field anomaly, (**c**) Free-air gravity anomaly and (**d**) Bouguer gravity anomaly. The magnetic data compilation is from Olesen *et al.* (1997b) that includes mostly total-intensity airborne measurements and some additional shipborne measurements. Flight altitudes, flying directions, and line-spacings of the aeromagnetic surveys vary widely. A reference to the Definite Geomagnetic Reference Field (DGRF 1965.0) was used to produce the total magnetic field anomaly grid with 1x1 km cells. The gravity data used in this study is a compilation by Skilbrei *et al.* (2000). The compilation consists of marine gravity data from the Geological Survey of Norway, the Norwegian Mapping Authority, the Norwegian Petroleum Directorate, Norwegian and foreign universities, and commercial

companies. Gravity data derived from satellite altimetry were used in the deep-water areas of the Norwegian-Greenland Sea (Laxon & McAdoo 1994, Andersen & Knudsen 1998). The International Standardization Net 1971 (IGSN 71) and the Gravity Formula 1980 for normal gravity were used to level the different surveys. From the compiled free-air dataset a Bouguer reduction at sea was carried out. The reduction was based on bathymetry data from Dehls *et al.* (2000) and a density of 2200 kg/m^3.

that new solutions should be considered to improve the sub-basalt and intrabasalt images (Planke *et al.* 1999b).

Intra-lava flow velocity variation, caused by compositional and structural variability within individual flows, combined with inter-layering between lava flows, sediments, tuff, sills, and hyaloclastites, contribute to the heterogeneous internal structure of the volcanic succession. This complex 3D structure attenuates, scatters and multiplies the reflection energy that gets transmitted into the basalt layers through the high impedance contrast at the top of the flows. Also, top and base basalt are not flat regular surfaces, but often have a complex topography, which compounds the disruptive effect on wave propagation. All these factors combine to substantially reduce the quality of sub-basalt seismic imaging (Martini *et al.* 2005).

The P-wave velocity in subaerial flow shows cyclical asymmetric variations related to emplacements and alteration processes and interbedding of flows and sediments. Planke (1994) developed a characteristic velocity and density basalt flow distribution (CFD) based on log responses in Ocean Drilling Program (ODP) hole 642E on the Vøring Marginal High. In single flows the velocity increases gradually from ~3 km/s at the top to 5.3 km/s, corresponding to a decreasing number of voids and cracks in the flow. The velocity in the massive central flow is 5.0-6.0 km/s, decreasing very rapidly near the base. The density logs often show a similar pattern, ranging from 2300 to 2800 kg/m^3 (Planke 1994, Planke *et al.* 1999a). This density and velocity distribution reflects changes in porosity, pore aspect ratio distribution, and alteration.

A useful technique in the presence of seismically problematical lithologies is utilization of potential field data (e.g. Smallwood *et al.* 2001). Density modelling can significantly improve the seismic interpretation and may especially help with understanding the structural interpretation under areas obscured by volcanics (Ashcroft *et al.* 1999). Density modelling has for example improved the geological interpretation of the sub-basaltic sedimentary fill and the depth to basement of the Faeroe-Shetland Basin (Ashcroft *et al.* 1999, England *et al.* 2005, White *et al.* 2005). The combined use of both gravity and magnetic potential fields adds a further constraint to the interpretations (e.g. Smallwood *et al.* 2001). Instruments measuring directly the gradients of the gravity field also hold the potential to resolve subsurface structures that seismic methods have difficulty to image (e.g. Smit *et al.* 2005). Gradient data were acquired in the Faeroe-Shetland Basin in 1999 for the purpose of resolving basalt complexity/characterisation and imaging sub-basalt geology. The results demonstrate the gradients ability to image basalt and the underlying geology (Murphy *et al.* 2002).

This study systematically investigates the utility of potential field data (gravity and magnetics) for basement mapping in sub-basaltic settings. The applied methods are Euler deconvolution on magnetic data, gravity gradients, and integrated 3D gravity and magnetic forward modelling. The different methods are tested on a synthetic model that has the same

dimensions, ambient magnetic field, and similar tectonic settings as the Møre margin. The results from the different methods are finally compared to a seismic line that extends from the Norwegian mainland to the oceanic domain west of the Møre Marginal High.

5.1 Tectonic settings

The Møre margin is part of the mid-Norwegian margin (Figure 5.1) that has been strongly affected by volcanism where extrusive and intrusive rocks form an important part of the basin fill (Planke *et al.* 1999a). The overall tectonic framework of the mid-Norwegian margin consists of a central area of NE-SW trending deep Cretaceous basins, the Vøring and Møre Basins, flanked by palaeo-highs and -platforms and the elevated mainland. The Basins are classical examples of intruded volcanic basins located on a rifted volcanic margin (e.g. Skogseid *et al.* 1992a, Skogly 1998, Berndt *et al.* 2000, Brekke 2000, Gernigon *et al.* 2003, Planke *et al.* 2005). The volcanic activity in these basins was associated with Late Paleocene rifting and continental breakup in the NE Atlantic. Similar intrusive basin provinces are located along the entire European NE Atlantic margin (e.g. Gibb & Kanaris-Sotiriou 1988, Bell & Butcher 2002, Smallwood & Maresh 2002) and onshore in central-east Greenland (e.g. Larsen & Marcussen 1992, Price *et al.* 1997).

The Møre margin is immediately flanked by the mainland to the east and the platform to the west is the Møre Marginal High that is characterized by thick, Early Eocene basalt flows overlying an unknown substrate. Regional information shows that the area is likely underlain by pre-Cretaceous sedimentary rocks varying in thickness between 3 and 10 km, which infill an older, uneven basement relief (Bøen *et al.* 1984, Eldholm & Mutter 1986, Skogseid & Eldholm 1989, Planke *et al.* 1991). The boundary between the marginal high and the basin area is formed by the Faeroe-Shetland Escarpment (Brekke 2000).

Potential field data (gravity and magnetics) have been used to estimate depth to top crystalline basement in the Møre Basin. The basement depths in the basin are reported to exceed 14 km based on magnetic depth estimates (Skilbrei *et al.* 1995, Skilbrei *et al.* 2002, Skilbrei & Olesen 2005). From density forward modelling studies the basin thickness is estimated 12-15 km (Skilbrei *et al.* 1995, Ebbing *et al.* 2006).

The magnetic anomalies in the study area (Figure 5.1b) range between -300 and 300 nT with the exception of the Frøya High that has a magnetic anomaly of approximately 1300 nT. A prominent magnetic high extends from the SW of the basin to the NE. The basin is generally characterized by a rather quiet magnetic field disturbed by occasional SW-NW trending anomalies that follow the main structural features. Westward of the Faeroe-Shetland Escarpment the magnetic characteristics change dramatically, probably caused by relatively shallow volcanics.

The free-air gravity anomaly (Figure 5.1c) has a range from -45 to 65 mGals in the study area and a general trend orientated SW-NE corresponding to the main structural features. A prominent gravity low exists in the eastern part of the basin adjacent to the Jan Mayen Lineament that seems to obliterate the gravity effect of the Vigra High and other basement highs in the area. The Bouguer gravity anomaly (Figure 5.1d) demonstrates that a part of this gravity low can be explained by the effect of deep bathymetry.

Comparison between the gravity anomaly maps and the magnetic anomaly map reveals some differences but the overall trend is similar. The most prominent difference in the basin

is associated with the SW-NE trending magnetic anomaly and considerable dissimilarities exist on the marginal high.

5.2 Methodology

To gain more insights into the sub-basalt problem, we make use of the gravity gradients, Euler deconvolution and forward modelling. The theoretical background is presented in the following sections.

5.2.1 Gravity gradients

Conventional gravimeters usually determine only the vertical component U_z of the three-component gravity acceleration vector at each measurement point. Gradiometers, in contrast, measure first-order changes in the gravity field, for example by measuring the difference field between two accelerometers placed closely together. These first-order changes form a nine-component tensor. Newton's theory of gravity implies, however, that only five of the nine components are independent and four are redundant (Figure 5.2). The measured gravity gradients thus provide a more detailed picture of the subsurface by better reflecting the edges, shape, and approximate depth of dominant mass anomalies (Huston *et al.* 1999, Smit *et al.* 2005).

Although fundamentally gravity gradient data contain no more information than conventional gravity data, both being governed by a single scalar potential satisfying Poisson's equation, they are of great interest from a practical point of view. Firstly, the horizontal resolution is about an order of magnitude better because of the absence of linear acceleration noise (the so-called common mode) inherent to gravity measurements. Secondly, gradients provide additional information in practice. The better S/N at shorter wavelengths has been shown to provide tighter constraints on overburden structure. Furthermore, the sensitivity of gradients to the geometrical structure of the anomaly is theoretically about 30% better than that of gravity vectors (Smit *et al.* 2005).

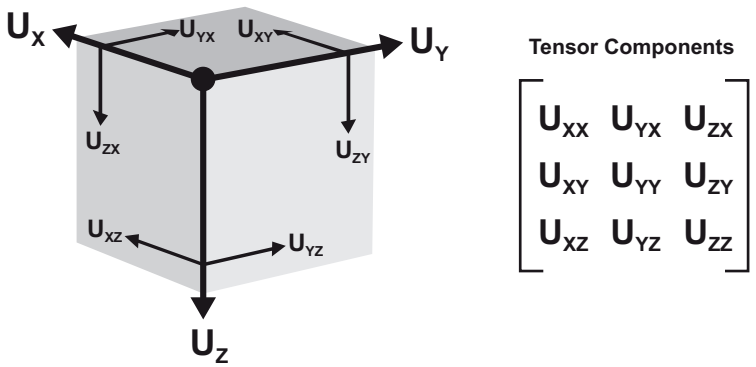

Figure 5.2. Gravity vector and tensor. The three components of the gravity vector are U_x, U_y and U_z. The gravity tensor has nine components but three are missing from the figure: U_{xx}, U_{yy} and U_{zz}. Five gradients are independent and four are redundant: $U_{xy}=U_{yx}$, $U_{xz}=U_{zx}$, $U_{yz}=U_{zy}$ and $U_{zz}=-(U_{xx}+U_{yy})$.

Horizontal derivatives are the most common method for detecting target edges and are commonly used (Nabighian *et al.* 2005). As this study had no access to measured gradient data the horizontal derivatives were computed from gravity data from the Møre margin. They emphasize the short-wavelength anomalies resulting from shallow sources but are also very sensitive to higher frequency noise. A 3x3 point convolution filter was applied to the gravity grid to produce a gradient map of the study area. Previous to the gradient filtering the grid was upward continued to 1 km to reduce the noise effect.

5.2.2 Euler depth estimation

Many depth estimation methods exist and the number keeps growing. The methods are often categorized as manual or automatic. The majority of automatic methods are theoretically independent of the susceptibility contrast and the magnetization direction (e.g. Li 2003). A commonly used automatic method is the Standard Euler deconvolution method (Reid *et al.* 1990).

The standard Euler deconvolution is based on Euler's homogeneity equation that can be re-stated as follows:

$$(x - x_0)\frac{\partial T}{\partial x} + (y - y_0)\frac{\partial T}{\partial y} + (z - z_0)\frac{\partial T}{\partial z} = N(B - T)$$

where (x_0, y_0, z_0) is the position of a magnetic source whose total field T is measured at (x, y, z). The total field has a regional value of B.

The equation relates the field (magnetic or gravity) and its gradient components to the location of the source, with the degree of homogeneity N, which may be interpreted as a structural index (Thompson 1982). The structural index is a measure of the rate of change with distance of the field. Thus, the magnetic field of a point dipole falls off as the inverse cube, giving the index of three, a vertical pipe gives rise to an inverse square field fall-off and an index of two.

The Geosoft system Euler 3D Deconvolution (Euler 3D) was used to perform the calculations. The system is an automatic location and depth determination software package for gridded data and is based on the method described by Reid *et al.* (1990) and Thompson (1982). The system uses a least squares method to solve Euler's equation simultaneously for each grid position within a sub-grid (window).

Magnetic depth estimates cannot be obtained everywhere on the gridded data and where no significant magnetic gradients exists it is not possible to acquire a valid depth estimate. It is only possible to obtain a depth estimate from magnetic data where there is some lateral discontinuity in magnetization, for example because of lithological variations within the basement or sediments or because of top-basement faulting.

The depth estimates provide a good starting point for a genuine structural interpretation (e.g. interactive modelling or a constrained inversion). As a strong magnetic contrast often exists between the sediments and the underlying crystalline basement the magnetic data can be used to estimate depth to the basement. This method has previously been used effectively on the mid-Norwegian margin (Åm 1970, Skilbrei & Olesen 2005). Skilbrei & Olesen (2005) studied the accuracy and the geological meaning of the 'magnetic basement' on the mid-Norwegian margin. They found generally good agreement between estimates made from magnetic anomalies and the depth to the Precambrian basement. In some areas there may exist non-magnetic Devonian basins, and non-magnetic Caledonian nappes can

overly the Precambrian basement. In the latter case, the true crystalline basement would lie above the 'magnetic basement'. Comparison of magnetic depth estimates and seismic-, borehole-, and petrophysical data yield errors that generally vary between 5% and 15% but uncertainty increased to the west of the study area where igneous sills and flows are known to exist (Skilbrei *et al.* 2002).

Ebbing *et al.* (2007) demonstrated the advantage of using multilevel magnetic data to acquire source depths at different levels. They used jointly a low-altitude aeromagnetic survey flown at 50 m altitude and a high-altitude aeromagnetic survey flown at 3400 m over the Oslo Graben. We test this method on the synthetic model to see if it is applicable to the Møre margin. As noise is absent in the synthetic model the field modelled in high-altitudes is almost identical to the upward continued field.

Upward continuation of potential field data is a common method to separate shallow sources from deeper sources. The process decreases the effect of shallow sources but enhances the effect of deeper sources (Jacobsen 1987). Only low altitude aeromagnetic surveys exist on the Møre margin and therefore in order to test the usability of different observation heights to separate the deep magnetic sources from the shallow sources on the Møre margin we employed upward continuation to the magnetic data. The upward continuation is expected to suppress the noise and enhance the effect of the deeper sources at the cost of the shallower sources in the data.

5.2.3 Forward modelling

Forward modelling of the density structure and the magnetic properties of the crust is nowadays used routinely in addition to seismic data to model the crustal structure of continental margins in a 2D or 3D sense (e.g. Skilbrei *et al.* 2002, Ebbing *et al.* 2006). But density modelling can also improve the geological interpretation of the sub-basaltic sedimentary fill, as has been proven for the Faroe-Shetland basin (Ashcroft *et al.* 1999, Smallwood *et al.* 2001, England *et al.* 2005, White *et al.* 2005). Forward modelling using seismic, gravity and magnetic data greatly improves the understanding of the extent of the flood basalts, as well as the thickness of the sub-volcanic sediments and the basement structure. No single one of these geophysical methods would have given all the information in isolation. In a forward density and magnetic model, the causative body of a gravity and/or magnetic anomaly is simulated by a model whose theoretical anomaly can be computed, and the model is altered until the computed anomaly closely matches the observed anomaly. Because of the inverse problem inherent in geophysical methods, the resulting model will not be the only possible interpretation. The ambiguity can be decreased by using other constraints on the nature and form of the anomalous body and where an acceptable number of constraints exist, a forward modelling study provides a powerful tool to image seismically problematic areas (Kearey *et al.* 2002).

The model calculation involves four steps. First a reasonable model is constructed, often from available seismic and well data. Then its effective gravity and magnetic signal is calculated and compared to the observed anomalies. Finally alteration of the model takes place to improve correspondence of observed and calculated anomalies. The process is iterative and the goodness of fit between observed and calculated anomalies is gradually improved.

The forward modelling system used in this study was the 3D modelling package IGMAS (Interactive Gravity and Magnetic Application System). The system uses polyhedrons

with triangulated surfaces to approximate bodies of constant density and/or susceptibility within the Earth, whose geometry is defined by a number of parallel vertical modelling sections. The system then calculates the potential field effect of the model at a designated station location (Götze & Lahmeyer 1988, Schmidt & Götze 1998, 1999).

5.3 Synthetic model

Two synthetic models were constructed to characterize sedimentary basins in different geological settings. A control model was created to represent a basin in non-volcanic setting and a test model was constructed to represent a basin influenced by basalt flows and intrusive sills (Figure 5.3). The models have the same basement structure and differ only in respect to emplacement of volcanic material of high density and high magnetization (Figure 5.4). Both models have a basin that is overlain by 2 km of water and 2 km of Cenozoic sediments. It is filled with Mesozoic sediments with a maximum depth of 18 km deep, and is 300 km wide and 400 km long. The basin is underlain by a magnetic basement that has four prominent highs and is symmetric about the deepest part of the model. The greatest structural variations are in the X direction but the basin shallows progressively in the Y direction from the deepest point, and hence has 3D characteristics. In order to exclude the effect of Moho undulations the base of the basement was kept flat at depth of 20 km. The basement is underlain by non-magnetic mantle. Only the basement has magnetic properties and has susceptibility of 0.01 SI and the remanent magnetization is equal to the induced magnetization (Q=1). The water was defined with density of 1030 kg/m^3, Cenozoic sediments with density of 2200 kg/m^3, Mesozoic sediments with density of 2500 kg/m^3, the basement with density of 2600 kg/m^3, and the mantle with density of 3300 kg/m^3.

In order to study the gravity and the magnetic response from the basement in volcanic settings a test model was constructed in addition to the previously described control model. In the test model the basin is partly overlain by a 1 km thick basalt layer and intruded by a sill at 7 km depth that is 100 m thick in the centre of the basin and thins to zero towards the edges. The basalt layer has a constant susceptibility of 0.01 SI and remanent magnetization that has the same polarity as the induced magnetic field but twice the intensity (Q=2). The sill has a susceptibility of 0.03 SI and the same remanent magnetization as the basalt layer. The basalt and the sill have densities of 2700 and 2900 kg/m^3, respectively. Petrophysical

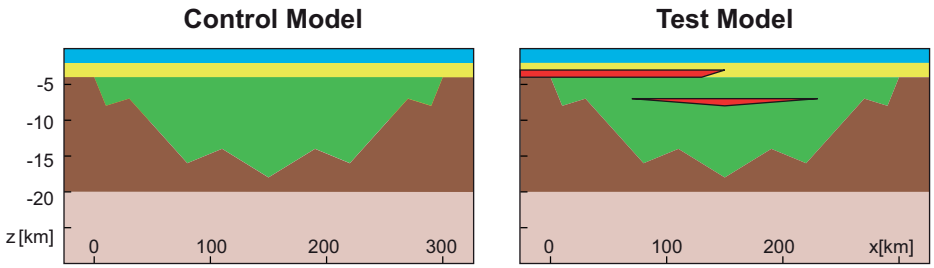

Figure 5.3. Synthetic model setup. Two synthetic models represent two different geological settings. The control model represents a basin in non-volcanic environment and the test model is influenced by volcanics. The petrophysical properties used in each model is given in Figure 5.7.

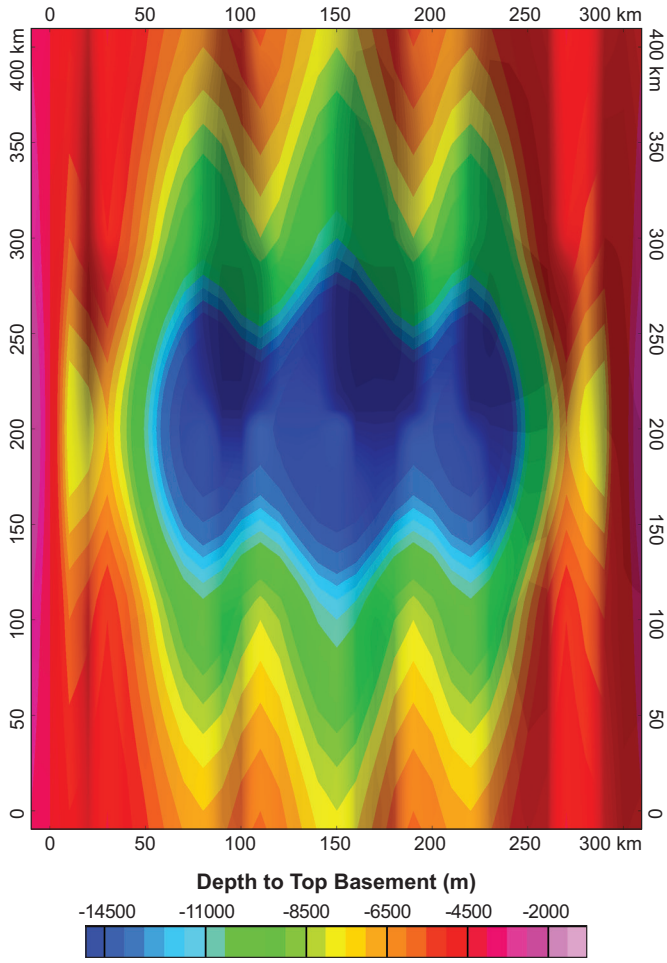

Figure 5.4. Synthetic Basement. The control model and the test model have identical Basement structure which is demonstrated here as a top to Basement map. The Basement depth varies both laterally (*x*-direction) and vertically (*y*-direction).

properties of both the control and test model are based on detailed petrophysical study that was used in a 3D forward model of the Møre margin (see Chapter 6).

The orientation of the basin and the induced magnetic field was configured to represent the present settings on the mid-Norwegian margin where the inclination is about 75°, declination 0° and the total normal magnetic field 50,000 nT. A reference density model was used to calculate absolute gravity anomalies from the model. The reference model is the same as used on the 3D model from the Møre margin.

The models were constructed in the modelling software IGMAS and the potential fields were calculated at stations on a regular grid with 5 km between stations. The gravity effect of the models was calculated at zero elevation and five different components of the gravity effect were calculated from the models: the *z*-component of the gravity (U_z), gradients of U_z (U_{xz}, U_{yz} and U_{zz}), *x* gradient of U_x (U_{xx}), and *y* gradient of U_y (U_{yy}). The total magnetic field (induced and remanent) was calculated at 0 and 3000 m elevation to represent low and high altitude aeromagnetic surveys.

5.3.1 Magnetic and gravity signals from the model

The difference between the total magnetic field anomalies of the control model and the test model demonstrates that the sills have a minor effect on the magnetic signal (Figure 5.5). The greatest effect is in the centre were the sill is thickest and overlies the deepest part of the basin. Superpositioning of the two volcanic sources severely disturbs the magnetic response of the underlying basin. The sill does not produce disturbances at its edges due to the very gradual thinning of the sill towards its edges. At the modelled depth the sill would have to have a continuous lateral extension of 10's of km and end abruptly in a thickness of considerably more than 100 m to produce edge disturbances in the magnetic signal that could be used to outline its lateral extension. The overlying basalt has a larger impact on the magnetic signal and the internal magnetic variation in the basalt further diffuse the image of the underlying basin. There is no indication of the small sub-basalt basin on the magnetic data from the test model and the indication of the sub-basaltic basin is considerably diminished.

Comparison between the gravity (U_z) anomalies from the control and test models demonstrates that the sill has an insignificant effect on the gravity signal but the shallower and thicker basalt has a more pronounced effect (Figure 5.5). The basalt does not completely obliterate the indication of deep basin but without any a priori information the sub-basaltic basin could easily be misinterpreted and its extent underestimated.

It is apparent from the gradient data (Figure 5.6) that the gravity signal contains considerably more data than can be read directly from the gravity maps. The five independent gravity gradients (or tensor components) from the control model clearly demonstrate that each gradient contains different information. The three tensor components of the z-component enhance different aspects of the basement structure. The U_{xz} brings out the edges of the basins and indicates how the basins deepen and shallow in the x-direction. The basement structure only mildly varies in the y-direction and this can be easily read from the U_{yz} tensor component as well as the general outline of the main basin. From the U_{zz} all the sub-basins and basement highs can easily be recognized. The U_{xx} and U_{yy} tensor components are very sensitive to lateral density contrasts in respective x- and y-directions and illuminate the edges of the underlying structures.

The gradients from the test model show that gradient data are much more sensitive to the overlying volcanic structures than the conventional gravity data. By comparing the gradient maps from the test model to the control model an indication of both the sill and basalt can be noticed. The signal from the sill is weak though and could hardly be observed without comparison to the control model. The shallower and thicker basalt has more influence on the gravity signal as also observed on the free-air gravity data. The U_{xz} and especially the U_{xx} clearly outline the edge of the basalt and could be used to map the lateral extension of the overlying body. The basement structure is also better retained in the gradient data. A much clearer indication of sub-basaltic basins is acquired from the gradient data than from the z-component data alone. The U_{xz} and U_{zz} both manage to indicate the small sub-basaltic basin but the deep centre basin is partly obliterated by the influence of the basalt edge.

5.3.2 Euler Deconvolution

Euler Deconvolution was applied to the magnetic grids from both the control and test models. Three parameters were varied, the observation height, the structural index, and the window size. The observation height was at zero level (0 m) and at 3000 m to represent the difference between low and high flying aeromagnetic surveys. The structural index varied

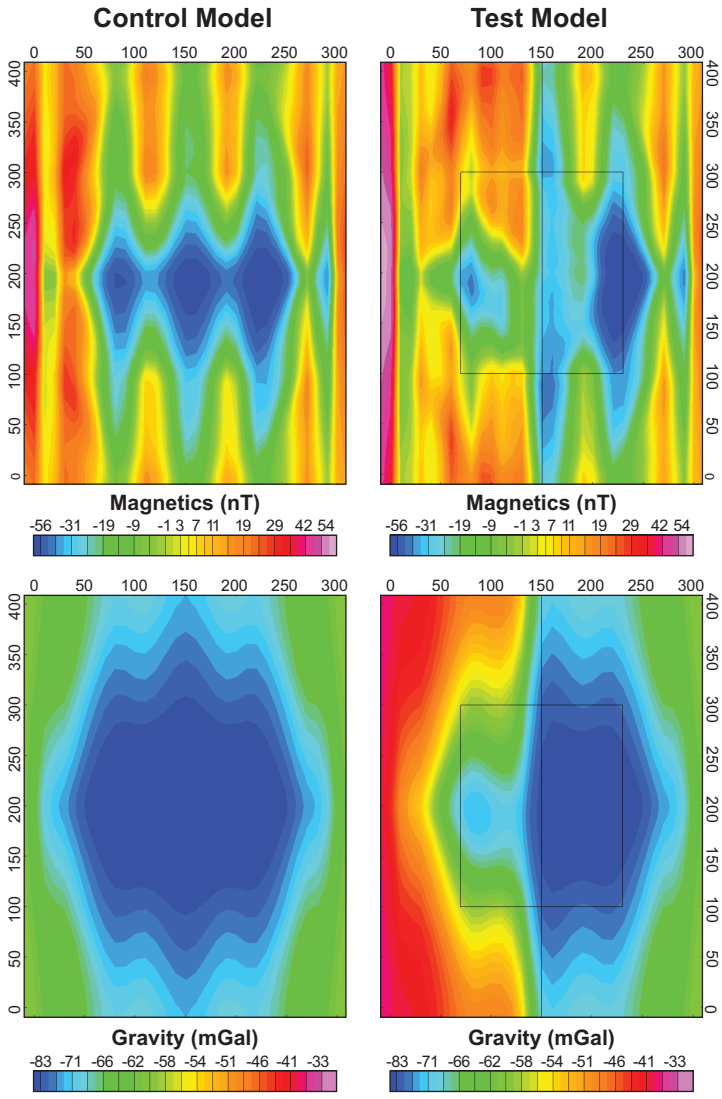

Figure 5.5. Gravity and magnetic anomalies of the synthetic models. The gravity and magnetic effect of the control and test models. The outlines of the volcanics are indicated by thin black lines.

between 0, 0.5, 1, and 1.5 and the window sizes were tested at 30, 60, 80, and 120 km for the control model. The same parameters were also used for the test model at the two different observation heights.

For all the window sizes a structural index of 0.5 best represents the basement structure in the control model (Figure 5.7). Solutions from a window size of 30 km are much dispersed in shallower parts and mostly lacking in deeper parts. A 60 km window sized gave dispersed solutions both in the deep and shallow parts. A window size of 80 km manages to give solutions that give good indications of the shallow to intermediate basin depth but poorly reflect the deepest part of the basin. Solutions produced with a window size of 120 km best reflect the overall basement structure but the deepest part is still underestimated.

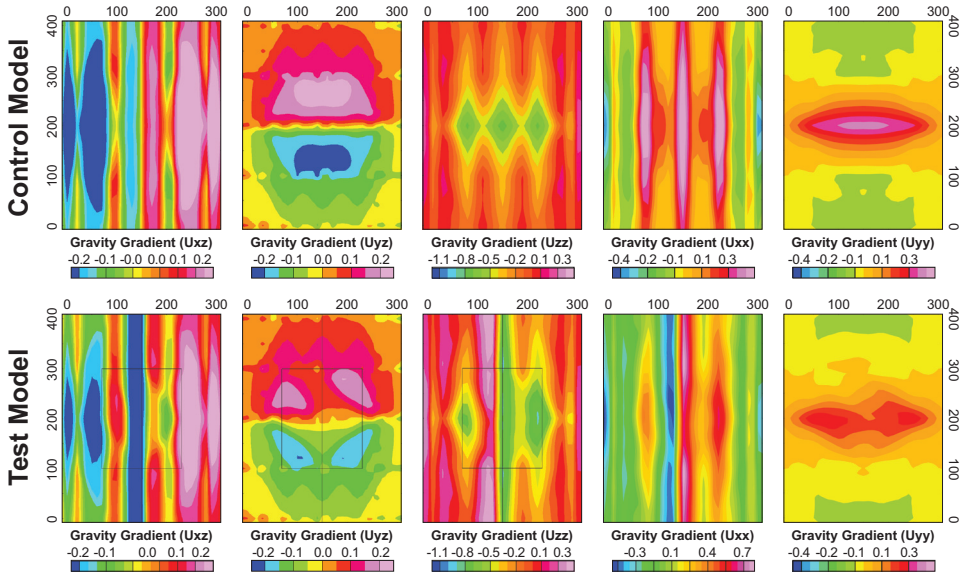

Figure 5.6. Gravity gradients of the synthetic models. The measured gravity gradient from control and test models. The outlines of the volcanics are indicated by thin black lines.

None of the structural index and window size combination gave an accurate estimate of the basement depth but might be regarded as a first order indication of the basement structure and used as a starting point in a forward model.

On the magnetic grid calculated from the test model (Figure 5.8) the Euler deconvolution was run with structural index of 0, 0.5, 1 and 1.5 and varying window sizes of 30, 60, 80 and 120 km. All the resulting solutions are disturbed by the magnetic sources overlying the basement. The greatest effect is at the edges of the sill and basalt and solutions for the deepest part of the basin are greatly disturbed. No combination of structural index and window size manages to produce solutions that accurately reflect the sub-basaltic basement structure. It is interesting to note, though, that structural index 0.5 and window sizes 80 and 120 km indicate the existence of the shallow sub-basin below the basalt (Figure 5.8). Even though the magnetic signal from the basement is greatly disturbed by the overlying volcanic structures the solutions do not manage to reflect the depth to the volcanics and only the edge of the basalt can be outlined.

The magnetic field from the test model was also calculated at 3000 m to see if the increased observation level would diminish the effect of the shallow volcanics on the magnetic signal from the basement. The increased acquisition height does not enhance the Euler depth solutions and generally results in shallower depth estimation, contrary to expectations (Figure 5.8).

5.3.3 Sensitivity of Forward Modelling

In order to test the sensitivity of a forward model in sub-basaltic settings the gravity and magnetic fields from the original test model were used as the observed fields. The physical parameters of the basalt were then altered and the calculated field adjusted to the observed one by changing the geometries of the model. It was assumed that a good geometrical

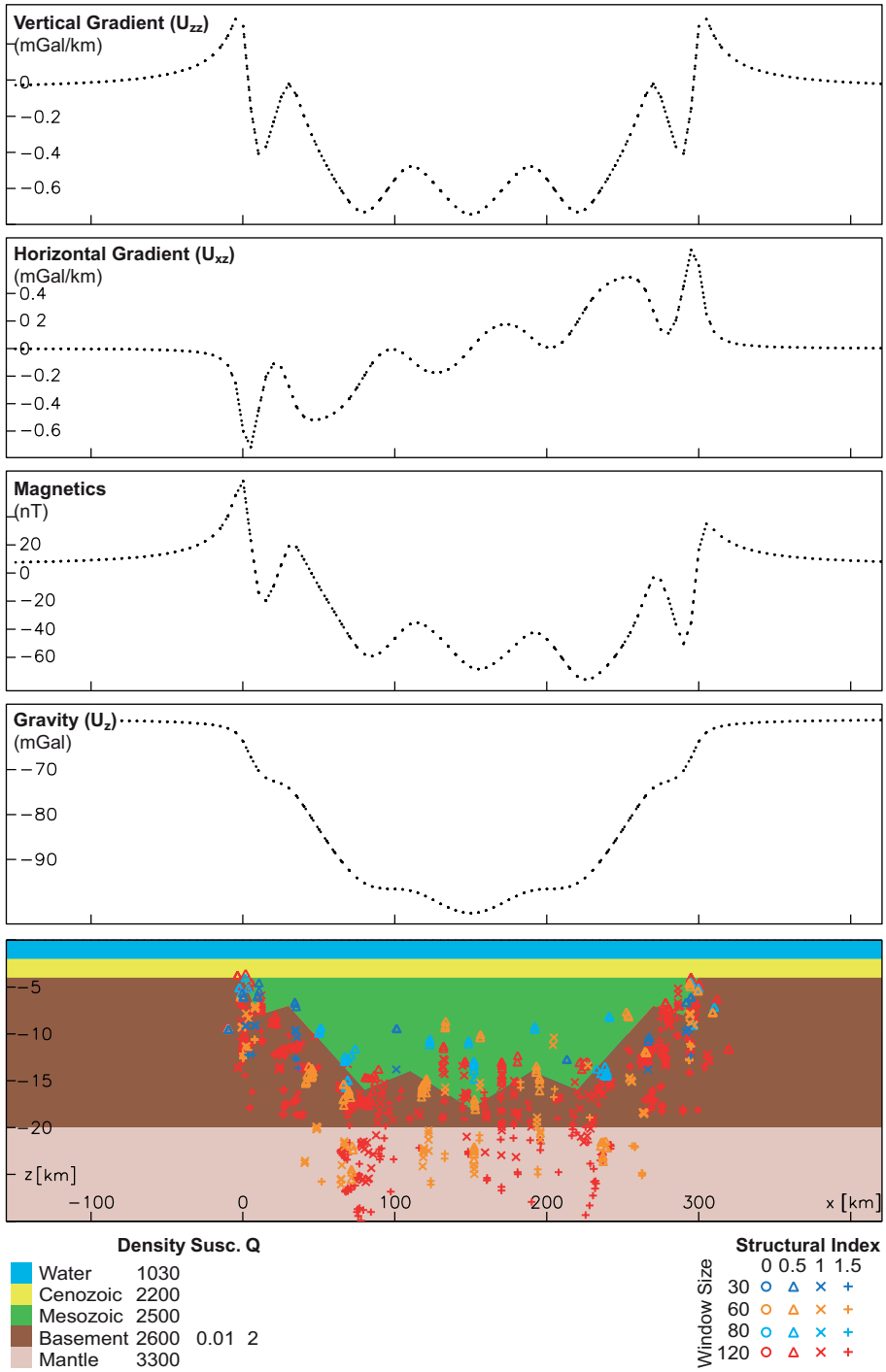

Figure 5.7. Profile of the control model. A profile view crossing the centre of the control model. The gravity and magnetic responses from the model are presented with black dotted lines. Euler solutions from variety of window sizes and structural indexes are drawn on the profile. Density is in kg/m^3, magnetic susceptibility (Susc.) is in SI units, and magnetic reamence is given as Königsberger ratio (Q).

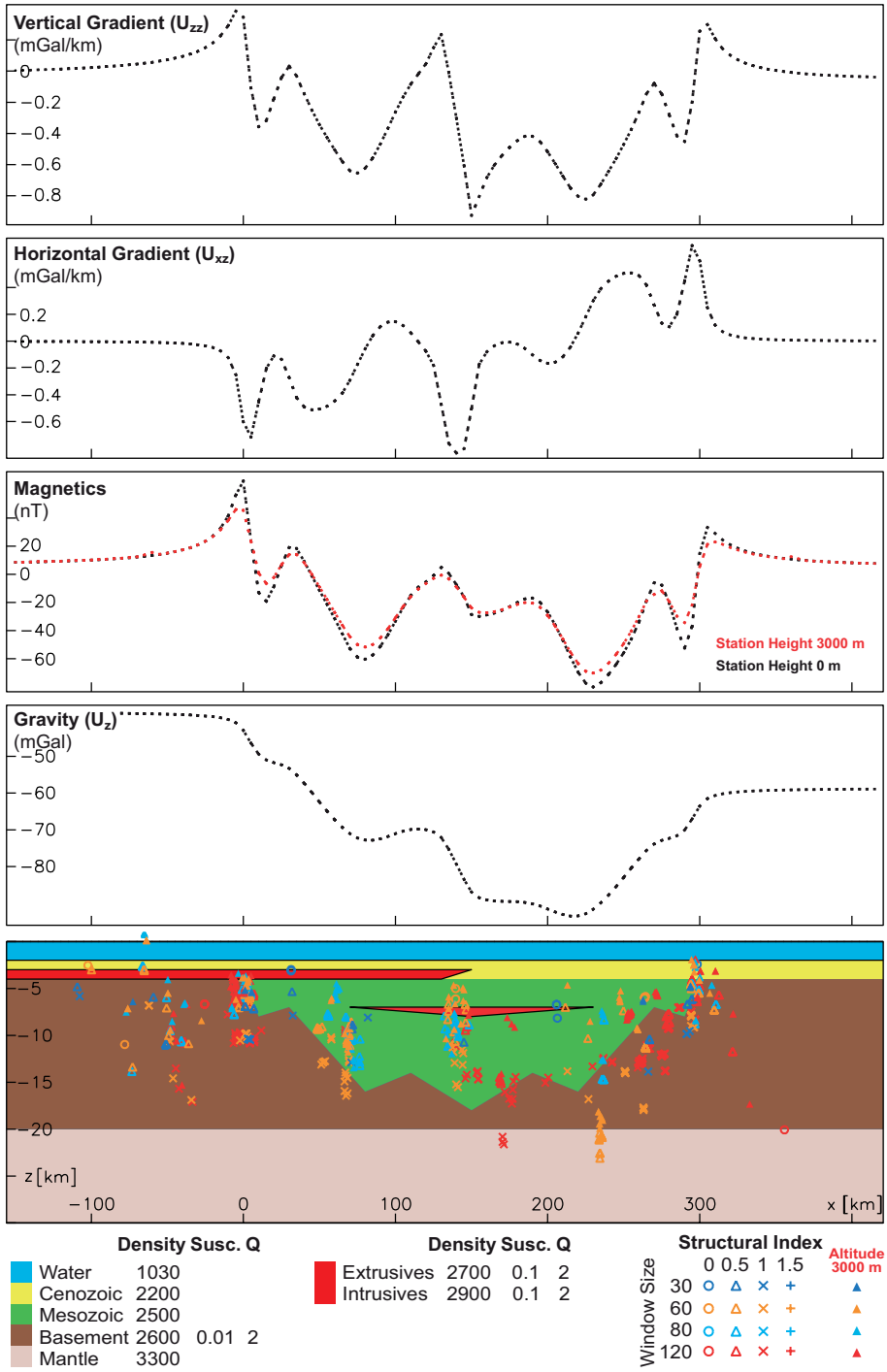

Figure 5.8. Profile of test model. A profile view crossing the centre of the test model. The gravity and magnetic responses from the model are presented with black dotted lines. Euler solutions from variety of window sizes and structural indexes are drawn on the profile. Density is in kg/m^3, magnetic susceptibility (Susc.) is in SI units, and magnetic reamence is given as Königsberger ratio (Q).

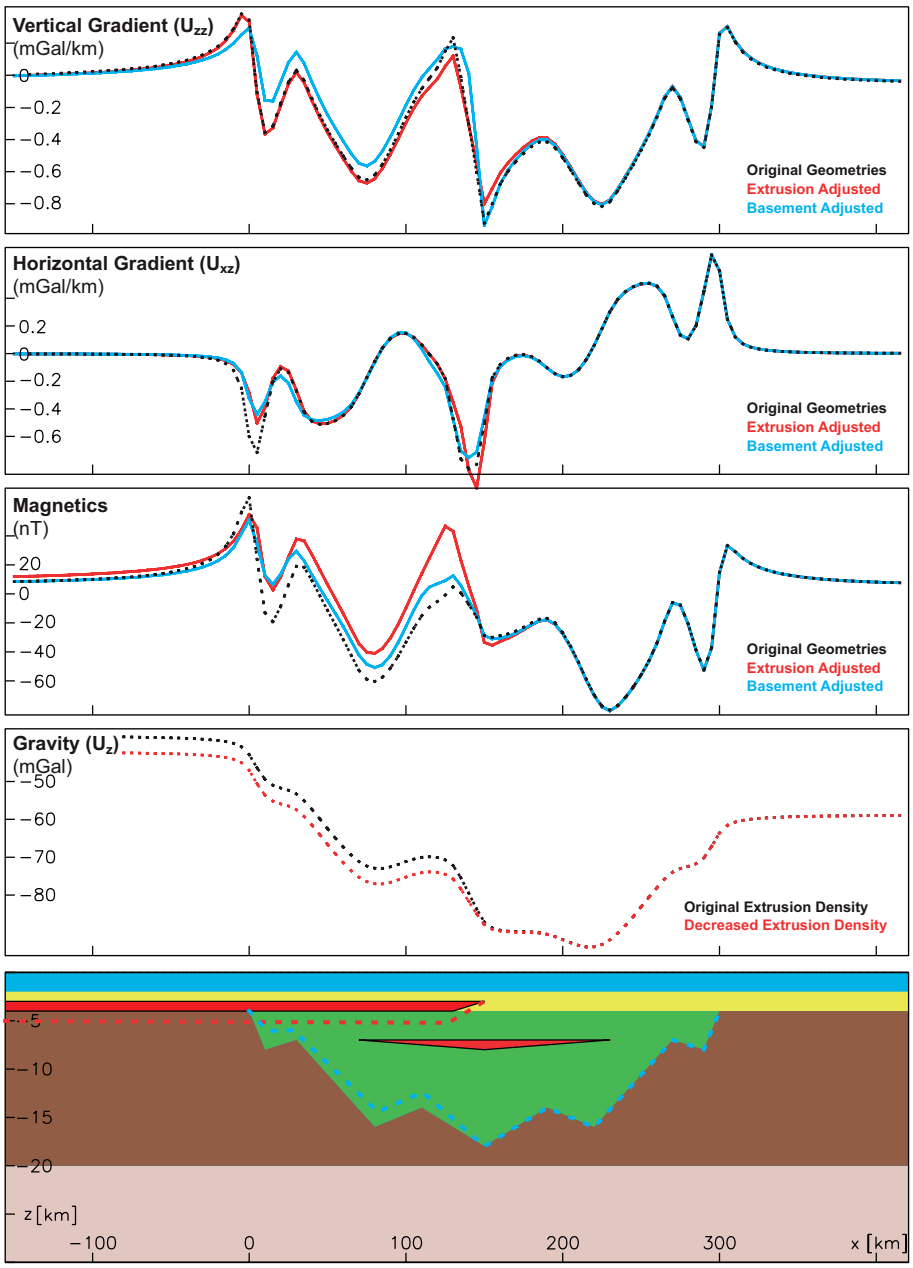

Figure 5.9. The effect of decreased basalt densities. Decreasing the density of the basalt flow decreases the gravity (U_z) effect of the model. To adjust the calculated gravity anomaly to the measured (before density change) it is both possible to change the geometry of the basalt body and the underlying basement. The dotted red line on the model profile indicates the change on the basalt necessary to adjust to the original gravity and the blue dotted line marks the change on the basement. The original potential field signature is given by black dotted lines, the red lines indicate the change resulting from adjustment of basalts and the blue lines reflect the effect on the potential fields by the basement shift. Note the reduced sub-basin depth from 8000 to 6000 m.

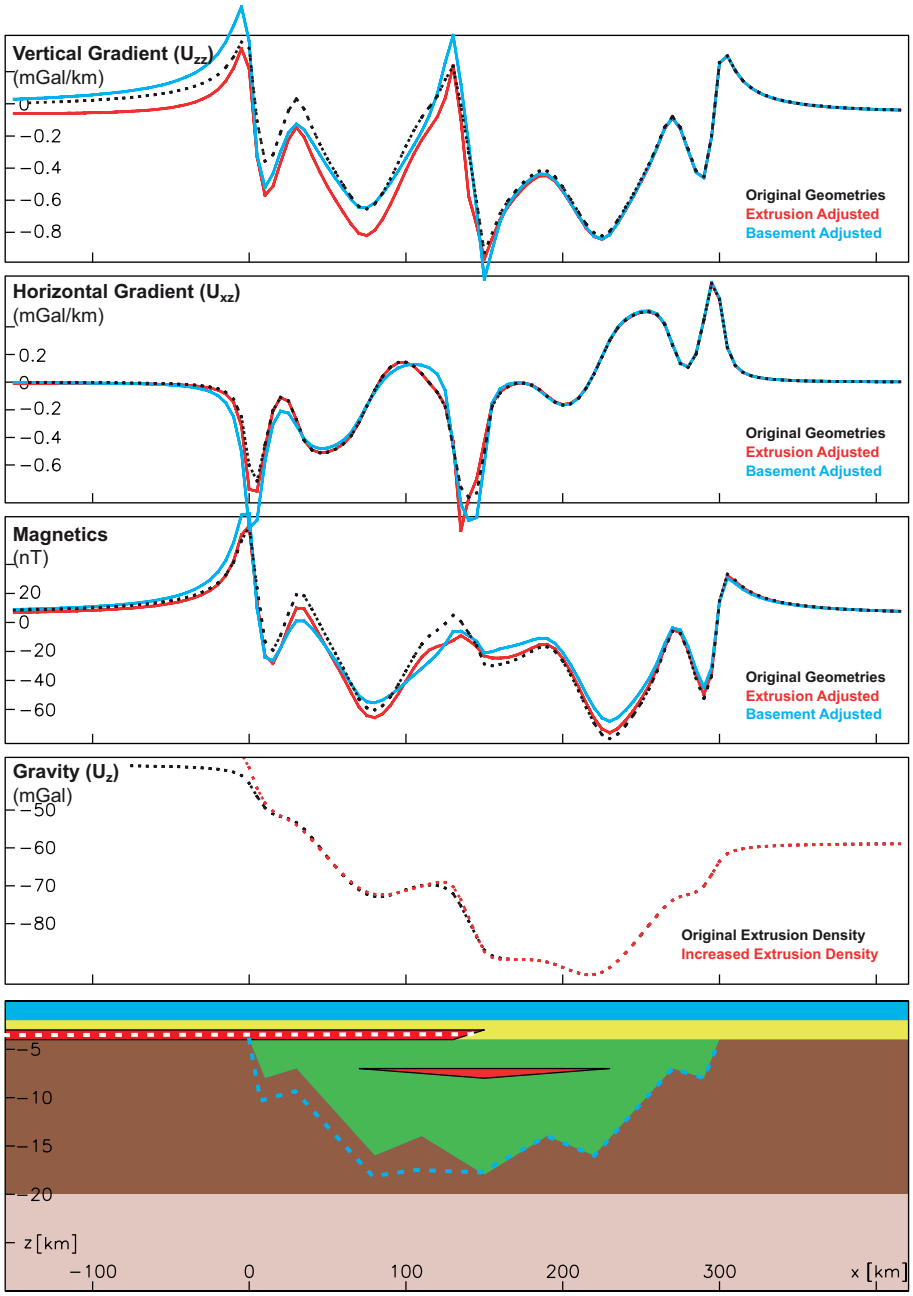

Figure 5.10. The effect of increased basalt densities. Increasing the density of the basalt flow increases the gravity (U_z) effect of the model. The calculated gravity anomaly was adjusted to the measured (before density change) by changing the geometry of the basalt body and the underlying basement. The dotted red line on the model profile indicates the change on the basalt necessary to adjust to the original gravity and the blue dotted line marks the change on the basement. The original potential field signature is given by black dotted lines, the red lines indicate the change resulting from adjustment of basalts and the blue lines reflect the effect on the potential fields by the basement shift. The depth of the sub-basin is now increased to more than 10 km.

(seismic) control existed on the bathymetry, sedimentary horizons, top basalt, top sill, and top basement where it is not overlain by volcanics. It was also assumed that the petrophysical properties (wells) were well constrained for the sediments. The density of the basalt was changed from 2700 kg/m^3 to 2600 and 2900 kg/m^3. Then the basalt and sedimentary thickness was altered to match the observed and calculated gravity field. The effect on the magnetic field, and U_{xz} and U_{zz} gravity gradients were observed as well.

Decrease in the basalt density from 2700 kg/m^3 to 2600 kg/m^3 results in a mismatch of approximately 5 mGal between the observed and calculated gravity but has almost no impact on the gradient fields and no effect on the magnetic field (Figure 5.9). For comparison satellite altimetry gravity data in the Norwegian-Greenland Sea is estimated to have ~3 mGal uncertainty (Engen *et al.* 2006) and shipboard surveys are estimated to contain ~1 mGal uncertainty (Dragoi-Stavar & Hall 2009). To fit the calculated field to the observed one the depth to the top of the basement was decreased by approximately 1500 m below the basalt. The 5 mGal difference remains on the west side of the model and could be taken as an indication of shallow Moho or gradual lateral variations in sediment density. Even if a good match between observed and calculated gravity fields is acquired in the basin area a slight mismatch exists on the gravity gradient fields. The magnetic anomalies also show slight mismatch.

Instead of changing the geometries of the basement it is also possible to increase the thickness of the basalt to acquire the same fit between the observed and calculated gravity fields. The change results in basalt thickness of 2.2 km which is an increase in thickness estimate of 1.2 km. The gravity gradients calculated from this new geometry are very similar to the gradients derived from the top basement depth decrease. The magnetic signal on the other hand shows a more pronounced mismatch (approximately 50 nT) at the edge of the basalt.

Increase in the basalt density from 2700 kg/m^3 to 2900 kg/m^3 results also in a mismatch of the calculated and observed gravity of approximately 10 mGals (Figure 5.10). Slight difference is also observed on the gravity gradient fields. Deepening the basement by 2000 m in order to fit the observed gravity signal to the calculated results in mismatch of the gravity gradients and magnetic anomalies to a similar degree as mentioned above. Thinning of the basalt plate to 500 m from 1 km produces the same fit between the observed and calculated gravity anomalies but the gradients are more affected at the basalt edge.

5.4 Application to the Møre margin

The study area has the same dimensions as the synthetic model and is defined by a 300x400 km rectangle. It includes the Møre Basin from the shallow continental coast to the Møre Marginal High and extends into the oceanic domain (Figure 5.1).

The magnetic anomalies in the study area (Figure 5.1b) range between -300 and 300 nT with the exception of the Frøya High that has a magnetic anomaly of approximately 1300 nT. A prominent magnetic high extends from the SW of the basin to the NE. The basin is generally characterized by a rather quiet magnetic field disturbed by occasional SW-NW trending anomalies that follow the main structural features. Westward of the Faroe-Shetland Escarpment the magnetic characteristics change dramatically, probably caused by relatively shallow volcanics.

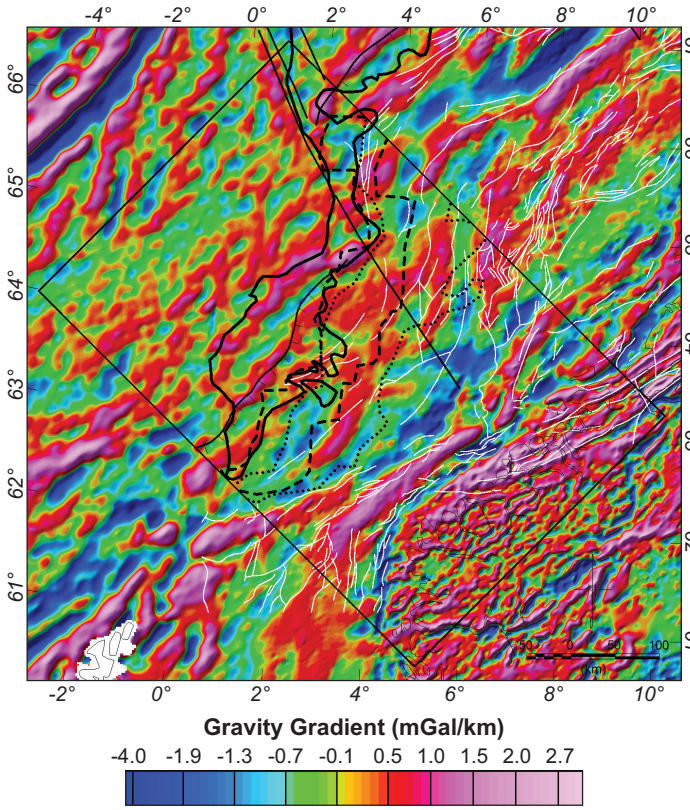

Figure 5.11. Gravity gradient of the Møre margin. Gravity gradient (U_{yz}) derived from the free-air gravity anomaly (U_z). The orientation of the gradient is across the main structural grain of the Møre margin or 315 degrees (SE-NW). Comparison with the overlying faults demonstrates the efficiency of the gradient as a boundary finder. Gravity gradient from the Møre margin compared to volcanic distribution. The black solid line outlines the distribution of basalt flows on the margin (from Planke *et al.* (2005)). The hatched line marks the areal distribution of saucer shaped sill intrusions and the dotted line indicates the extend of deeper sills in the Møre Basin.

The free-air gravity anomaly (Figure 5.1c) has a range from -45 to 65 mGals in the study area and a general trend orientated SW-NE corresponding to the main structural features. A prominent gravity low exists in the eastern part of the basin adjacent to the Jan Mayen Lineament that seems to obliterate the gravity effect of the Vigra High and other basement highs in the area. The Bouguer gravity anomaly (Figure 5.1d) demonstrates that a part of this gravity low can be explained by the effect of deep bathymetry.

Comparison between the gravity anomaly maps and the magnetic anomaly map reveals some differences but the overall trend is similar. The most prominent difference in the basin is associated with the SW-NE trending magnetic anomaly and considerable dissimilarities exist on the marginal high.

The gradient direction was set perpendicular to the general structural trend on the Møre margin. The resulting gradient map (Figure 5.11) shows very good agreement with previously mapped large scale structures in the area, enhances the basement highs and lows, and indicates structural variability on the marginal high.

A preliminary 3D gravity and magnetic model of the Møre margin from the Norwegian coast to the oceanic domain constrained by seismic, and petrophysical data provided an approximation to the regional structures of the margin (see Chapter 6 for details on model). The petrophysical properties used in the 3D model are listed in Figure 5.12. A profile from the model along the seismic line GMNR102-94, that has been used to study the volcanostratigraphy of the Møre margin (Planke & Alvestad 1999, Berndt *et al.* 2001b), was used to constrain the sub-basaltic basement structure (Figure 5.12). The line was depth converted by using interval velocities obtained from exploration well (NPD 6204/11-1) and published seismic refraction studies in the vicinity of the line (Ólafsson *et al.* 1992). The geometries from the seismic line were adjusted to the gravity and magnetic fields. The resulting model slightly deviates from the seismic interpretation but the general trend is similar. The model indicates a sub-basaltic basin on the marginal high (marked A on Figure 5.12). The profile shows how the gravity gradients correlate to the modelled basement structure. Considerable difference exists between the modelled gradients and gradients derived from the Bouguer gravity compilation which illustrates that incorporation of the gradients in the modelling process would improve the model. The basins labelled B and C on Figure 5.12 produce responses in the calculated gradients that also differ considerably from the gradients derived from the gravity compilation of the study area. The gradients reflect the edges and shape of the basement structure and incorporation of the observed gradients in the modelling process would therefore provide valuable constraints to the model.

Euler deconvolution solutions along the profile manage to reflect the main basement structures relatively well in the basin and even give an indication of sub-basaltic basement lows (marked B and C on Figure 5.12). Where the basalt gets shallower and thicker no indication of the sub-basaltic basin is acquired from the Euler solutions. Experiments with different window sizes and structural indexes for the Euler deconvolution showed that a structural index of 0.5 gave the best basement depth estimates but varying the window size between 30, 60, 80 and 120 km did not have much effect (Figure 5.12). Upward continuation of the magnetic grid to diminish the effect of the shallow volcanics did not produce solutions that better reflected the underlying basement structure.

5.5 Discussion

The construction of synthetic models and calculation of the gravity and magnetic response of models with and without volcanics provides means to visualize and estimate the effect of volcanics on the different methods applied to the gravity and magnetic data. The synthetic models are a simple representation of the Møre margin and have a limited frequency spectrum. Even though the models are constructed in 3D the structural variations are much greater in the *x*-direction than in the *y*-direction and therefore only provide limited representation of a real geological setting in three dimensions. Nevertheless, the models provide basic insights into the usability and limitations of the potential field methods in offshore volcanic settings.

Modelling experiments on the Møre margin have demonstrated that sills at the modelled depth (7 km) cannot be identified from the potential field data unless considerably thicker than 100 m and with thicker edges. A shallower and, 1 km thick basalt layer has a clearer effect on both the magnetic and gravity signals. The gradient data enhanced and clearly brought out the basalt edge. No lucid indication of volcanics could be acquired from the

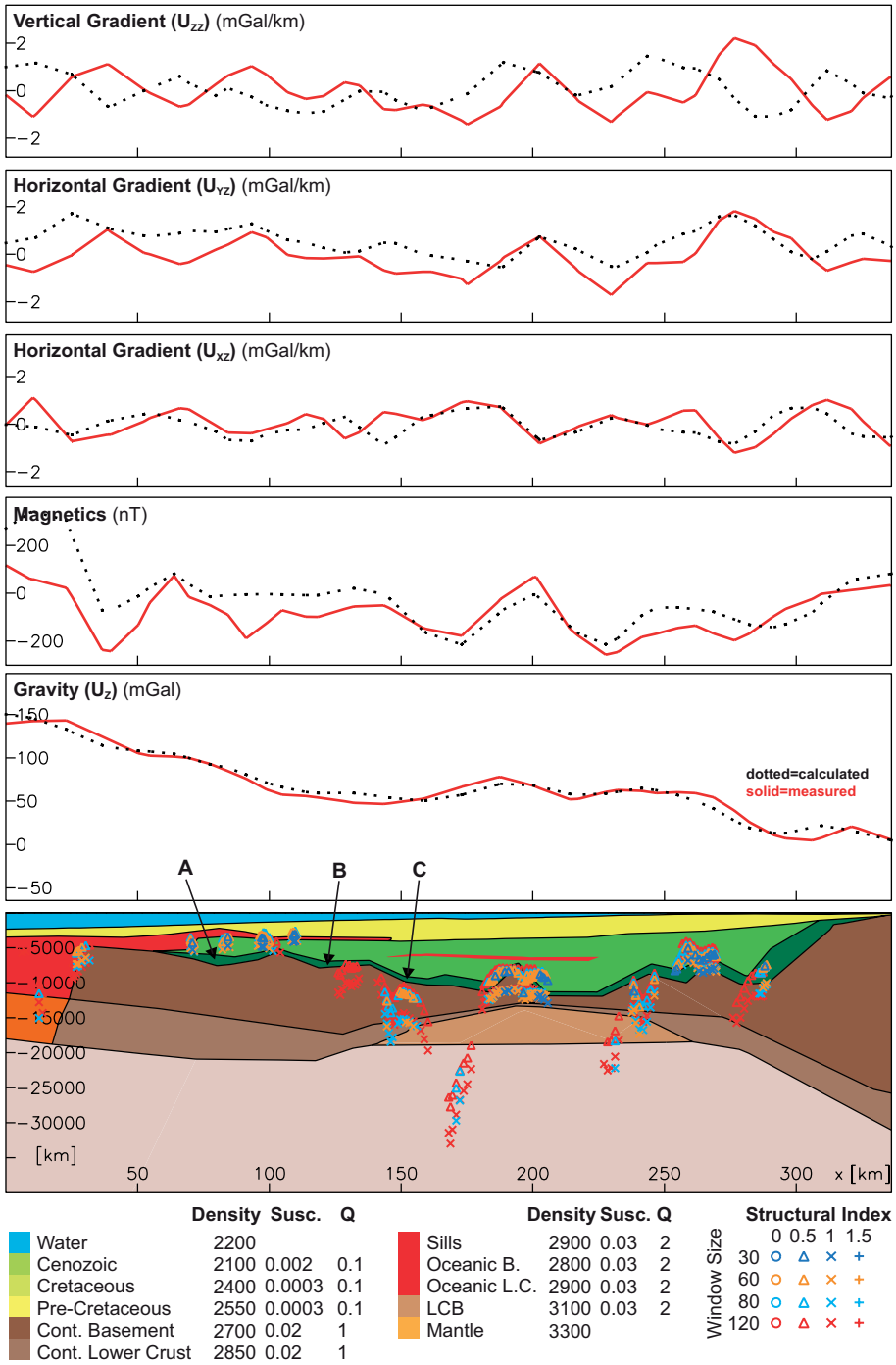

Figure 5.12. A profile view from the Møre margin from a 3D density and magnetic model along the the GMNR94-102 seismic line (see location of profile a-a' on Figure 5.1). Letters A, B and C indicate sub-basaltic basins mentioned in the text. Density is in kg/m^3, magnetic susceptibility (Susc.) is in SI units, and magnetic reamence is given as Königsberger ratio (Q).

gravity and magnetic data from the Møre margin. Lateral distribution of the sills and basalt flows could not be linked consistently with any gravity or magnetic signal in the study area. The gravity gradient calculated from the free-air grid didn't give any clear indication of the volcanics edges either (Figure 5.11). The fact that the synthetic gravity gradient data clearly expresses the basalt edges that can not be observed on the gravity data from the Møre margin, implies a practical difference between observed gravity gradient data and gravity gradient calculated from conventional gravity data. The noise inherent in the conventional gravity data is amplified with calculation of the gradient and interferes with shorter wavelengths. Measured gravity gradient data, as represented by the synthetic model, do not contain linear acceleration noise like the conventional gravity data and therefore provide more information at the shorter wavelengths.

The sub-basaltic basement structure of the synthetic model is difficult to resolve from the magnetic and gravity anomalies but the gravity gradient data give a much better image of the sub-basaltic basin (Figures 5.5 and 5.6). The same observations are made on the data from the Møre margin, the gravity gradient map indicates basement structure neither indicated by the magnetic nor by the free-air or Bouguer anomalies. A profile view of the 3D density and magnetic model demonstrates how well the horizontal gravity gradient relates to the basement undulations in the study area (Figure 5.12). The profile also shows a considerable agreement between the forward model and the calculated gradient in positioning of the sub-basaltic basin on the Møre Marginal High. The noise content of the conventional gravity does not appear to interfere as much with the signal from the basement as with the signal from the shallower volcanics.

Experiments with Euler deconvolution on the magnetic grids, both from the synthetic models and the Møre margin, demonstrated that the method can be useful to estimate the basement structure where little volcanic disturbance exists. The method gave an indication of the sub-basaltic basin in the synthetic model but produced no solutions in the sub-basaltic basin on the Møre Marginal High indicated by the forward model and the horizontal gravity gradient. Tests on increased observation levels on the synthetic model and an upward continued grid of the Møre margin did not enhance the results. The reason for this is probably how the upward continuation method attenuates the high wavenumbers (low frequency) relative to the low wavenumbers (high frequency). The process involves multiplication in the Fourier domain of the transformed data and not only enhances the low frequency but also attenuates the high frequencies. The result is hidden attenuated noise in a smooth appearing grid. The Euler deconvolution utilizes the gradient of the field and is therefore very sensitive to the noise in the data and the unexpected results from the upward continued data are most likely product of this. Results from the synthetic model show that Euler solutions can be used as volcanic edge detector but this could not be demonstrated on the Møre margin probably because of the great water depth and burial depth of the volcanics.

The forward models demonstrate how sensitive the gravity and magnetic signals are to the extent and geometry of the volcanics. Deep sills have almost no effect on the signals and can not be mapped in the setting presented in this study. Shallower basalt flows have much greater impact on the gravity and magnetic fields. The impact is on a wide frequency range as the large scale basaltic plate has a long wavelength signal but the small scale geometric undulations and edges have short wavelength effect. The gravity anomalies are more sensitive to the large scale variations but the magnetic anomalies are more responsive to the small scale structures.

In order to estimate basalt thickness and sub-basaltic sedimentary thickness from a forward model good geometrical constraints on the model are vital. Top basalt can easily be constrained by seismic interpretations and magnetotellurics (MMT) can be used to acquire the top basement structure (Heincke *et al.* 2006, Reynisson *et al.* 2008). As demonstrated on the synthetic model, measured gravity gradients help in detecting edges and lateral structural variations that provide further geometrical constraints. The remaining unsolved horizon is the contact between the basalts and the sediments. The location of this horizon is heavily dependent upon the geophysical properties used in the model. The values defining the physical properties can only be assumed based on well data and parameter studies and create considerable uncertainty in the estimates. Volcanic density of 2700 kg/m^3 instead of 2600 kg/m^3 would result in approximately 1 km difference in thickness estimates. As demonstrated on the synthetic model the integrated modelling of the gravity and magnetics reduces the freedom of property variations and therefore tightens the thickness estimates.

5.6 Conclusions

Volcanics affect the gravity and magnetic signals over a wide range of wavelengths, making it very difficult to distinguish between overlying basalts and underlying basement. The longer wavelengths interfere with the signal from the basement structure and the shorter wavelengths are greatly disturbed by noise and therefore the recognition of both basement and volcanics is problematic in the sub-basaltic environment.

Euler deconvolution, as an example of a routinely used magnetic depth estimate method provides valuable depth solutions in the volcanic environment but is not capable of identifying a basin overlain by basalts approaching 1 km thickness. High observation levels and an upward continuation did not enhance the solutions.

Forward density and magnetic models provide a valuable tool to estimate both the basalt and sub-basaltic sedimentary thickness but are limited by the ambiguity inherent in the potential field methods. Integration of gravity and magnetic in the modelling process provides better constraints than modelling each geophysical property in isolation. In particular, the use of gravity gradients further decreases the available model solutions and provides boundary detection even in sub-basaltic settings. Even with the increased availability of FTG data and increase in FTG technology geometrical constraints provided by seismic are vital to the potential field methods, as are well studies and other investigations that provide control on the petrophysical properties.

Sub-basaltic seismic imaging remains problematic and therefore the integration of other available geophysical methods (i.e. electromagnetic methods) is important to further enhance sub-basaltic images. Careful characterization of the volcanics and the sub-basaltic sediments are also very important to better control geophysical interpretations.

Acknowledgements
We would like to thank two anonymous reviewers and the editor M. Fedi for helpful comments which led to significant improvements in the manuscript. This study is part of a PhD project titled 'Sub-basalt exploration using integrated gravimetric-, magnetometric- and seismic- (velocity) models, with isostatic considerations' financed by Shell. The Geological Survey of Norway and TGS-NOPEC provided the gravity, magnetic and bathymetry data. The 3D modelling was performed using the software package IGMAS.

Chapter 6
A regional 3D model of the Møre margin

Reynisson, R. F. & Ebbing, J. In prep. Deep structure of the Møre margin, offshore Norway. Part 1: a regional 3D model of the Møre margin.

The mid-Norwegian margin has been subject to extensive interest from both industry and academia for the past four decades. Numerous geophysical experiments have been undertaken that have shed light on the crustal structure of the margin and its evolution. The margin is classically defined as a volcanic passive margin that went from rift to drift in Early Cenozoic (e.g. Eldholm *et al.* 1989, Skogseid & Eldholm 1989). New ideas on the tectonic style and the margin's development have been emerging (Osmundsen *et al.* 2002, White *et al.* 2005, Osmundsen & Ebbing 2008) fuelled by studies on magma-poor passive margins (e.g. Boillot & Froitzheim 2001, Whitmarsh *et al.* 2001, Manatschal 2004, Lavier & Manatschal 2006, Reston & Pèrez-Gussinyé 2007). It is suggested that observed detachment faults have the potential to reduce the crustal thickness to a level where the whole crust becomes brittle and paths the way for mantle exhumation (Osmundsen & Ebbing 2008).

The distal parts of the mid-Norwegian margin are greatly masked by magmatic products from the Cenozoic breakup phase. The lavas on the marginal high severely impede seismic imaging of the deep crustal structure. Sills and the mere thickness of the sedimentary successions in the basins also impede imaging of the deeper crust. In order to address the architecture of the margin from the coast to the COB a 3D potential field model was constructed. The model provides new and relevant constraints on the maximum extent of the continental crystalline basement, sub-basalt geometry, the nature of the rift and proto-ridge structures and the distribution of lower crustal bodies along the margin. This study focuses on the Møre margin segment (Figure 6.1) and how the deeper crustal structures relate to the newly established ideas on the mid-Norwegian margin.

Information about the gross crustal structure can be obtained by modelling potential field data, especially gravity, if the basin sediment fill and the water column contributions can be removed successfully from the total gravity field. The free-air gravity anomaly has a range from -45 to 65 mGal in the study area and a general trend orientated SW-NE corresponding to the main structural features. A prominent gravity low exists in the eastern part of the basin adjacent to the Jan Mayen Lineament that seems to obliterate the gravity effect of the Vigra High and other basement highs in the area. The Bouguer gravity anomaly (Figure 6.2a) demonstrates that this gravity low can largely be explained by the effect of deep bathymetry. The magnetic anomalies in the study area range between -300 and 300 nT

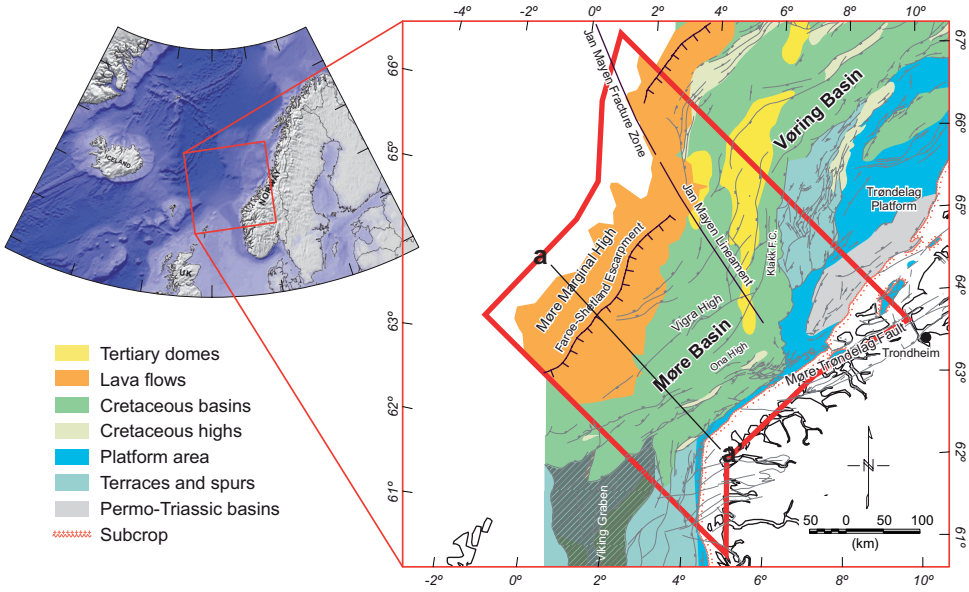

Figure 6.1. Overview of the study area. The thick red line outlines the modelled area. Structure map modified from Mosar (2002). Profile a-a' is shown in Figure 6.6.

with the exception of the Frøya High that has a magnetic anomaly of approximately 1300 nT. Along the central axis of the Møre Basin a prominent linear magnetic high extends from the SW of the basin to the NE (Figure 6.2b). This magnetic anomaly, dubbed the Møre Basin Magnetic Anomaly (MBMA), has a complex reletion to the gravity anomaly. The basin is generally characterized by a rather quiet magnetic field disturbed by occasional SW-NW trending anomalies that follow the main structural features. Westward of the Faroe-Shetland Escarpment the magnetic characteristics change dramatically, probably caused by interference of relatively shallow volcanics with deeper sources.

6.1 Data Sources

6.1.1 Potential Field Data

The gravity data is a compilation from the the Geological Survey of Norway (NGU) of Norway and adjacent ocean areas (Skilbrei *et al.* 2000). The data used in the compilation contains offshore measurements of ~59 000 km of marine gravity profiles that have been acquired by the Norwegian Petroleum Directorate, various oil companies, universities, and the Norwegian Mapping Authority. Gravity data from satellite altimetry (Laxon & McAdoo 1994, Andersen & Knudsen 1998) were used to fill in data gaps in the deep ocean area. The International Gravity Standardization Net 1971 (IGSN 71) and the Gravity Formula of 1980 for normal gravity were used in the derivation of the anomaly values. The combined data set consists of free-air anomaly offshore and terrain-corrected Bouguer anomaly onshore that were interpolated to square cells of two km using the minimum curvature method. In order to eliminate the effect of the bathymetry on the gravity signal a complete Bouguer anomaly was calculated offshore. A bathymetry compilation from the Geological Survey of Norway by Dehls *et al.* (2000) and a reduction density of 2200 kg/m^3 was used for this purpose.

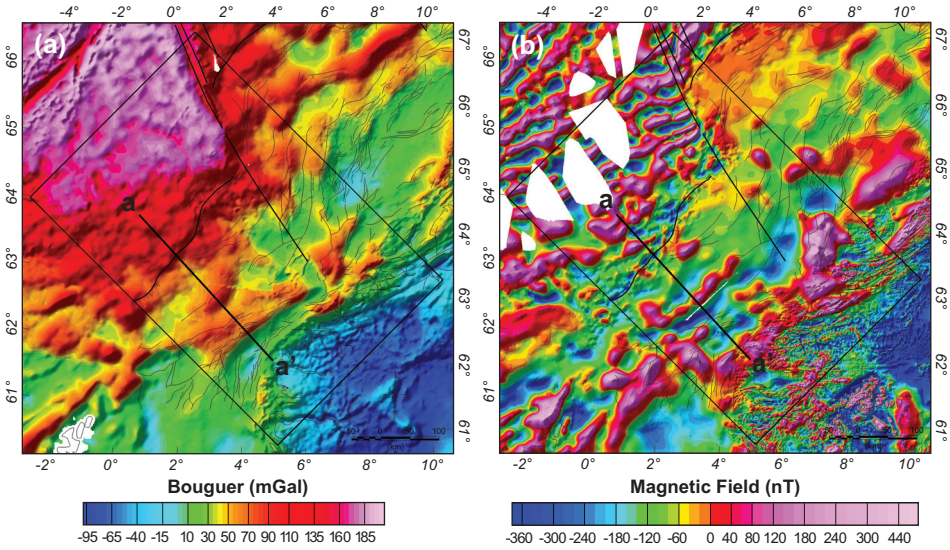

Figure 6.2. Gravity and magnetic anomaly maps of the Møre margin. (**a**) Bouguer gravity anomaly and (**b**) total magnetic field anomaly. Fault boundaries are marked by thin black lines and major tectonic features with thick black lines (after Blystad *et al.* 1995). The box outlines the study area and the thick black line marks the profile a-a' (GMNR94-102) presented in Figure 6.6. The magnetic data compilation is from Olesen *et al.* (1997b) and the gravity data is a compilation by Skilbrei *et al.* (2000). The Bouguer reduction was based on bathymetry data from Dehls *et al.* (2000) and a density of 2200 kg/m^3.

High-resolution satellite derived free-air data is estimated to have an altimetric resolution of ~4 mGal over 10–15 km wavelengths on the African margin (Fairhead *et al.* 2001a, Fairhead *et al.* 2001b). The resolution is assumed to increase with higher latitudes because of better crossing angles between satellite tracks. Overlapping satellite and marine gravity measurements in the Arctic Ocean differ 2.64–3.11 mGal (Childers *et al.* 2001). On this Engen *et al.* (2006) estimated their satellite altimetry gravity data compilation in the Norwegian-Greenland Sea to have ~3 mGal uncertainty. The resolution of shipboard surveys is estimated to be ~1 mGal over 5–10 km wavelengths (Dragoi-Stavar & Hall 2009). Based on this we assume that the NGU compilation grid (Skilbrei *et al.* 2000) has between ~1 and ~3 mGal uncertainty, increasing from shore to deep sea.

The magnetic data is from a magnetic anomaly map of Norway and adjacent ocean areas compiled by Olesen *et al.* (1997a). The data sources in our study area are total-intensity airborne measurements with flight altitudes varying between 200 and 500 m. The line spacings were smallest over mainland Norway (0.5–2.5 km), intermediate over the continental shelf (3–8 km) and largest over deep oceanic area in the Norwegian and Greenland Seas (10–15 km). Inaccuracy in navigation affects the continuity of some sea floor spreading anomalies. No attempt was made to transform magnetic-anomaly data to a common altitude. The aeromagnetic data from mainland Norway and the Norwegian continental shelf are based on a 500x500 m grid interpolated from digitised hand-drawn contour maps. After some level adjustments the grids were combined into a single grid with 1x1 km cells.

6.1.2 Seismic Data

The seismic data used in this study comprises both reflection and refraction data. The majority of the reflection seismic is a proprietary industrial data provided by Shell but all of the refraction data is based on previous publications.

Ten seismic lines from the MNR survey (Figure 6.3) recently acquired by Fugro Multi Client Services (FMCS) in cooperation with TGS-NOPEC Geophysical Company were used to address the deep structure of the Møre margin. The MNR data was acquired with a 10 km streamer, a relatively large source and with a record length of 10 seconds. These long offset data are of high quality and provide a novel view on the regional geology in the study area. As can be seen on Figure 6.3 the MNR lines in our database are focused on the eastern part of the study area. The lines were depth converted by utilizing Shell's stacking velocity cube of the mid-Norwegian margin.

A long-offset seismic line (GMNR94-102) that has been used to study the volcanostratigraphy of the Møre margin (Planke & Alvestad 1999, Berndt *et al.* 2001b) was used to acquire deep view on the central part of the study area. The line was depth converted using interval velocities obtained from exploration well (NPD 6204/11-1) and published seismic refraction studies in the vicinity of the line (Ólafsson *et al.* 1992) (Table 6.1).

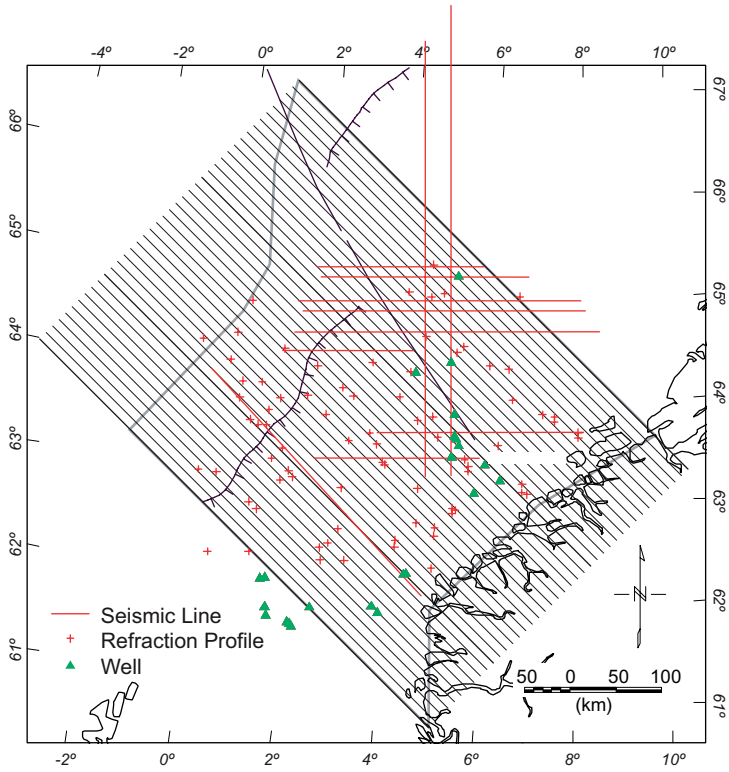

Figure 6.3. Supplementary data. The black parallel lines show the location of all the sections of the 3D model. The thick black lines indicate the location of the sections in Figure 6.12. Red lines indicate the seismic lines used in this study. Red crosses show location of seismic wide-angle experiments used to constrain deeper structures. Triangles represent NPD exploration wells that provided petrophysical information for the study.

Table 6.1. Petrophysical properties applied in model. Density is in kg/m^3, velocity is m/s, magnetic susceptibility (Susc.) is in SI units, and magnetic remanence is given as Königsberger ratio (Q).

	Density	Velocity	Susc.	Q
Water	1030	1460	0	0
Cenozoic	2100	1800–2600	0.001	0.4
Cretaceous	2500	3000–4400	0.0003	0.4
Pre-Cretaceous	2600	4000–5000	0.0003	0.4
Continental Basement	2750	6000–6500	0.02	1
Lower Continental Crust	2900	6000–6500	0.005	0.5
Oceanic Basement	2700	4500–7000	0.02	2
Lower Oceanic Basement	3100	7000	0.02	2
Volcanic flows	2700	4500–7000	0.02	2
Volcanic intrusions	2700		0.05	0
Lower Crustal Body	3100	7000	0.01	0.5
Mantle	3295–3300	8000	0	0

In addition to lines from the MNR survey Shell provided access to their seismic database on the mid-Norwegian margin. The Base Cretaceous and Base Tertiary unconformities interpretations in the Møre Basin were extracted from this dataset. The horizons extend from the Norwegian coastline towards the Faroe-Shetland escarpment where the seismic signal deteriorates as a consequence of volcanic emplacement. The dataset was also used to map the distribution of igneous rocks on the Møre margin (Figure 6.4).

Data from seismic wide-angle experiments in the study area were provided by the Universities of Oslo and Bergen. The data are from four different experimental setups, unreversed sonobuoys (Talwani & Eldholm 1972, Eldholm & Mutter 1986), reversed sonobuoys (Ewing & Ewing 1959), expanding spread profiles (Ólafsson *et al.* 1992), and OBS profile 8A-96 (Raum 2000).

6.1.3 Well Data

Composite logs from 21 NPD exploration wells on the Møre margin were analysed to acquire petrophysical data on the sediments in the study area. Few logs also contained data on the crystalline basement. An average on 20 m intervals was recorded for both density and sonic logs. The lithostratigraphic units on the logs were grouped into three main groups: Cenozoic, Cretaceous, Pre-Cretacous, and basement (Figure 6.5, Table A.1).

No well in the study area provided information on the petrophysical properties of the igneous rocks in the area. Scientific drilling has provided data on volcanics on the neighboring Vøring margin (Kent & Opdyke 1978, Eldholm *et al.* 1987, Planke 1994, Planke & Eldholm 1994) and intrusives have been sampled in NPD well 6607/5-2 (Berndt *et al.* 2000).

6.2 Seismic Interpretation

The main focus of the seismic interpretation was the deep structure of the margin from affecting Base Cretaceous and deeper levels. The goal was to obtain the configuration

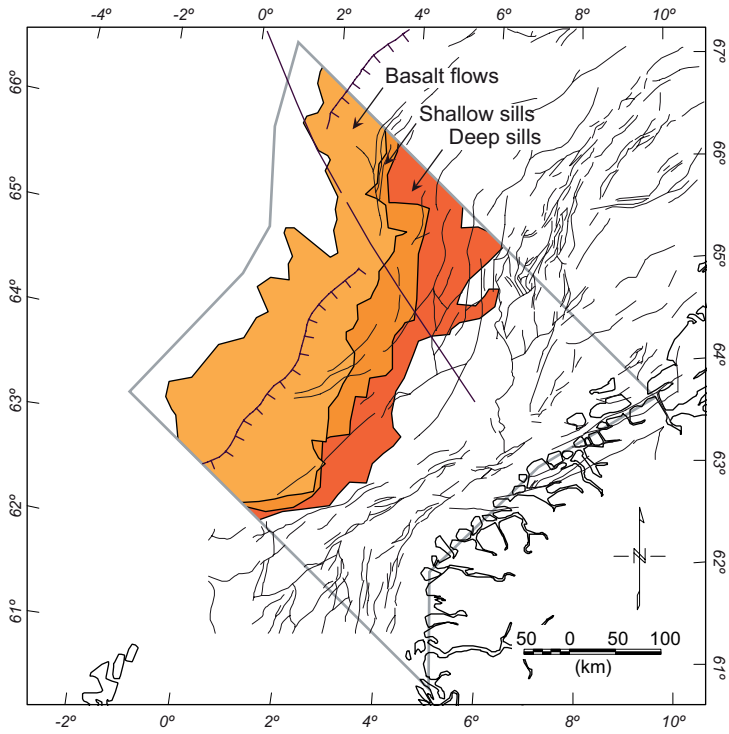

Figure 6.4. The distribution of magmatic rocks in the study area based on seismic interpretation.

and style of the deep-seated structures to provide a geological input in the potential field model. The lateral distribution of both extrusives and intrusives was also a primary focus to constrain the top of the lava flows and intrusions in the study area.

The MNR lines and the GMNR line, recorded to 10 and 14 s two-way time (TWT), provided means to address the deep structure of the study area. Shell's interpretation of the near-base Cretaceous unconformity (BCU) provided a starting point to the interpretation. The base of the Cretaceous corresponds to a strong seismic marker (e.g. Bukovics & Ziegler 1985, Blystad *et al.* 1995, Gabrielsen *et al.* 1999, Brekke 2000) and is well defined as an onlap surface. Within the basin areas itself the BCU lies very deep and is difficult to interpret. Towards the west sills further hamper the interpretation of the BCU and deeper structures. Below the BCU dipping reflector packages can be observed and are interpreted to represent pre-Cretaceous sediments. The seismic basement is defined as the deepest continuous reflection and as noted by Osmundsen *et al.* (2002) it is likely that the seismic basement conceals pre-Middle Triassic successions. The deepest observed reflections are disconnected reflector bands comparable to those described by Osmundsen and Ebbing (2008).

The intrusions (sills) were divided in two different units based on the seismic signature and depth. Both units are characterized by high amplitude reflection, local transgression and abrupt terminations. The shallower unit is recognized by its saucer-shape and rough seismic character. The deeper unit has a smooth seismic character, strong amplitude signal, and a large degree of continuity. The shallower sills were easily recognized in the basin on seismic data, but oceanward of the escarpment they are very difficult to observe. The

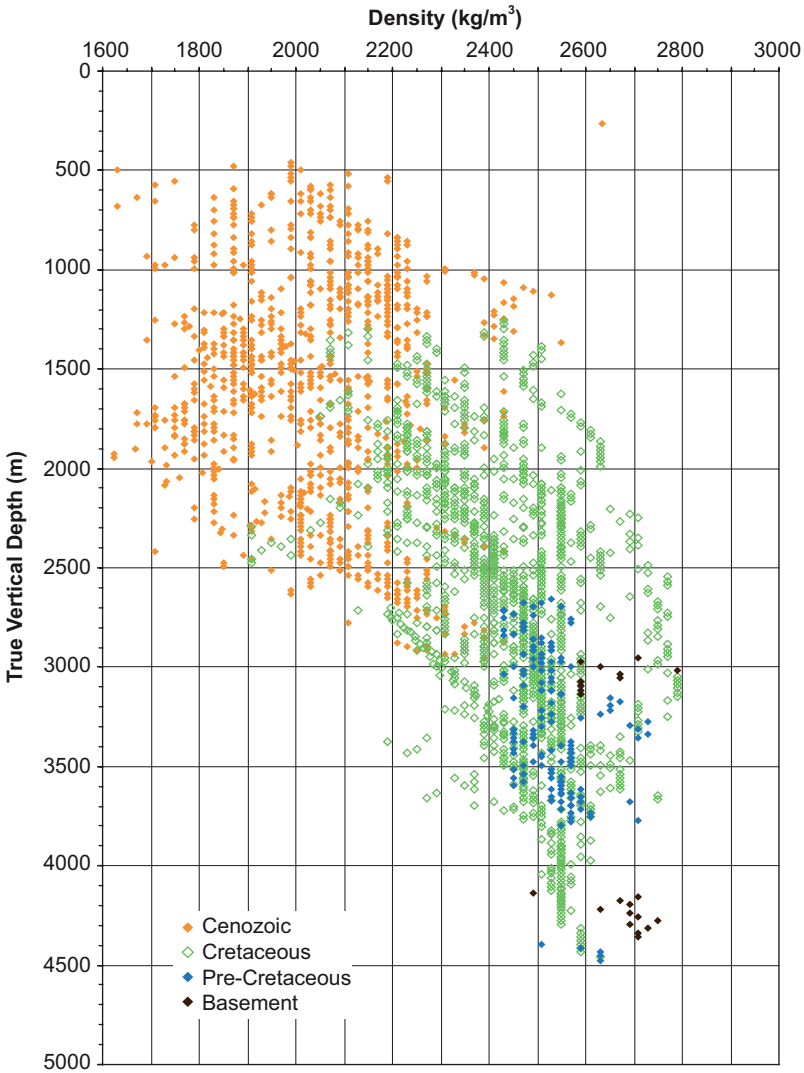

Figure 6.5. Density from NPD wells. The figure shows the trend of density with depth of four main lithological units from 21 exploration wells on the Møre margin (see Figure 6.3 for location of the wells).

deeper sills could be mapped with relative ease in the basin but are untraceable beyond the escarpment. The extrusives (lavas) were interpreted as one body which was relatively easily identified because of the high impedance contrast between post-rift sediments and the top-basalts, resulting in a strong reflector.

6.3 3D Potential Field Model

In general, forward model calculation involves four steps. First a reasonable model is constructed, often from available seismic and well data. Then its effective gravity and magnetic signal is calculated and compared to the observed anomalies. Finally alteration

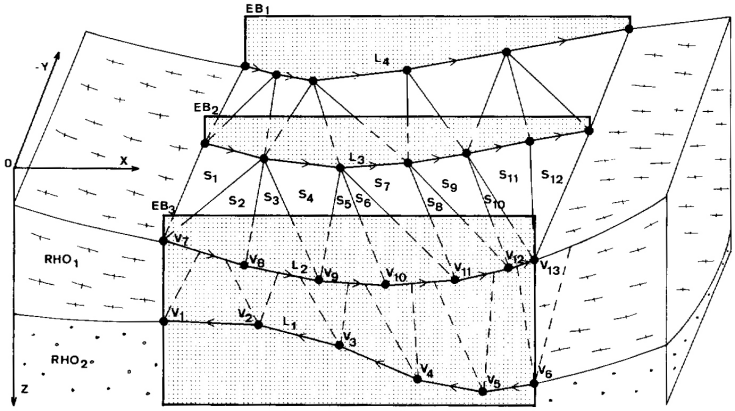

Figure 6.6. A simple two-layer structure modelled with three vertical sections where *EB* are vertical sections, *V* are model vertices, *L* are lines and *S* are triangles (Götze & Lahmeyer 1988).

of the model takes place to improve correspondence of observed and calculated anomalies. The process is iterative and the goodness of fit between observed and calculated anomalies is gradually improved. The forward modelling system used in this study was the 3D modelling package IGMAS (Interactive Gravity and Magnetic Application System). The system uses polyhedrons with triangulated surfaces to approximate bodies of constant density and/or susceptibility within the Earth. Their geometry is defined by a number of parallel vertical modelling sections. The model is divided into vertical sections as shown in Figure 6.6. All the other elements of the model (geometric and material parameters) are contained in these planes. Within individual planes a series of vertices comprises a line which marks the layer boundary with the respective plane. The layer boundaries stabilize the 3D model structure by encompassing the lines of neighbouring planes which are separated by identical parameters (density or susceptibility) complexes. Thus, in Figure 6.6 the lines L_2, L_3, and L_4 are brought together into a layer boundary surface. Each layer boundary consists of triangles which have the V_i as their vertices. The vertices which are encompassed by the basic element layer lines are joined into triangles within a layer (Götze & Lahmeyer 1988). The system then calculates the potential field effect of the model at a designated station location. The analytical solution of the volume integral for the gravity and magnetic effect of a homogeneous body is based on the reduction of the volume integral to an integral over the bounding triangles (Götze 1984, Götze & Lahmeyer 1988). In the modelling interface, after geometry changes the gravity effect of the model can quickly be updated because only the changed triangles have to be recalculated. Changes of the model geometry are restricted to predefined parallel vertical sections. This is a small restriction to the flexibility but makes geometry changes easy. No complex 3D editor is needed. The vertical sections are displayed together with the measured and calculated gravity fields, the geometry is updated and the gravity recalculated immediately after each change. The next section is then displayed and changed (Lahmeyer *et al.* 2010).

The constructed model consists of 42 cross-sections with a regular spacing of 10 km (Figure 6.3). Each cross-section is made of several geometrical bodies with varying physical properties (Table 6.1). Each geometrical body is representative of a regional geological structure and has constant density and magnetic properties. The geometry of each section

in the model was configured to match all available data, first the constraint data and then the gravity and magnetic data.

6.3.1 Model Geometry

The model consists of water, sediments, crystalline crust, igneous rocks, lower crustal body, and halfspace (upper mantle) that extends to a depth of 200 km. The sediments were subdivided in three units based on seismic data. The different units represent Cenozoic, Cretaceous, and Pre-Cretaceous. The igneous rocks accounted for in the model were lava flows on the marginal high and intrusions in the basin. Both the continental and oceanic crystalline crust was divided in two subunits to account for increase in density with depth and vertical variation in magnetic properties.

Depth converted horizons of the Base Cretaceous and Base Tertiary unconformities in the Møre Basin provided geometrical constraints for the main sedimentary structures. These horizons are based on extensive proprietary industrial dataset and gave as good geometrical control to the model as possible to date. The horizons extend from the Norwegian coastline towards the Faroe-Shetland escarpment where the seismic signal deteriorates as a consequence of volcanic emplacement. The top of the extrusives was interpreted from reflection seismic data and imported in the model. Estimation of depth to magnetic basement provided a starting point for modelling the top basement horizon. Structural index 0.5 and a window size of 50 km was used which is in concordance to results from a feasibility study on the use of Euler Deconvolution in basement mapping on the

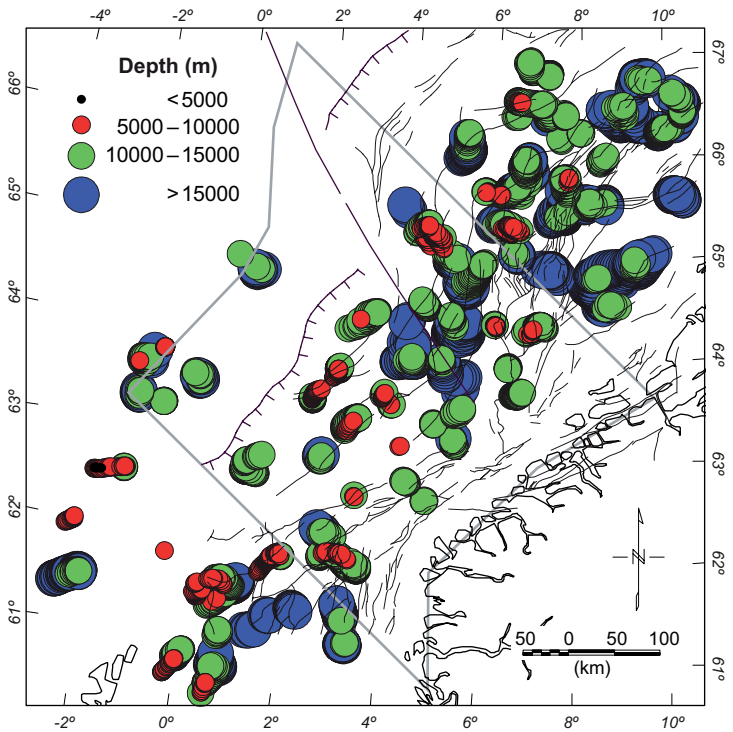

Figure 6.7. Euler 3D Deconvolution depth solutions. Depth to magnetic basement from a structural index 0.5, window size 40 km and statistical depth uncertainty 3%.

Møre margin (Chapter 5). The resulting depth estimates tend to cluster vertically beneath the true location of the causative body and magnetic basement was interpreted as the top of the vertical cluster. The results (Figure 6.7) provide a good and independent starting point for the location of the basement in the 3D model, especially in the eastern part of the study area where igneous rocks don't obscure the underlying basement. The Moho was constrained at the coastline of Norway with the compilation by Kinck *et al.* (1993) and its modifications by Olesen *et al.* (2002) and Ebbing *et al.* (2006). Data from seismic wide-angle experiments also provided constraints to the basement and Moho.

In order to use absolute densities in the model a reference model was constructed to represent the normal lithospheric density. The reference model used in this study has three layers: the upper crust (0–12 km: 2700 kg/m^3), the lower crust (12–30 km: 2900 kg/m^3), and the upper mantle (30–200 km: 3300 kg/m^2) and is in general agreement to global scale velocity and density distribution in the lithosphere (Dziewonski & Anderson 1981). To avoid edge effects the model was extended 500 km from the limits of the study area.

6.3.2 Layer Properties

Each model body was assigned a density, susceptibility, and magnetic remanence, which for consistency was kept constant for each body throughout the model. Table 6.1 summarizes the petrophysical database used in this study. Log data from exploration wells in the area and seismic refraction profiles provided density values for the sedimentary rocks. The magnetic properties are based on Hunt *et al.* (1995) and Mørk *et al.* (2002). Properties of the crystalline crust are based on previous modelling and petrophysical studies in the area (Mjelde *et al.* 1998, Mjelde *et al.* 2001, Olesen *et al.* 2002, Raum *et al.* 2002, Skilbrei *et al.* 2002, Fernàndez *et al.* 2004, Ebbing *et al.* 2006, Slagstad *et al.* 2008) (Tables A.2, A.3, A.4). Thermal modelling has showed that the Curie isotherm doesn't coincide with the Moho in the study area (Scheck-Wenderoth & Maystrenko 2008) but Ebbing *et al.* (2009) demonstrated that the depth extent of the magnetic sources on the mid-Norwegian margin are controlled by the overall geometry of the crystalline crust. In order to keep the model simple and not introduce internal variations to the modelled bodies it was decided to let the Moho define the boundary between magnetic and non-magnetic bodies. The effect of this is well within the sensitivity of the model as the magnetic anomaly was only modelled to fit the shape and not the amplitude. Density values for the LCB and Mantle are based on properties in a 3D model of the Vøring margin (Ebbing *et al.* 2006). These properties are based on velocity data that were acquired in OBS experiments on the mid-Norwegian margin (Mjelde *et al.* 1998, Mjelde *et al.* 2001, Raum *et al.* 2002). The velocity-density relations are estimated to contain errors in the order of +/-100 kg/m^3 (cf. Ebbing *et al.* 2006).

The petrophysical properties of the igneous rocks in the model are based on wells on the neighbouring Vøring margin. Magnetic properties were acquired from the Deep Sea Drilling Project (DSDP) Leg 38 and Ocean Drilling Program (ODP) Leg 104 in 1974 and 1985, respectively (Kent & Opdyke 1978, Eldholm *et al.* 1987). Cores from ODP well 642E provided bulk densities for over 900 m of volcanic rocks. An extensive wire line logging program recorded physical property variations of the upper volcanic section that resulted in average density of 2500 kg/m^3 but the individual lava flows showed cyclic pattern with densities ranging from about 2300 to about 2800 kg/m^3 (Planke 1994, Planke & Eldholm 1994). The lava flows and interbedded sediments at Site 642 are similar to the upper basalt

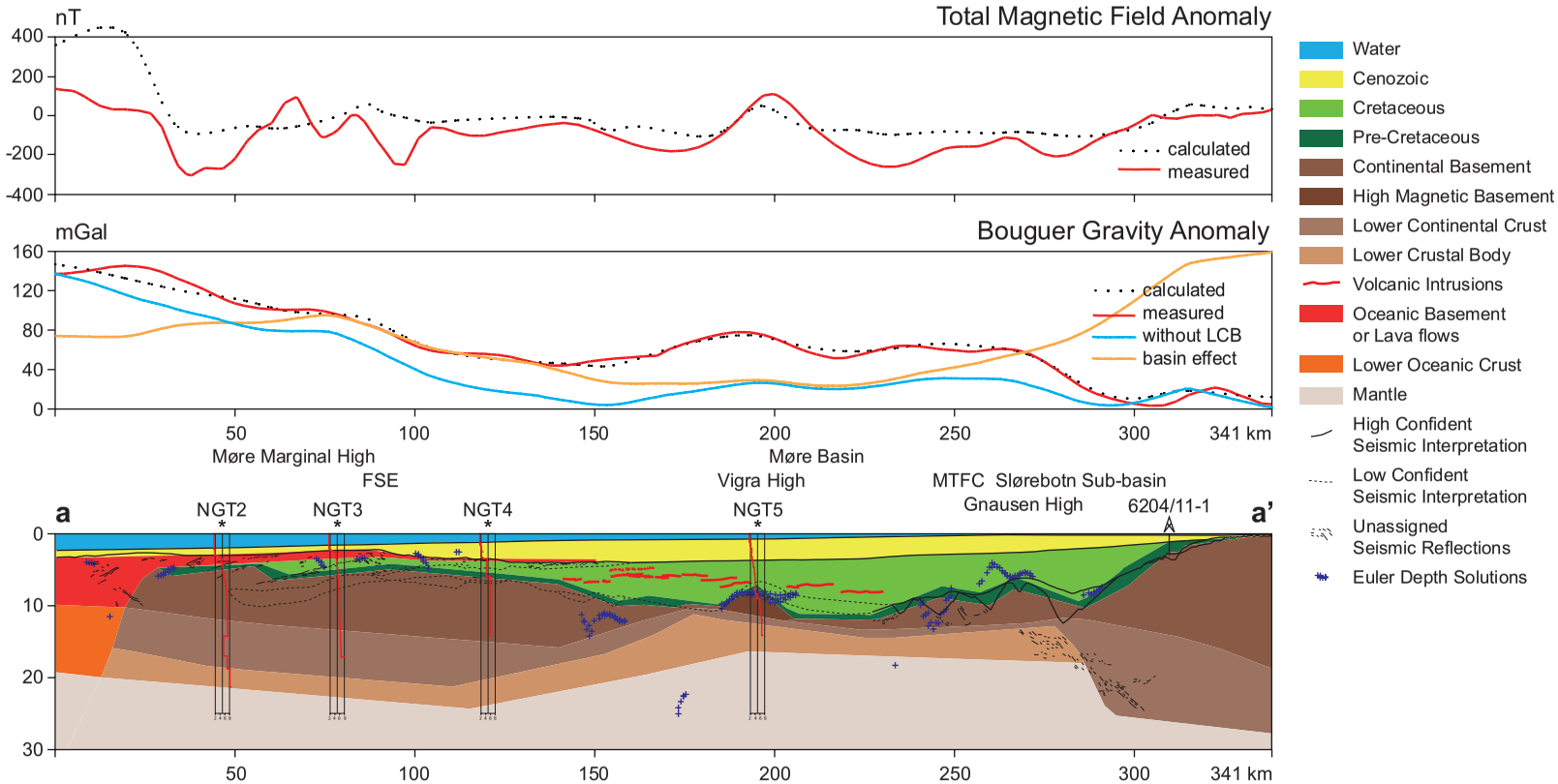

Figure 6.8. Profile a-a' (see Figure 6.1 for location) along seismic line GMNR94-102. The figure shows a typical cross section from the Møre margin extending from the coast to the COB. The fit between observed and modelled potential fields are shown. The gravity response of the model without LCB is shown by the blue line. The relative gravity response of the sedimentary basin is given by the yellow line. Properties for each model unit are given in Table 6.1. The solid colours represent the 3D modelling results, the black lines show the seismic interpretation and blue crosses are Euler depth solutions. The red lines are the velocity trend of refraction profiles. It is apparent that the 3D model lacks the detail of the seismic reflection data but in genereal there is a good agreement between the two different geophysical methods.

series of the three Faroes basalt series. Iceland extrusive formations also show similarities to the volcanics encountered at Site 642 (Planke & Eldholm 1994). Because only very limited number of wells have penetrated volcanics on the mid-Norwegian margin measurements from the Faroe Islands and Iceland have been collected to extend the petrophysical database on igneous rocks (Table A.5, A.6). Saxov and Abrahamsen (1966) studied the densities of lava formations on the Faroes Islands. Their investigation concluded in a mean density value of 2860 kg/m^3 for the whole area. The Lopra-1 and Vestmanna-1 wells provided considerable amount of petrophysical data on the Faroes (Balling *et al.* 1984, Nielsen *et al.* 1984, Schoenharting & Abrahamsen 1984) and deepening of the Lopra-1 well increased the database further (Abrahamsen & Waagstein 2006, Boldreel 2006). The Iceland Research Drilling Project (IRDP) was undertaken in 1978 and resulted in a 1920 m deep drill hole that provided samples of the upper 3 km of Icelandic crust (Friðleifsson 1982). Densities and magnetic properties were acquired from both cores and logs of the whole well. The National Energy Authority of Iceland published in 1984 a report containing 346 density measurements on lava flows and volcanic intrusions (Pálsson *et al.* 1984). The average density of basalt flows from these measurements is 2780 kg/m^3.

6.3.3 Modelling Procedure

The initial setup of the model was based on all available geometrical constraints and layer properties as described above. The gravity was then calculated at station locations with 5 km spacing over the whole study area and compared to the observed gravity. The long wavelength misfit was first addressed by adjusting the Moho configuration in every section of the model until a reasonable fit was acquired. The next step was to expand the LCB to the centre of the basin to further adjust the long wavelength signal. The horizon dividing the basement layer from the lower crust layer was kept constant for regions of normal oceanic and continental crust. For stretched continental crust associated with crustal thinning the lower crust was thinned more than the overlying more rigid basement. The basement structure was then adjusted to fit the gravity and the magnetic signature. The base-basalt was mainly based on the gravity signal and to a lesser extent on the magnetic signature.

The final model has a standard deviation of approximately 6.5 mGals for the gravity, which is in the order of the error in marine gravity data (~3 mGal). The deviations of the modellled gravity field are mainly in the short wavelength domain and below the resolution of the model. The standard deviation for the magnetic is 145 nT, somewhat larger than for the gravity as expected because the modelling of the magnetic field was focused on fitting general trend of the magnetic signature without expecting a close fit on the absolute magnetic value. An attempt was made to fit the gravity anomalies as good as possible without re-configuring the sediment and top basalt horizons. Given the greater uncertainty and complexity of the magnetic properties the magnetic anomalies were not anticipated to fit as well as the gravity anomalies. When an acceptable fit between the gravity anomalies was acquired for the whole model the basement structure was fine tuned to fit the calculated magnetic anomalies to the measured anomalies. Greater emphasizes was on fitting the general shape of the calculated and measured anomalies than fitting the absolute values of the anomalies.

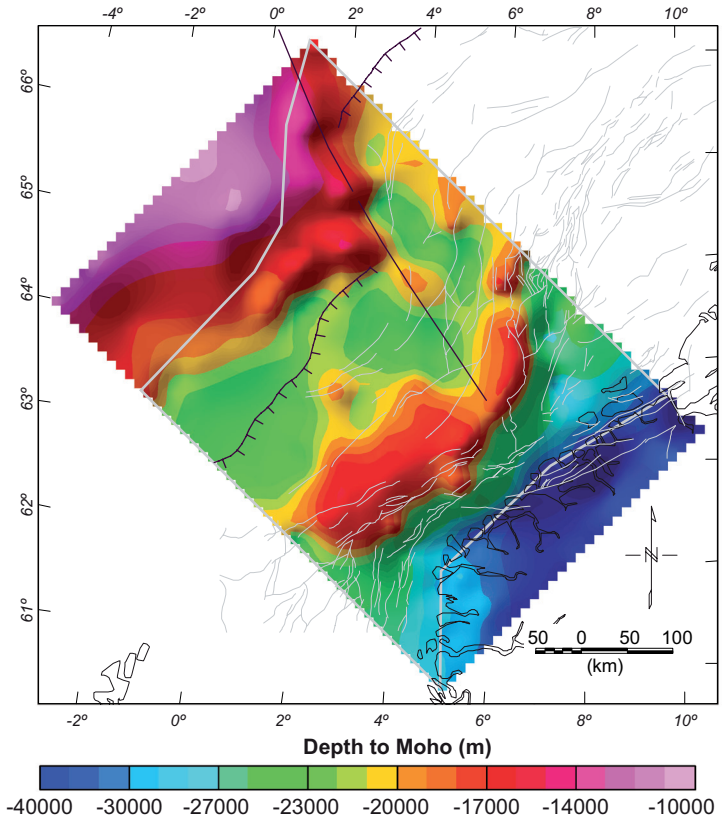

Figure 6.9. Depth to Moho from the 3D model.

6.4 Modelling Results

Because of the ambiguity of potential field interpretation the model presented here is one of several possible models, which has been developed by an iterative, interactive procedure, trying to satisfy as much constraining data as presently available. The greatest uncertainty is on the outer margin where only poor or no seismic control exists. Nevertheless, the sub-basaltic structure on the marginal high is supported by reflections observed on the GMNR94-102 line that were not employed in the construction of the initial model. Figure 6.8 presents a comparison of modelled cross-section to the GMNR94-102 line. It is apparent that the model lacks the detail of the seismic lines but on the other hand it gives an indication of structures that are hardly or not at all visible on the seismic.

The accuracy of the model also depends on the quality of the data. The gravity and magnetic compilations used in this study did not include all existing surveys in the area as they are non-released industrial data. Several gravity surveys are missing from the compilation and two high quality magnetic surveys (NB-07 and MBAM-97) are also missing from this study. A denser dataset could be used to construct a more localized model that would decrease the geometrical uncertainty of the modelled bodies.

The results from the model provided some key horizons from the Møre margin. These are the crust-mantle boundary (Moho) (Figure 6.9), top of the lower crustal body (LCB)

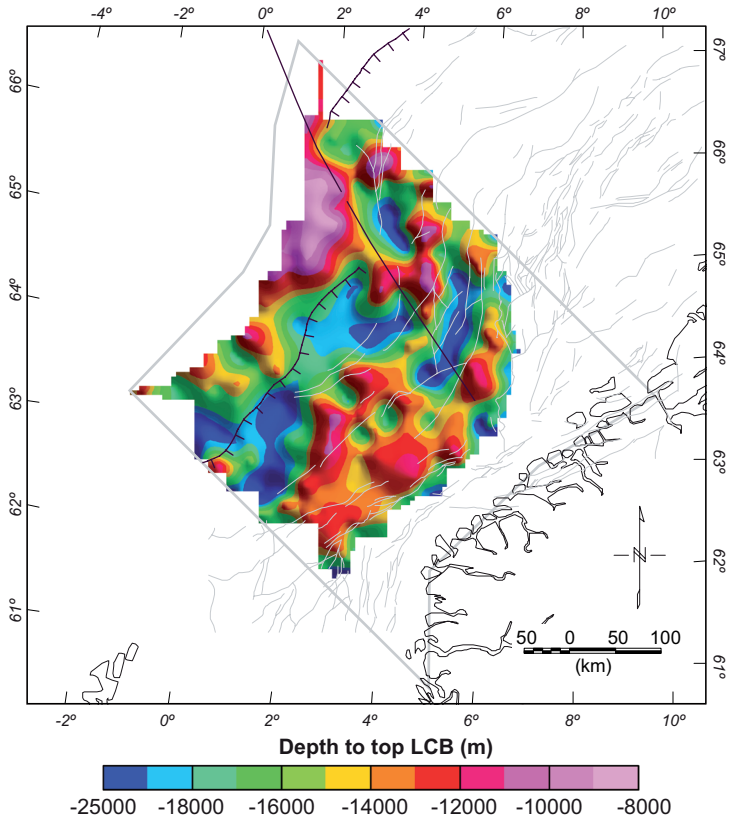

Figure 6.10. Depth to top LCB from the 3D m odel.

(Figure 6.10), top crystalline continental crust (basement) (Figure 6.11), base Cretaceous, and base basalt. The resulting horizons also provided means to acquire estimates of sediments, LCB, crustal, and basalt thickness across the margin (Figure 6.12). Cross-sections across the general strike of the margin illustrate the gross structural characteristics of the Møre margin (Figure 6.13). A major characteristic of the margin is the rapid deepening of the basin from the coastline to about 12 km in the depocenter over a horizontal distance less than 100 km. The deepening of the basin is associated with shallowing of the Moho which indicates a sever thinning of the crust. Another major characteristic is the existence of a lower crustal body that is thickest below the centre of the basin and extends to the COB.

The depth to Moho in the study area ranges from 30 km at the coastline to 15 km in the oceanic domain (Figure 6.9). Just 100 km from the coast the Moho rises to less than 20 km depth and displays a pronounced 100 km wide high in the centre of the Møre Basin. Towards the Møre Marginal High the Moho deepens again to little less than 30 km and at the COB it shallows rapidly to 15 km. The Jan Mayen Lineament coincides with a significant Moho signature. A similar signature is observed in the centre of the basin as well indicating a lineament cross-cutting the Møre Basin (Figure 6.9).

The general trend of the LCB resulting from the model (Figure 6.10) follows the strike of the margin. Its depth ranges from nearly 25 km below the Faroe-Shetland Escarpment to less than 12 km at its peaks. Three ridge trends along the margin's strike can be observed on the depth map, two of them in the basin that follow the main structural trends, and one

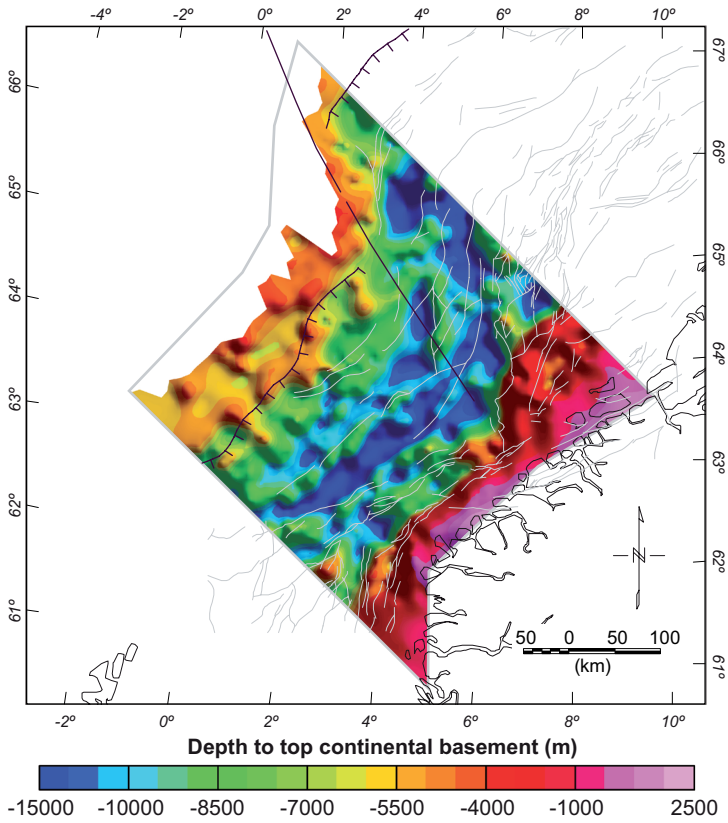

Figure 6.11. Depth to top continental basement from the 3D model.

below the Møre Marginal High in an unknown structural setting. The ridge trends are more pronounced on the LCB isopach map (Figure 6.12d), which are locally up to more than 10 km thick. The distribution of the LCB extends to the limits of the study area on three sides but to the SE it terminates at Møre-Trøndelag and Klakk fault complexes.

The LCB accounts for a considerable part of the gravity signal on the margin. By substituting the density of the LCB (3100 kg/m^3) with the density of the lower crust (2900 kg/m^3) the gravity signal of the Bouguer anomaly without the effect of the LCB was calculated from the model (Figure 6.14a). As expected a more pronounced gravity low now is observed in central axis of the basin but surprisingly a prominent high still remains in the SW part of the basin. By subtracting the gravity anomaly without the LCB from the Bouguer anomaly the gravity effect of LCB was acquired (Figure 6.14b). The main gravity effect of the LCB is in the axial part of the basin and decreases sharply in the SW part. It is apparent that the LCB is a necessity in the model as higher sediment densities could not account for all this gravity effect. A shallower Moho could not account for this gravity effect either as it would have to cross seismically constrained horizons.

The depth to basement map (Figure 6.11) demonstrates that the modelled results fit closely to seismic observations in the Møre Basin as the flanks of basement highs coincide with major faults in the study area. The model provides map of the basement from the Norwegian coast to the COB and gives an indication of the structural settings for the whole

continental margin. The depth to top basement is approximately 12 km at its maximum in the centre of basin. This deep part of the basin follows the main structural trend for about 170 km, extending from just south of the Vigra High towards the southwest. The rather regular architecture of the basement is significantly disturbed at the location of the Jan Mayen Lineament. Considerable basement structure exists below the marginal high where the basement rises in general compared to the basin region. The sub-marginal basement structures vary in depth from approximately 5 km for the highs and approximately 7 km for the lows, indicating accommodation space for substantial sub-basaltic basins.

The crust thins from 30 km at the coastline to 20 km at the Slørebotn detachment where the crust tapers to about 10 km and thins to less than 8 km in a 100 km wide area in the centre of the basin. Then towards the escarpment the crust thickens again up to 18 km

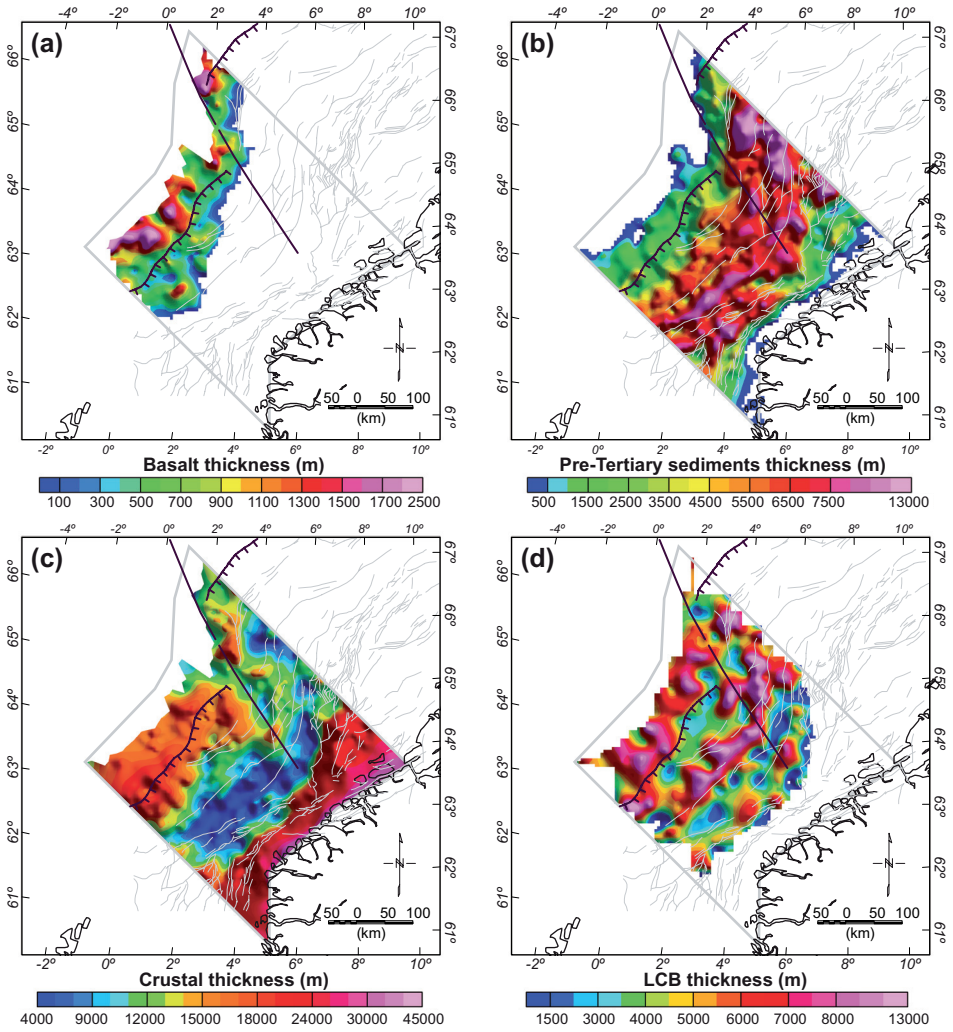

Figure 6.12. Isopachs from the 3D model. (**a**) Basalt thickness, (**b**) Pre-Tertiary sediments thickness, (**c**) crustal thickness, and (**d**) thickness of the LCB.

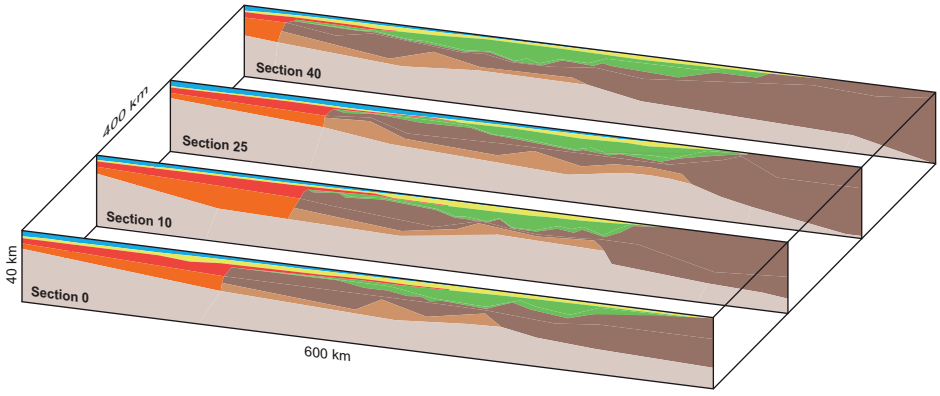

Figure 6.13. Perspective view of four sections from the 3D model (see Figure 6.3 for location).

and thins again towards the COB. The Jan Mayen Lineament coincides with a change in thickness of the crust from SW to NE. To the north the lineament seems to cut the crust but at the southern tip the lineament coincides with a thicker than adjacent crust. By assuming an original crustal thickness of 30 km a total stretching factor for the margin was calculated (Figure 6.15a). The centre of the basin has been severely thinned and the main thinning follows the trend of the main faults. The thinning of the crust on the Møre Marginal high is up to 200% but is still only half of the thinning in the central axis of the basin. If the top of the LCB is taken as the base of the crust the results are even more dramatic (Figure 6.15b). In this case the thinning of the crust is severe on the whole margin NW of the landward marginal faults.

The sub-basaltic basement structure (and consequently sedimentary thickness) is of a major interest with respect to hydrocarbon exploration. The model presented in this study predicts these features but as this is a large scale regional model the results can only be viewed as an indication. The extrusive volcanics on the Møre margin have been interpreted in terms of volcanic eruption, emplacement, and sedimentation history based on different seismic facies units (Alvestad 1997, Planke & Alvestad 1999, Planke *et al.* 1999a). In this study the extrusive volcanics were interpreted as one body because the potential field model is insensitive to the internal subdivisions of the volcanic pile. The top of the extrusives was interpreted from seismic reflection data. The top reflection is relatively easily identified because of the high impedance contrast between post-rift sediments and the top-basalts, resulting in a strong reflector. The base of the basalt was extracted from the model as the part of the base-Cenozoic horizon that extended below the top-basalt. The base-basalt horizon interpretation has few constraints and relies mainly on gravity modelling and to a lesser extent on the magnetic. On a regional scale the confidence level of this horizon is acceptable but as the choice of parameters affects the thickness estimate at the scale of 100s of meters the confidence level is low on a local scale. By subtracting the depth to base-basalt from the top-basalt horizon the basalt thickness was acquired (Figure 6.12a). The average thickness of the basalt layer is ~1 km and the maximum thickness is ~2.5 km.

The interpretations on intrusions (sills) in the study area rely only on seismic reflection data. The shallower unit is recognised by its saucer-shape and rough seismic character. The deeper unit has a smooth seismic character and a large degree of continuity. The shallower

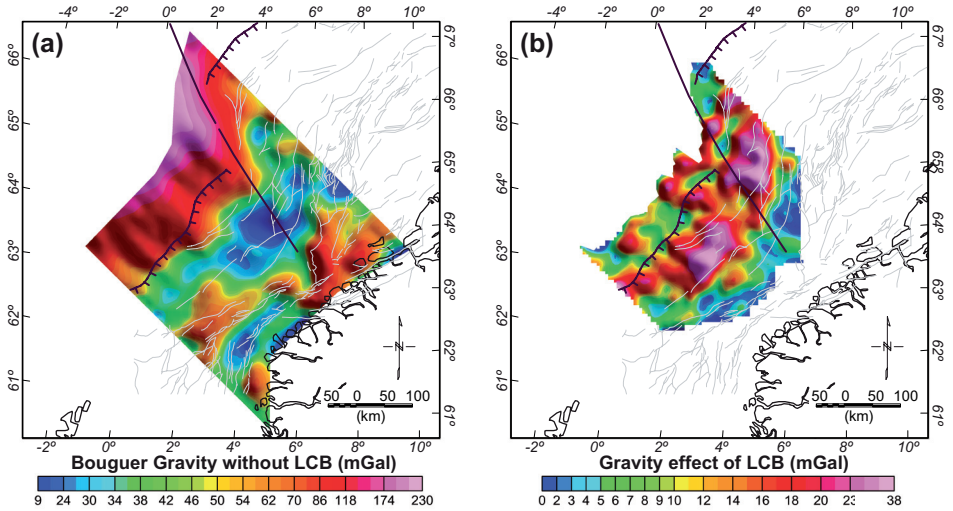

Figure 6.14. Effect of the LCB on the gravity signal. (**a**) Bouguer gravity anomaly from the model without the LCB present. (**b**) The gravity effect of the LCB.

sills were easily recognized in the basin on seismic data, but oceanward of the escarpment they are very difficult to observe. The deeper sills could be mapped with relative ease in the basin but are untraceable beyond the escarpment. It was not possible to produce the base of the intrusives from the potential field model because they are too deep and thin to be detected in the gravity and magnetic signal.

The base Tertiary was well constrained by seismic reflection data and has a high confidence level throughout the study area. For most of the area the base Cretaceous was also well constrained but in the deeper parts of the basin and below sills and especially on the marginal high the confidence reduces dramatically. It is impossible to distinguish between Cretaceous and Pre-Cretaceous sediments in the basaltic areas. Only the low density and magnetic properties of sediments give an indication of their presence below the basalts and hence the top basement structure. Even on the more landward part of the margin the top basement cannot be easily determined from seismic data and its modelled structure relies to a high degree on the potential field response. An isopach of the pre-Tertiary sediments was acquired by subtracting the depth to top basement from the base-Tertiary horizon combined with base-basalt (Figure 6.12b). The thickness of the resulting sedimentary layer is at maximum in the axial part of the basin where it is approximately 13 km but on average the thickness is ~4.5 km in the study area. Considerable variations in pre-Tertiary sedimentary thickness is observed below the basalts in the vicinity of the marginal high. The thickness varies mainly between 1.5 and 2.5 km but locally it is up to ~4.5 km.

6.5 Discussion

Despite of the extensive amounts of geophysical data acquired on the Møre margin during the past decades, considerable ambiguity exists with respect to the deeper structures. This ambiguity is mainly the effect of imaging problems caused by the substantial thickness of

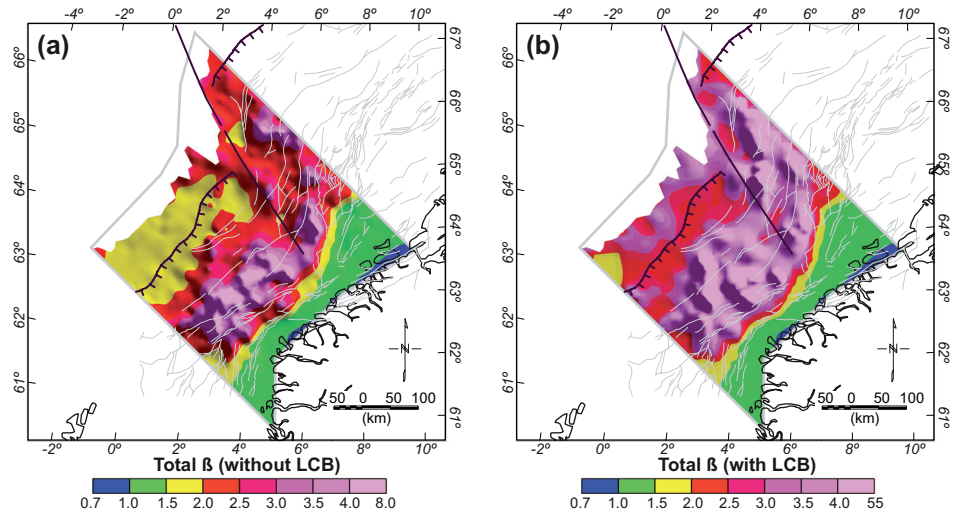

Figure 6.15. Total thinning factor of the Møre margin. The factor is the ratio of the assumed original crustal thickness of 30 km against the current crustal thickness (original thickness / current thickness). Current crustal thickness of 30 km would give a factor of 1 and current crustal thickness of 15 km would give a factor of 2. (**a**) thinning factor assuming LCB as part of the crust and (**b**) thinning factor assuming LCB part of the mantle.

Cretaceous strata and large volumes of volcanic bodies in the area. By integration of various geophysical data and implementation of a 3D potential field model a more complete image of the deep structure of the Møre margin has been acquired than previously attained.

A basement map covering the whole mid-Norwegian margin was produced by Skilbrei *et al.* (2002) based on magnetic depth estimates and seismic constraints (see Figure 6 in Skilbrei *et al.* 2002). The regional trend is similar to the results from this study, but there is considerable difference in the absolute depth that increases towards the escarpment in this study. It is not surprising that differences exists between the two maps as a great uncertainty is associated with the magnetic depth method.

Ebbing *et al.* (2006) used a similar approach as was used in this study but their model was focused on the Vøring margin. The extent of their basement map was limited to the escarpments bordering the Vøring and Møre marginal highs in contrast to the COB in this study. The basement map from Ebbing *et al.* (2006) includes the northern part of the Møre margin and allows comparison of the two studies. In general there is a good agreement between the two studies both in regards to overall crustal architecture and actual depth (compare Figure 6.11 and Fig. 8a in Ebbing *et al.* 2006). The main difference is oceanward of the Vigra High where this study indicates a shallower basement than that of Ebbing *et al.* (2006) and a more pronounced shallowing of the basement towards the COB. The greatest basement depth in this study is concentrated along an axial trend landward of the Vigra High.

Osmundsen & Ebbing (2008) addressed the structural style and mechanisms of crustal thinning of the mid-Norwegian margin by integrating interpretation of deep seismic reflection data with 3D gravity and magnetic model. Their model incorporates the Lofoten, Vøring, and northern part of the Møre margin. They demonstrate how the

basement is reduced from a thickness of ~32 km at the coast to between 5 and 12 km over a horizontal distance of ~60 km and prevails thin from the tapered area to the COB. The most important difference between the results of Osmundsen & Ebbing (2008) is that in this study the basement thickness increases from the area of maximum thinning towards the COB (compare Figure 6.12c with Figure 5a in Osmundsen & Ebbing 2008). Thickening of the basement from the axial part of the Møre basin towards the COB is in agreement with seismic refraction studies in the Møre Basin (Ólafsson *et al.* 1992, Raum 2000).

Scheck-Wenderoth *et al.* (2007) constructed a 3D structural model of the mid-Norwegian margin (Vøring and Møre) from five major unconformity maps and extensive OBS database. The unconformity maps constrained the geometry of the sedimentary packages and the deep structure of the model was constructed by interpolating the 2D OBS profiles. Their results indicate the maximum depth of the Møre basin ~18 km and the maximum thinning of the crust below most of the basin in contrast to maximum depth of ~12 km and maximum thinning focused along the basins's axis (see Figure 6 in Scheck-Wenderoth *et al.* (2007)). They don't indicate any LCB in the Møre basin but it is caused by the lack of available OBS data in the basin which limits the interpretation of the deeper structures.

In spite of differences in the distal part of the Møre margin between the studies a considerable agreement exists in the proximal part. The basement tapers from 30 km at the coast to less than 10 km over a horizontal distance of ~70 km (Figure 6.12c). The width of the zone of minimum thickness is ~60 km and beyond that the crustal thickness increases to up to 20 km towards the COB. Figure 6.15 shows the crustal thickness in relation to a reference thickness of 30 km both by assuming the LCB as part of the crust (Figure 6.15a) and by assuming the LCB as part of the mantle (Figure 6.15b). By assuming the LCB as a part of the mantle a broader crustal thinning is observed that is persistent towards the COB and is in better agreement to the studies by Osmundsen & Ebbing (2008) and Scheck-Wenderoth *et al.* (2007). Whether the LCB is better assigned a crustal or mantle origin is addressed in Chapter 7.

The LCB thickness map (Figure 6.12d) shows three main ridges that follow the general strike of the margin. The innermost one follows the trend of the Ona High outboard of the Slørebotn Sub-basin and must represent either the deepest part of the crust or sepentinised upper mantle rocks as suggested by Osmundsen & Ebbing (2008). The middle and most pronounced ridge underlying the Vigra High follows the trend of the maximum thinning and might therefore be interpreted as high density lower crust or exhumed upper mantle. By comparing this ridge to the distribution of magmatic rocks in the study area (Figure 6.4) it is apparent that the middle LCB ridge falls within the border defining the extent of sills. This indicates a magmatic origin of the LCB as the source of the sills in the basin as suggested by Skilbrei *et al.* (2002) and Mjelde *et al.* (2009a).

Given the regional scale of the model (400x600 km) and its simple structure with only 12 bodies differing in density and magnetic parameters it is necessary to address the limitations of the model. Each body in the model is given a constant density and magnetic parameter and is assumed to represent a regional geological feature. The bodies are homogenous and the boundaries between them are sharp. This is a gross simplification of the real world as most geological features (such as a sedimentary unit, continental crust or basalt flow) are very heterogeneous and complex. It is impossible to address this complexity in a regional model and therefore a large scale average needs to be estimated. Then it is important to

tie the geometry of each body to as many constraints as possible (e.g. seismic horizons). The number of available constraints is reduced with depth which reflects the increased uncertainty of the model with depth. For example, the lower-crustal body (LCB) is given a constant density for the whole modelled area. The real world is probably not this simple as both the lower crust and upper mantle densities most likely fade into the intermediate LCB densities. A sharp boundary between the different bodies does therefore probably not exist as indicated by the model. On the other hand, the model strongly suggests that an anomalously dense body exists between the mantle and lower-crust in the study area. The lateral distribution of this anomaly is well expressed in the model but its absolute thickness variations are much more uncertain. Maps based on the results from the model's deep structure can therefore only be viewed as an indicator of the structural variations and not exact position of a real geological body.

6.5 Conclusions

A 3D model of the Møre margin was constructed by forward modelling employing the gravity and magnetic fields. Numerous independent data were used to diminish the nonuniqueness of the method. The resulting model consists of several horizons that divide the main geological bodies in the study area. The results from the model provided some key horizons from the Møre margin. These are the crust-mantle boundary (Moho), top of the lower crustal body (LCB), top crystalline continental crust (basement), base Cretaceous, and base basalt. The resulting horizons also provided means to acquire estimates of sediments, LCB, crustal, and basalt thickness across the margin. In addition three horizons were based on reflection seismic interpretation only. These are the top of the lava flows and top of the intrusions. The intrusions (sills) were divided in two different units based on the seismic signature and depth.

The resulting horizons have provided means to address the large scale geolgocal features of the Møre margin. A major characteristic of the margin is the rapid deepening of the basin from the coastline to ~12 km in the depocenter over a horizontal distance less than 100 km. Another major characteristic is the existence of a lower crustal body that is thickest below the centre of the basin and extends to the COB.

The depth to Moho in the study area ranges from 30 km at the coastline to 15 km in the oceanic domain. Just 100 km from the coast the Moho rises to less than 20 km depth and displays a pronounced 100 km wide high in the centre of the Møre Basin.

The Jan Mayen Lineament coincides with a significant Moho signature. A similar signature is observed in the centre of the basin as well indicating a lineament cross-cutting the Møre Basin.

The general trend of the LCB resulting from the modelfollows the strike of the margin. Its depth ranges from nearly 25 km below the Faroe-Shetland Escarpment to less than 12 km at its peaks. Three ridge trends along the margin's strike can be observed on the depth map, two of them in the basin that follow the main structural trends, and one below the Møre Marginal High in an unknown structural setting.

The model provides map of the basement from the Norwegian coast to the COB and gives an indication of the structural settings for the whole continental margin. The depth to top basement is ~12 km at its maximum in the centre of basin.

Considerable basement structure exists below the marginal high where the basement rises in general compared to the basin region. The sub-marginal basement structures vary in depth from approximately 5 km for the highs and approximately 7 km for the lows, indicating accommodation space for substantial sub-basaltic basins.

The average thickness of the basalt layer is ~1 km and the maximum thickness is ~2.5 km. An isopach of the pre-Tertiary sediments was acquired and the thickness of the resulting sedimentary layer is at maximum in the axial part of the basin where it is approximately 13 km but on average the thickness is ~4.5 km in the study area. Considerable variations in pre-Tertiary sedimentary thickness is observed below the basalts in the vicinity of the marginal high. The thickness varies mainly between 1.5 and 2.5 km but locally it is up to ~4.5 km.

Acknowledgements

The Geological Survey of Norway and TGS-NOPEC provided the gravity, magnetic and bathymetry data. Shell provided the depth converted BCU and base Tertiary horizons from the Møre Basin. Seismic lines from the MNR survey acquired by Fugro Multi Client Services in cooperation with TGS-NOPEC Geophysical Company were used in this study. Asbjørn Breivik provided the ESP and sonoboyu profiles. The 3D modelling was performed using the software package IGMAS.

Chapter 7

Origin of lower crustal bodies on the Møre margin from isostatic considerations

Reynisson, R. F., Ebbing, J. & Osmundsen, P. T. In prep. Deep structure of the Møre margin, offshore Norway. Part 2: origin of lower crustal bodies on the Møre margin from isostatic considerations.

A high-velocity, high-density layer at the base of the crust, which is detected by OBS seismic experiments with a seismic P-wave velocity of 7.0–7.9 km/s (e.g. Raum *et al.* 2002, Raum *et al.* 2005, Tsikalas *et al.* 2008, Mjelde *et al.* 2009a) is characteristic for the mid-Norwegian margin and volcanic margins in general. We refer to this layer as lower crustal body (LCB) to follow convention, but suggest that it can be part of the mantle as well as the crust. The LCB is however, often referred to as magmatic underplating (van Wijk *et al.* 2004) but, while the high velocity/high density of the LCB may be considered as an objective observation, its origin as a layer of underplated material is an interpretation that dates back to work by e.g. White *et al.* (1987). In recent years, there has been a renewed discussion about the interpretation of the LCB (e.g. Gernigon *et al.* 2004, Mjelde *et al.* 2005, Ebbing *et al.* 2006). Ebbing *et al.* (2006) proposed that the LCB could be remnants of the Caledonian root and Gernigon *et al.* (2006) propose that the LCB characteristics may partly be explained by the presence of pre-existing high-velocity rocks, such as eclogites or migmatites. A non-magmatic interpretation of the LCB would lower the estimated NAIP melt volumes (Eldholm & Grue 1994) significantly. This, in turn, would affect most conventional models for NAIP formation that generally link melt volumes to potential mantle temperature (White & McKenzie 1989). It is still common to propose that the LCB represents magmatically underplated material (e.g. Mjelde *et al.* 2005, Mjelde *et al.* 2009a), and that their internal density and velocity distribution may signify differences in the magma composition, in turn possibly reflecting asthenospheric temperatures or compositional inhomogeneities in the asthenospheric source.

This study focuses on the LCB on the Møre margin (Figure 7.1), that has been detected and mapped by wide angle seismic studies (Ólafsson *et al.* 1992, Raum *et al.* 2002, Mjelde *et al.* 2009b). Results from a 3D regional model of the Møre margin (Chapter 6) and implementation of the concept of isostasy and flexure of the lithosphere can provide new insights into the characteristics and possible origin of the LCB.

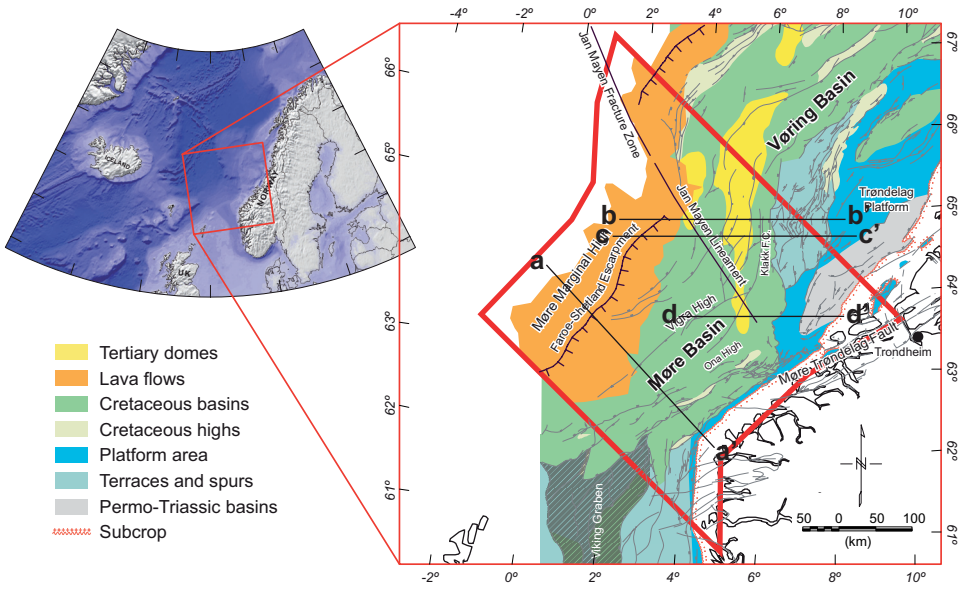

Figure 7.1. Overview of the study area. The thick red line outlines the 3D model (Chapter 6). Tectonic map from Mosar *et al.* (2002). Profile a-a' is shown in Figure 7.5. Profiles b-b', c-c' and d-d' are shown in Figure 7.8.

7.1 Deep structure of the Møre margin from a 3D model

The results from the regional model described in Chapter 6 provided key horizons for this study. The depth to Moho in the study area ranges from 30 km at the coastline to 15 km in the oceanic domain (Figure 6.8). Below the coast the Moho is at 30 km depth and just 100 km from the coast the Moho is at less than 20 km depth and displays a pronounced 100 km wide high in the centre of the Møre Basin. Towards the Møre Marginal High the Moho deepens again to about 25 km and below the marginal high its depth decreases to less than 15 km. The Jan Mayen Lineament coincides with a significant Moho signature. A similar signature is observed in the centre of the basin as well, indicating a lineament cross-cutting the Møre Basin.

The general trend of the LCB resulting from the model (Figure 6.9) follows the strike of the margin. Its depth ranges from nearly 25 km below the Faroe-Shetland Escarpment to less than 12 km at its peaks. Three ridge trends along the margin's strike can be observed on the depth map, two of them in the basin that follow the main structural trends, and one below the Møre Marginal High in an unknown structural setting. The distribution of the LCB extends to the limits of the study area on three sides but to the SE it terminates at Møre-Trøndelag and Klakk fault complexes.

By subtracting the model Moho from the modelled top basement horizon a crustal thickness was acquired. The map shows that a very thin crystalline crust (less than 5 km) exists below the centre of the Møre Basin. Comparing the crustal thickness to the LCB distribution shows that in the Møre Basin the thinnest crust spatially coincides with the most landward ridge of the LCB (Figure 7.2). Comparison of LCB distribution and volcanic distribution on Figure 7.3 reveals that all the LCB are overlain by volcanics apart from a

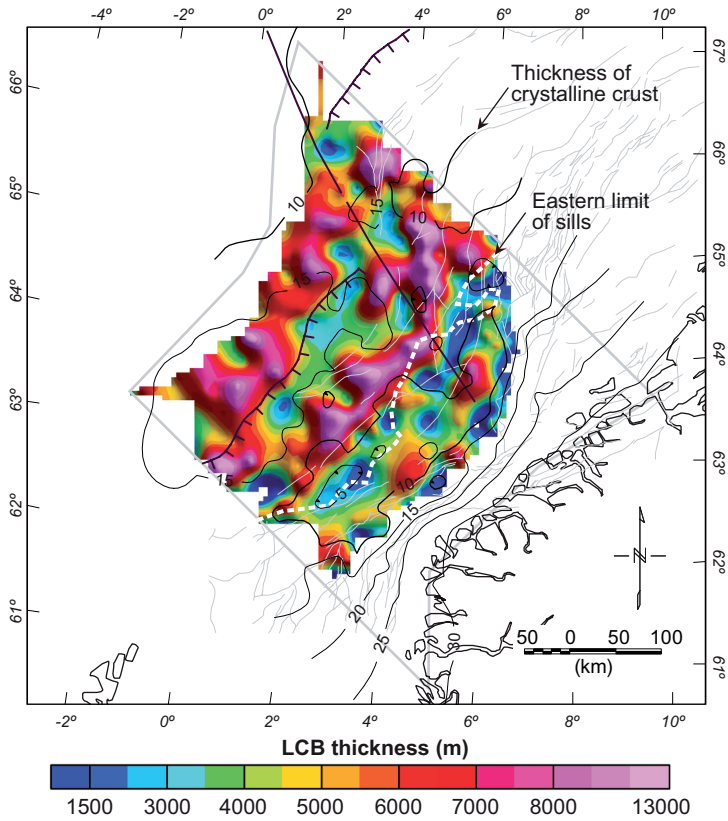

Figure 7.2. LCB vs. crustal thickness and magmatic distribution. Comparing the crustal thickness to the LCB distribution shows that in the Møre Basin the thinnest crust spatially coincides with the most landward ridge of the LCB. The two more distal ridges follow the trend of the magmatic distribution.

landward ridge that coincides with the very thin crust in the proximal part of the basin. How the LCB relates spatially to thin crust and magmatic sills can give an indication to its origin, i.e. whether the LCB is a serpentinised mantle or magmatic underplate. These two different cases will have different effects on the isostatic state of the lithosphere. Comparison of the model results to a system in isostatic equilibrium can shed light on the origin of the LCB.

7.2 Isostatic Flexural Moho

Isostatic compensation requires all topographic masses (loading) and sediments (deloading) to be compensated at lithospheric level. When no loading or deloading exists, the Moho interface has no undulations and is at the normal crustal depth. In the presence of a crustal load (or deload) a compensation takes place and the Moho undulates accordingly. How the Moho undulates is related to both the crustal load and the strength of the lithospheric plate.

The parameter that characterizes the apparent flexural strength of the lithosphere is the flexural rigidity (D), which is commonly expressed through the elastic thickness (T_e) of the lithosphere (Turcotte & Schubert 2002). For a homogeneous isotropic elastic thin plate,

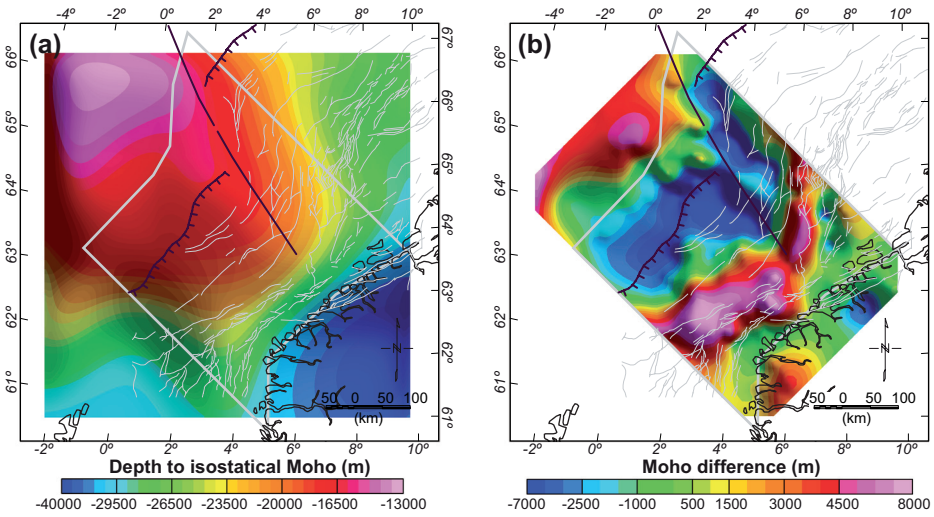

Figure 7.3. Isostatic flexural Moho. (**a**) The isostatic Moho shows the same first-order trends as the model Moho (Figure 6.9) with a regional increase from the coast towards the oceanic plate. (**b**) The difference map was acquired by subtracting the depth to the model Moho from the depth to the flexural Moho. Positive difference, indicating model Moho shallower than flexural Moho, is mainly located in the landward part of the basin and follows the trend of the Møre Trøndelag Fault Complex. The negative difference, reflecting modelled Moho deeper than the flexural Moho, is largely located below the Faroe-Shetland Escarpment.

such as the lithosphere at large scale, the flexure $w(x,y)$ of the plate loaded by a load $h(x,y)$ is defined in frequency space by (Watts 2001):

$$W(k) = -\frac{\rho_c}{\rho_m - \rho_c}\left(1 + \frac{16\pi^4 k^4 D}{(\rho_m - \rho_c)g}\right)^{-1} H(k) \qquad (7.1)$$

where $W(k)$ is the Fourier transform (FT) of the flexure of the plate, $H(k)$ is the FT of the load, ρ_m is the density of the mantle, ρ_c density of the crust, g is the normal gravity, and D is the flexural rigidity. When D=0 Nm, the isostatic compensation is identical to an Airy-Heiskanen isostatic model.

Assuming that the Møre margin is in isostatic equilibrium, we calculated the isostatic compensation for the de-loading of the margin by the relatively low-density sedimentary infill and water. For the isostatic calculation, we used the spectral method of the software LithoFlex (Braitenberg *et al.* 2006). The loading of the sediments was calculated by applying a linear depth-dependent density function from 2200 kg/m^3 at sea surface to 2700 kg/m^3 in 10 km depth and constant below. The surrounding basement density has been chosen with 2750 kg/m^3. The simplified density distribution leads to de-loading of the lithosphere, which in an isostatic concept leads to crustal thinning to balance the loading. A relatively low effective elastic thickness value (T_e=10 km), as estimated for the Viking Graben by Kuznir *et al.* (1991), was applied. The reference depth was chosen 30 km and the density contrast at the isostatic flexural base with 400 kg/m^3, which correlates to a lower crust density of 2900 kg/m^3 and a mantle density of 3300 kg/m^3.

The resulting isostatic Moho (Figure 7.3a) shows the same first-order trends as the model Moho (Figure 6.8) with a regional increase from the coast towards the oceanic plate. The difference map (Figure 7.3b) highlights substantial differences between the isostatic and model Moho and gives valuable insight into the margin. The difference map was acquired by subtracting the depth to the model Moho from the depth to the flexural Moho. Positive difference, indicating model Moho shallower than flexural Moho, is mainly located in the landward part of the basin and follows the trend of the Møre Trøndelag Fault Complex. The negative difference, reflecting model Moho deeper than the flexural Moho, is largely located below the Faroe-Shetland Escarpment.

7.3 Isostatic effect of the LCB

The LCB is by many workers believed to consist of magmatic material that has underplated the crust (e.g. Skogseid *et al.* 1992a, van Wijk *et al.* 2004, Mjelde *et al.* 2005). Spatial correlation between the distribution of the modelled LCB and the volcanics also suggest a magmatic origin for at least parts of the LCB (cf. Skilbrei *et al.* 2002, Mjelde *et al.* 2009a). The presumed magmatic underplate will disturb the state of isostasy as it has a negative density contrast with respect to the mantle and thus induces both uplift and deepening of the Moho. By assuming Airy-type response of the crust to the emplacement of a high-density body at the base of the crust we can estimate the amount of depressed Moho. From a simple model of magmatic underplating (Figure 7.4a) we have:

$$u\rho_w + T_c\rho_c + T_m\rho_m + \rho_a r = T_c\rho_c + v\rho_x + T_m\rho_m \qquad (7.2)$$

where u is the amount of uplift, v is the thickness of the LCB, r is the depression of the Moho (r=v–u), T_c is the crustal thickness and T_m is the thickness of the sub-crustal lithosphere.

Given: $u\rho_w + \rho_a r = v\rho_x$

We get from equation 7.2: $u\rho_w + \rho_a(v-u) = v\rho_x$

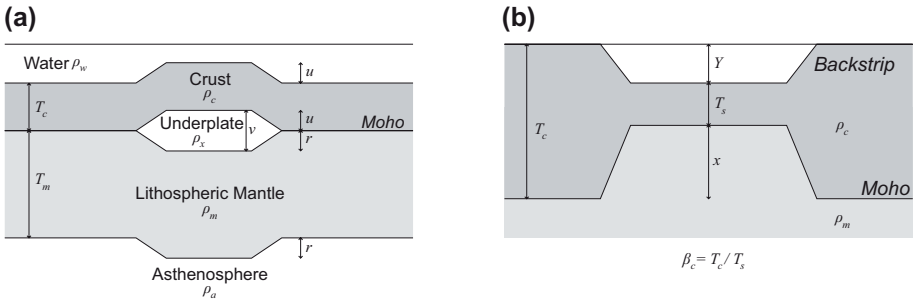

Figure 7.4. Isostatic and flexural effect of the LCB. (**a**) Simple model of magmatic underplating of a crust of uniform thickness. (**b**) The relationship between the amount of stretching and crustal thinning Redrawn from Watts (2001).

And therefore the uplift caused by the underplate (u) is:

$$u = v\frac{(\rho_a - \rho_x)}{(\rho_a - \rho_w)} \qquad (7.3)$$

If v=5 km (the average thickness of the modelled LCB), ρ_a=3300 kg m^{-3}, ρ_x=3100 kg m^{-3} and ρ_w=1030 kg m^{-3} then u=0.4 km and r=4.6 km. These results state that a 5 km thick underplate added to the base of the crust will result in an uplift of 0.4 km and deepening of the Moho by 4.6 km, given that the crust has no internal strength during the emplacement of the magmatic underplate and that no erosion has occurred. If the water level at the time of the underplate emplacement was less than the uplift erosion would have amplified the uplift and consequently reduced the deepening of the Moho by up to 2 km (Tiley *et al.* 2004).

The negative difference between the modelled Moho and the flexural Moho is up to 7 km (Figure 7.3b). The main difference in the two models that were used to produce the different Moho maps is the LCB as the basement map from the forward model was used as to define the geometry of the sedimentary load. The LCB was accounted for in the 3D forward model but was not included in the calculations of the isostatic Moho. The difference between the two models is also caused by lateral property variations (density and magnetic) not accounted for in the forward model and a more simple sedimentary structure in the isostatic model. It is feasible to assume that the LCB is accountable for majority of this difference as comparison of Figures 7.2 and 7.3b shows that the two LCB ridges outboard the eastern limit of sills are in the same area as the negative Moho difference and the positive difference covers very similar area as the inner most LCB ridge inboard of the sills limit (see also Figure 7.7). The negative difference is in the order of 5 km in the area of the two outboard LCB ridges which is well within the range of expected Moho suppression caused by magmatic underplating of dimensions resulting from the forward model.

7.4 Flexural effect of the LCB

Crustal strength and isostatic adjustments play a major role in the evolution history of a margin. By applying the results from our model to the concept of isostasy and flexure of the lithosphere we can acquire an approximation to the gross-scale evolution of the Møre margin. Active faulting and high heat flows accompany the early stages of rifting and therefore is an Airy isostatic model or low T_e applicable during this period. However, postrift sediments are gently dipping and of wide extent, suggesting that flexure takes over at some stage after the end of rifting (Allen & Allen 2005). Watts (1982) argued that the characteristic pattern of stratigraphic onlap on the eastern Atlantic and other margins suggested an increasing rigidity of the lithosphere with time, which is the expected result of an elastic lithosphere heated during the rifting stage and subsequently cooling.

By applying a method of flexural backstripping (Watts 2001) to a basement structure from the 3D model we can acquire an estimate on the geometry of the Moho by taking into account flexure during and following rifting. The method flexurally backstrips sediments in a rift-type basin and then, restores the crustal structure underlying the basin. The restoration assumes that rifting is accompanied by crustal thinning and that sediments flexurally load the crust during and following rifting.

If local isostasy is assumed during rifting the amount of crustal thinning (β) is computed from the backstrip (Y) assuming:

$$\beta = \frac{(\rho_m - \rho_c)T_c}{(\rho_m - \rho_c)T_c - (\rho_m - \rho_w)Y} \qquad (7.4)$$

where T_c is the initial crustal thickness, and ρ_c, ρ_m *and* ρ_w are the densities of the crust, mantle and water respectively (Figure 7.4b). Watts (2001) showed that given densities of ρ_c=2800 kg/m^3, ρ_m=3330 kg/m^3 and ρ_w=1030 kg/m^3 the relationship between β and Y is similar as acquired from McKenzie's thermal model assuming an age of rifting between 120 and 180 Ma.

In order to take into account finite strength of the margin lithosphere during rifting a flexural model is needed. Kooi *et al.* (1992) and Weissel & Karner (1989) formulated a model in which the amount of extension depends on depth of necking (Z_{neck}). This parameter is considered to be the depth to strength maxima in the lithosphere (Kooi *et al.* 1992) or depth to a detachment surface (Weissel & Karner 1989). Irrespective of its physical meaning the depth of necking concept allows lithospheric strength during rifting in the backstripping process. Watts and Stewart (1998) demonstrated the use of a flexural model offshore West Africa and showed:

$$\beta = \frac{Z_{neck}\Phi(k) + q_0}{Q_0(k) - Y^*(k)\Phi(k)} \qquad (7.5)$$

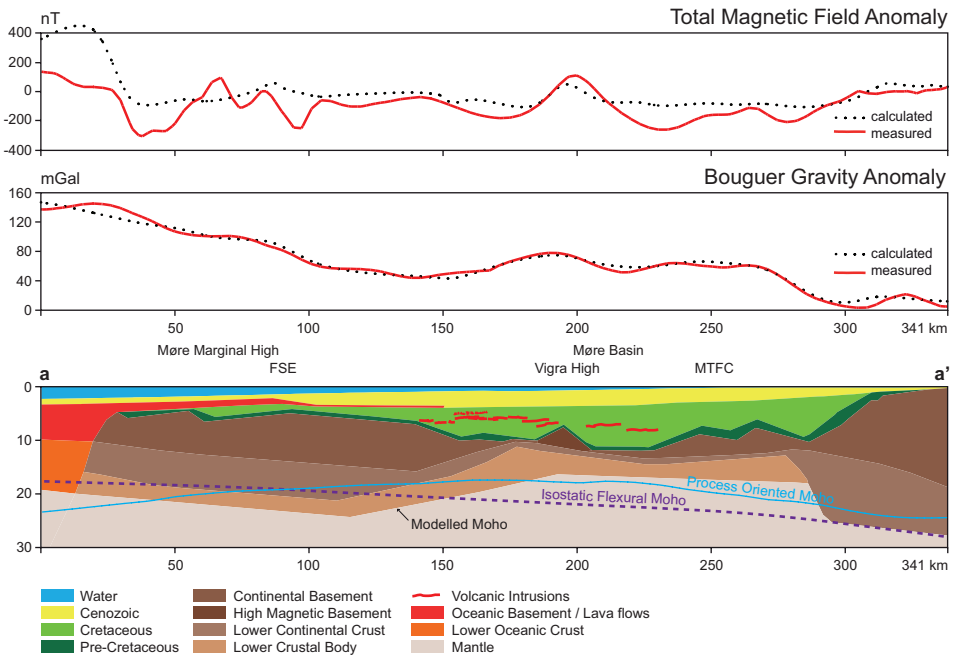

Figure 7.5. Profile a-a' (see Figure 7.1 for location) from the regional 3D model along seismic line GMNR94-102. Two differently acquired Mohos are compared to the model Moho. The flexural Moho is calculated by assuming T_e=10 km for the whole margin and without including the effect of the LCB. The process oriented Moho assumes T_e=5 km during rifting and T_e=25 km during sedimentation and is capable of reflecting the broad Moho architecture in the centre of the basin.

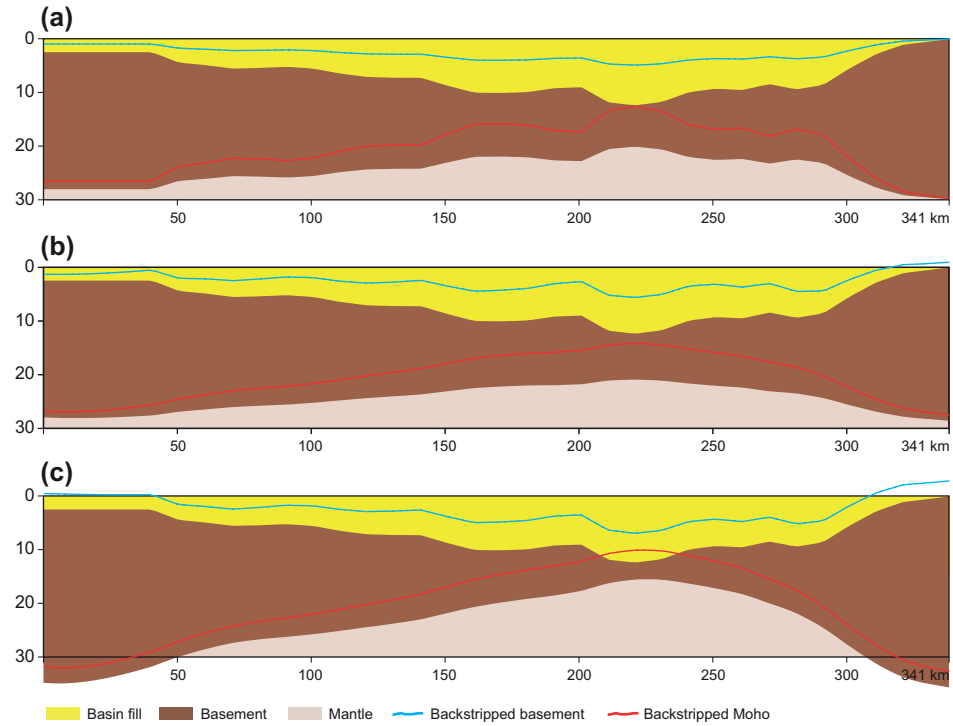

Figure 7.6. The isostatic Moho is not only dependent on the crustal strength regime at current time but is heavily affected by the crustal strength during rifting and subsequent sedimentation. (**a**) Local isostasy (T_e=0) during both rifting and loading of basin. (**b**) Weak crust (T_e=5 km) during both rifting and loading of the basin. (**c**) Weak crust (T_e=5 km) during rifting and strong crust (T_e=25 km) during sedimentation. The backstripped basement and Moho horizons indicate the horizons without the suppressing effect of the sedimentary load.

where the uppercase variables represent the Fourier transform of the lowercase variables. $\Phi(k)$ is given by $(Dk^4+(\rho_m-\rho_w)g)$, where D is the flexural rigidity. The computational steps in the process are further outlined in Watts (1988) and Watts (2001). The usefulness of this equation is that it allows the Moho architecture to be determined from the backstripped profile Y, taking into account the possibility of strength during rifting.

For the basement structure we used the modelling results along seismic profile GMNR94-102 (Figure 7.5). For simplicity we used a three layered model that contains mantle, crust and basin fill (water or sediments). We assumed that during rifting the basin is water filled and after rifting the basin is completely filled with sediments. We compare three different scenarios, local isostasy (T_e=0) during both rifting and loading of basin (Figure 7.6a), weak crust (T_e=5 km) during both rifting and loading of the basin (Figure 7.6b), and weak crust (T_e=5 km) during rifting and strong crust (T_e=25 km) during sedimentation (Figure 7.6c). In the first case, where we assume local isostasy both during rifting and during sedimentation, there is an exact correspondence between the shape of the basement and the resulting Moho geometries. The difference between the first and second case lies only in the stronger crust for the second case. The main effect is that the "ruggedness" of the Moho is greatly reduced but follows same trend and is at similar depths. By introducing difference in elastic thickness during rifting and

sedimentation (T_e=5 vs. T_e=25 km) we acquire a Moho that has the same "smoothness" as in the second case but lies much shallower in the centre of basin. The high Moho relief is preserved from the rifting period when the crust was weak and during sedimentation the crust is rigid and therefore distributes the load caused by the sedimentary fill over larger areas of the crust resulting in a very shallow Moho in the centre of the basin.

The case of weak crust (T_e=5 km) during rifting and strong crust (T_e=25 km) during sedimentation best fits the profile from the Møre margin (Figure 7.5) which is similar to results obtained by Karner *et al.* (2005) in the Ross Sea region. They studied the effect, on sedimentary basins, of different rigidity of the lithosphere at the time of rifting and at the time of sedimentation. They observed similar anti-correlation as is observed on the Møre margin (Figure 7.5) where the gravity anomalies are anti-correlated with the sedimentary thickness. They noted that three independent factors must exist for this to be possible: 1) the flexural rigidity of lithosphere during rifting needs to be thermally reset by the extension process, 2) the basins need to be sediment starved following rifting for a significant period, and 3) during the main phase of sedimentation, the flexural strength of the post-rift lithosphere needs to be relatively high compared to the rift phase.

The underplate is related to the Early Tertiary continental break-up (e.g. White *et al.* 1987, Eldholm & Grue 1994) which is much later than the main rifting period on the margin in the Early Cretaceous (Lundin & Doré 1997) and after the most of the sediment

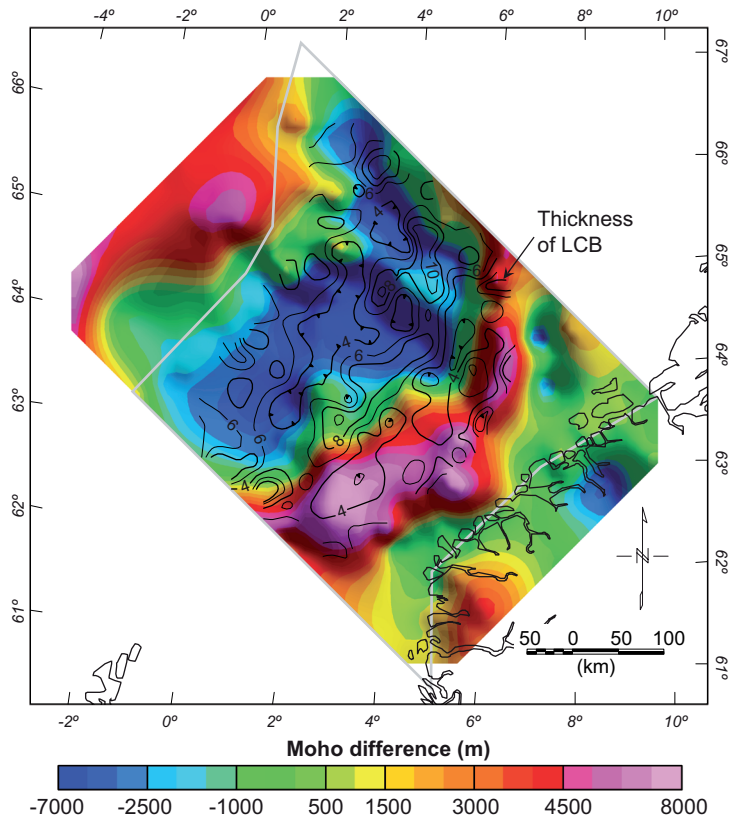

Figure 7.7. Moho difference vs. LCB thickness. Positive Moho difference coincides with the most proximal part of the LCB underlying very thin crust.

infill. If magmatic underplate exists below the centre of the basins the crust would reflect more local isostatic architecture because high heat flows and consequently weak crust are the effects of magmatic underplating which is in disagreement with the necessity of a rigid lithosphere (T_e=25 km) during the whole sedimentation period. The positive difference between the modelled and the flexural Moho that coincides with the most landward LCB ridge can therefore not be explained by emplacement of a high-density body at the base of a weak crust. The high-density body would rather fit a model of multiple intrusions in the lower crust as proposed by White *et al.* (2008) which do not elevate the temperature in the crust to the same degree as the magmatic underplate. The distance from the continent-ocean transition (COT) and the location of the inner most LCB ridge in relation to the distribution of sills make this a less feasible explanation but White *et al.* (2008) observed the lower-crustal intrusions near the Faroe Islands on a narrow zone ~50 km wide on the COT. Another possibility is that the modelled LCB related to positive Moho difference is not a high-density crust but a low-density mantle. The origin of the low-density mantle would be unroofed mantle rocks that have undergone serpentinization. Such settings are prone to develop detachments at the crust/serpentinized mantle transition (e.g. Reston 2009), which in turn can lead to core complex-like structural geometries as observed on the Møre margin.

7.5 Implications for evolution of the margin

Comparing the distribution of volcanics to the architecture of the modelled LCB in the study area (Figure 7.2) indicates a strong genetic link between the igneous bodies and a part of the LCB. A considerable part of the high density body correlates spatially with the distribution of deep-seated sill complexes and shallower volcanics. This implies at least partly an igneous origin of the LCB. The most landward modelled LCB high is not overlain by volcanics but coincides with the deepest part of the basement and the thinnest crust (Figure 7.2). The LCB at this location could represent high-grade metamorphic rocks, remnant from the Caledonian orogenic root (Gernigon *et al.* 2003, Gernigon *et al.* 2004, Ebbing *et al.* 2006). This would though require a high degree of coincidence between thin crust and the location of the high-grade metamorphic body. Another possibility would be that the LCB represents a partly serpentinised upper mantle as proposed by Osmundsen and Ebbing (2008). Serpentinisation of the upper mantle under highly thinned continental

Figure 7.8. Model profiles along MNR seismic lines (see Figure 7.1 for location of profiles). Lines on the profiles indicate seismic interpretation and the solid coloured bodies are from the regional model. Thick red lines indicate location of faults that have possibly ruptured the crust. Note the occurrence of magnetic anomalies in (**a**) and (**b**) not successfully accounted for in the model and the prominent anomaly in (**c**). These anomalies seem to be related to the deep cutting faults and the shallow LCB. The LCB has high density properties and if it represents serpentinite it is a low grade serpentinite. A higher grade serpintinite has density similar to the crust but higher magnetic properties than usual crust and this can explain both that the deep reflector band are not always following the top of the LCB and the location of the magnetic anomalies laterally shifted from the location of the shallow LCB.

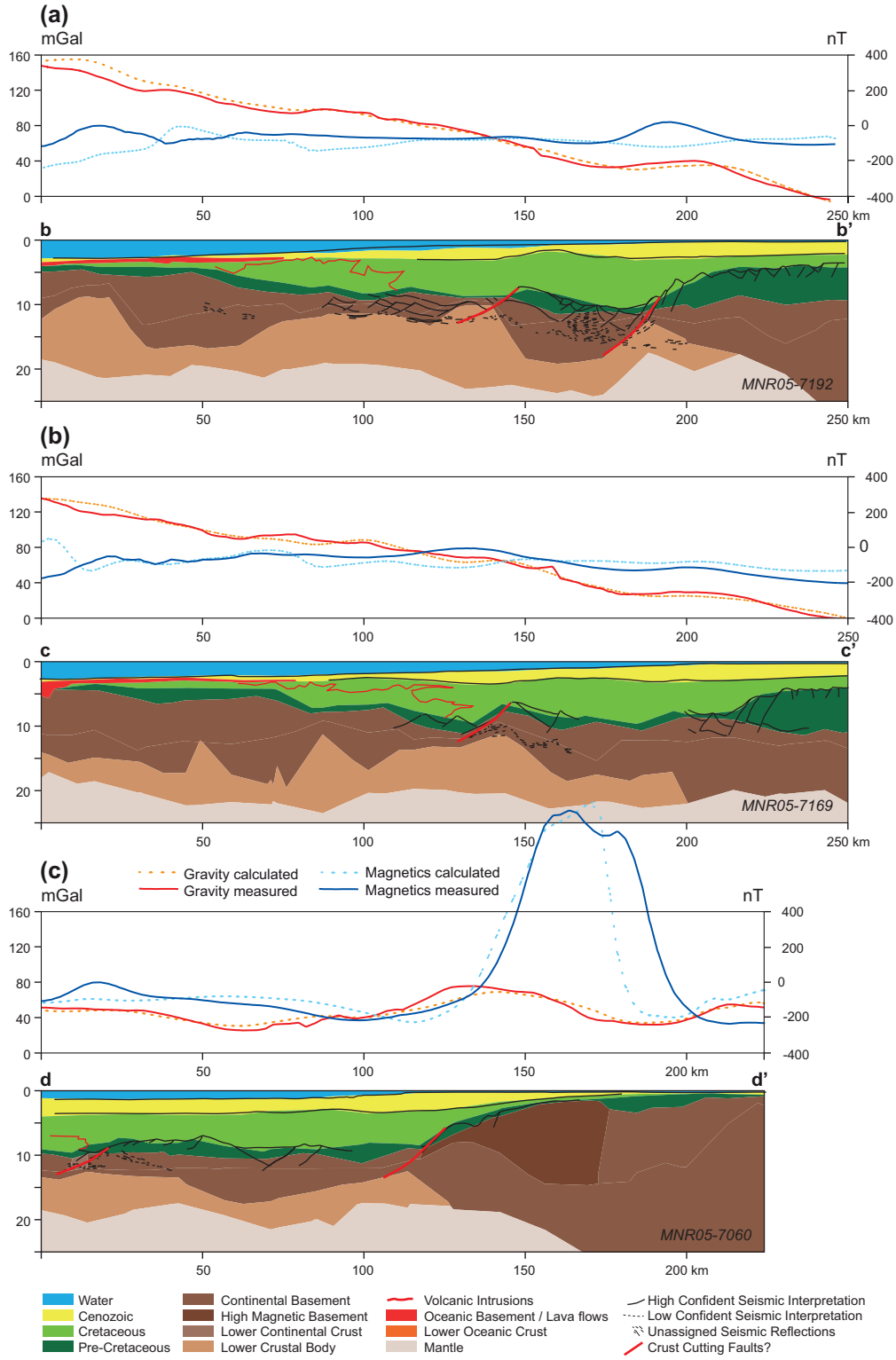
(a)
mGal
nT
160
120
80
40
0
400
200
0
-200
-400
50
100
150
200
250 km
b
b'
0
10
20
MNR05-7192
(b)
mGal
nT
c
c'
MNR05-7169
(c)
Gravity calculated
Gravity measured
Magnetics calculated
Magnetics measured
200 km
d
d'
MNR05-7060
Water
Cenozoic
Cretaceous
Pre-Cretaceous
Continental Basement
High Magnetic Basement
Lower Continental Crust
Lower Crustal Body
Volcanic Intrusions
Oceanic Basement / Lava flows
Lower Oceanic Crust
Mantle
High Confident Seismic Interpretation
Low Confident Seismic Interpretation
Unassigned Seismic Reflections
Crust Cutting Faults?

crust has been documented on the Iberian margin and from the fossil continent-ocean transition preserved in the Eastern Alps. Where extension is large enough for the entire crust to become brittle, cross-cutting faults have caused serpentinisation of the underlying upper mantle (e.g. Manatschal 2004).

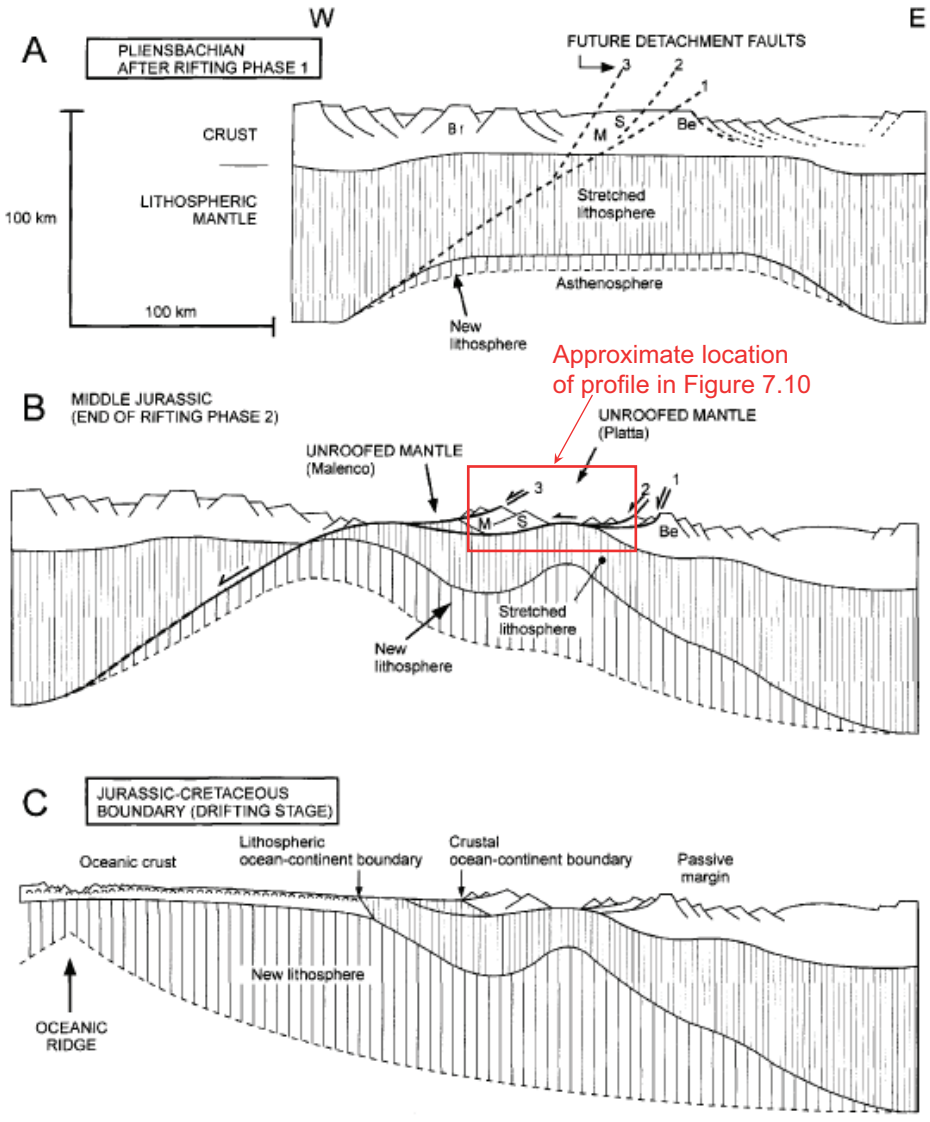

Figure 7.9. An evolution model based on Froitzheim & Manatschal (1996) that fits the main structural features and proposed LCB origin on the Møre margin. Syn- and postrift sedimentary units are not shown. (**a**) Situation after overall pure-shear extension in first rifting phase, with traces of future, second-phase detachment faults indicated. (**b**) Situation after second rifting phase, immediately preceding continental breakup: sequentially active, west-dipping detachment faults have accommodated exhumation of mantle in two areas. (**c**) Drifting stage.

Isostatic considerations point towards a at least twofold origin of the LCB on the Møre margin. The gravity signal calculated from the starting model, after the Moho had been isostatically adjusted, was considerably less than the observed gravity signal. This can have three explanations, the unloading effect of the sediments is more than accounted for, the margin is not in isostatic equilibrium and the margin is experiencing subsidence, or there is more mass in the crust than accounted for in the starting model. To account for the mismatch by unloading, the sediments would have to have densities much lower than realistically possible. There is no indication of lateral movement in the study area that allow us to believe the area is not close to isostatic equilibrium. Therefore we have to assume the existence of a body of anomalous density at the crust-mantle interface. This body can either be a high density crustal body or a low density mantle body. From isostatic and flexural considerations, as described above, it is feasible to assign this body to the crust where the modelled Moho is below the isostatic Moho and to the mantle where the modelled Moho is above. By subtracting the isostatic Moho from the modelled Moho we note that the positive values correspond to the most proximal part of the LCB underlying very thin crust and therefore reinforce the postulation of a mantle origin (Figure 7.7).

Several authors have suggested that the Møre Basin started to open as an ocean in the Cretaceous (Bott 1975, Roberts *et al.* 1981). This interpretation was not supported by Eldholm *et al.* (1984). However, Lundin & Rundhovde (1993) later proposed that nearly successful rifting took place in the basin. A NW-oriented refraction profile across the Møre margin (Ólafsson *et al.* 1992) supports the results of this study that only a few km of crust remains in the central part of the basin. The profile crosses a series of NE-trending positive magnetic anomalies (maximum amplitude of anomalies of approx. 450 nT) in the central Møre Basin, the pronounced crustal thinning coincides with the magnetic anomalies. These anomalies have been interpreted as seamounts (Lundin & Rundhovde 1993), by analogy with characteristics of such features in the northern Red Sea (Cochran & Martinez 1988). If so, their presence implies a nearly successful rift event (Lundin & Doré 1997). Evidence of Early Cretaceous magmatic activity in the region includes report of pyroclastic rocks in the North Sea (Crittenden *et al.* 1991), off mid-Norway (Dalland 1980), and on East Greenland (Lundin & Doré 1997, Doré *et al.* 1999). Skilbrei *et al.* (2002) claim that the absence of a coinciding belt of pronounced gravity anomalies along the axis of the basin makes it unlikely that Cretaceous seamounts exist at the centre of the Møre Basin. They suggest an alternative interpretation that is a combination of high-grade basement highs, possibly with increased magnetization due to intrusions that form a 'Christmas tree' of dykes and sills. Osmundsen & Ebbing (2008) suggested that serpentinised mantle under the highly extended continental crust of the Møre Basin is fully possible. Serpentinisation decreases the density (Miller & Christensen 1997) of the original manle rock but increases the magnetic susceptibility (Dunlop & Prévot 1982). During serpentinisation a crystallization magnetic remanence is acquired because of the growth of newly formed magnetite grains in the ambient geomagnetic field (Dunlop & Prévot 1982). Oufi & Cannat (2002) showed that the magnetic susceptility remains modest for degrees of serpentinisation less than 75% but increases sharply for degrees of serpentinisation higher than 75%. The density of peridotite serpentinised to a degree of 75% is between 2700 and 2800 kg/m^3 (Miller & Christensen 1997) which is the same as the density of the crystalline basement. The high density body modelled below the central axis of the Møre Basin labelled lower crustal body (LCB) can represent a lightly serpentinsed mantle and the body labelled high magnetic basement in

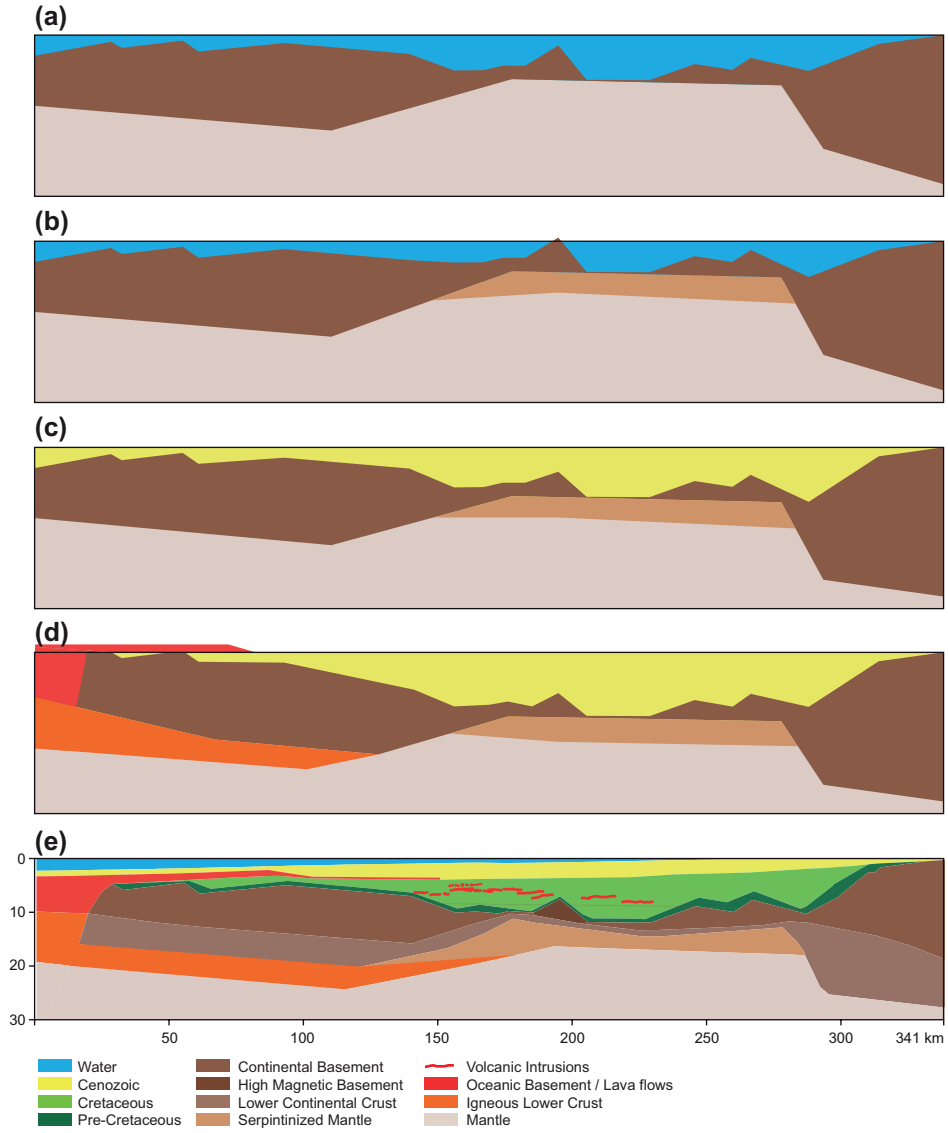

Figure 7.10. Evolution of the Møre margin from the end of main rifting phase to current setting. (**a**) At the end of the main rifting phase the whole crust is brittle and severely thinned in the axial part of the basin. (**b**) Eventual embrittlement of the entire crustal section results in isostatic response of a volume increase at the crust-mantle boundary that causes crustal uplift in the axial part of the basin. (**c**) Subsequent sedimentation loads the crust which subsides by the isostatic response to the load. (**d**) At the time of breakup the margin becomes strongly magmatic. Magmatic underplating and/or highly intruded lower crust change the crustal density structure and consequently trigger isostatic response that causes uplift of the marginal high. (**e**) Further post-drift sedimentation and thermal contraction develops the margin to the present state.

Figure 7.5 has the same properties as highly serpentinised peridotite. The SW extension of the Vigra High has geometrical and property resemblance to the Hobby High on the Iberia margin (Manatschal *et al.* 2001), which is a crustal remanence overlying exhumed mantle that has been capped by a detachment fault (Manatschal 2004). The distinctive SW-NE trending magnetic anomaly and lack of coinciding gravity anomaly in the Møre Basin could therefore be explained by the existence of serpentinised peridotites below the basin.

The profiles on Figure 7.8 show combined seismic interpretation and model results. They demonstrate that the top of the LCB as indicated by the model has a resemblance in the seismic signature as deep-reflector bands as described by Osmundsen *et al.* (2002). As noted by Osmundsen & Ebbing (2008) incision of the deep reflector band by Jurassic-Creaceous faults indicates that the LCB in the Møre Basin was in place long before Tertiary magmatic activity and it is therefore highly unlikely that the LCB is of underplate origin. The profiles also demonstrate how the variation of LCB thickness across the margin. On profile A in Figure 7.8 it is apparent that where the crust has been severely faulted the LCB is thick. It is feasible to assume these faults may be responsible for crosscutting the crust and consequent serpentinisation of the underlying mantle. On the more distal part it cannot be ruled out the LCB has magmatic origin as it coincides with the distribution on sills in the basin, which in turn might suggest a genetic link between the LCB and sills.

In general terms crust thins from ~30 km at the coastline to less than 10 km in the axial part of the Møre Basin, thickens below the Faroe-Shetland Escarpment to ~15 km and gradually thins towards the COB. These first-order observations fit a kinematic evolution model by Froitzheim & Manatschal (1996). Based on field observations in the Alpine former margins they suggest a discontinuous, two-stage evolution of rifting, with a fundamental reorganization of fault patterns between the two stages. During the second rifting stage two the mantle is unroofed in two locations and in between resides considerable residue of continental crust, which would be represented by the Møre Marginal High on the Møre margin. The drift and creation of oceanic crust would be facilitated by the more distal unroofed mantle location (Figure 7.9).

A conceptual sketch of the evolution of the Møre margin based on our observations and the kinematic model by Froitzheim & Manatschal (1996) is provided in Figure 7.10. The sketch shows the evolution of the margin from the end of the main rifting phase to present day setting along seismic line GMNR94-102 (Figure 7.5). At the end of the main rifting phase the whole crust is brittle and severly thinned in the axial part of the basin (Figure 7.10a). Eventual embrittlement of the entire crustal section paths the way for water to percolate into the upper mantle and changes the petrophysical state of the mantle material which results in decreased density and increased volume of the upper mantle rocks. The isostatic response of the volume increase at the crust-mantle boundary results in crustal uplift in the axial part of the basin (Figure 7.10b). Subsequent sedimentation loads the crust which subsides caused by the isostatic response to the load (Figure 7.10c). At the time of breakup the margin becomes strongly magmatic and magmatic products in the form of intrusions and lava flows affect the distal part of the margin. Magmatic underplating and/or highly intruded lower crust change the crustal density structure and consequently trigger isostatic response that causes uplift of the marginal high (Figure 7.10d). Further post-drift sedimentation and thermal contraction develops the margin to the present state (Figure 7.10e).

7.6 Conclusions

Implementation of the concept of isostasy and flexure of the lithosphere to the results from the 3D model of the Møre margin provided new insights into the characteristics and possible origin of the LCB on the margin.

Isostatic considerations strongly suggest the existence of a body of anomalous density at the crust-mantle interface. This body can either be a high density crustal body or a low density mantle body. It is feasible to assign this body to the crust where the modelled Moho is below the isostatic Moho and to the mantle where the modelled Moho is above. By subtracting the isostatic Moho from the modelled Moho we note that the positive values correspond to the most proximal part of the LCB underlying very thin crust and therefore reinforce the postulation of a mantle origin.

Combined seismic interpretation and model results demonstrate that the top of the LCB as indicated by the model has a resemblance in the seismic signature as deep-reflector bands. The incision of the deep reflector band by Jurassic-Creaceous faults indicates that the LCB in the Møre Basin was in place long before Tertiary magmatic activity and it is therefore highly unlikely that the LCB is of underplate origin.

Where the crust has been severely faulted the LCB is thick and it is proposed that these faults may be responsible for crosscutting the crust and consequent serpentinisation of the underlying mantle. On the more distal part it cannot be ruled out the LCB has magmatic origin as it coincides with the distribution on sills in the basin, which in turn might suggest a genetic link between the LCB and sills.

Acknowledgements
Seismic lines from the MNR survey acquired by Fugro Multi Client Services in cooperation with TGS-NOPEC Geophysical Company were used in this study. The software Lithoflex was used to acquire the flexural Moho. The flexural backstripping was calculated by utilization of Mathcad files provided by Watts (2001).

Chapter 8

Properties and distribution of lower crustal bodies on the mid-Norwegian margin

Reynisson, R. F., Ebbing, J., Lundin, E. & Osmundsen, P. T. In print. Properties and distribution of lower crustal bodies on the mid-Norwegian margin. In: *From Mature Basins to New Frontiers*. Proceedings of the 7th Petroleum Geology Conference. Geological Society, London.

This study addresses the origin of the LCB on the whole mid-Norwegian continental margin (Figure 8.1). The mid-Norwegian margin was formed by episodic extensional events during Late Paleozoic-Triassic, Late-Jurassic-Early Cretaceous and Late Cretaceous-Paleocene times (Ziegler 1988, Blystad *et al.* 1995, Doré *et al.* 1999, Brekke 2000). Early Tertiary continental break-up and initial seafloor spreading between Eurasia and Greenland was characterized by emplacement of significant volumes of magmatic rocks (e.g. Eldholm & Grue 1994). The magmatic rocks were partially extruded on the surface as flood basalts and tuffs and partially intruded as central complexes, sills and dikes into the sedimentary rocks and the crystalline crust. In addition, a lower crustal high-velocity body has been recognized along many parts of the margin, and is commonly interpreted to represent magmatic material added beneath the crust (e.g. Eldholm & Grue 1994, Mjelde *et al.* 2001), or intruded in the lower crust (e.g. White *et al.* 1987, White *et al.* 2008, White & Smith 2009). Notably, the interpreted magmatic body has been proposed to constitute between 60% and 80% of the total magmatic rock volume in the NAIP (White *et al.* 1987, Eldholm & Grue 1994, White *et al.* 2008). In the southernmost Vøring basin, however, the lower crustal layer shows anomalously high P-wave velocities (8.4 km/s) and has been interpreted as eclogite by Raum *et al.* (2006) and Mjelde *et al.* (2009b). In the remainder of the basin the layer is interpreted as mafic intrusions emplaced during the last phase of rifting, but it cannot be excluded that the body consists of older (Caledonian?) mafic rocks (Ebbing *et al.* 2006, Mjelde *et al.* 2009a). Determining the nature of the LCB clearly is relevant for the thermal history of volcanic margins, and arguably also for the entire concept of the development of such margins.

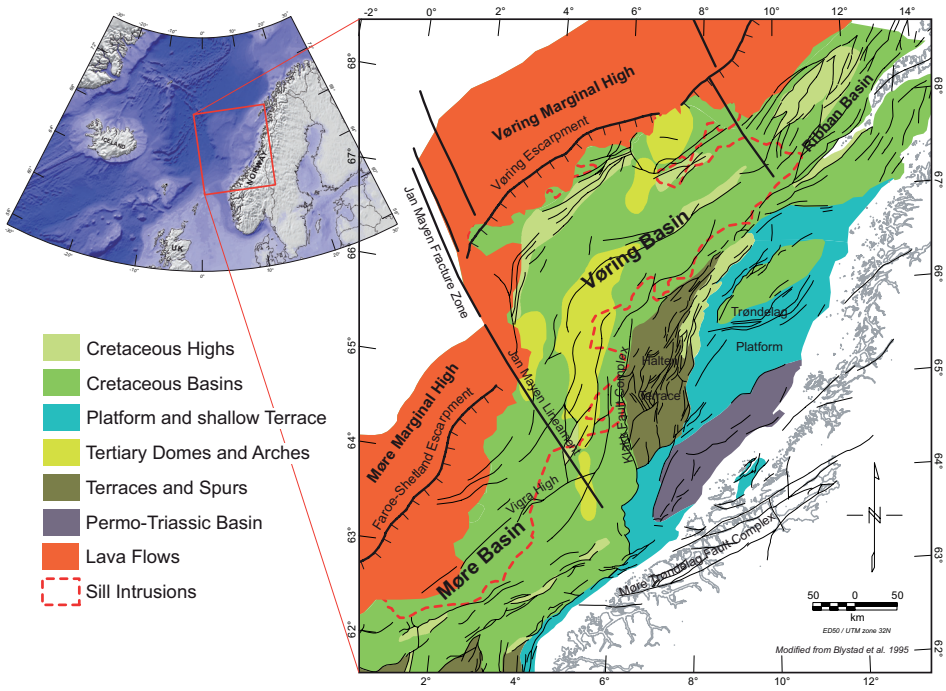

Figure 8.1. The study area is the mid-Norwegian margin, a part of the NE Atlantic margin, and comprises the Møre, Vøring and Lofoten-Vesterålen margin segments. The figure shows the main geological and structural features of the margin based on Blystad *et al.* (1995).

8.1 Compilation of 3D models

The geometries of the deeper crust and the upper mantle on the mid-Norwegian margin are reasonably well defined in 2D by OBS data. From 3D potential field models, which have been integrated in the current study, different horizons can be mapped, which allow discussing regional changes in the geometry of the study area. The spatial extension of the horizons, with the exception of the Moho, is limited to the NW by the main escarpments and to the SE by the coast of Norway. Here, we utilize top crystalline basement, top LCB, and Moho horizons in alliance with seismic interpretation and isostatic considerations to shed light on the properties of the LCB.

Figure 8.2 shows the thickness of the high-density lower crustal body (LCB) as defined by the integrated 3D models and seismic data. The LCB is primarily modelled on the Møre and Vøring margins and extends from the escarpments well into the basins. The overall structural trend of the LCB follows the general strike of the margin as indicated by seismically mapped faults. Two distinct LCB ridges that are up to 10 km thick exist on the Møre margin. The Vøring margin contains an LCB that is somewhat more evenly distributed, varying between 3 and 8 km thickness. The Lofoten margin has only a veneer of LCB that is little more than 1 km thick and is not present north of the supposed Jennegga Transfer Zone (Tsikalas *et al.* 2008).

By subtracting the Moho from the top basement horizon a crustal thickness map was acquired (Figure 8.3). The map shows a very thin crystalline crust (less than 5 km) below

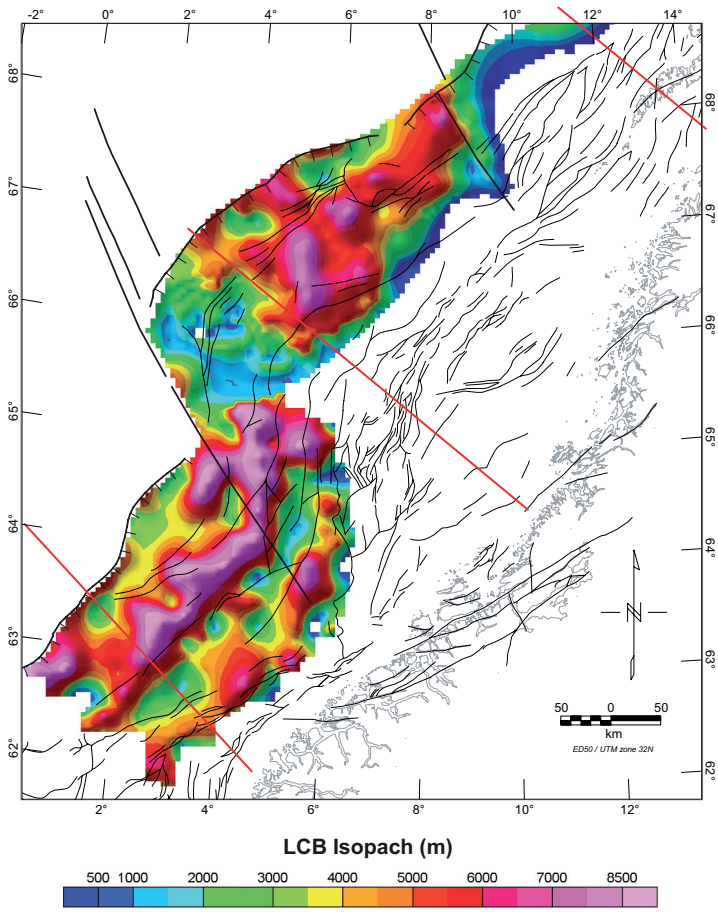

Figure 8.2. LCB isopach resulting from integrated 3D models of the mid-Norwegian margin. The structural features are the same as in Figure 8.1. The red lines indicate the location of profiles in Figure 8.8.

the centre of the Møre Basin. Thin crust (less than 10 km) is noted along the whole mid-Norwegian margin and coincides with the extent of the Cretaceous depocentres, suggested to relate to Early Cretaceous rifting (Lundin & Doré 1997). Comparison of the crustal thickness with the LCB distribution reveals a strong first order correlation along the entire mid-Norwegian margin. Locally, there is not always a one-to-one correlation between thickest modelled LCB and thinnest modelled crust. There are several possibly explanations for this, such as different origin of the LCB (magmatic, metamorphic, serpentinised). Particularly, densities of serpentinised mantle rocks may overlap with densities of crustal rocks and may therefore not be recognized by gravity modelling.

The distribution of volcanics in the study area was compiled from a seismic study (Chapter 6) and from previously published maps (Blystad *et al.* 1995, Olesen *et al.* 2002, Planke *et al.* 2005). Comparison of distributions of the LCB and the limit of lavas and sills (Figure 8.4) reveals that all the LCB on the Vøring margin is overlain by volcanics and so is a considerable part on the Lofoten margin. On the Møre margin the LCB is overlain by volcanics apart from the landward LCB ridge that coincides with the very thin crust.

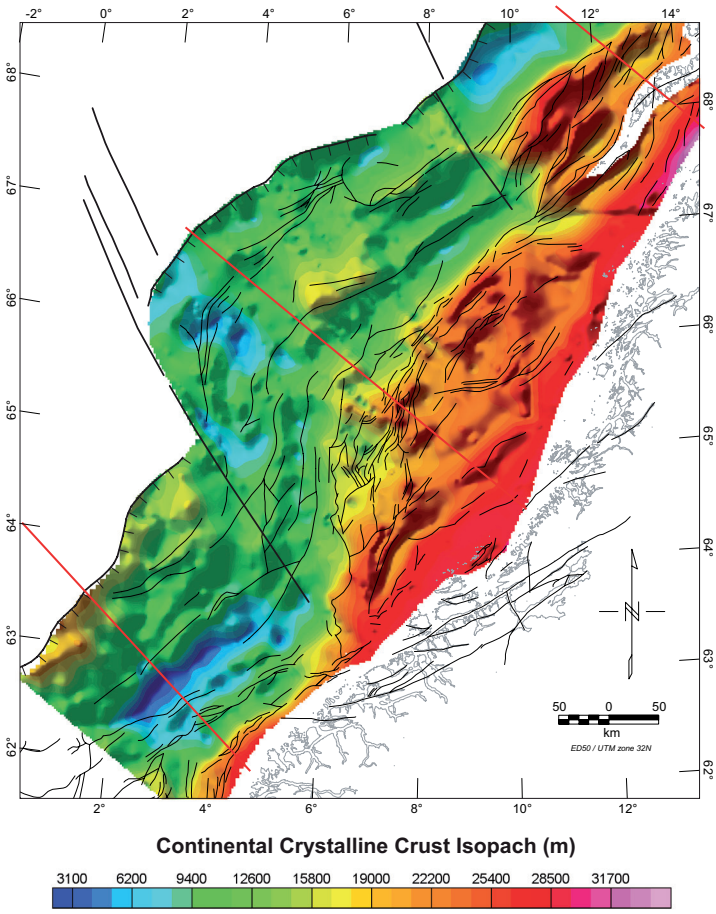

Figure 8.3. Thickness of continental crystalline crust. The map shows that a very thin crystalline crust (less than 5 km) exists below the centre of the Møre Basin. Thin crust (less than 10 km) is noted locally on the whole mid-Norwegian margin and coincides with the extent of the Cretaceous depocentres, suggested to relate to Cretaceous rifting (Lundin & Doré 1997). The structural features are the same as in Figure 8.1. The red lines indicate the location of profiles in Figure 8.8.

8.2 Isostatic considerations

The Moho boundary is assumed to reflect the isostatic equilibrium surface at the base of the lithosphere. Because the Moho is shallower than the base lithosphere and has a high density contrast it is the main contributor of isostatic compensation to the gravity field. Comparison of the Moho from the integrated models with an isostatic compensation surface provides insight into the characteristics of the whole crust in the study area. By comparing the two differently acquired Mohos, it is proposed that a distinction can be made between whether the LCB should be assigned to the crust or the mantle. This distinction has a profound

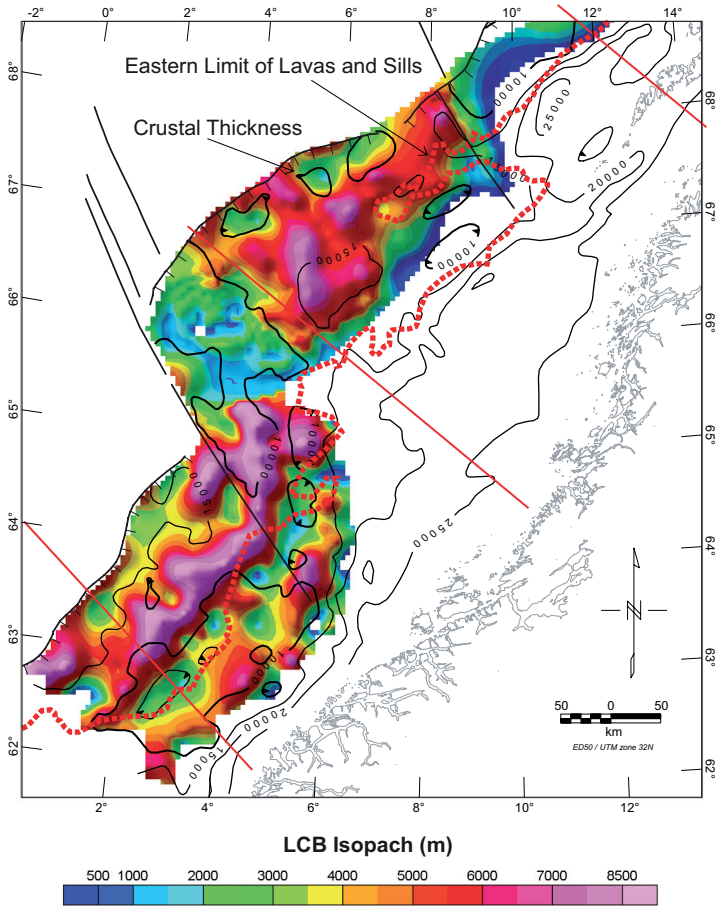

Figure 8.4. LCB distribution compared to magmatic rocks and crustal thickness. The black lines are contours of the crust thickness in Figure 3 and are drawn with 5000 m interval. The red dotted line presents the eastern limit of lavas and sills on the margin. Comparison of LCB distribution and volcanic distribution reveals that all the LCB on the Vøring margin is overlain by volcanics and considerable part on the Lofoten margin. On the Møre margin the LCB is overlain by volcanics apart from the landward ridge that coincides with the very thin crust. Comparing the crustal thickness to the LCB distribution shows that in the Møre Basin the thinnest crust spatially coincides with the most landward ridge of the LCB. The landward edge of the LCB in the Vøring Basin coincides with underlying thin crust. On the Lofoten margin the whole LCB coincides with thin crust. Main lineaments are the same as in Figure 8.1. The red lines indicate the location of profiles in Figure 8.8.

influence on the genetic origin of the LCB. Crust originated LCB indicates underplated or intruded igneous material in the lower crust and mantle originated LCB reflects a low density mantle. It is feasible to interpret the LCB associated to the mantle as seprnentinized mantle and further that this body spatially coincides with very thin crust.

Assuming that the mid-Norwegian margin is in isostatic equilibrium, we calculated the isostatic compensation for the de-loading of the margin by the relatively low-density sedimentary infill and water. For the isostatic calculation, we used the LithoFlex software

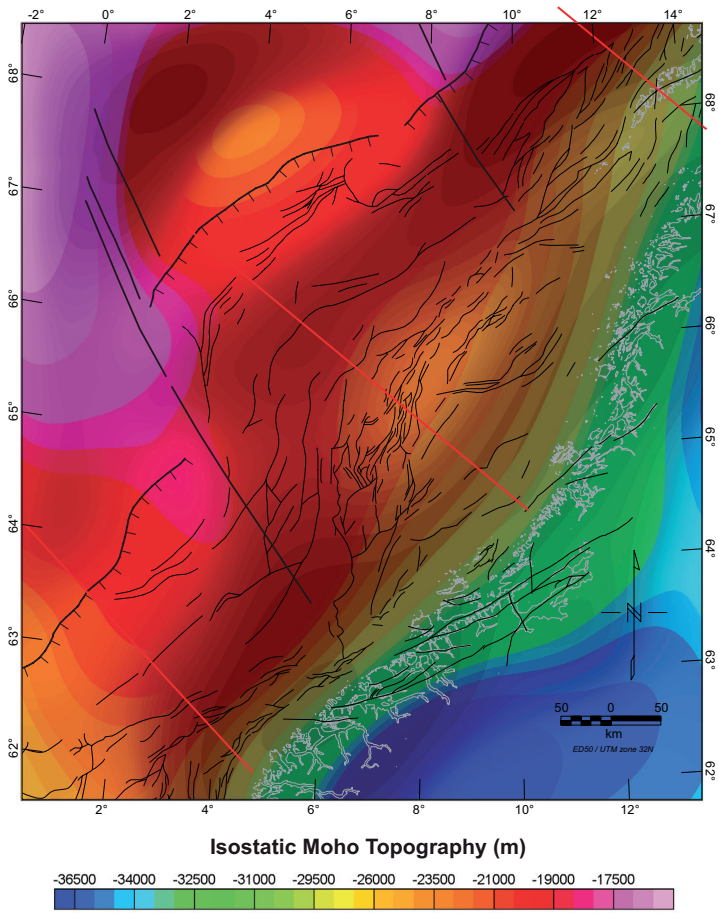

Figure 8.5. Isostatic flexural Moho. Relatively low value for the strength of the lithosphere (T_e=10 km) was applied to calculate the Isostatic flexural Moho. The reference depth was chosen 30 km and the density contrast at the isostatic flexural base with 400 kg/m^3, which correlates to a lower crust density of 2900 kg/m^3 and a mantle density of 3300 kg/m^3. The structural features are the same as in Figure 8.1. The red lines indicate the location of profiles in Figure 8.8.

(Braitenberg *et al.* 2002, Wienecke *et al.* 2007). The loading of the sediments was calculated by applying a linear depth-dependent density function from 2200 kg/m^3 at sea surface to 2700 kg/m^3 at 10 km depth and constant below this level. The surrounding basement had density of 2750 kg/m^3. The simplified density distribution leads to de-loading of the lithosphere, which in an isostatic concept requires crustal thinning to balance the load. A relatively low value for the strength of the lithosphere (T_e=10 km) was applied. The reference depth was 30 km and the density contrast at the isostatic flexural base was 400 kg/m^3, which corresponds to a lower crust density of 2900 kg/m^3 and a mantle density of 3300 kg/m^3.

The resulting isostatic Moho (Figure 8.5) shows a similar regional trend as the model Moho (Figure 8.6) with depth decreasing from the coast to the axial part of the basins and increasing again towards the marginal high. The difference map (Figure 8.7) highlights

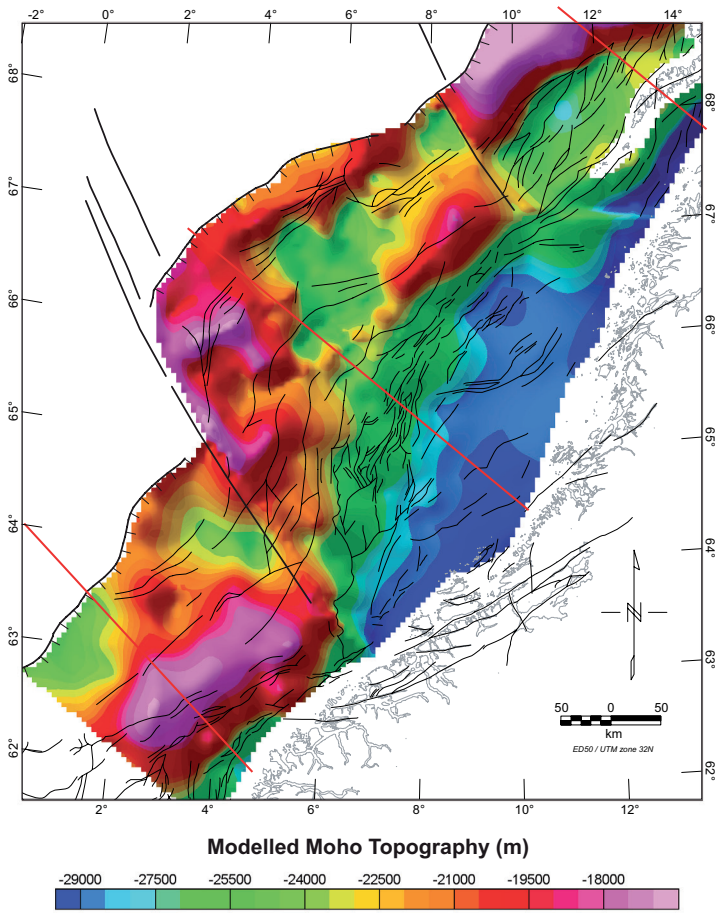

Figure 8.6. Model Moho. Moho configuration resulting from the compiled 3D models. The structural features are the same as in Figure 8.1. The red lines indicate the location of profiles in Figure 8.8.

substantial differences between the isostatic and modelled Moho and gives valuable insight into the margin. A positive difference reflects that the model Moho is shallower than the isostatic Moho and negative difference indicates locations where the model Moho is deeper. In the southern Vøring, the isostatic and model Moho are at similar depth, while in the central and northern Vøring margin the isostatic Moho is more than 4 km shallower than the model Moho, corresponding to the thickness of the LCB. The same observation is made for the outer Møre margin. In the inner Møre margin and the Lofoten margin, the isostatic Moho is deeper than the model Moho. Three profiles representative for each margin segment further illustrate the difference between the isostatic and model Moho (Figure 8.8).

The lateral volcanic distribution coincides mainly with negative Moho difference but the location of thin crust is most often associated with positive difference or a modelled Moho shallower than isostatic Moho (compare figures 8.4 and 8.7). Most of the LCB has a distribution that follows the trend of the negative Moho difference although the most inboard part of the LCB on the Møre and Vøring margins and the whole LCB on the Lofoten

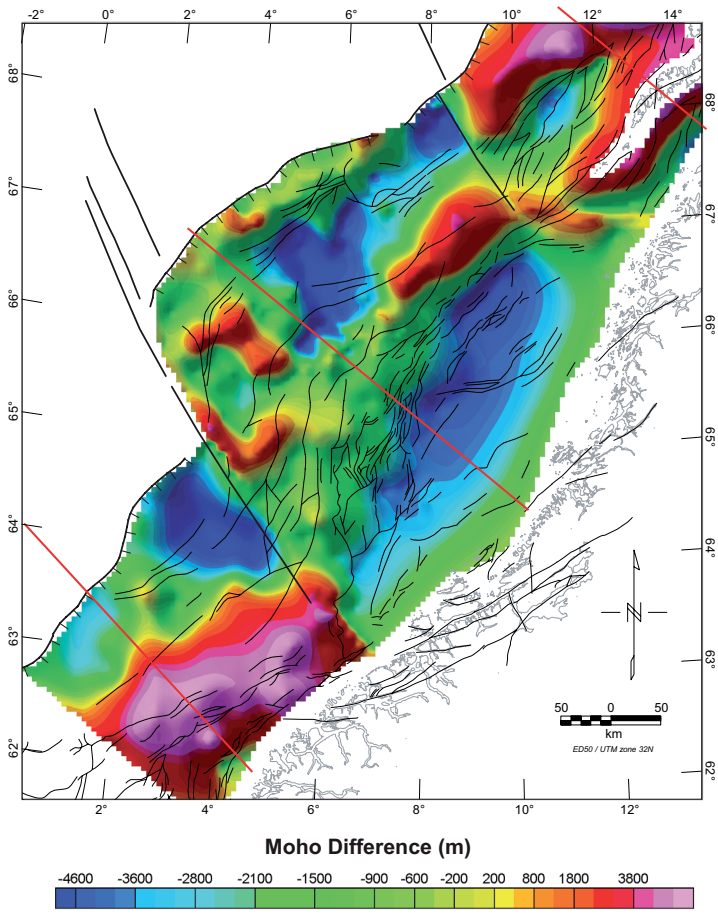

Figure 8.7. Moho difference. Positive difference reflects scenarios where the model Moho is shallower than the isostatic Moho and negative difference indicates locations where the model Moho is deeper. The difference map highlights substantial differences between the isostatic and model Moho. In the southern Vøring, the isostatic and model Moho are at similar depth, while on the central and northern Vøring margin the isostatic Moho is more than 4 km shallower than the model Moho. The same observation can be made on the outer Møre margin. On the inner Møre margin and the Lofoten margin, the isostatic Moho is deeper than the model Moho. The structural features are the same as in Figure 8.1. The red lines indicate the location of profiles in Figure 8.8.

margin are spatially associated with positive Moho difference and thin crust. The positive difference coinciding with LCB introduces a problem to a static crustal model if the LCB is assumed part of the crust. This is because the high density body is included in the model but not in the isostatic calculations. From isostatic considerations a high density body of LCB in the crust should suppress the Moho. It is therefore more feasible to assign the LCB in these scenarios to the mantle than the crust. Kimbell *et al.* (2004) compared Moho depth based on isostatic consideration with Moho depth observed in seismic data and noted discrepancies where estimated Moho was both shallower and deeper than observed Moho. Amongst several possibilities to explain the isostatic Moho being deeper than the seismic

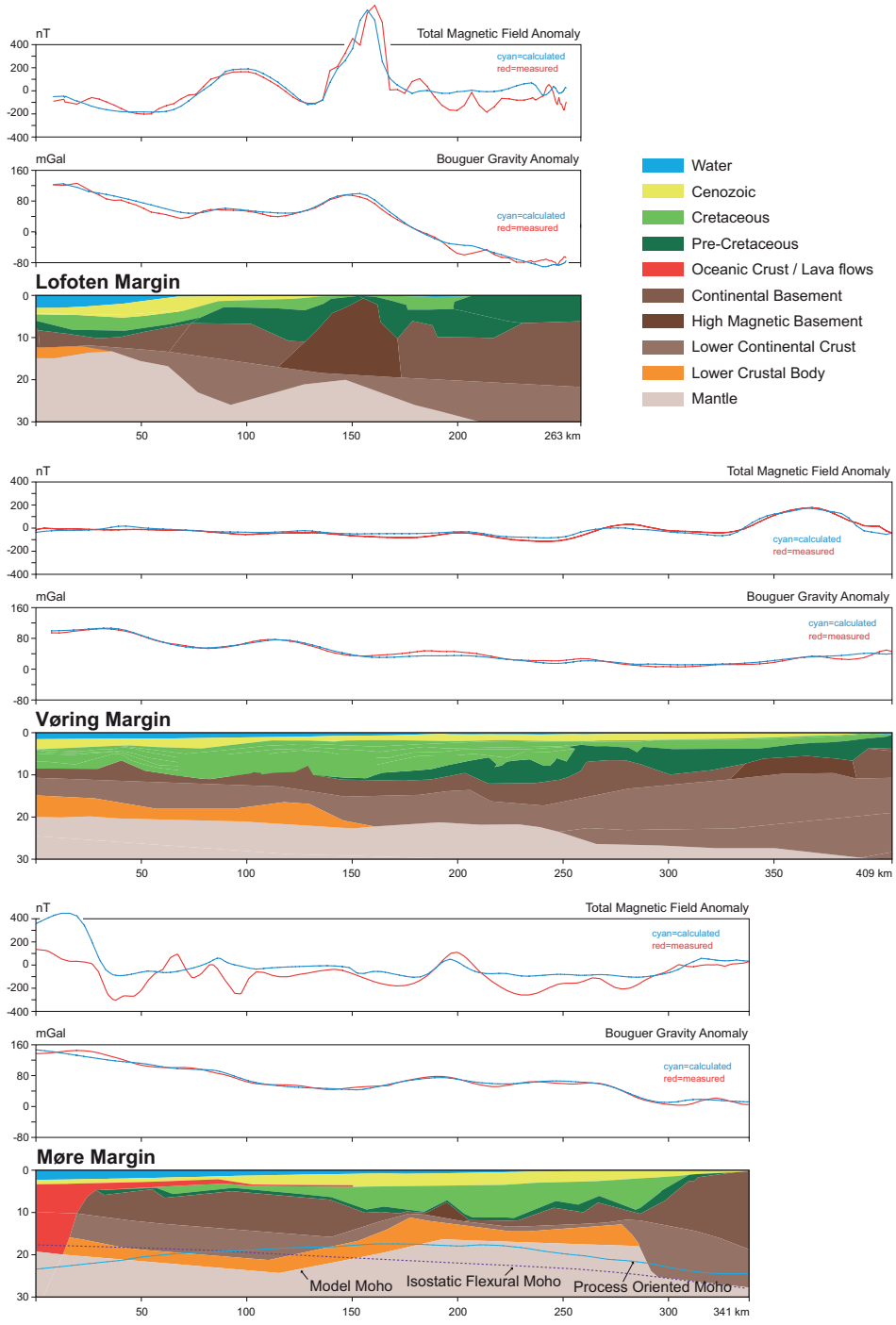

Figure 8.8. Representative profiles of the mid-Norwegian margin segments. Three profiles representative for each margin segment illustrate the main geological bodies of the mid-Norwegian margin. The properties used in the potential field models are listed in Table 8.1. See the Møre profile for comparison of different Moho types. The location of the profiles is shown with thick red lines in figures 8.2-8.7.

Table 8.1. Petrophysical properties applied in models. Density is in kg/m^3, magnetic susceptibility (Susc.) is in SI units (10^5), and magnetic remanence is given as Königsberger ratio (Q).

	Density	Susceptibility	Remenance
Water	2200	0	0
Cenozoic	2050-2500	10-100	0.2-0.4
Cretaceous	2200-2500	30-250	0.2-0.3
Pre-Cretaceous	2600-2650	30-250	0.2-0.3
Oceanic Crust / Lava flows	2700	2000	2
Continental Basement	2680-2750	750	0.5-0.7
High Magnetic Basement	2680-2750	2000-3000	1.0-1.5
Lower Continental Crust	2850-2950	1000-2000	0.4-0.5
Lower Crustal Body	3100	500-750	0.4
Mantle	3300	0-250	0-0.4

Moho Kimbell *et al.* (2004) favoured a negative upper mantle density anomaly. This means that the modelled high-density LCB is not a part of the crust but a low-density mantle and the model Moho is defined at the top of the LCB which results in even larger positive Moho difference.

8.3 Process oriented approach

A profile from the Møre margin demonstrates the Moho configuration and the discrepancy between model Moho and isostatic Moho (Figure 8.8). Accepting that LCB coinciding with a positive Moho difference represents a low-density mantle, the Moho is defined at the top of the LCB in the centre of the basin but at the base of the LCB at the flanks of the basin. In order to reconstruct this Moho configuration with isostatic and flexural considerations a process oriented approach (Watts 2001) is needed. This approach allows us to take into account different crustal strength regimes during rifting and subsequent sedimentation. We used elastic thickness values T_e=5 km during rifting and T_e=25 km during sedimentation to reconstruct the Moho geometry below the basin. The high Moho relief is preserved from the rifting period when the crust was weak. During sedimentation the crust is more rigid and therefore, distributes the load caused by the sedimentary fill over larger areas of the crust. The resulting Moho configuration resembles the model Moho configuration in a very shallow Moho in the centre of the basin. This approach demonstrates how the positive difference between the model Moho and the isostatic Moho can exist and still be isostatically reasonable.

From the above, it possible to exclude that the LCB coinciding with positive Moho difference is magmatic underplate or highly intruded lower crust. An underplated or intruded lower crust would be related to the Early Tertiary continental break-up (e.g. White *et al.* 1987, Eldholm & Grue 1994), which is much later (in the order of 80 m.y.) than the main rifting period on the margin in the Late Jurassic-Early Cretaceous (Lundin & Doré 1997) and likewise after most of the sediment infill had taken place. If the lower crust is underplated or greatly intruded below the axial part of the basins the crust would reflect a more local isostatic architecture because high heat flows and consequently weak crust

are the effects of magmatic underplating, which would be in disagreement with a strong crust (T_e=25 km) during the whole sedimentation period. The spatial coincidence of very thin crust, positive Moho difference and LCB further point towards a mantle origin of the LCB. From this it is more feasible to assign the origin of the LCB to unroofed mantle rocks that have undergone serpentinisation. Such settings are prone to develop decollements at the crust/serpentinised mantle interface (e.g. Reston 2009), which in turn can lead to core complex-like structural geometries. A modelled Moho deeper than isostatic Moho can on the other hand be explained by isostatic readjustments of weak crust caused by igneous underplate or intrustions in the lower crust.

8.4 Regional considerations

Geologic history predating separation of the mid-Norwegian margin from that of East Greenland included two events that are particularly important with respect to the discussion of LCB origin. The first event was the Late Silurian-Early Devonian Caledonian Orogeny, which was succeeded by Devonian-Early Carboniferous extension and unroofing (e.g. Osmundsen *et al.* 2006). High-grade metamorphic rocks formed during this orogeny are well preserved in outcrop on both conjugate margins and it can readily be concluded that the deeper crust of the original Caledonian root also consisted of high-grade rocks. The protoliths of this orogenic root probably varied considerably. Even so, it appears very likely that remnants from the orogenic root likely would have achieved P-wave velocities in the 7-8 km/sec range (c.f. Hürich *et al.* 2001).

The second important tectonic event was the Late Jurassic-Early Cretaceous rifting, which established the pre-cursor to our current NE Atlantic margins (Doré *et al.* 1999). Following the mid-Jurassic opening of the Central Atlantic, Early Cretaceous rifting followed by plate separation that propagated northward from Iberia-Newfoundland into the Bay of Biscay, Rockall Trough, and Labrador Sea (e.g. Johnston *et al.* 2001). Severe Early Cretaceous rifting also extended from the Rockall Trough via the Faroe-Shetland Basin, Møre Basin, Vøring Basin, Lofoten-NE Greenland margins into the Tromsø and Bjørnøya Basins of the SW Barents margin (e.g. Shannon 1991, Faleide *et al.* 1993, Lundin & Doré 1997). Of the mentioned areas the Iberia and Newfoundland margins have been sampled via several academic drilling campaigns, proving the presence of exhumed and serpentinised mantle (e.g. Tucholke *et al.* 2007 and references therein). For quite some time it has been clear that the Labrador Sea conjugate margins are characterized by belts of exhumed mantle (Louden & Chian 1999, Srivastava & Roest 1999). The Rockall Trough has also been interpreted to be underlain by exhumed and serpentinised mantle (O'Reilly *et al.* 1996, Morewood *et al.* 2005). The highly stretched southern axial part of the Porcupine Basin, where the so-called Median Volcanic Ridge is located, is now considered to be highly thinned continental crust underlain by serpentinised mantle (Reston 2009). A review of the mentioned magma-poor margins is provided by Reston (2009). Our contribution in this paper illustrates that also the Møre Basin likely is underlain by serpentinised mantle, and we argue that the Vøring basin probably also is underlain by serpentinised mantle, at least in part. Like the Møre Basin, the Vøring Basin is characterized by a thick Cretaceous sedimentary fill, and the basin lacks significant Cenozoic extension except in the outermost part (e.g. Lundin & Doré, 1997, Roberts *et al.* 1997).

While mantle exhumation in the Porcupine Basin probably relates to Late Jurassic rifting, the other mentioned areas were thinned during Cretaceous time. Notably, the plate separation rates were slow during the Cretaceous, consistent with the development of the mentioned magma-poor margins (Bown & White 1995). During the Early Eocene opening of the magma-rich NE Atlantic however, the plate separation rates increased dramatically for a short period. Commonly, this increase in plate separation rate and the magma-rich opening of the NE Atlantic is associated with the arrival of a mantle plume (e.g. White *et al.* 1987). High P-wave velocities of a lower crustal body along the continent-ocean transition has been interpreted to represent magmatic intrusion in the lower crust or underplating, stemming from rapid decompressional melting of anomalously hot mantle related to the mantle plume (e.g. White & McKenzie 1989, Eldholm & Grue 1994). Numerous OBS studies by Mjelde and co-workers along the mid-Norwegian margin (see Mjelde *et al.* 2009a and references therein) have outlined an extensive LCB under the mid-Norwegian margin, and this LCB has generally been interpreted to represent Early Cenozoic magmatic underplating.

Ascribing the LCB along the Edoras-Hatton margin and the conjugate SE Greenland margin to Early Cenozoic magmatic intrusion or underplating (White *et al.* 1987, White & Smith 1989) appears reasonable. In this area break-up of Pangea occurred within the Laurentian plate and the presence of Caledonian high grade metamorphic rocks is unlikely. As mentioned the path of Early Cretaceous rifting and related mantle serpentinisation went via the Rockall Trough into the mid-Norwegian margin. Lack of evidence for major Cretaceous extension along the SE Greenland/Edoras-Hatton Bank part of the NE Atlantic also makes mantle serpentinisation an unlikely explanation for the LCB here. However, the situation is quite different along the mid-Norwegian / East Greenland margins. Break-up of this part of the NE Atlantic certainly reopened the Caledonian Orogen, and both the mid-Norwegian Basins and Thetis Basin off NE Greenland were severely thinned during the Early Cretaceous rift event. Thus, the LCB beneath the mid-Norwegian margins in all likelihood relates to at least three different processes: 1) magmatic underplating or lower-crustal intrusion during Early Eocene break-up, 2) high grade metamorphism during the Caledonian orogeny, and 3) mantle serpentinisation during Late Jurassic-Early Cretaceous rifting. Of these processes, it appears that Early Cretaceous mantle serpentinisation may be the dominant process. Recent work along the Hatton-Edoras margin reveals that the LCB there is confined to a relatively narrow body, ca 40 km in width (White *et al.* 2008, White & Smith 2009). We have no problem accepting that this LCB relates to Early Cenozoic intrusions of the lower crust as proposed. However, the much wider LCB, observed on the mid-Norwegian margin coincides closely with the deep Cretaceous basins and we propose a genetic relationship between the severe Cretaceous extension and the LCB. Notably, V_p/V_s ratios along regional transects across the mid-Norwegian margin reveal ratios in the 1.8-1.9 range for large areas. Such V_p/V_s ratios are consistent with serpentinised mantle, but also with gabbro (Miller & Christensen 1997, Escartin *et al.* 2001). The weakness in interpreting this part of the mid-Norwegian LCB as underplated material (Mjelde *et al.* 2009b) lies foremost in the absence of Cenozoic extension.

8.5 Discussion and conclusion

The origin of the LCB is still under discussion and different interpretations exist for the body and the strong deep crustal reflectors, which are often associated with it (e.g. Gernigon *et al.* 2003). The early proposal that the anomalously high velocity may reflect the concentration of MgO within magmatically underplated or intruded material, which in turn was suggested to reflect mantle temperature (White & McKenzie 1989), has subsequently been challenged (Eldholm *et al.* 1995, Gernigon *et al.* 2004). Nevertheless, it is still common that workers (e.g. Mjelde *et al.* 2005) propose that the LCB represents magmatically underplated material, and that the density and velocity distribution may

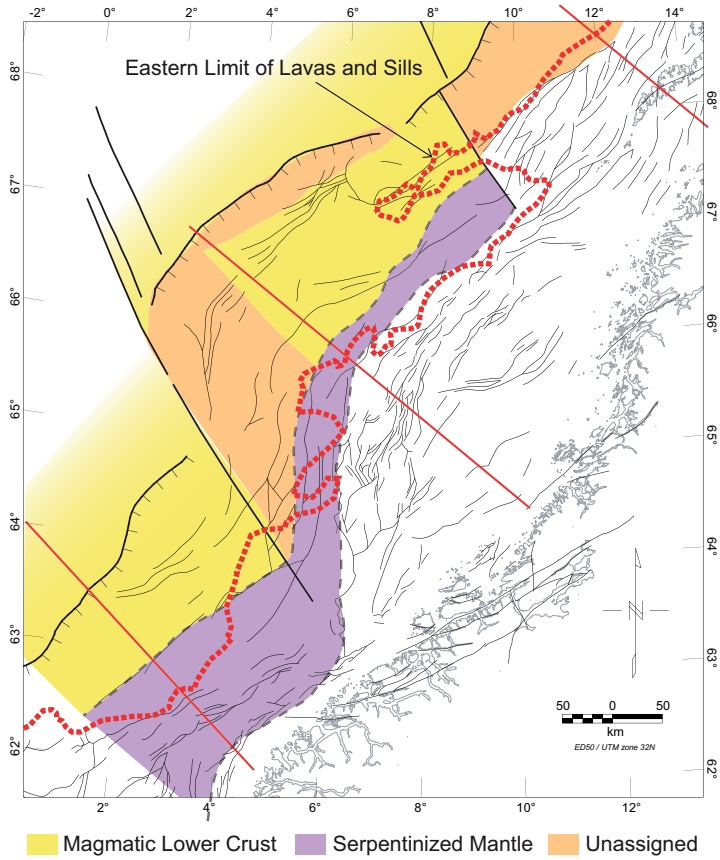

Figure 8.9. Proposed properties of LCB on the mid-Norwegian margin. The main conclusions are summarized in this figure which shows the distribution of LCB on the margin and its varying properties. The yellow colour indicates LCB most likely of magmatic intrusive or underplate origin. The violet colour defines the distribution of LCB that may represent serpentinised mantle. LCB that has indecisive origin is shown in orange. Here, the origin could be any of the proposed origins: 1) high grade metamorphic, 2) mantle serpentinisation, or 3) magmatic underplating. The red dotted line presents the eastern limit of lavas and sills on the margin. The structural features are the same as in Figure 8.1. The red lines indicate the location of profiles in Figure 8.8.

signify differences in the magma composition, in turn possibly reflecting asthenospheric temperatures or compositional inhomogeneities in the asthenospheric source. OBS studies indicate large variations in the thickness and velocity within the lower crustal body, and these have been proposed to relate to the distribution of mantle melts via feeder dykes (Mjelde *et al.* 2002). The velocities of this layer varies between 7.0–7.7 km/s, and have been reinterpreted as functions of differences in the magma composition due to inhomogeneities in the asthenospheric source (Mjelde *et al.* 2005) or as a function of mafic differentiation inside the LCB (Gernigon *et al.* 2006). White *et al.* (2008) suggest that variations in seismic velocity in the LCB may reflect variable percentages of intruded igneous rock into pre-existing continental crust.

Gernigon *et al.* (2003, 2004) discussed a range of possible origins for the LCB, where ultra high-pressure metamorphic rocks were the preferred alternative. Upper amphibolite to eclogite facies metamorphic rocks of a mafic composition have the same velocity range as those of the LCB (Hürich *et al.* 2001). The crust of the Horda Platform (Christiansson *et al.* 2000) and the Møre coastal area (Ólafsson *et al.* 1992) are interpreted to be underlain by eclogite. Raum *et al.* (2006) and Mjelde *et al.* (2009b) interpreted the lower crust in the southwestern corner of the Vøring Basin as in situ eclogite based on anomalously high P-wave velocities (8.4 km/s). The apparent correlation between the boundaries of the LCB and the interpreted offshore extensions of the post-Caledonian detachments support this interpretation (Ebbing *et al.* 2006), but it is unlikely that the entire region has the composition of eclogite. After all, only parts of the western gneiss region, onshore Norway, consist of these rocks and the bulk composition is a granitic or granodioritic gneiss. Depending on the protolith, metamorphism to upper amphibolite-eclogite facies can result in the same velocity range (~7–8 km/s) as the rocks that traditionally are interpreted as magmatically underplated material (Hürich *et al.* 2001). Thus, based on P-wave velocity alone it is not possible to distinguish between these alternatives and magmatic underplating. The V_p/V_s ratio should be distinctive (Eccles *et al.* 2009) but V_p/V_s ratios of LCB on the mid-Norwegian margin are reported between 1.8 and 1.9 (Mjelde *et al.* 2009a, 2009b). Such V_p/V_s ratios are compatible with mafic rocks of both igneous and metamorphic origin, but also with serpentinised mantle (Miller & Christensen 1997, Escartín *et al.* 2001).

In order to address the possible genetic relationship between the LCB and interpretations of magmatic underplating, it is important to consider the tectonic setting of the layer. For instance, the LCB extends far inboard of the eastern limit of significant Tertiary extension, while it apparently stops abruptly against the Bivrost Lineament. The abrupt termination of the LCB against the Bivrost Lineament is difficult to explain since it is clear that the passive margin continues north to the Senja Fracture Zone. Seen from a regional perspective, Tertiary extension does not terminate against the Bivrost Lineament. Thus, it is difficult to attribute the lack of a LCB body north of the Bivrost Lineament to the lack of Tertiary extension since it is obvious that the Lofoten margin segment also went to break-up.

Some authors (Eldholm & Grue 1994) have proposed that magmatic underplating will preferentially be located at pre-existing Moho relief locations. This concept could possibly explain how Early Cenozoic underplated material could be preferentially located under the Mesozoic Møre and Vøring basins. However, the explanation appears unlikely, The Rockall Trough is an example of a highly thinned basin that ought to have been ideally situated to preferentially receive Early Cenozoic magmatic underplating – yet it did not. It appears far

easier to propose a mechanism that links the LCB in the central Møre and Vøring basins in time to the Mesozoic crustal thinning, i.e. suggesting a serpentinised mantle origin. From isostatic considerations it is also unlikely as it is not reasonable to sustain a Moho relief with material added to the base of a rifted crust without assuming an unrealistically rigid crust.

On the mid-Norwegian margin, the presence of the LCB is linked to the differences between the isostatic and seismic Moho. The occurrence of LCB is either a response of the subsidence and rift history of the margin or the LCB has influenced the rift and subsidence history of the margin. Our proposal that the mid-Norwegian margin LCB can be related to at least three different geologic events (Figure 8.9) and processes influences several issues. The magmatic rock volume of the North Atlantic large igneous province may be significantly less than previously thought, considering that, 60–80% of the volume of this LIP has been estimated to reside in the LCB (White *et al.* 1987, Eldholm & Grue 1994, White *et al.* 2008). An origin other than magmatic underplating for the LCB will change the heat flow history of the margin significantly (to a cooler scenario).

In order to further enhance our understanding of the LCB observed on passive margins world wide it is important not only to integrate different geophysical methods but also to integrate different geological scale studies. The regional Moho configuration acquired by isostatic and modelling studies compared to seismically obtained Moho can shed light on the properties of LCB on all passive margins and improve understanding on the evolution of the margins.

Acknowledgments

The Geological Survey of Norway and TGS-NOPEC provided the gravity, magnetic and bathymetry data. The 3D modelling was performed using the software package IGMAS. This study is part of a PhD project titled 'Sub-basalt exploration using integrated gravimetric-, magnetometric- and seismic- (velocity) models, with isostatic considerations' financed by Shell. Odleiv Olesen is thanked for constructive feedback that led to modifications of the manuscript. We are also grateful to Robert S. White and Tony Doré that provided helpful reviews that improved the manuscript considerably.

Chapter 9
Concluding remarks

Volcanics affect the gravity and magnetic signals over a wide range of wavelengths, making it very difficult to distinguish between overlying basalts and underlying basement. The longer wavelengths interfere with the signal from the basement structure and the shorter wavelengths are greatly disturbed by noise and therefore the recognition of both basement and volcanics is problematic in the sub-basaltic environment.

Euler deconvolution provides valuable depth solutions in the volcanic environment but is not capable of identifying a basin overlain by basalts approaching 1 km thickness. High observation levels and an upward continuation did not enhance the solutions.

Forward density and magnetic models provide a valuable tool to estimate both the basalt and sub-basaltic sedimentary thickness but are limited by the ambiguity inherent in the potential field methods. Integration of gravity and magnetic in the modelling process provides better constraints than modelling each geophysical property in isolation. In particular, the use of gravity gradients further decreases the available model solutions and provides boundary detection even in sub-basaltic settings. Even with the increased availability of full tensor gravity data (FTG) data and increase in FTG technology geometrical constraints provided by seismic are vital to the potential field methods, as are well studies and other investigations that provide control on the petrophysical properties.

Isostatic considerations provide a first order approximation to the Moho depth which can be used as a regional guideline in a forward model. Comparison of the isostatic Moho and modelled Moho provide means to understand the evolution of the overlying crust. By comparing the two differently acquired Mohos a distinction can be made of whether the LCB should be assigned to the crust or the mantle. This distinction has a profound influence on the genetic origin of the LCB and hence the evolution history of the margin. Crust originated LCB indicates underplated or intruded igneous material in the lower crust and mantle originated LCB reflects a low density mantle.

Sub-basaltic seismic imaging remains problematic and therefore the integration of all available geophysical methods (i.e. electromagnetic methods) is important to further enhance sub-basaltic images. Careful characterization of the volcanics and the sub-basaltic sediments are also very important to better control geophysical interpretations. A feasibility study was undertaken in co-operation with EMGS to test the use of EM (both CSEM and MT) in sub-basalt exploration (Fanavoll *et al.* 2008). Three different models were run through the EMGS 3D modelling software, varying thickness as well as resistivity of the volcanics and basement. The presence of volcanics was clearly detected by the CSEM method. However, there is an upper threshold value of the thickness/resistivity product,

where the CSEM method becomes insensitive to variations in either thickness of the layer, or the resistivity. Below this threshold value variations in thickness and resistivity will influence the results. 2D inversion of three synthetic MT models was done in this feasibility study. One model included only a simple basalt structure. The MT response was not sensitive to this structure, because the contrast to the background resistivity was too small. In the second model the basement was added, in addition to the basalt. The basement boundary could be seen clearly from the inversion results and in the individual receiver responses. Finally, an increase in the basalt thickness was tested. The MT results were now sensitive to the basalt layer, but failed to resolve the sediments between the basalts and the basement where the thickness reaches its minimum values (1500 m).

In order to further enhance our understanding on passive margins it is important not only to integrate different geophysical methods but also to integrate different geological scale studies. The regional Moho configuration acquired by isostatic and modelling studies compared to seismically obtained Moho can shed light on the properties of LCB on all passive margins and therefore improve our understanding of their evolution.

Bibliography

Abrahamsen, N. & Waagstein, R. 2006. Magnetic logs from the Lopra-1/1A and Vestmanna-1 wells, Faroe Islands. *Geological Survey of Denmark and Greenland Bulletin* **9**, 41-49.

Allen, P. A. & Allen, J. R. 2005. *Basin analysis: priciples and applications*. Blackwell Publishing, Oxford.

Alvestad, E. 1997. Seismisk karakterisering og dannelse av det ekstrusive oppsprekkningskomplekset på Møre marginen. Unpublished MS thesis, University of Oslo.

Åm, K. 1970. Aeromagnetic investigations on the continental shelf of Norway, Stad-Lofoten (62°-69° N). *Norges geologiske undersøkelse* **266**, 49-61.

Andersen, M. S. 1988. Late Cretaceous and Early Tertiary extension and volcanism around the Faroe Islands. In: *Early Tertiary Volcanism in the North Atlantic* (edited by Morton, A. C. & Parson, L. M.). *Special Publications* **39**. Geological Society, London, 115-122.

Andersen, O. B. & Knudsen, P. 1998. Gravity anomalies derived from the ERS-1 satellite altimetry. Kort og Martykelstyrelsen, Copenhagen.

Andersen, T. B. & Jamtveit, B. 1990. Uplift of deep crust during orogenic extensional collapse: A model based on field studies in the Sogn-Sunnfjord Region of western Norway. *Tectonics* **9**, 1097-1111.

Ashcroft, W. A., Hurst, A. & Morgan, C. J. 1999. Reconciling gravity and seismic data in the Faero-Shetland Basin, West Shetland. In: *Petroleum Geology of Northwest Europe: Proceedings of the 5th Conference* (edited by Fleet, A. J. & Boldy, S. A. R.). Geological Society, London, 595-600.

Balling, N., Kristiansen, J. I. & Saxov, S. 1984. Geothermal measurements from the Vestmanna-1 and Lopra-1 boreholes. In: *The deep drilling project 1980-1981 in the Faeroe Islands* (edited by Berthelsen, O., Noe-Nygaard, A. & Rasmussen, J.). Føroya Fróðskaparfelag, Tórshavn, 137-147.

Barton, A. J. & White, R. S. 1997. Volcanism on the Rockall continental margin. *Journal of the Geological Society* **154**(3), 531-536.

Barton, P. & Barker, N. 2003. Velocity imaging by tau-p transformation of refracted seismic traveltimes. *Geophysical Prospecting* **51**(3), 195-203.

Basile, C., Mascle, J., Popoff, M., Bouillin, J. P. & Mascle, G. 1993. The Ivory Coast-Ghana transform margin: a marginal ridge structure deduced from seismic data. *Tectonophysics* **222**(1), 1-19.

Bell, B. R. & Butcher, H. 2002. On the emplacement of sill complexes: evidence from the Faroe-Shetland Basin. In: *The North Atlantic Igneous Province: Stratigraphy, Tectonic, Volcanic and Magmatic Processes* (edited by Jolley, D. W. & Bell, B. R.). *Special Publication* **197**. The Geological Society, London, 307-329.

Berndt, C., Skogly, O. P., Planke, S., Eldholm, O. & Mjelde, R. 2000. High-velocity breakup-related sills in the Voring Basin, off Norway. *Journal of Geophysical Research-Solid Earth* **105**(B12), 28443-28454.

Berndt, C., Mjelde, R., Planke, S., Shimamura, H. & Faleide, J. I. 2001a. Controls on the tectono-magmatic evolution of a volcanic transform margin: the Voring Transform Margin, NE Atlantic. *Marine Geophysical Researches* **22**(3), 133-152.

Berndt, C., Planke, S., Alvestad, E., Tsikalas, F. & Rasmussen, T. 2001b. Seismic volcanostratigraphy of the Norwegian Margin: constraints on tectonomagmatic break-up processes. *Journal of the Geological Society* **158**, 413-426.

Blakely, R. J. 1996. *Potential theory in gravity and magnetic applications*. Cambridge University Press, Cambridge.

Blystad, P., Brekke, H., Færseth, R. B., Larsen, B. T., Skogseid, J. & Tørudbakken, B. 1995. *Structural elements of the Norwegian continental shelf. Part II: The Norwegian Sea Region*. p.

Boillot, G. & Froitzheim, N. 2001. Non-volcanic rifted margins, continental break-up and the onset of sea-floor spreading: some outstanding questions. In: *Non-Volcanic Rifting of Continental Margins: A Comparison of Evidence from Land and Sea* (edited by Wilson, R. C. L., Whitmarsh, R. B., Taylor, B. & Froitzheim, N.). *Geological Society London Special Publications* **187**, 9-30.

Boldreel, L. O. 2006. Wire-line log-based stratigraphy of flood basalts from the Lopra-1/1A well, Faroe Islands. *Gelogical Survey of Denmark and Greenland Bulletin* **9**, 7-22.

Bott, M. H. P. 1975. Structure and evolution of the Atlantic Floor between northern Scotland and Iceland. *Norges geologiske undersøkelse Bulletin* **316**, 195-199.

Braitenberg, C., Ebbing, J. & Götze, H.-J. 2002. Inverse modelling of elastic thickness by convolution method - the eastern Alps as a case example. *Earth and Planetary Science Letters* **202**, 387-404.

Braitenberg, C., Wienecke, S. & Wang, Y. B. 2006. Basement structures from satellite-derived gravity field: South China Sea ridge. *Journal of Geophysical Research* **111**(B05407), 1-15.

Breivik, A., Mjelde, R., Faleide, J. I. & Murai, Y. 2006. Rates of continental breakup magmatism and seafloor spreading in the Norway Basin–Iceland plume interaction. *Journal of Geophysical Research* **111**(B07102).

Brekke, H., Dahlgren, S., Nyland, B. & Magnus, C. 1999. The prospectivity of the Vøring and Møre basins of the Norwegian Sea continental margin. In: *Petroleum Geology of Northwest Europe: Proceedings of the 5th Conference* (edited by Fleet, A. J. & Boldy, S. A. R.). Geological Society, London, 261-274.

Brekke, H. 2000. The tectonic evolution of the Norwegian Sea Continental Margin with emphasis on the Vøring and Møre Basin. In: *Dynamics of the Norwegian Margin* (edited by Nøttvedt, A.). *Special Publication* **167**. Geological Society, London, 327-378.

Buck, W. R., Martinez, F., Steckler, M. S. & Cochran, J. R. 1988. Thermal consequences of lithospheric extension: pure and simple. *Tectonics* **7**, 213-234.

Bugge, T., Befring, S., Belderson, R. H., Eidvin, T., Jansen, E., Kenyon, N. H., Holtedahl, H. & Sejrup, H. P. 1987. A giant three-stage submarine slide off Norway. *Geo-Marine Letters* **7**, 191-198.

Bukovics, C., Cartier, E. G., Shaw, N. D. & Ziegler, P. A. 1984. Structure and development of the mid-Norway Continental Margin. In: *Petroleum Geology of the North European Margin* (edited by Heier, K. S. & Spencer, A. M.). Graham & Trotman, 407-423.

Bukovics, C. & Ziegler, P. A. 1985. Tectonic development of the Mid-Norway continental margin. *Marine and Petroleum Geology* **2**, 2-22.

Byrkjeland, U., Bungum, H. & Eldholm, O. 2000. Seismotectonics of the Norwegian continental margin. *Journal of Geophysical Research* **105**(B3), 6221-6236.

Bøen, F., Eggen, S. & Vollset, J. 1984. Structures and basins of the margin from 62–69° N and their development. In: *Petroleum Geology of the North European Margin* (edited by Spencer, A. M.). Norwegian Petroleum Society, Graham and Trotman, London, 253-270.

Cartwright, J. A. 1992. Fundamental crustal lineaments and transverse structural zones in continental rifts. In: *Basement Tectonics* (edited by Mason, R.) **7**. Kluwer, Netherlands, 209-217.

Chave, A., Constable, S. & Edwards, R. 1991. Electrical exploration methods for the seafloor. In: *Electromagnetic methods in applied geophysics*, Vol. 2 (edited by Nabighian, M. N.). Soc. Expl. Geophys., 931–966.

Childers, V. A., McAdoo, D. C., Brozena, J. M. & Laxon, S. W. 2001. New gravity data in the Arctic Ocean- Comparison of airborne and ERS gravity. *Journal of Geophysical Research* **106**(B5).

Christiansson, P., Faleide Jan, I. & Berge Anker, M. 2000. Crustal structure in the northern North Sea; an integrated geophysical study; Dynamics of the Norwegian margin. *Geological Society Special Publications* **167**, 15-40.

Christie, P. A. F. & Robein, E. 2005. Recent advances in geophysical technology: introduction and review. In: *Petroleum Geology: North-West Europe and Global Perspectives - Proceedings of the 6th Petroleum Geology Conference* (edited by Doré, A. G. & Vining, B. A.). Geological Society, London, 1369-1376.

Cochran, J. R. & Martinez, F. 1988. Evidence from the northern Red Sea on the transition from continental to oceanic rifting. *Tectonophysics* **153**, 25-53.

Constable, S. C., Orange, A. S., Hoversten, G. M. & Morrison, H. F. 1998. Marine magnetotellurics for petroleum exploration; Part I, A sea-floor equipment system. *Geophysics* **63**(3), 816-825.

Coward, M. P. 1993. The effect of Late Caledonian and Variscan continental escape tectonics on basement structure: Paleozoic basin kinematics and subsequent Mesozoic basin development in NW Europe. In: *Petroleum Geology of Northwest Europe: Proceedings of the 4th Conference* (edited by Parker, J. R.). Geological Society, London, 1095-1108.

Crawford, W. C. 2002. The sensitivity of seafloor compliance measurements to sub-basalt reservoirs. *Lithos Science Report* **4**, 139-147.

Crawford, W. C. 2004. The sensitivity of seafloor compliance measurements to sub-basalt sediments. *Geophysical Journal International* **157**(3), 1130-1145.

Crittenden, S., Cole, J. & Harlow, C. 1991. The Early to "middle" Cretaceous lithostratigraphy of the Central North Sea (UK Sector). *Journal of Petroleum Geology* **14**, 387-416.

Dalland, A. 1980. The sedimentary sequence of Andøya, northern Norway-Depositional and structural history. In: *Geology of the North Atlantic Borderlands* (edited by Kerr, J. W., Ferguson, A. J. & Machan, L. C.). *Memoirs* **14**. Canadian Society of Petroleum Geologists, 387-416.

Dean, K., McLachlan, K. & Chambers, A. 1999. Rifting and the development of the Faroe-Shetland Basin. In: *Petroleum Geology of Northwest Europe: Proceedings of the 5th Conference* (edited by Fleet, A. J. & Boldy, S. A. R.). Geological Society, London, 533-544.

Dehls, J. F., Olesen, O., Bungum, H., Hicks, E., Lindholm, C. D. & Riis, F. 2000. Neotectonic map: Norway and adjacent areas (1:3 milljon). Geological Survey of Norway, Trondheim.

Dillon, W. 1988. On underplating. *Geology* **16**(10), 958-959.

Doré, A. G. 1991. The structural foundation and evolution of Mesozoic seaways between Europe and the Arctic. *Palaeogeography Palaeoclimatology Palaeoecology* **87**, 441-492.

Doré, A. G. 1992. Synoptic palaeogeography of the Northeast Atlantic seaway: late Permian to Cretaceous. In: *Basins on the Atlantic Seaboard: Petroleum Geology, Sedimentology and Basin Evolution* (edited by Parnell, J.). *Special Publications* **62**. Geological Society, London, 421-446.

Doré, A. G. & Lundin, E. R. 1996. Cenozoic compressional structures on the NE Atlantic margin: nature, origin and potential significance for hydrocarbon exploration. *Petroleum Geoscience* **2**, 299-311.

Doré, A. G., Birkeland, Ø., Eliassen, P. E. & Jensen, L. N. 1997a. The NE Atlantic margin: implications of late Mesozoic and Cenozoic events for hydrocarbon prospectivity. *Petroleum Geoscience* **3**, 117-131.

Doré, A. G., Lundin, E. R., Fichler, C. & Olesen, O. 1997b. Patterns of basement structure and reactivation along the NE Atlantic margin. *Journal of the Geological Society* **154**, 85-92.

Doré, A. G., Lundin, E. R., Jensen, L. N., Birkeland, Ø., Eliassen, P. E. & Fichler, C. 1999. Principal tectonic events in the evolution of the northwest European Atlantic margin. In: *Petroleum Geology of Northwest Europe: Proceedings of the 5th Conference* (edited by Fleet, A. J. & Boldy, S. A. R.). Geological Society, London, 41–61.

Dragoi-Stavar, D. & Hall, S. 2009. Gravity modeling of the ocean-continent transition along the South Atlantic margins. *Journal of Geophysical Research (Solid Earth)* **114**(B13), 09401.

Dunlop, D. J. & Prévot, M. 1982. Magnetic properties and opaque mineralogy of drilled submarine intrusive rocks. *Geophys. J. R. astr. Soc.* **69**, 763-802.

Dziewonski, A. M. & Anderson, D. L. 1981. Preliminary Reference Earth Model. *Physics of the Earth and Planetary Interiors* **25**(4), 297-356.

Ebbing, J., Lundin, E., Olesen, O. & Hansen, E. K. 2006. The mid-Norwegian margin; a discussion of crustal lineaments, mafic intrusions, and remnants of the Caledonian root by 3D density modelling and structural interpretation. *Journal of the Geological Society* **163**(1), 47-59.

Ebbing, J., Skilbrei, J. R. & Olesen, O. 2007. Insights into the magmatic architecture of the Oslo Graben by petrophysically constrained analysis of the gravity and magnetic field. *Journal of Geophysical Research-Solid Earth* **112**, B044404, doi:10.1029/2006JB004694.

Ebbing, J., Olesen, O., Gernigon, L., Reynisson, R. F. & the Continental Shelf Geophysics Team at the Geological Survey of Norway. 2008. Gravity and magnetic data provide evidence of old structures on the Norwegian shelf. In: *Geology for society for 150 years - The legacy after Kjerulf* (edited by Slagstad, T. & Dahl, R.). *Gråsteinen* **12**.

Ebbing, J., Gernigon, L., Pascal, C., Olesen, O. & Osmundsen, P. T. 2009. A discussion of structural and thermal control of magnetic anomalies on the mid-Norwegian margin. *Geophysical Prospecting* **57**, 665-681.

Eccles, J. D., White, R. S. & Christie, P. A. F. 2009. Identification and inversion of converted shear waves: case studies from the European North Atlantic continental margins. *Geophysical Journal International* **179**(1), 381-400.

Eidesmo, T., Ellingsrud, S., MacGregor, L.M., Constable, S., Sinha, M.C., Johansen, S., Kong, F.N. & Westerdahl, H. 2002. Sea Bed Logging (SBL), a new method for remote and direct identification of hydrocarbon filled layers in deepwater areas. *First Break* **20**, 144-152.

Eldholm, O. & Coffin, M. F. 2000. Large igneous Provinces and plate tectonics. *Geophysical monograph* **121**, 309-326.

Eldholm, O. & Grue, K. 1994. North-Atlantic Volcanic Margins - Dimensions and Production-Rates. *Journal of Geophysical Research-Solid Earth* **99**(B2), 2955-2968.

Eldholm, O. & Mutter, J. C. 1986. Basin structure on the Norwegian margin from analysis of digitally recorded sonobuoys. *Journal of Geophysical Research* **91**(B3), 3763-3783.

Eldholm, O., Sundvor, E., Myhre, A. M. & Faleide, J. I. 1984. Cenozoic evolution of the continental margin of Norway and western Svalbard. In: *Petroleum Geology of the North European Margin* (edited by Spencer, A. M.). Graham & Trotman, 3-18.

Eldholm, O., Thiede, J. & Taylor, E. 1987. Proceeding Oceanic Drilling Program, Initial Reports 104, College Station, TX (Ocean Drilling Program).

Eldholm, O., Thiede, J. & Taylor, E. 1989. Evolution of the Vøring volcanic margin. *Proceedings of the Ocean Drilling Program, Scientific Results* **104**, 1033-1065.

Eldholm, O., Skogseid, J., Planke, S. & Gladczenko, T. P. 1995. Volcanic margin concepts. In: *Rifted Ocean–Continent Boundaries* (edited by Banda, E.). *NATO ASI* **5**. Kluwer Acad., Norwell, Mass., 1–16.

Eldholm, O., Tsikalas, F. & Faleide, J. I. 2002. Continental margin off Norway 62-75°N: Palaeogene tectono-magmatic segmentation and sedimentation. In: *The North Atlantic Igneous Province: Stratigraphy, Tectonic, Volcanic and Magmatic Processes* (edited by Jolley, D. W. & Bell, B. R.). *Special Publication* **197**. Geological Society, London, 39-68.

Engen, Ø., Frazer, N. L., Wessel, P. & Faleide, J. I. 2006. Prediction of sediment thickness in the Norwegian-Greenland Sea from gravity inversion. *Journal of Geophysical Research* **111**.

England, R. W., Mcbride, J. H. & Hobbs, R. W. 2005. The role of Mesozoic rifting in the opening of the NE Atlantic: evidence from deep seismic profiling across the Faroe-Shetland Trough. *Journal of the Geological Society* **162**, 661-673.

Escartín, J., Hirth, G. & B., E. 2001. Strength of slightly serpentinized peridotites: Implications for the tectonics of oceanic lithosphere. *Geology* **29**, 1023-1026.

Evans, D. J. 1997. Estimates of the eroded overburden and the Permian-Quaternary history of the area west of Orkney. *Scottish Journal of Geology* **33**(2), 169-182.

Ewing, J. & Ewing, M. 1959. Seismic-refraction measurements in the Atlantic ocean basins, in the Mediterranean sea, on the mid-Atlantic ridge, and in the Norwegian sea. *Geological Society of America Bulletin* **70**(3), 291-318.

Fairhead, J. D., Green, C. M. & Dickson, W. G. 2001a. Oil exploration from space: fewer places to hide. *First Break* **19**(9), 514-519.

Fairhead, J. D., Green, C. M. & Odegard, M. E. 2001b. Satellite-derived gravity having an impact on marine exploration. *The Leading Edge* **August**.

Faleide, J. I., Vagnes, E. & Gudlaugsson, S. T. 1993. Late Mesozoic-Cenozoic evolution of the south-western Barents Sea in a regional rift-shear tectonic setting. *Marine and Petroleum Geology* **10**(3), 186-214.

Faleide, J. I., Solheim, A., Fiedler, A., Hjelstuen, B. O., Andersen, E. S. & Vanneste, K. 1996. Late Cenozoic evolution of the western Barents Sea-Svalbard continental margin. *Global and Planetary Change* **12**, 53-74.

Fanavoll, S., Reynisson, R. F., Waag, G., Walker, P. & Ebbing, J. 2008. *Feasibility study of integrated electromagnetic, gravimetric, aeromagnetic and seismic sub-basalt exploration techniques*. NGU Report 2008.003. The Geological Survey of Norway, 66 p.

Fernàndez, M., Torne, M., Garcia-Castellanos, D., Vergés, J., Wheeler, W. & Karpuz, R. 2004. Deep structure of the Vøring Margin: the transition from a continental shield to a young oceanic lithosphere. *Earth and Planetary Science Letters* **221**(1-4), 131-144.

Fernàndez, M., Ayala, C., Torne, M., Verges, J., Gomez, M. & Karpuz, R. 2005. Lithospheric structure of the mid-Norwegian margin; comparison between the More and Voring margins. *Journal of the Geological Society* **162**(6), 1005-1012.

Fichler, C., Rundhovde, E., Olesen, O., Sæther, B. M., Rueslåtten, H., Lundin, E. & Doré, A. G. 1999. Regional tectonic interpretation of image enhanced gravity and magnetic data covering the mid-Norwegian shelf and adjacent mainland. *Tectonophysics* **306**, 183-197.

Firth, J. & Taylor, R. 2009. True 3D Seismic—Wide Azimuth Comes Of Age. *PESA News* **October/November**, 40-44.

Fliedner, M. M. & White, R. S. 2001. Seismic structure of basalt flows from surface seismic data, borehole measurements, and synthetic seismogram modeling. *Geophysics* **66**(6), 1925-1936.

Fliedner, M. M. & White, R. S. 2003. Depth imaging of basalt flows in the Faeroe-Shetland Basin. *Geophysical Journal International* **152**(2), 353-371.

Fowler, C. M. R. & Nisbet, E. G. 1982. The Thermal Background to Metamorphism-II Simple Two-Dimensional Conductive Models. *Geoscience Canada* **9**(4).

Friðleifsson, I. B. 1982. The Iceland Research Drilling Project in relation to the geology of Iceland. *Journal of Geophysical Research* **87**(B8), 6363-6370.

Froitzheim, N. & Manatschal, G. 1996. Kinematics of Jurassic rifting, mantle exhumation, and passive-margin formation in the Austroalpine and Penninic nappes (eastern Switzerland). *Geological Society of America Bulletin* **108**(9), 1120-1133.

Fruehn, J. & Sugrue, M. 1999. Sub-basalt imaging improvements - west of Hebrides. *SEG Expanded Abstracts*.

Fruehn, J., Fliedner, M. M. & White, R. S. 2001. Integrated wide-angle and near-vertical subbasalt study using large-aperture seismic data from the Faeroe-Shetland region. *Geophysics* **66**(5), 1340-1348.

Furlong, K. P. & Fountain, D. M. 1986. Continental crustal underplating: Thermal considerations and seismic-petrologic consequences. *Journal of Geophysical Research* **91**(B8), 8285-8294.

Færseth, R. B., Gabrielsen, R. H. & Hurich, C. A. 1995. Influence of basement in structuring of the North Sea basin, offshore southwest Norway. *Norsk Geologisk Tidsskrift* **75**, 105-119.

Gabrielsen, R. H., Faerseth, R., Hamar, G. & Roennevik, H. 1984. Nomenclature of the main structural features on the Norwegian continental shelf north of the 62nd parallel. In: *Petroleum Geology of the North European Margin* (edited by Spencer, A. M.). Norwegian Petroleum Society, Graham and Trotman, London, 41–60.

Gabrielsen, R. H., Odinsen, T. & Grunnaleite, I. 1999. Structuring of the Northern Viking Graben and the More Basin; the influence of basement structural grain, and the particular role of the More-Trondelag Fault Complex. *Marine and Petroleum Geology* **16**(5), 443-465.

Gernigon, L., Ringenbach, J. C., Planke, S., Le Gall, B. & Jonquet-Kolstø, H. 2003. Extension, crustal structure and magmatism at the outer Voring Basin, Norwegian margin. *Journal of the Geological Society* **160**(2), 197-208.

Gernigon, L., Ringenbach, J. C., Planke, S. & Le Gall, B. 2004. Deep structures and breakup along volcanic rifted margins: insights from integrated studies along the outer Voring Basin (Norway). *Marine and Petroleum Geology* **21**(3), 363-372.

Gernigon, L., Lucazeau, F., Brigaud, F., Ringenbach, J. C., Planke, S. & Le Gall, B. 2006. A moderate melting model for the Voring margin (Norway) based on structural observations and a thermo-kinematical modelling: Implication for the meaning of the lower crustal bodies. *Tectonophysics* **412**(3-4), 255-278.

Gibb, F. G. F. & Kanaris-Sotiriou, R. 1988. The geochemistry and origin of the Faeroe-Shetland sill complex. In: *Early Tertiary Volcanism and the Opening of the NE Atlantic* (edited by Morton, A. C. & Parson, L. M.). *Geological Society Special Publication* **39**, 241-252.

Gradstein, F. M. & Backstrøm, S. 1996. Cenozoic biostratigraphy and paleobathymetry, northern North Sea and Haltenbanken. *Norsk Geologisk Tidsskrift* **76**, 3-32.

Gradstein, F. M., Kaminski, M. A. & Agterberg, F. P. 1999. Biostratigraphy and paleoceanography of the Cretaceous seaway between Norway and Greenland. *Earth Science Reviews* **46**, 27-98.

Grunnaleite, I. & Gabrielsen, R. H. 1995. Structure of the More Basin, mid-Norway continental margin. *Tectonophysics* **252**(1-4), 221-251.

Götze, H.-J. & Lahmeyer, B. 1988. Application of three-dimensional interactive modeling in gravity and magnetics. *Geophysics* **53**(8), 1096-1108.

Hall, B. D. & White, N. 1994. Origin of anomalous Tertiary subsidence adjacent to North Atlantic continental margins. *Marine and Petroleum Geology* **11**, 702-714.

Hamar, G. P. & Hjelle, K. 1984. Tectonic framework of the Møre Basin and the northern North Sea. In: *Petroleum Geology of the North European Margin* (edited by Spencer, A. M.). Norwegian Petroleum Society, Graham & Trotman, London, 349–358.

Handy, M. R. & Streit, J. E. 1999. Mechanics and mechanisms of magmatic underplating: inferences from mafic veins in deep crustal mylonite. *Earth and Planetary Science Letters* **165**(3), 271-286.

Hartz, E. & Andersen, A. 1995. Caledonian sole thrust of central East Greenland: A crustal scale Devonian extensional detachment? *Geology* **23**, 637-640.

Heincke, B., Jegen, M. & Hobbs, R. W. 2006. Joint Inversion of MT, Gravity and Seismic Data applied to sub-basalt Imaging. In: *SEG Annual Meeting*, New Orleans.

Herzberg, C. T., Fyfe, W. S. & Carr, M. J. 1983. Density constraints on the formation of the continental Moho and crust. *Contributions to Mineralogy and Petrology* **84**(1), 1-5.

Hinz, K. 1981. A hypothesis on terrestrial catastrophes: wedges of very thick oceanward dipping layers beneath passive continental margins - their origin and palaeoenvironment significance. *Geologische Jahrbuch, Serie E* **22**, 3-28.

Hinz, K., Dostman, H. J. & Hanisch, J. 1982. Structural framework of the Norwegian Sea. In: *Offshore Norhtern Seas*. Norwegian Petroleum Society, Oslo, 1–22.

Hinz, K. 1987. Symmetric conjugation of continent-ocean boundary structures along the Norvwegian and East Greenland margins. *Marine and petroleum geology* **4**(3), 166.

Hitchen, K., Stoker, M. S., Evans, D. & Beddoe-Stevens, B. 1995. Permo-Triassic sedimentary and volcanic rocks in basins to the north and west of Scotland. In: *Permian and Triassic Rifting in Northwest Europe* (edited by Boldy, S. A. R.). *Special Publications* **91**. Geological Society, London, 87-102.

Hjelstuen, B. O., Eldholm, O. & Skogseid, J. 1997. Vøring Plateau diapirs and their structural and depositional settings. *Marine Geology* **144**, 33-57.

Hjelstuen, B. O., Eldholm, O. & Skogseid, J. 1999. Cenozoic evolution of the northern Vøring margin. *Geological Society of America Bulletin* **111**, 1792-1807.

Holbrook, W. S., Larsen, H. C., Korenaga, J., Dahl-Jensen, T., Reid, I. D., Kelemen, P. B., Hopper, J. R., Kent, G. M., Lizarralde, D. & Bernstein, S. 2001. Mantle thermal structure and active upwelling during continental breakup in the North Atlantic. *Earth planet. Sci. Lett* **190**(3-4), 251–266.

Hospers, J. 1951. Remanent Magnetism of Rocks and the History of the Geomagnetic Field. *Nature* **168**, 1111-1112.

Hoversten, G. M., Morrison, H. F. & Constable, S. C. 1998. Marine magnetotellurics for petroleum exploration; Part II, Numerical analysis of subsalt resolution. *Geophysics* **63**(3), 826-840.

Hunt, C. P., Moskowitz, B. M. & Banerjee, S. K. 1995. Magnetic properties of rocks and minerals (Vol. 3). Rock physics and phase relations. A handbook of physical constants. *AGU Reference Shelf, American Geophysical Union*, 189-204.

Hürich, C. A., Deemer, S. J. & Indares, A. 2001. Compositional and metamorphic controls on velocity and reflectivity in the continental crust: An example from the Grenville Province of eastern Québec. *Journal of Geophysical Research* **106**(B1), 665-682.

Huston, H. H., Sestak, H. & Lyman, G. D. 1999. Methodology for interpreting 3-D marine gravity gradiometry data. *The Leading Edge* **18**(4), 482-485.

Jacobsen, B. H. 1987. A Case for Upward Continuation as a Standard Separation Filter for Potential-Field Maps. *Geophysics* **52**(8), 1138-1148.

Jegen, M., Hautot, S., Cairns, G. & Tarits, P. 2002. Use of electromagnetics to image sub-basalt sediments. In: *Sub-basalt imaging. Journal of Conference Abstracts* **7**. Cambridge Publications, Cambridge, UK, 154-155.

Karner, G. D., Studinger, M. & Bell, R. E. 2005. Gravity anomalies of sedimentary basins and their mechanical implications; application to the Ross Sea basins, West Antarctica. *Earth and Planetary Science Letters* **235**(3-4), 577-596.

Kearey, P., Brooks, M. & Hill, I. 2002. *An Introduction to Geophysical Exploration*. Blackwell Publishing, Oxford.

Kent, D. V. & Opdyke, N. D. 1978. Paleomagnetism and magnetic properties of igneous rock samples - Leg 38. In: *Initial Reports of the Deep Sea Drilling Project 38-41* (edited by White, S. M., Supko, P. R., Natland, J., Gardner, J. & Herring, J.). Texas A & M University, Ocean Drilling Program, College Station, TX, Washington.

Kimbell, G. S., Gatliff, R. W., Ritchie, J. D., Walker, A. S. D. & Williamson, J. P. 2004. Regional three-dimensional gravity modelling of the NE Atlantic margin. *Basin Research* **16**(2), 259-278.

Kinck, J. J., Husebye, E. S. & Larsson, F. R. 1993. The Moho Depth Distribution in Fennoscandia and the Regional Tectonic Evolution from Archean to Permian Times. *Precambrian Research* **64**(1-4), 23-51.

Kusznir, N. J., Marsden, G. & Egan, S. S. 1991. A flexural-cantilever simple-shear/pure-shear model of continental lithosphere extension: applications to the Jeanne d'Arc Basin, Grand Banks and Viking Graben, North Sea. *Geological Society, London, Special Publications* **56**(1), 41-60.

Kooi, H., Cloetingh, S. & Burrus, J. 1992. Lithospheric Necking and Regional Isostasy at Extensional Basins 1. Subsidence and Gravity Modeling With an Application to the Gulf of Lions Margin (SE France). *Journal of Geophysical Research* **97**(B12), 17553-17551.

LaFehr, T. R. 1991. Standardization in gravity reduction. *Geophysics* **56**(8), 1170-1178.

Lahmeyer, B., Götze, H.J., Schmidt, S., Alvers, M.R., Plonka, C. & Fichler, C. 2010. Interactive 3D Gravity and Magnetic Modelling in IGMAS+ and the Integration in the Depth Imaging Workflow. In: 72nd EAGE Conference & Exhibition incorporating SPE EUROPEC 2010.

Larsen, H. C. & Marcussen, C. 1992. Sill-intrusion, flood basalt emplacement and deep crustal structure of the Scoresby Sund region, East Greenland. In: *Magmatism and the Causes of Continental Break-up* (edited by Storey, B. C., Alabaster, T. & Pankhurst, R. J.). *Special Publications* **68**. Geological Society, London, 365–386.

Larsen, H. C. & Saunders, A. D. 1998. Tectonism and volcanism at the southeast Greenland rifted margin: a record of plume impact and later continental rupture. *Proceedings of the Ocean Drilling Program, Scientific Results* **152**, 503-533.

Lavier, L. L. & Manatschal, G. 2006. A mechanism to thin the continental lithosphere at magma-poor margin. *Nature* **440**, 324-328.

Laxon, S. & McAdoo, D. 1994. Arctic Ocean Gravity Field Derived From ERS-1 Satellite Altimetry. *Science* **265**.

Le Pichon, X. & Hayes, D. E. 1971. Marginal offsets, fracture zones and the early opening of the South Atlantic. *Journal of Geophysical Research* **76**, 6283–6293.

Li, X. 2003. On the use of different methods for estimating magnetic depth. *The Leading Edge* **22**(11), 1090-1099.

Lister, J. R. & Kerr, R. C. 1991. Fluid-mechanical models of crack propagation and their application to magma transport in dykes. *Journal of Geophysical Research* **96**(B6), 10049-10077.

Lundin, E. & Doré, A. G. 1997. A tectonic model for the Norwegian passive margin with implications for the NE Atlantic: Early Cretaceous to break-up. *Journal of the Geological Society* **154**, 545-550.

Lundin, E. R. & Rundhovde, E. 1993. Structural domains in the Møre Basin, Norway - from digital images of aeromagnetic data. Extended abstract. In: *EAPG-5th conference*, Stavanger, Norway.

MacGregor, L. & Sinha, M. 2000. Use of marine controlled-source electromagnetic sounding for sub-basalt exploration. *Geophysical Prospecting* **48**(6), 1091-1106.

MacGregor, L. & Sinha, M. 2002. Sub-basalt imaging using marine controlled source electromagnetic sounding. In: *Sub-basalt imaging. Journal of Conference Abstracts* **7**. Cambridge Publications, Cambridge, UK, 172-173.

Manatschal, G., Froitzheim, N., Rubenach, M. & Turrin, B. D. 2001. The role of detachment faulting in the formation of an ocean-continent transition: insights from the Iberia Abyssal Plain. In: *Non-Volcanic Rifting of Continental Margins: A Comparison of Evidence from Land and Sea* (edited by Wilson, R. C. L., Whitmarsh, R. B., Taylor, B. & Froitzheim, N.). *Geological Society London Special Publications* **187**, 405-428.

Manatschal, G. 2004. New models for evolution of magma-poor rifted margins based on a review of data and concepts from West Iberia and the Alps. *Int J Earth Sci*, 432-465.

Martini, F. & Bean, C. J. 2002. Interface scattering versus body scattering in subbasalt imaging and application of prestack wave equation datuming. *Geophysics* **67**(5), 1593-1601.

Martini, F., Hobbs, R. W., Bean, C. J. & Single, R. 2005. A complex 3D volume for sub-basalt imaging. *First Break* **23**(7), 41-51.

Meyer, R., van Wijk, J. & Gernigon, L. 2007. The North Atlantic Igneous Province: A review of models for its formation. In: *Plates, plumes, and planetary processes: Geological Society of America Special Paper 430* (edited by Foulger, G. R. & Jurdy, D. M.), 525-552.

Miller, D. J. & Christensen, N. I. 1997. Seismic velocities of lower crustal and upper mantle rocks from the slow-spreading mid-Atlantic ridge, south of the Kane tronsform zone (Mark). In: *Proceedings of the Ocean Drilling Program, Scientific Results* (edited by Karson, J. A., Cannat, M., Miller, D. J. & Elthon, D.) **153**, 437-454.

Milton, N. J., Bertram, G. T. & Vann, I. R. 1990. Early Palaeogene tectonics and sedimentation in the Central North Sea. In: *Tectonic Events Responsible for Britain's Oil and Gas Reserves* (edited by Hardman, R. P. F. & Brooks, J.). *Special Publications* **55**. Geological Society, London, 339-351.

Mjelde, R., Kodaira, S., Shimamura, H., Kanazawa, T., Shiobara, H., Berg, E. W. & Riise, O. 1997. Crustal structure of the central part of the Vøring Basin, mid-Norway margin, from ocean bottom seismographs. *Tectonophysics* **277**(4), 235-257.

Mjelde, R., Digranes, P., Shimamura, H., Shiobara, H., Kodaira, S., Brekke, H., Egebjerg, T., Sorenes, N. & Thorbjornsen, S. 1998. Crustal structure of the northern part of the Vøring Basin, mid-Norway margin, from wide-angle seismic and gravity data. *Tectonophysics* **293**(3-4), 175-205.

Mjelde, R., Digranes, P., Van Schaack, M., Shimamura, H., Shiobara, H., Kodaira, S., Naess, O., Sørenes, N. & Vågnes, E. 2001. Crustal structure of the outer Vøring Plateau, offshore Norway, from ocean bottom seismic and gravity data. *Journal of Geophysical Research-Solid Earth* **106**(B4), 6769-6791.

Mjelde, R., Kasahara, J., Shimamura, H., Kamimura, A., Kanazawa, T., Kodaira, S., Raum, T. & Shiobara, H. 2002. Lower crustal seismic velocity-anomalies; magmatic underplating or serpentinized peridotite? Evidence from the Vøring Margin, NE Atlantic. *Marine Geophysical Researches* **23**, 169-183.

Mjelde, R., Raum, T., Breivik, A., Shimamura, H., Murai, Y., Takanami, T. & Faleide, J. I. 2005. Crustal structure of the Vøring Margin, NE Atlantic: a review of geological implications based on recent OBS data. In: *Petroleum Geology: North-West Europe and Global Perspectives - Proceedings of the 6th Petroleum Geology Conference* (edited by Doré, A. G. & Vining, B. A.). Geological Society, London, 804-813.

Mjelde, R., Faleide, J. I., Breivik, A. J. & Raum, T. 2009a. Lower crustal composition and crustal lineaments on the Vøring Margin, NE Atlantic: A review. *Tectonophysics* **472**, 183-193.

Mjelde, R., Raum, T., Kandilarov, A., Murai, Y. & Takanami, T. 2009b. Crustal structure and evolution of the outer Møre Margin, NE Atlantic. *Tectonophysics* **468**, 224-243.

Moore, J. G., Phillips, R. L., Grigg, R. W., Peterson, D. W. & Swanson, D. A. 1973. Flow of Lava into the Sea, 1969-1971, Kilauea Volcano, Hawaii. *Bulletin of the Geological Society of America* **84**(2), 537-546.

Morley, C. K., Nelson, R. A., Patton, T. & Munn, S. G. 1990. Transfer zones in the East Africa rift system and their relevance to hydrocarbon exploration in rifts. *American Association of Petroleum Geologists Bulletin* **74**, 1234-1253.

Mosar, J., Eide, E. A., Osmundsen, P. T., Sommaruga, A. & Torsvik, T. H. 2002. Greenland - Norway separation: A geodynamic model for the North Atlantic. *Norwegian Journal of Geology* **82**(4), 281-298.

Mosar, J. 2003. Scandinavia's North Atlantic passive margin. *Journal of Geophysical Research-Solid Earth* **108**(B8).

Mudge, M. R. 1968. Depth control of some concordant intrusions. *Bulletin of the Geological Society of America* **79**(3), 315-332.

Murphy, C. M., Gary, R. M. & Stalin, F. 2002. Resolving basalt and sub-basalt geology with high precision high resolution gravity gradient data. In: *Sub-basalt imaging. Journal of Conference Abstracts* **7**. Cambridge Publications, Cambridge, UK, 178-179.

Mutter, J. C., Talwani, M. & Stoffa, P. L. 1982. Origin of seaward-dipping reflectors in oceanic crust off the Norwegian margin by "subaerial sea-floor spreading". *Geology* **10**, 353-357.

Mutter, J. C., Buck, W. R. & Zehnder, C. M. 1988. Convective partial melting 1. A model for the formation of thick basaltic sequences during the initiation of spreading. *Journal of Geophysical Research* **93**(B2), 1031-1048.

Mørk, M. B. E., McEnroe, S. A. & Olesen, O. 2002. Magnetic susceptibility of Mesozoic and Cenozoic sediments off Mid Norway and the role of siderite: implications for interpretation of high-resolution aeromagnetic anomalies. *Marine and Petroleum Geology* **19**(9), 1115-1126.

Nabighian, M. N., Ander, M. E., Grauch, V. J. S., Hansen, R. O., LaFehr, T. R., Li, Y., Pearson, W. C., Peirce, J. W., Phillips, J. D. & Ruder, M. E. 2005. Historical development of the gravity method in exploration. *Geophysics* **70**(6), 63ND-89ND.

Naylor, P. H., Bell, B. R., Durnall, P., Fredsted, R. & Jolley, D. W. 1999. Paleogene magmatism in the Faero-Shetland Basin: influences on uplift history and sedimentation. In: *Petroleum Geology of Northwest Europe: Proceedings of the 5th Conference* (edited by Fleet, A. J. & Boldy, S. A. R.). Geological Society, London, 545-558.

Nielsen, P., Stefánsson, V. & Tulinius, H. 1984. Geophysical logs from Lopra-1 and Vestmanna-1. In: *The deep drilling project 1980-1981 in the Faeroe Islands* (edited by Berthelsen, O., Noe-Nygaard, A. & Rasmussen, J.). Føroya Fróðskaparfelag, Tórshavn, 115-135.

Olesen, O., Gellein, J., Håbrekke, H., Kihle, O., Skilbrei, J. R. & Smethurst, M. A. 1997a. Magnetic anomaly map: Norway and adjacent ocean areas (1:3 milljon). Geological Survey of Norway, Trondheim.

Olesen, O., Torsvik, T. H., Tveten, E., Zwaan, K. B., Løseth, H. & Henningsen, T. 1997b. Basement structure of the continental margin in the Lofoten-Lopphavet area, northern Norway: constraints from potential field data, on-land structural mapping and palaeomagnetic data. *Norsk Geologisk Tidsskrift* **77**, 15-30.

Olesen, O., Lundin, E., Nordgulen, O., Osmundsen, P. T., Skilbrei, J. R., Smethurst, M. A., Solli, A., Bugge, T. & Fichler, C. 2002. Bridging the gap between the onshore and offshore geology in Nordland, northern Norway. *Norwegian Journal of Geology* **82**(4), 243-262.

Olesen, O., Ebbing, J., Lundin, E., Mauring, E., Skilbrei, J. R., Torsvik, T. H., Hansen, E. K., Henningsen, T., Midbøe, P. & Sand, M. 2007. An improved tectonic model for the Eocene opening of the Norwegian-Greenland Sea: use of modern magnetic data. *Marine and Petroleum Geology* **24**, 53-66.

Osmundsen, P. T. & Andersen, T. B. 1994. Caledonian compressional and late-orogenic extensional defromation in the Staveneset area, Sunnfjord, western Norway. *Journal of Structural Geology* **16**, 1385-1401.

Osmundsen, P. T., Sommaruga, A., Skilbrei, J. R. & Olesen, O. 2002. Deep structure of the Mid Norway rifted margin. *Norwegian Journal of Geology* **82**(4), 205-224.

Osmundsen, P. T. & Ebbing, J. 2008. Styles of extension offshore mid-Norway and implications for mechanisms of crustal thinning at passive margins. *Tectonics* **27**.

Oufi, O. & Cannat, M. 2002. Magnetic properties of variably serpentinized abyssal peridoties. *Journal of Geophysical Research* **107**(B5), EPM 3.

Ólafsson, I., Sundvor, E., Eldholm, O. & Grue, K. 1992. More Margin - Crustal Structure from Analysis of Expanded Spread Profiles. *Marine Geophysical Researches* **14**(2), 137-162.

Parsons, M., MacQueen, J., Undli, T. H., Berstad, S. & Horstad, I. 2001. A tale of three methods: Volcanics in the Abrolhos Banks, Brazil. *SEG Technical Program Expanded Abstracts*, 634-637.

Pálmason, G. 1980. A continuum model of crustal generation in Iceland; kinematic aspects. *Journal of Geophysics* **47**, 7–18.

Pálsson, S., Haraldsson, G. I. & Vigfússon, G. H. 1984. *Eðlismassi og poruhluti bergs*. OS-84048/VOD-18 B. 35 p.

Pedersen, A. K., Larsen, L. M., Pedersen, G. K. & Dueholm, K. 1996. Filling and plugging of a marine basin by volcanic rocks: The Tonoqqu Member of the Lower Tertiary Veigat Formation on Nuussuaq, Central West Greenland. *Bull. Grønlands Geologiske Undersøgelser*(171), 5-28.

Pedersen, T. & Skogseid, J. 1989. Vøring Plateau volcanic margin: extension, melting and rifting. In: *Proceedings of the Ocean Drilling Program, Scientific Results* (edited by Eldholm, O., Thiede, J. & Taylor, E.) **104**, 985-991.

Planke, S. 1994. Geophysical Response of Flood Basalts from Analysis of Wire Line Logs - Ocean Drilling Program Site-642, Voring Volcanic Margin. *Journal of Geophysical Research-Solid Earth* **99**(B5), 9279-9296.

Planke, S. & Alvestad, E. 1999. Seismic volcanostratigraphy of the extrusive breakup complexes in the northeast Atlantic: implications from ODP/DSDP drilling. *Proceedings of the Ocean Drilling Program, Scientific Results* **163**, 3-16.

Planke, S. & Eldholm, O. 1994. Seismic Response and Construction of Seaward Dipping Wedges of Flood Basalts - Voring Volcanic Margin. *Journal of Geophysical Research-Solid Earth* **99**(B5), 9263-9278.

Planke, S., Skogseid, J. & Eldholm, O. 1991. Crustal structure off Norway, 62° to 70° north. *Tectonophysics* **189**(1-4), 91-107.

Planke, S., Alvestad, E. & Eldholm, O. 1999a. Seismic characteristics of basaltic extrusive and intrusive rocks. *The Leading Edge* **18**(3), 342-348.

Planke, S., Cerney, B., Bücker, C. J. & Nilsen, O. 1999b. Alteration effects on petrophysical properties of subaerial flood basalts: Site 990, southeast Greenland margin. *Proceedings of the Ocean Drilling Program, Scientific Results* **163**, 17-28.

Planke, S., Symonds, P. A., Alvestad, E. & Skogseid, J. 2000. Seismic volcanostratigraphy of large-volume basaltic extrusive complexes on rifted margins. *Journal of Geophysical Research-Solid Earth* **105**(B8), 19335-19351.

Planke, S., Rasmussen, R., Rey, S. S. & Myklebust, R. 2005. Seismic characteristics and distribution of volcanic intrusions and hydrothermal vent complexes in the Vøre and Møre basins. In: *Petroleum Geology: North-West Europe and Global Perspectives - Proceedings of the 6th Petroleum Geology Conference* (edited by Doré, A. G. & Vining, B. A.). Geological Society, London, 833-844.

Price, S., Brodie, J., Whitham, A. & Kent, R. 1997. Mid-Tertiary rifting and magmatism in the Traill Ø region, East Greenland. *Journal of the Geological Society* **154**, 419-434.

Raum, T. 2000. Crustal Structure and Evolution of the Faeroe, Møre and Vøring margins From Wide-angle Seismic and Gravity Data. Unpublished Dr. Scient. thesis, University of Bergen.

Raum, T., Mjelde, R., Digranes, P., Shimamura, H., Shiobara, H., Kodaira, S., Haatvedt, G., Sorenes, N. & Thorbjornsen, T. 2002. Crustal structure of the southern part of the Voring Basin, mid-Norway margin, from wide-angle seismic and gravity data. *Tectonophysics* **355**(1-4), 99-126.

Raum, T., Mjelde, R., Berge, A. M., Paulsen, J. T., Digranes, P., Shimamura, H., Shiobara, H., Kodaira, S., Larsen, V. B., Fredsted, R., Harrison, D. J. & Johnson, M. 2005. Sub-basalt structures east of the Faroe Islands revealed from wide-angle seismic and gravity data. *Petroleum Geoscience* **11**, 291-308.

Raum, T., Mjelde, R., Shimamura, H., Murai, Y., Bråstein, E., Karpuz, R. M., Kravik, K. & Kolstø, H. J. 2006. Crustal structure and evolution of the southern Vøring Basin and Vøring Transfrom Margin, NE Atlantic. *Tectonophysics* **415**, 167-202.

Reid, A. B., Allsop, J. M., Granser, H., Millett, A. J. & Somerton, I. W. 1990. Magnetic interpretation in three dimensions using Euler deconvolution. *Geophysics* **55**(1), 80-91.

Reid, I. 1989. Effects of lithospheric flow on the formation and evolution of a transform margin. *Earth and Planetary Science Letters* **95**(1-2), 38-52.

Ren, S., Skogseid, J. & Eldholm, O. 1998. Late Cretaceous-Paleocene extension on the Vøring Volcanic Margin. *Marine Geophysical Researches* **20**(4), 343-369.

Reston, T. J. 2009. The structure, evolution and symmetry of the magma-poor rifted margins of the North and Central Atlantic: A synthesis. *Tectonophysics* **468**, 6-27.

Reston, T. J. & Pèrez-Gussinyé, M. 2007. Lithospheric extension from rifting to continental brakup at magma-poor margins: rheology, serpentinisation and symmetry. *Int J Earth Sci* **96**, 1033-1046.

Reynisson, R. F., Ebbing, J. & Skilbrei, J. R. 2007. Magnetic and gravity fields in an integrated approach to the sub-basalt imaging problem. In: *EGM 2007 International Workshop. Innovation in EM, Grav and Mag Methods: a new Perspective for Exploration*, Capri, Italy.

Reynisson, R. F., Fanavoll, S., Waag, G. & Ebbing, J. 2008. Fesibility study of electromagnetic, gravimetric and aeromagnetic methods in sub-basaltic settings. In: *70th EAGE Conference & Exhibition*, Rome, Italy.

Reynisson, R. F., Ebbing, J. & Skilbrei, J. R. 2009. The use of potential field data in revealing the basement structure in sub-basaltic settings: an example from the Møre margin, offshore Norway. *Geophysical Prospecting* **57**(4), 753-771.

Reynisson, R. F., Ebbing, J., Lundin, E. & Osmundsen, P. T. in press. Properties and distribution of lower crustal bodies on the mid-Norwegian margin. In: *From Mature Basins to New Frontiers. Proceedings of the 7th Petroleum Geology Conference*. Geological Society, London.

Reynolds, J. M. 1997. *An introduction to applied and enironmental geophysics*. John Wiley & Sons Ltd, Chichester, West Sussex.

Roberts, A. W., White, R. S., Lunnon, Z. C., Christie, P. A. F., Spitzer, R. & iSIMM Team. 2005. Imaging magmatic rocks on the Faroes Margin. In: *Petroleum Geology: North-West Europe and Global Perspectives - Proceedings of the 6th Petroleum Geology Conference* (edited by Doré, A. G. & Vining, B. A.). Geological Society, London, 755-766.

Roberts, D. G., Masson, D. G. & Miles, P. R. 1981. Age and strucure of the southern Rockall Trough: new evidence. *Earth and Planetary Science Letters* **52**, 115-128.

Roberts, D. G., Thompson, M., Mitchener, B., Hossack, J., Carmichael, S. & Bjørnseth, H. M. 1999. Palaeozoic to Tertiary rift and basin dynamics: mid-Norway to the Bay of Biscay–a new context for hydrocarbon prospectivity in the deep water frontier. In: *Petroleum Geology of Northwest Europe: Proceedings of the 5th Conference* (edited by Fleet, A. J. & Boldy, S. A. R.). Geological Society, London, 7–40.

Rutter, E. H., Brodie, K. H. & Evans, P. J. 1993. Structural geometry, lower crystal magmatic underplating and lithospheric stretching in the Ivrea-Verbano zone, northern Italy. *Journal of Structural Geology* **15**(3-5), 647-662.

Ryan, P. D. & Dewey, J. F. 1997. Continental eclogites and the Wilson Cycle. *Journal of the Geological Society* **154**, 437-442.

Rønnevik, H., Bergsager, E., Moe, A., Øvrebø, O. & Navrestad, H. 1975. The Geology of the Norwegian Continental Shelf. In: *Petroleum and the continental shelf of North West Europe* (edited by Woodland, A. W.) **1**. Applied Science Publishers, London, 117-129.

Saunders, A. D., Fitton, J. G., Kerr, A. C., Norry, M. J. & Kent, R. W. 1997. The North Atlantic Igneous Province. *Geophysical monograph* **100**, 45-93.

Saxov, S. & Abrahamsen, N. 1966. Some geophysical investigations in the Faroe Islands. *Zeitschrift für Geophysik* **32**, 455-471.

Scheck-Wenderoth, M., Raum, T., Faleide, J. I., Mjelde, R. & Horsfield, B. 2007. The transition from the continent to the ocean: a deeper view on the Norwegian margin. *Journal of the Geological Society* **164**, 855-868.

Scheck-Wenderoth, M. & Maystrenko, Y. 2008. How warm are passive continental margins? A 3-D lithosphere-scale study from the Norwegian margin. *Geology* **36**, 419-422.

Schmidt, S. & Götze, H.-J. 1998. Interactive visulization and modification of 3D models using GIS functions. *Physics and Chemistry of the Eart* **23**(3), 289-296.

Schmidt, S. & Götze, H.-J. 1999. Integration af data constraints and potential field modelling - an example from Southern Lower Saxony, Germany. *Physics and Chemistry of the Eart, Part A* **24**(3), 191-196.

Schoenharting, G. & Abrahamsen, N. 1984. Magnetic investigations on cores from the Lopra-1 drillhole, Faeroe Islands. In: *The deep drilling project 1980-1981 in the Faeroe Islands* (edited by Berthelsen, O., Noe-Nygaard, A. & Rasmussen, J.). Føroya Fróðskaparfelag, Tórshavn, 109-114.

Scrutton, R. A. 1979. On sheared passive continental margins. *Tectonophysics* **59**, 293–305.

Séranne, M. & Séguret, M. 1987. The Devonian basins of western Norway: tectonics and kinematics of extending crust. In: *Continental Extensional Tectonics* (edited by Dewey, J. F. & Hanckock, P. L.). *Special Publications* **28**. Gelogical Society, London, 537-548.

Sinton, C. W., Hitchen, K. & Duncan, R. A. 1998. ^{40}Ar-^{39}Ar geochronology of silic and basic volcanic rocks on the margins of the North Atlantic. *Geological Magazine* **135**, 161-170.

Skilbrei, J. R., Sindre, A., McEnroe, S. A., Robinson, P. T. & Kihle, O. 1995. *Combined interpretation of potential field-, petrophysical data and topography from Central Norway and the continental shelf between 62° N and 65° N, including a preliminary report on paleomagnetic dating of faults near Molde*. Report 95.027, Geological Survey of Norway.

Skilbrei, J. R., Kihle, O., Olesen, O., Gellein, J., Sindre, A., Solheim, D. & Nyland, B. 2000. Gravity anomaly map: Norway and adjacent ocean areas (1:3 milljon). Geological Survey of Norway, Trondheim.

Skilbrei, J. R., Olesen, O., Osmundsen, P. T., Kihle, O., Aaro, S. & Fjellanger, E. 2002. A study of basement structures and onshore-offshore correlations in Central Norway. *Norwegian Journal of Geology* **82**(4), 263-279.

Skilbrei, J. R. & Olesen, O. 2005. Deep structure of the Mid-Norwegian shelf and onshore-offshore correlations: Insights from potential field data. In: *Onshore-Offshore Relationships on the North Atlantic Margin* (edited by Wandas, B. T. G., Nystuen, J. P., Eide, E. A. & Gradstein, F.). *NPF Special Publication* **12**. Norwegian Petroleum Society (NPF), 43-68.

Skogly, O. P. 1998. Seismic characterization and emplacement of intrusives in the Vøring Basin. Unpublished MS thesis, University of Oslo.

Skogseid, J. & Eldholm, O. 1987. Early Cenozoic crust at the Norwegian Continental Margin and the conjugate Jan Mayen Ridge. *Journal of Geophysical Research* **92**(B11), 11471-11492.

Skogseid, J. & Eldholm, O. 1989. Vøring Plateau continental margin: Seismic interpretation, Stratigraphy, and vertical movements. In: *Proceedings of the Ocean Drilling Program, Scientific Results* (edited by Eldholm, O., Thiede, J. & Taylor, E.) **104**, 993–1030.

Skogseid, J., Pedersen, T., Eldholm, O. & Larsen, B. T. 1992a. Tectonism and magmatism during NE Atlantic continental break-up: the Vøring Margin. In: *Magmatism and the Causes of Continental Break-up* (edited by Storey, B. C., Alabaster, T. & Pankhurst, R. J.). *Special Publications* **68**. Geological Society, London, 305–320.

Skogseid, J., Pedersen, T. & Larsen, V. B. 1992b. Vøring Basin: subsidence and tectonic evolution. In: *Structural and Tectonic Modelling and its Application to Petroleum Geology* (edited by Larsen, R. M., Brekke, H., Larsen, B. T. & Talleraas, E.). *Norwegian Petroleum Society (NPF), Special Publication* **1**. Elsevier, Amsterdam, 55-82.

Skogseid, J., Planke, S., Faleide, J. I., Pedersen, T., Eldholm, O. & Neverdal, F. 2000. NE Atlantic continental rifting and volcanic margin formation. In: *Dynamics of the Norwegian Margin* (edited by Nøttvedt, A.). *Special Publication* **167**. Geological Society, London, 295-326.

Slagstad, T., Barrére, C., Davidsen, B. & Ramstad, R. K. 2008. Petrophysical and thermal properties of pre-Devonian basement rocks on the Norwegian continental margin. *Geological Survey of Norway Bullettin* **448**, 1-6.

Smallwood, J. R. & Maresh, J. 2002. The properties, morphology and distribution of igneous sills: modelling, borehole data and 3D seismic from the Faroe-Shetland area. In: *The North Atlantic Igneous Province: Stratigraphy, Tectonic, Volcanic and Magmatic Processes* (edited by Jolley, D. W. & Bell, B. R.). *Special Publication* **197**. Geological Society, London, 271-306.

Smallwood, J. R., White, R. S. & Staples, R. S. 1998. Deep crustal reflectors under Reydarfjordur, eastern Iceland: crustal accretion above the Iceland mantle plume. *Geophysical Journal International* **134**(1), 277-290.

Smallwood, J. R., Towns, M. J. & White, R. S. 2001. The structure of the Faeroe-Shetland Trough from integrated deep seismic and potential field modelling. *Journal of the Geological Society* **158**, 409-412.

Smit, D.-J., Biegert, E. & Mondt, J. 2005. Advances in subsurface imaging using potential field technology: gravimetry sensors and applications. In: *Petroleum Geology: North-West Europe and Global Perspectives - Proceedings of the 6th Petroleum Geology Conference* (edited by Doré, A. G. & Vining, B. A.). Geological Society, London, 1453-1459.

Smythe, D. K., Chalmers, J. A., Skuce, A. G., Dobinson, A. & Mould, A. S. 1983. Early opening history of the North Atlantic - I. Structure and origin of the Faeroe-Shetland Escarpment. *Geophysical Journal of the Royal Astronomical Society* **72**, 373-398.

Solheim, A., Riis, F., Elverhoi, A., Faleide, J. I., Jensen, L. N. & Cloetingh, S. 1996. Impact of glaciations on basin evolution: data and models from the Norwegian margin and adjacent areas - introduction and summary. *Global and Planetary Change* **12**, 1-9.

Stuevold, L. M. & Eldholm, O. 1996. Cenozoic uplift of Fennoscandia inferred from a study of the mid-Norwegian margin. *Global and Planetary Change* **12**, 359-386.

Stuevold, L. M., Skogseid, J. & Eldholm, O. 1992. Post-Cretaceous uplift events on the Vøring continental margin. *Geology* **20**, 919-922.

Surlyk, F. 1990. Timing, style and sedimentary evolution of Late Palaeozoic-Mesozoic extensional basins of East Greenland. In: *Tectonic Events Responsible for Britans's Oil and Gas Reserves* (edited by Hardman, R. P. F. & Brooks, J.). *Special Publications* **55**. Geological Society, London, 107-125.

Surlyk, F., Piasecki, S., Rolle, F., Stemmerik, L., Thomsen, E. & Wrang, P. 1984. The Permian basin of East Greenland. In: *Petroleum Geology of the North European Margin* (edited by Spencer, A. M.). Norwegian Petroleum Society, Graham & Trotman, London, 303–315.

Svensen, H., Planke, S., Malthe-Sorenssen, A., Jamtveit, B., Myklebust, R., Eidem, T. R. & Rey, S. S. 2004. Release of methane from a volcanic basin as a mechanism for initial Eocene global warming. *Nature* **429**(6991), 542-545.

Symonds, P. A., Planke, S., Frey, Ø. & Skogseid, J. 1998. Volcanic evolution of the Western Australian continental margin and its implications for basin development. In: *The Sedimentary Basins of Western Australia: Proc. of Pet. Expl. Soc. of Australia Symp.* (edited by Purcell, P. G. & Purcell, R. R.) **2**, Perth, 33–54.

Talwani, M. & Eldholm, O. 1972. Continental margin off Norway: A geophysical study. *Geological Society of America Bulletin* **83**, 3573-3606.

Talwani, M. & Eldholm, O. 1977. Evolution of the Norwegian-Greenland Sea. *Bulletin of the Geological Society of America* **88**(7), 969-999.

Thiede, J., Eldholm, O. & Taylor, E. 1989. Variability of Cenozoic Norwegian-Greenland Sea paleoceanography and northern hemisphere paleoclimate. In: *Proceedings of the Ocean Drilling Program, Scientific Results* (edited by Eldholm, O., Thiede, J. & Taylor, E.) **104**, 1067-1118.

Thompson, D. T. 1982. EULDPH - A new technique for making computer-assisted depth estimates from magnetic data. *Geophysics* **47**, 31-37.

Tiley, R., White, N. & Al-Kindi, S. 2004. Linking Paleogene denudation and magmatic underplating beneath the British Isles. *Geological Magazine* **141**, 345-351.

Torske, T. & Prestvik, T. 1991. Mesozoic detachment faulting between Greenland and Norway: Inferences from Jan Mayen Fracture Zone system and associated alkalic volcanic rocks. *Geology* **19**, 481-484.

Torsvik, T. H., Carlos, D., Mosar, J., Cocks, L. R. M. & Malme, T. N. 2002. Global reconstructions and North Atlantic paleogeography 440 Ma to Recent. In: *BATLAS - Mid Norway plate reconstruction atlas with global and Atlantic perspectives* (edited by Eide, E.). Gelogical Survey of Norway, 18-39.

Tsikalas, F., Faleide, J.I. & Eldholm, O. 2001. Lateral variations in tectono-magmatic style along the Lofoten-Vesteralen volcanic margin off Norway. *Marine and Petroleum Geology* **18**(7), 807-832.

Tsikalas, F., Faleide, J. I. & Kusznir, N. J. 2008. Along-strike variations in rifted margin crustal architecture and lithosphere thinning between northern Vøring and Lofoten margin segments off mid-Norway. *Tectonophysics* **458**, 68-81.

Turcotte, D. L. & Schubert, G. 2002. *Geodynamics*. Cambridge University Press, Cambridge.

van Wijk, J. W., van der Meer, R. & Cloetingh, S. A. P. L. 2004. Crustal thickening in an extensional regime: application to the mid-Norwegian Vøring margin. *Tectonophysics* **387**(1-4), 217-228.

Vogt, P. R., Cherkashev, G., Ginsburg, G., Ibanov, G., Milikov, A., Crane, K., Lein, A., Sundvor, E., Pimenov, N. & Egorov, A. 1997. Haakon Mosby mud volcano provides unusual example of venting. *Eos* **78**, 549-557.

Walker, G. P. L. 1993. Basaltic-volcano systems. In: *Magmatic Processes and Plate Tectonics* (edited by Prichard, H. M., Alabaster, T., Harris, N. B. W. & Neary, C. R.). *Special Publications* **76**. Geological Society, London, 3-38.

Wang, Y. B. & Singh, S. C. 2003. Separation of P- and S-wavefields from wide-angle multicomponent OBC data for a basalt model. *Geophysical Prospecting* **51**(3), 233-245.

Warner, M., Morgan, J., Chironi, C., Tong, C. H. & Stekl, I. 2002. Sub-basalt: what's the problem? In: *Sub-basalt imaging. Journal of Conference Abstracts* **7**. Cambridge Publications, Cambridge, UK, 197-198.

Watts, A. B. 1982. Tectonic subsidence, flexure and global changes of sea level. *Nature* **297**(5866), 469-474.

Watts, A. B. 1988. Gravity anomalies, crustal structure and flexure of the lithosphere at the Baltimore Canyon Trough. *Earth and Planetary Science Letters* **89**, 221-238.

Watts, A. B. & Stewart, J. 1998. Gravity anomalies and segmentation of the continental margin offshore West Africa. *Earth and Planetary Science Letters* **156**, 239-252.

Watts, A. B. 2001. *Isostasy and flexure of the lithosphere*. Cambridge University Press, Cambridge.

Weber, M. E., Lyman, G. & Anderson, B. S. 2000. Enhancing seismic depth migration with simultaneous gravity. *Offshore* **60**(10).

Weissel, J. K. & Karner, G. D. 1989. Flexural Uplift of Rift Flanks Due to Mechanical Unloading of the Lithosphere During Extension. *J. Geophys. Res.* **94**(B10), 13919-13950.

White, R. S. 1988. A hot-spot model for Early Tertiary volcanism in the North Atlantic. In: *Early Tertiary Volcanism in the North Atlantic* (edited by Morton, A. C. & Parson, L. M.). *Special Publications* **39**. Geological Society, London, 241-252.

White, R. S. & McKenzie, D. 1989. Magmatism at Rift Zones - the Generation of Volcanic Continental Margins and Flood Basalts. *Journal of Geophysical Research-Solid Earth and Planets* **94**(B6), 7685-7729.

White, R. S., Spence, G. D., Fowler, S. R., McKenzie, D. P., Westbrook, G. K. & Bowen, A. N. 1987. Magmatism at rifted continental margins. *Nature* **330**, 439-444.

White, R. S., Smallwood, J. R., Fliedner, M. M., Boslaugh, B., Maresh, J. & Fruehn, J. 2003. Imaging and regional distribution of basalt flows in the Faeroe-Shetland Basin. *Geophysical Prospecting* **51**(3), 215-231.

White, R. S., Spitzer, R., Christie, P. A. F., Roberts, A. W., Lunnon, Z., Maresh, J. & Group, i. W. 2005. Seismic imaging through basalt flows on the Faroes Shelf. In: *Faroe Islands Exploration Conference: Proceedings of the 1st Conference. Annales Societatis Scientiarum Færoensis, Supplementum 43* **43**, Tórshavn, 1-7.

White, R. S., Smith, L. K., Roberts, A. W., Christie, P. A. F., Kusznir, N. J. & iSIMM Team. 2008. Lower-crustal intrusion on the North Atlantic continental margin. *Nature* **452**(7186), 460-U6.

White, R. S. & Smith, L. K. 2009. Crustal structure of the Hatton and the conjugate east Greenland rifted volcanic continental margins, NE Atlantic. *J. Geophys. Res.* **114**.

Whitmarsh, R. B., Minshull, T. A., Russell, S. M., Dean, S. M., Louden, K. E. & Chian, D. 2001. The role of syn-rift magmatism in the rift-to-drift evolution of the West Iberia continental margin: geophysical observations. In: *Non-Volcanic Rifting of Continental Margins: A Comparison of Evidence from Land and Sea* (edited by Wilson, R. C. L., Whitmarsh, R. B., Taylor, B. & Froitzheim, N.). *Geological Society London Special Publications* **187**, 107-124.

Wienecke, S., Braitenberg, C. & Götze, H. J. 2007. A new analytical solution estimating the flexural rigidity in the Central Andes. *Geophysical Journal International* **169**(3), 789-794.

Zelt, C. A. 1999. Modelling strategies and model assessment for wide-angle seismic traveltime data. *Geophys. J. Int.* **139**, 183-204.

Ziegler, P. A. 1988. Evolution of the Arctic-North Atlantic and the western Tethys. *American Association of Petroleum Geologists Memoirs* **43**.

Ziolkowski, A., Hanssen, P., Gatliff, R., Jakubowicz, H., Dobson, A., Hampson, G., Li, X. Y. & Liu, E. R. 2003. Use of low frequencies for sub-basalt imaging. *Geophysical Prospecting* **51**(3), 169-182.

Appendix

Summary of petrophysical properties representative for the Møre margin

Table A.1. Densities based on 21 composite well logs from NPD exploration wells in the Møre basin. Units are kg/m^3. Minimum value (min), maximum value (max), average value (ave) and standard deviation for a specific geological body.

	min	**max**	**ave**	**std**
Neogene	1 630	2 370	2 092	140
Paleogene	1 623	2 550	2 024	179
Cretactous	1 910	2 790	2 438	142
Jurassic	2 150	2 810	2 551	111
Triassic	2 430	2 730	2 534	66
Basement	2 490	2 790	2 664	69

Table A.2. Magnetic properties of basement rocks on the Norwegian mainland and the mid-Norwegian shelf. Number of samples (no) and average value (ave) a for a specific rock type. Susceptibility is in SI units.

Area / Lithology	**Susceptibility**		**Q-value**	**Well**	**Reference**
	no	ave	ave		
Western Gneiss Region	1989	0.00339	0.25		NGU 89.164
Central Norway basem. window	419	0.00910	1.04		Olesen *et al.* (2002)
Brecciated siltstone	1	0.00046	0.53	6305/12-2	Slagstad *et al.* (2008)
Leucogabbro	1	0.00284	0.52	6306/10-1	Slagstad *et al.* (2008)
Leucogabbro	1	0.00100	0.50	6306/10-1	Slagstad *et al.* (2008)
Granite	1	0.00119	2.29	6407/10-3	Slagstad *et al.* (2008)

Table A.3. Densities of basement rocks on the Norwegian mainland and the mid-Norwegian shelf. Number of samples (no) and average value (ave) a for a specific rock type. Density units are kg/m^3.

Area / Lithology	Density		Well	Reference
	no	ave		
Western Gneiss Region	1989	2 762		NGU 89.164
Central Norway basem. window	419	2 729		Olesen *et al.* (2002)
Brecciated siltstone	1	2740	6305/12-2	Slagstad *et al.* (2008)
Leucogabbro	1	2 767	6306/10-1	Slagstad *et al.* (2008)
Leucogabbro	1	2 732	6306/10-1	Slagstad *et al.* (2008)
Granite	1	2 631	6407/10-3	Slagstad *et al.* (2008)

Table A.4. Densities applied in previous studies on the Mid-Norwegian margin. Units are kg/m^3.

	Mjelde *et al.* (1998)	**Mjelde *et al.* (2001)**	**Raum *et al.* (2002)**	**Olesen *et al.* (2002)**	**Fernàndez *et al.* (2004)**	**Ebbing *et al.* (2006)**
Water	1030	1030	1030	1030	1030	1030
Cenozoic	1950-2200	1900-2150	1950-2250	2200	2200	2050-2100
Cretaceous	2450-2670		2400-2650	2350-2500	2400-2650	2300-2600
Pre-Cretaceous	2830	2700-2810	2680-2760		<2600	2650-2700
Continental Crust	2700-2950	2820-2900	2820-2840	2750-2950	2650-2950	2650-3000
Continental Basement						2650-2850
Lower Continental Crust						2950-3000
Volcanic flows		2700-2770			2500	
Volcanic intrusions		2620-2800				
LCB	3100-3230	3110-3220	3000-3120	3100	3000	3100
Mantle	3330	3330-3360	3300-3340	3250	3200	3300

Table A.5. Densities of igneous rocks on the Vøring margin, Faeroe Islands and Iceland. Number of samples (no), average value (ave) and standard deviation (std) of each unit in a study. Units are kg/m^3.

	Density			Location	Reference
	no	ave	std		
Volcanic section above 1089 mbsf		2 660		ODP 642E	Eldholm *et al.* (1987)
Volcanic section below 1089 mbsf		2 440		ODP 642E	Eldholm *et al.* (1987)
Volcanic section above 1089 mbsf		2 500		ODP 642E	Planke & Eldholm (1994)
Upper lava series	25	2 870	60	Faroe Islands	Saxov & Abrahmsen (1966)
Middle lava seris	71	2 820	90	Faroe Islands	Saxov & Abrahmsen (1966)
Lower lava series	29	2 900	40	Faroe Islands	Saxov & Abrahmsen (1966)
Intrusions	7	2 970	60	Faroe Islands	Saxov & Abrahmsen (1966)
Tuffs	8	2 170	120	Faroe Islands	Saxov & Abrahmsen (1966)
Middle lava series	11	2 760		Vestmanna-1	Balling *et al.* (1984)
Lower lava series	3	2 920		Vestmanna-1	Balling *et al.* (1984)
Lower lava series	4	2 970		Lopra-1	Balling *et al.* (1984)
Flow unit		2 850		Lopra-1/1A	Boldreel (2006)
Core		2 900		Lopra-1/1A	Boldreel (2006)
Crust		2 660		Lopra-1/1A	Boldreel (2006)
Lava flows		2 740		Lopra-1/1A	Boldreel (2006)
Intrusions		2 900		Lopra-1/1A	Boldreel (2006)
Sediments		2 580		Lopra-1/1A	Boldreel (2006)
Lower lava series	32	2 680	270	Lopra-1/1A	Abrahamsen (2006)
Lava flows	237	2 784	145	Iceland	Pálsson *et al.* (1984
Intrusions	13	2 740	230	Iceland	Pálsson *et al.* (1984)
Lava flows		2 800	220	IRDP	Jónsson & Stefánsson (1982)
Intrusions		2 940	180	IRDP	Jónsson & Stefánsson (1982)
Lava flows	90	2 850	160	IRDP	Christensen & Wilkens (1982)
Intrusions	45	2 950	70	IRDP	Christensen & Wilkens (1982)

Table A.6. Magnetic properties of igneous rocks in wells on the Vøring margin, Faeroe Islands and Iceland. Number of samples (no) and average value (ave) of each unit in a study. Susceptibility is given in SI units.

	Susceptibility		**Q-value**	**Location**	**Reference**
	no	ave	ave		
Igneous rock	7	0.01600	4.84	DSDP 38-338	Kent & Opdyke (1978)
Igneous rock	3	0.01500	2.33	DSDP 38-342	Kent & Opdyke (1978)
Igneous rock	221	0.03000	4.17	ODP 104-642E	Eldholm *et al.* (1987)
Middle lava series	420			Vestmanna-1	Abrahamsen *et al.* (1984)
Lower lava series	420	0.02000		Vestmanna-1	Abrahamsen *et al.* (1984)
Lower lava series		0.01925	4.61	Lopra-1	Schoenharting & Abrahamsen (1984)
Lower lava series (basalt)	46	0.02210		Lopra-1/1A	Abrahamsen & Waagstein (2006)
Lower lava series (tuff)	17	0.08500		Lopra-1/1A	Abrahamsen & Waagstein (2006)
Lower lava series	46	0.02210	2.16	Lopra-1/1A	Abrahamsen (2006)
Lava flows	258	0.05044	1.84	IRDP	Bleil *et al.* (1982)
Intrusions	110	0.05801	3.37	IRDP	Bleil *et al.* (1982)